Performance of Low-Cost Radio-over-Fibre Systems

A thesis submitted to the University of Kent for the degree of
Doctor of Philosophy in Electronic Engineering

by

Anjali Das

February 2008

ABSTRACT

The research presented in this thesis has focused on the use of radio-over-fibre (RoF) technology for improving the quality of mobile/wireless coverage within buildings. The primary aim was to minimise overall system costs by employing commercially available components. For this purpose, a distributed antenna system using low-cost vertical-cavity surface-emitting lasers (VCSELs) operating at 850 nm and multimode fibre (OM1/OM2) has been designed and implemented.

A detailed link budget analysis has been performed which allows for the prediction of maximum achievable ranges for the transmission of different wireless systems over the RoF link, while taking into account practical restrictions that are important for bi-directional link operation (e.g. crosstalk and noise emissions). The analysis indicates that when optimised component parameter values are utilised, reasonable cell sizes may be achieved for systems such as GSM, UMTS and WLAN. The link budget predictions were verified for the transmission of 'real' WLAN signals over the designed RoF link and complete coverage of a standard office room was demonstrated.

The majority of previous research into low-cost RoF links has primarily involved characterisation of the optical path. In this investigation, signal strength and throughput measurements were conducted for the combined optical and wireless paths in order to verify the operation of the complete fibre-fed WLAN system. Throughput values close to 5 Mbps for IEEE 802.11b and 20 Mbps for IEEE 802.11g were recorded. Additionally, the transmission of different combinations of emulated mobile/wireless systems in a dual-band configuration over another radio-over-fibre link (also employing 850 nm VCSELs and MMF) has been successfully demonstrated.

Experimental investigations have been carried out for the first time to analyse the performance of WLAN-over-fibre networks using different MAC mechanisms such as fragmentation and the use of RTS/CTS in the presence of hidden nodes. Finally, scenarios involving multiple clients accessing a single remote antenna unit and multiple remote antenna units being fed by a single access point have been demonstrated.

ACKNOWLEDGEMENTS

There have been many people who have helped in the completion of this research and thesis. I shall always remain indebted to each one of them.

I would like to express my sincere gratitude to my supervisor, **Dr. Nathan Gomes**, without whose helpful guidance and support, this Ph.D. could not have been completed. I would like to thank **Dr. David Wake**, for so generously sharing with us his knowledge and insight into RoF technologies, particularly during the link budget spreadsheet development and WLAN system demonstrator measurements.

I am indebted to the **University of Kent/ROSETTE** and the **Institution of Engineering and Technology**, for providing me with financial support during the course of my Ph.D.

I am extremely grateful for the persistent support of **Anthony Nkansah**. His suggestions and advice throughout the duration of my Ph.D. have been most helpful. For our memorable 'tea-time chats', I thank **Denyse Menne** (my fairy godmother!), **Yiquing Liang**, **Majlinda Mjeku** and **Olanike Folayan.** Thanks to **Majlinda** also for her help and suggestions during the hectic days of the WLAN MAC experiments, and for carrying out the OPNET simulations.

Additionally, I wish to thank **Benito Sanz** and **Ignacio Garcia** for designing and building the antenna used in the measurements.

This research could not have been completed without the tireless efforts of our laboratory technician, **Mr. Robert Davis** (Department of Electronics) in helping with the set-up of a number of our experiments. I am also grateful to **Mr. Clive Birch**, **Mr. Terry Rockwell** and **Mr. Simon Jakes** (Department of Electronics).

I would like to express my gratitude to **Dr. Lethien** (IEMN, Lille) and **Dr. Vilcot** (IEMN, Lille) without whose help and co-operation, it would have been impossible for the dual-band RoF measurements to have been made.

I would also like to thank the **University of Kent Library**, for helping in the timely acquisition of numerous publications through inter-library loans over the three years of my research.

As a final personal note, I wish to express my deepest appreciation and gratitude to my family and friends: in particular, my wonderful parents, **Sati** and **Mohandas**, my Cheriamma, **Kamala**, my uncle, **Ravi**, my grandparents, my sister **Pooja**, my brother **Akhilesh**, my ever-supporting parents (in-law), **Lotika** and **Paul, Roma Mausi** and my close friends, **Sohini, Veena** and **Bindu**. Their love, wisdom and support over the years have been a constant source of inspiration to me. Thank you to each one of them. Lastly, I am very grateful to my husband and best friend, **Salil**, for always being there for me. Without his never-ending patience, love and encouragement (and indeed his editorial skills!), I would not have been able to complete this PhD.

Anjali Das
February 2008

CONTENTS

LIST OF PUBLICATIONS

The following is a list of the publications (in chronological order) that have been produced during the duration of work reported in this thesis.

[1] A. Das., A. Nkansah, and N.J. Gomes, "Characterization of VCSELs for use in multimode ROF links," *NEFERTITI Winterschool Conference* (NEFERTITI: Network of Excellence on Broadband Fibre Radio Techniques and its Integration Technologies), York, United Kingdom, February 2004.

[2] I.J. Garcia Zuazola, J. Batchelor, R.J. Langley, A. Das, A. Nkansah, D. Wake, and N.J. Gomes, "Photonic Antenna Units Containing Bi-Directional Amplification for TDD and FDD in Picocell Systems," *Proceedings of the Loughborough Antennas and Propagation Conference 2005*, ISBN 0947974334, Loughborough, United Kingdom, April 2005.

[3] A. Das, A. Nkansah, I.J. Garcia, N.J. Gomes, J.C. Batchelor, and D. Wake, "Demonstration of Multimode Fibre-fed Indoor Wireless Network," *NEFERTITI workshop on Photonics in Wireless Communications*, Gothenburg, Sweden, June 2005.

[4] A. Das, A. Nkansah, I.J. Garcia, N.J. Gomes, J.C. Batchelor, and D. Wake, "Low-cost Multimode Fibre-fed Indoor Wireless Network," *UK National URSI Symposium*, Abingdon, United Kingdom, July 2006.

[5] A. Das, A. Nkansah, N.J. Gomes, I.J. Garcia, J C. Batchelor, and D. Wake, "Design of Low-cost Multimode Fibre-fed Indoor Wireless Networks," *IEEE Transactions on Microwave Theory and Techniques*, Volume 54, Issue 8, pp. 3426-3432, August 2006.

[6] N.J. Gomes, A. Das, A. Nkansah, M. Mjeku, and D. Wake, "Multimode Fiber-fed Indoor Wireless Networks," Invited Paper, *International Topical Meeting on Microwave Photonics (MWP)*, Grenoble, France, October 2006.

[7] A. Nkansah, A. Das, N.J. Gomes, P. Shen, and D. Wake, "VCSEL-based Single-mode and Multimode Fiber Star/Tree Distribution Network for Millimeter-wave Wireless Systems," *International Topical Meeting on Microwave Photonics (MWP)*, Grenoble, France, October 2006.

[8] A. Nkansah, A. Das, C. Lethien, J. Vilcot, N.J. Gomes, I.J. Garcia, J.C. Batchelor, and D. Wake, "Simultaneous Dual Band Transmission over Multimode Fibre-fed Indoor Wireless Network," *IEEE Microwave and Wireless Component Letters*, Volume 16, Issue 11, pp. 627-629, November 2006.

[9] A. Nkansah, A. Das, N.J. Gomes, and P. Shen, "Multilevel Modulated Signal Transmission over Serial Single-Mode and Multimode Fiber Links using Vertical-Cavity Surface-Emitting Lasers for Millimeter-wave Wireless Communications," *IEEE Transactions on Microwave Theory and Techniques*, Vol. 55, No. 6, pp. 1219-1228, June 2007.

[10] A. Das, M. Mjeku, A. Nkansah, and N.J. Gomes, "Effects on IEEE 802.11 MAC Throughput in Wireless LAN over Fiber Systems," *Journal of Lightwave Technology*, Vol. 25, Issue 11, pp. 3321-3328, November 2007.

LIST OF ACRONYMS

ACK: Acknowledgement (frame)

ACLR: Adjacent channel leakage ratio

AP: Access point

AU: Antenna unit

BER: Bit error ratio

BPSK: Binary phase-shift keying

BSS: Basic service set

CCK: Complementary code keying

CNR: Carrier-to-noise ratio

CO: Central office

CSMA/CA: Carrier sense multiple access with collision avoidance

CTS: Clear to send

CU: Central unit

DAS: Distributed antenna system

DCF: Distributed coordination function

DCS: Digital cellular system

DECT: Digital Enhanced Cordless Telecommunications

DFB: Distributed feedback (laser)

DIFS: Distributed inter frame space

DL: Downlink

DS: Distribution system

DPRS: DECT packet radio service

DPSK: Differential phase-shift keying

DSSS: Direct sequence spread spectrum

EAM: Electroabsorption modulator

EDGE: Enhanced Data-Rates for GSM Evolution

EMB: Effective modal bandwidth

ERP: Extended rate PHY

ESS: Extended service set

ETSI: European Telecommunications Standard Institute

EVM: Error vector magnitude

FDD: Frequency division duplex

FER: Frame error rate

FHSS: Frequency-hopping spread spectrum

FP: Fabry-Perot (laser)

GMSK: Gaussian minimum shift keying

GPRS: General Packet Radio Service

GSM: Global System for Mobile Communications / Groupe Special Mobile

HIPERLAN: High Performance Radio Local Area Network

IBSS: Independent basic service set

IEEE: Institute of Electrical and Electronics Engineers

IF: Intermediate frequency

IIP3: Third-order input intercept point

IM3: Third-order intermodulation (products)

IMDD: Intensity modulation direct-detection

IP3: Third-order intercept point

IR: Infrared

ITU: International Telecommunication Union

LOS: Line-of-sight

MAC: Medium access control (layer)

MMF: Multi-mode fibre

MPDU: MAC protocol data unit

MR: Mobile receiver

MSDU: MAC service data unit

MT: Mobile transmitter

MU: Mobile unit

NAV: Network allocation vector

OFDM: Orthogonal frequency division multiplexing

OIP3: Third-order output intercept point

PBCC: Packet binary convolutional code

PCF: Point coordination function

PCS: Personal Communication Service

PD: Photodiode

PHS: Personal Handyphone System

PHY: Physical (layer)

QAM: Quadrature amplitude modulation

QPSK: Quaternary phase-shift keying

RAU: Remote antenna unit

RF:	Radio frequency
RIN:	Relative intensity noise
RoF:	Radio-over-fibre
RTS:	Request to send
SCM:	Sub-carrier multiplexing
SFDR:	Spurious-free dynamic range
SIFS:	Short inter frame space
SMF:	Single-mode fibre
SNR:	Signal-to-noise ratio
TCP:	Transmission control protocol
TDD:	Time division duplex
TMT:	Theoretical maximum throughput
UDP:	User datagram protocol
UL:	Uplink
UMTS:	Universal Mobile Telecommunication System
VCSEL:	Vertical-cavity surface-emitting laser
VSA:	Vector signal analyser
VSG:	Vector signal generator
WiMAX:	Worldwide Interoperability for Microwave Access
WLAN:	Wireless Local Area Network

LIST OF FIGURES

Figure **Page**

LIST OF TABLES

Table **Page**

To my late Amma

CHAPTER 1
INTRODUCTION

The aim of any communication system, be it wired or wireless, is to enable the transfer of information from one point to another. Wireless communication systems have come a long way since the introduction of the 1st generation (1G) systems in the 1970s. The emergence of subsequent generations – 2G, 3G and the future 4G systems – has been triggered by the rapidly growing user density and the demand for higher speeds and more services; this naturally leads to greater bandwidth requirements. One way of satisfying these bandwidth requirements and, therefore, increasing capacity is by the implementation of smaller-sized cells (for example, microcells and picocells). An effective way of interconnecting these microcells or picocells is to use optical fibres. In addition to providing high transmission capacities, optical fibres also offer advantages such as low attenuation, low weight and minimal susceptibility to external interference. This integration of fibre-optics with wireless communications is termed radio-over-fibre (RoF) technology.

1.1 Radio-over-Fibre Technology

Radio-over-fibre technology involves distribution of RF signals over optical fibre from a central location to several remote antenna sites. An RoF transmission system is analogue in nature since the distributed signal is an analogue waveform (though it may be digitally modulated as in GSM, UMTS, WLAN or WiMAX) [1]. Based on the transmission frequency, RoF systems may be classified as microwave RoF (frequencies < 30 GHz) and millimetre-wave RoF (frequencies > 30 GHz) [2].

One of the main motivations behind RoF technology is the provision of high quality mobile/wireless services for dense user populations in buildings such as shopping centres, airports, medical centres or corporate offices [1], [3]. The entire building may be divided into a number of picocells, each of which is serviced by a remote antenna unit (RAU). With optical fibre as the transmission medium, RF signals can be distributed throughout the building using a distributed antenna system (DAS).

An example of a DAS implementation using RoF is shown in Figure 1.1. As shown, the DAS transports radio carriers from a central unit (CU) to a number of remote antenna units. Consequently, the access points (in WLAN, for example) or base stations (in GSM, for example) do not need to be located in different rooms of the building, rather in a central location, such as the basement. Thus, in addition to making maintenance and upgrading simpler (with all the complexity concentrated at the CU), such a system also results in very simple RAUs that require only optoelectronic conversion and amplification mechanisms. One can also imagine scenarios where the base stations or access points can be switched to different RAUs to cater for variations in demand. Moreover, the transmission of different radio signals over the same fibre optic infrastructure in a DAS can result in operational benefits by enabling the provision of shared infrastructure costs for different service providers and operators.

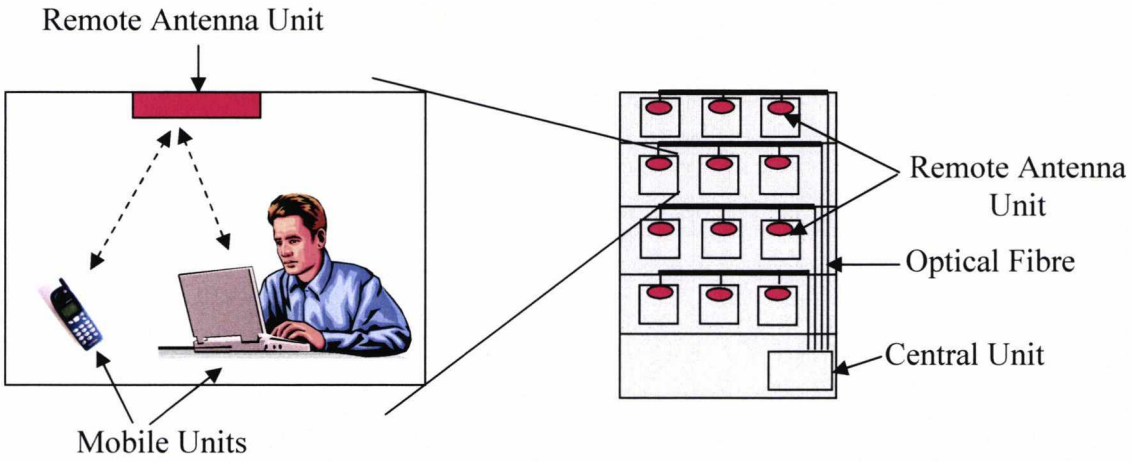

Figure 1.1. Implementation of a distributed antenna system using radio-over-fibre

1.1.1 Transportation Techniques for Radio-over-Fibre Links

The simplest method of distributing an RF signal over optical fibre is by using intensity modulation direct detection (IMDD) [4]. Using the IMDD method, the intensity of the optical source (located at the CU) is modulated by applying an RF signal. After transportation over the optical fibre, the RF signal is recovered by using a photodiode (located at the RAU). This process is called direct detection. The IMDD technique is further divided into two types, based on how the intensity modulation is performed. The first type called direct modulation, involves the direct application of the modulating signal to the laser source. The alternative way is to use external modulation: here the laser operates at a constant optical power and an external device is used to modulate the optical intensity. It should be noted that both intensity modulation techniques (i.e.,

direct modulation and external modulation) use direct detection [4]. The simplicity and hence reduced costs of using direct modulation IMDD makes it a popular choice for microwave RoF systems [1].

The RF signal may be transported over the optical fibre at the RF frequency (RF-over-fibre), at an intermediate frequency (IF-over-fibre) or as a baseband signal (baseband-over-fibre) [5]. In the RF-over fibre technique, the RF signal is directly transported over the optical fibre or in other words, the laser source (or external modulator) is modulated at the radio transmission frequency. In the IF-over-fibre or baseband-over-fibre technique, the IF or the baseband signal (respectively) is transmitted over the fibre with the necessary up-conversion taking place at the RAU. For the uplink transmission in this case, the received RF signal is down-converted to an IF or baseband signal before transmission back to the CU. Of the three techniques, the RF-over-fibre method is the most cost-effective as it results in simple RAUs without the use of extra electronics (such as local oscillators and mixers) for any up/down conversion. It is, therefore, the most widely implemented transportation method for microwave RoF systems. The IF/baseband-over-fibre techniques, on the other hand, are more popular for millimetre-wave RoF systems [5] (examples of such systems are presented in Section 3.5, Chapter 3).

1.1.2 Examples of RoF Application Areas

Due to the simplicity and cost-effectiveness of RoF technology, it has been applied extensively in a number of areas. RoF technology applied in mobile telephone networks can be used to provide coverage extension in shadowed or obstructed areas such as tunnels and railways; it can also be used for capacity distribution in urban areas, airports and shopping centres [1]. Notable examples of RoF implementations in the 'real world' include the Bluewater shopping centre in the United Kingdom [1] and the Sydney Olympic Games village [6]. Four UK cellular operators (two at 900 MHz and two at 1800 MHz) share the single-mode fibre-based RoF network in the Bluewater shopping centre. The huge capacity at the Sydney Olympics was served by the Tekmar (now Andrew Corporation) BriteCell single-mode fibre-fed DAS. In this system, depending on the demand, coverage could be switched between the various venues across the Olympic village.

RoF has also been conceptually applied in the development of road-to-vehicle multiple-service communication systems as discussed in [1]. Specifically, the road-to-vehicle communication system (an Intelligent Transportation System service), utilises the 36–37 GHz millimetre-wave band and aims at providing services such as vehicle information and communication, electronic toll collection and mobile telephony as an integrated broadband signal. A more recent investigation into the use of radio-over-fibre technology for road-vehicle communications is presented in [7]. Figure 1.2 illustrates the basic architecture for such a system. Finally, in order to cater for the steadily increasing demand for broadband services in rural areas, a RoF-based wireless access network architecture has been proposed in [8].

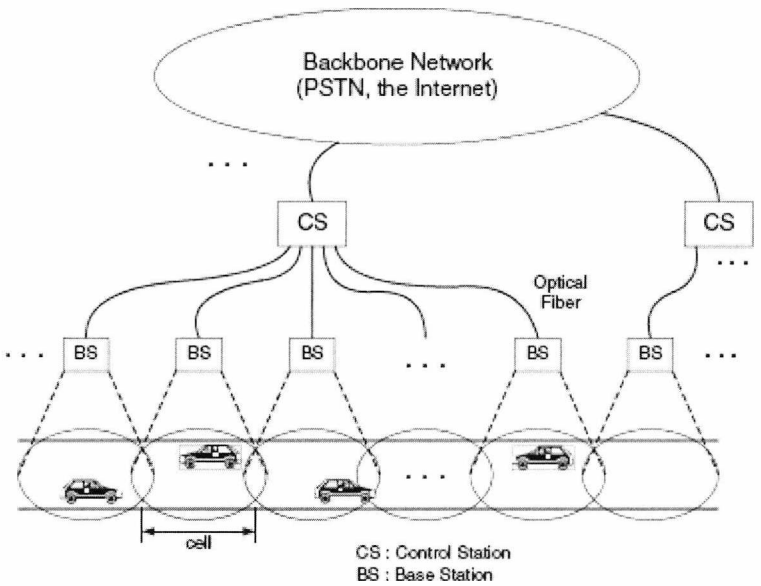

Figure 1.2. Basic architecture of an RoF-based road-vehicle communication system (reproduced from [7])

1.2 Objectives of Research

A number of DAS products available in the market today use single-mode fibre (SMF) for RF signal distribution. This fact is highlighted in Table 1.1 which presents a comparison of some of the currently available commercial fibre-based DAS products. While single-mode fibre is preferred over multimode fibre (MMF) due to better bandwidth performance, multimode fibre is still a more cost-effective option as it is pre-installed in most building backbones today [9].

Additionally, the preferred optical sources for use in these commercial DAS products operate at wavelengths of around 1300 nm (Table 1.1). However, such optical sources are known to be expensive. In this respect, vertical-cavity surface-emitting lasers (VCSELs) operating at 850 nm are a more cost-effective option. Compared to 1300 nm optical sources, these commercially available VCSELs are also more efficiently coupled with multimode fibre. Therefore, the main aim of the research presented in this thesis was to design and implement a distributed antenna system fed by VCSEL-MMF-based optical links for improving in-building coverage.

TABLE 1.1 COMPARISON OF SOME OF THE CURRENTLY AVAILABLE COMMERCIAL DAS PRODUCTS

Product	Fibre used	Wavelength of operation of the optical source (nm)	Examples of wireless systems supported
Andrew ION-B series [10]	SMF	1310	GSM 900, GSM 1800, UMTS 2100
PowerWave's UniServ [11]	SMF	1310	GSM 900, GSM 1800
Zinwave 2700 [12]	SMF	1310	GSM, UMTS, WLAN
	MMF		
Inter-Reach Unison LGC Wireless [13]	SMF	Information not available	GSM 900, GSM 1800, EDGE, UMTS
	MMF		
ADC Digivance [14]	SMF	1310	GSM 900, GSM 1800, EDGE, UMTS
	MMF	850	

Any practical RoF-based distributed antenna system should ideally enable the transmission of multiple wireless systems. In this respect, the transmission performance of different combinations of emulated wireless systems in a dual-band configuration has been experimentally investigated in this work.

The IEEE 802.11 medium access control (MAC) protocol is popular in current wireless networks due to its simplicity. However, the distributed nature of the protocol makes it less tolerant (compared to centralised MAC schemes such as HiperLAN/2) to the additional propagation delay introduced by the insertion of optical fibre [15]. It, therefore, becomes important to experimentally address the WLAN MAC protocol issues with respect to the transmission of the signal over the fibre (in addition to wireless transmission). In the past, the effect of introducing this extra propagation delay on the timing constraints imposed by the IEEE 802.11 MAC protocol has only been investigated either by means of theoretical analysis [16] or by simulation [17], [18].

Another IEEE 802.11 MAC-related issue that has received considerable attention for conventional WLAN networks (non-fibre based) is that of hidden nodes and the use of the request to send/clear to send (RTS/CTS) mechanism as a solution. Only recently (by means of simulation studies) has the use of RTS/CTS in the hidden-node scenario been investigated in the context of WLAN-over-fibre networks [19]. Thus, the final aim of the research is to experimentally analyse the WLAN-over-fibre link performance in terms of the IEEE 802.11 WLAN MAC protocol.

1.3 Original Contribution

The unique contributions made in this thesis have been listed below:

- A link budget analysis has been developed that allows theoretical range predictions for the transmission of different wireless systems such as GSM, UMTS and WLAN over an RoF link. The link budget not only allows the calculation of maximum achievable ranges for different wireless systems, but also takes into account restrictions such as crosstalk and noise emissions which are important for practical system transmissions. Using this analysis, it has been theoretically calculated that reasonable cell sizes may be achieved for the transmission of several mobile/wireless systems (up to a transmission frequency of 2.5 GHz).

- A distributed antenna system using low-cost components such as commercially available 850 nm VCSELs and OM1/OM2 MMF has been designed. A remote antenna unit was developed which was successfully implemented as part of the DAS. Transmission of 'real' WLAN signals over the designed RoF link has been demonstrated and complete coverage of a standard office room was achieved.

- Signal strength measurements aided in verifying the link budget predictions for the transmission of IEEE 802.11b and IEEE 802.11g over the complete optical and wireless paths. Additionally, further evaluation of the WLAN-over-fibre link performance in terms of the throughput was also carried out. Finally, the link quality was assessed by streaming video signals over the WLAN-over-fibre link.

- The transmission of different combinations of emulated mobile/wireless systems in a dual-band configuration over another radio-over-fibre link (also employing 850 nm VCSELs and multimode fibre) has been demonstrated for the first time.

- For the investigation of the WLAN-over-fibre link performance in terms of the IEEE 802.11 MAC protocol, effects of fibre propagation delay, fragmentation and the use of RTS/CTS on the wireless network throughput are experimentally examined. Additionally, realistic issues such as the presence of multiple clients and the simultaneous operation of multiple RAUs (fed by a single WLAN access point) are also addressed.

1.4 Outline of the Thesis

The outline of the thesis is as follows:

Since radio-over-fibre links are essentially analogue in nature, Chapter 2 of this thesis provides a background on some of the key aspects of analogue fibre-optic links. In particular, the main components of a fibre-optic link such as optical fibres, optical sources and photodiodes are briefly discussed. The main aim of presenting such a discussion is to highlight the advantages of some of the components (such as VCSELs and multimode fibre) for use in low-cost indoor RoF links. Additionally, two performance metrics used for RF fibre optic links are also examined.

Chapter 3 presents a detailed review of past research in the field of low-cost RoF systems. The focus is primarily on microwave RoF systems. Examples of research on the use of 850 nm VCSELs in RoF links and successful RF transmission over multimode fibre are discussed. A brief outline of millimetre-wave RoF systems with particular focus on the different transportation techniques used is also presented.

Chapter 4 describes and presents the component characterisation experiments carried out in order to obtain the different component parameter values that are important to the design of a radio-over-fibre link. Furthermore, two RAU designs are proposed for implementation in the designed fibre-based distributed antenna system.

Chapter 5 outlines the theory behind the link budget calculations. A link budget spreadsheet has been developed for analysing the bi-directional operation of the designed RoF link. The component parameter values obtained using the characterisation measurements in the previous chapter are used as input to the link budget spreadsheet. The analysis aims to optimise the link component parameter values to obtain the best possible range while accounting for restrictions such as crosstalk and noise emissions.

In Chapter 6, the implementation of a distributed antenna system using the proposed RAU designs for the transmission of WLAN signals is presented. The WLAN system demonstrator uses the optimised amplifier gain values from the link budget calculations and is used as a means for verifying the link budget range predictions. The performance of the RoF link for the transmission of IEEE 802.11b signals (at 11 Mbps) and IEEE 802.11g signals (at 54 Mbps) is characterised by means of signal strength and throughput measurements. The chapter also presents theoretical range predictions for other wireless systems such as GSM 900, GSM 1800 and UMTS using the link budget. Finally, the simultaneous dual-band transmission of different combinations of wireless signals (e.g. GSM, DPRS, UMTS and IEEE 802.11g) over the link has been demonstrated.

The performance of the WLAN demonstrator using different IEEE 802.11 MAC mechanisms has been examined in Chapter 7 by means of experiments supported by simulations (using OPNET Modeler) wherever possible. Throughput measurements carried out for the transmission of IEEE 802.11b and IEEE 802.11g signals via the two different RAU configurations, evaluate the effect of fragmentation, fibre propagation delay and the hidden node mechanism. Furthermore, the network performance in the presence of multiple clients accessing the AP via a single RAU, or clients accessing the AP via multiple RAUs has also been discussed.

Finally, Chapter 8 contains a summary of the work described in the thesis. The key achievements of the research work are also highlighted. Additionally, the chapter outlines possibilities for future work into the design and implementation of low-cost radio-over-fibre systems.

References

[1] H. Al-Raweshidy and S. Komaki (Editors), "*Radio over Fiber Technologies for Mobile Communications Networks*," Artech House, Inc., 2002.

[2] D. Wake, L.D. Westbrook, N.G. Walker, and I.C. Smith, "Microwave and millimeter-wave radio fibre," *BT Technology Journal*, Vol. 11, No. 2, pp. 77-88, April 1993.

[3] D. Wake, "Trends and prospects for radio over fibre picocells," *Proceedings of the International Topical Meeting on Microwave Photonics (MWP '02)*, pp. 21-24, November 2002.

[4] C.H. Cox III, "*Analog Optical Links: Theory and Practice*," Cambridge University Press, 2004.

[5] D. Novak, A. Nirmalathas, C. Lim, C. Marra, and R.B. Waterhouse, "Fibre-radio – challenges and possible solutions," *Proceedings of the International Topical Meeting on Microwave Photonics (MWP '03)*, pp. 49-56, September 2003.

[6] N. Anscombe, "Demand for indoor coverage drives radio-over-fibre," *Wireless Europe*, pp. 35-36, Feb./March 2005.

[7] H.B. Kim, M. Emmelmann, B. Rathke, and A. Wolisz, "A radio over fiber network architecture for road vehicle communication systems," *Proceedings of the IEEE Vehicular Technology Conference (VTC 2005 Spring)*, Stockholm, Sweden, May 2005.

[8] H.B. Kim and A. Wolisz, "A radio over fiber based wireless access network architecture for rural areas," *Proceedings of the 14th IST Mobile & Wireless Communication Summit*, Dresden, Germany, June 2005.

[9] A. Flatman, "In-premises optical fibre installed base analysis to 2007," presented to *IEEE 802.310GBE over FDDI Grade Fibre Study Group*, Orlando, FL, March 2004.

[10] www.andrew.com, Andrew ION-B series listed under coverage and capacity solutions.

[11] www.powerwave.com, Powerwave's coverage systems – LinkNet convergence platform.

[12] www.zinwave.com, Zinwave 2700 Distributed Antenna System.

[13] www.lgcwireless.com, InterReach Unison listed under LGC Wireless In-building solutions.

[14] www.adc.com, ADC Digivance Indoor Coverage Solutions (ICS) listed under wireless solutions.

[15] B.L. Dang, V. Prasad, and I. Niemegeers, "On the MAC protocols for radio over fiber networks," *International Conference on Communication and Electronics (ICCE) 2006, Hanoi*, October, 2006.

[16] M.G. Larrode, A.M.J. Koonen, and P.F.M. Smulders, "Impact of radio-over-fibre links on the wireless access protocols," *Proceedings NEFERTITI Workshop, Belgium*, January, 2005.

[17] B.L. Dang and I. Niemegeers, "Analysis of IEEE 802.11 in Radio over Fiber Home Networks," *Proceedings of the 30th IEEE Conference on Local Computer Networks (LCN) 2005*, pp. 744-747, November, 2005.

[18] N.J. Gomes, A. Das, A. Nkansah, M. Mjeku, and D. Wake, "Multimode fiber-fed indoor wireless network," Invited paper, *International Topical Meeting on Microwave Photonics (MWP) 2006*, October, 2006.

[19] M. Mjeku and N.J. Gomes, "Analysis of RTS/CTS exchange in WLAN over fiber networks," *IEEE Transactions for Wireless Communications*, submitted for publication, 2006.

CHAPTER 2
GENERAL ASPECTS OF ANALOGUE FIBRE-OPTIC LINKS

2.1 Introduction

Chapter 1 briefly discussed radio-over-fibre technology and outlined the reasons for its increasing popularity for providing in-building coverage. It was also mentioned that even though the transmitted system over a radio-over-fibre link may be digitally modulated, RoF transmission is essentially analogue in nature. This chapter therefore discusses the basic components of an analogue fibre-optic link with a view to justifying the use of specific components in the design of low-cost in-building RoF links. Specifically, Sections 2.2–2.4 present discussions on the types of optical fibres, modulation devices and photodetection devices that may be used in analogue fibre-optic links. Finally, Section 2.5 briefly examines two parameters that are utilised to assess the performance of radio-over-fibre links.

2.2 Optical Fibre

An optical fibre is a cylindrical dielectric waveguide with a core made of glass surrounded by a glass cladding. The core has a higher refractive index than the cladding and the light propagates within the fibre using the principle of total internal reflection. Based on the number of propagating modes supported, optical fibres may be classified as single-mode fibres or multimode fibres [1], [2]. A single-mode fibre has a core-diameter between 8 and 12 μm and supports only one mode of propagation. A multimode fibre, with larger core-diameters like 50 μm and 62.5 μm, supports multiple modes.

The different modes in a multimode fibre may be grouped into mode groups and each of the mode groups is associated with a unique propagation delay. The difference in transmission times between the slowest and fastest mode group results in the broadening of a pulse launched into the multimode fibre [3]. This effect is called intermodal dispersion which occurs along with chromatic dispersion. Intermodal dispersion results in lower bandwidths in MMF. It is also known that multimode step-

index fibres exhibit large amounts of intermodal dispersion. A solution to this problem is offered by graded-index fibres where the refractive index profile can be engineered to reduce intermodal dispersion [4], [5].

Chromatic dispersion occurs in both single-mode and multimode fibres due to the finite spectral width of the optical source [1], [2]. The finite spectral width results in the optical source emitting a band of wavelengths (instead of a single wavelength). Propagation delay differences between the spectral components of the launched light arise either due to the material of the fibre or as a result of the waveguiding effects within the fibre [1]. These effects cause a broadening of each transmitted mode.

2.2.1 Classifications of MMF

Intermodal dispersion is characterized by the modal bandwidth specification of the fibre [3]. Additionally, the dispersion or pulse broadening increases with increase in the length of the fibre. Due to this dependence on fibre length, modal bandwidth is also represented as the bandwidth-length product and uses the unit MHz.km. One of the specifications used for MMF is the overfilled-launch (OFL) bandwidth which is measured under the assumption that all the modes of the fibre are equally excited. For example, some varieties of 50 μm-core MMF are specified by an OFL bandwidth of 500 MHz.km at 850 nm and 500 MHz.km at 1300 nm. Similary, some varieties of 62.5 μm core-diameter MMF have OFL bandwidth specifications of: a) 160 MHz.km at 850 nm and 500 MHz.km at 1300 nm, also called the FDDI-grade fibre, and b) 200 MHz.km at 850 nm and 500 MHz.km at 1300 nm.

Multimode fibres are also classified as OM1, OM2 and OM3 fibres by the International Standards Organization (ISO) [6]. The 62.5 μm-core MMF with OFL bandwidth specifications of 200/500 MHz. km (850 nm/1300 nm) are called OM1 fibres while the 50 μm-core MMF with an OFL bandwidth specification of 500/500 MHz. km (850 nm/1300 nm) are called OM2 fibres. A third class of MMF is the recently developed laser-optimized 50 μm-core variety with a bandwidth-length product of 2000 MHz.km[1] at 850 nm, also referred to as OM3 fibres [10].

[1] Note that this is an effective modal bandwidth (EMB) specification (not an OFL specification). EMB characterises the fibre performance for a particular light source based on launch distribution created by the source [7], [8] and [9].

2.2.2 MMF in Short-Haul Communication Links

As multimode fibre suffers from intermodal dispersion, single-mode fibre is preferred for long-distance communication links and metropolitan networks. However, MMF continues to be a popular choice for short-haul communications links (premises links), especially for in-building deployment and campus backbones. The popularity of MMF is mainly due to relaxed alignment tolerances and ease of handling (compared to SMF) which in turn, lowers the cost of connectors, transceiver equipment and installation.

A study conducted in [11] presents details of the current distribution of MMF and SMF in world-wide building backbones. It must be noted that this study was conducted in 2004 and that the most recent results have been extrapolated based on assumptions that can be found in [11]. The results indicate that for in-building backbones, link lengths up to 300 m are the most widely deployed (approximately 89% in 2007). Figure 2.1 depicts the relative shares of different fibre types in such links (i.e., building backbone links up to 300 m) between 2003 and 2007. The fibre types include three varieties of 50 μm-core MMF (400/400 MHz.km, OM2 fibre and OM3 fibre), two varieties of 62.5 μm-core MMF (FDDI grade and OM1 fibre) and SMF. The dominance of MMF over SMF within building backbones is clear from the figure. Another point to note is that even though the share of 50 μm-core MMF is significant, 62.5 μm-core MMF is more widely installed (approximately 45% of the total share in 2007) than 50 μm-core MMF. In particular, the OM1 type of fibre has been the most widespread contributing to approximately 33% of the total share in 2007[2].

[2] Note that 62.5 μm-core MMF have been more popular compared to 50 μm-core MMF because of their larger core-diameters, which, in turn, meant better light gathering capability [12].

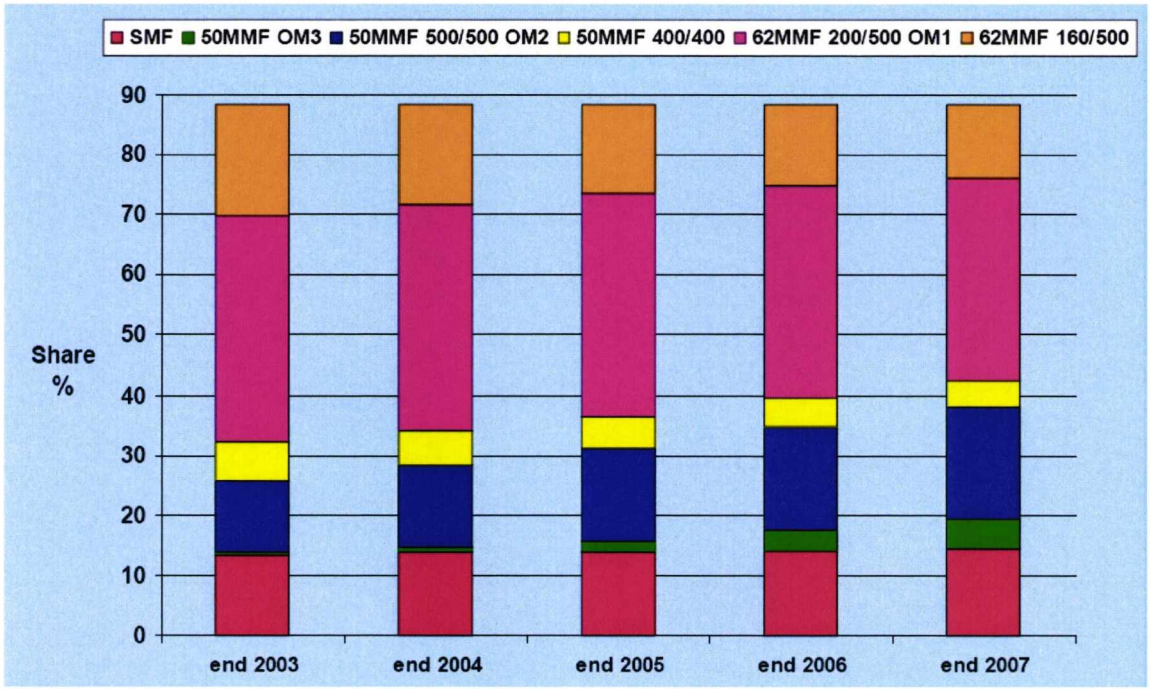

Figure 2.1. Share of building-backbone links up to 300 m in world-wide installed base (reproduced from [11])

2.3 Modulation Device

As discussed in Section 1.1.1, intensity modulation may be performed either using direct modulation or using external modulation. Direct modulation analogue fibre-optic links have been primarily employed in the research presented in this thesis and are, therefore, the focus of this section. Information on the use of external modulators in IMDD links may be found in [13] - [18].

An important consideration in direct modulation links is that the RF signal bandwidth should be within the modulation bandwidth of the laser source being used. One of the most popular lasers that exhibits adequate modulation bandwidth and efficiency, enabling it to be practically implemented in direct modulation links is the semiconductor laser [13]. With reference to semiconductor lasers, stimulated emission in forward-biased p-n junctions was first demonstrated in the early 1960s [19], [20]. The small physical size, high electric power-to-light conversion efficiency and the excellent coupling to optical fibres, makes the semiconductor laser popular in the mass consumer market [21]. Another advantage associated with semiconductor lasers is that they can be modulated at several GHz, unlike the light-emitting diode (LED) for which modulation frequencies are limited up to a few hundred MHz.

Based on the manner of light propagation through the laser structure, semiconductor lasers may be classified as edge-emitting lasers and vertical-cavity surface-emitting lasers. The following sub-sections briefly outline the two different types of semiconductor lasers and also provide a comparison highlighting the advantages of surface-emitting lasers over edge-emitting lasers for use in short-haul fibre-optic links.

2.3.1 Edge-Emitting Lasers

In these types of lasers, the optical cavity is in the plane of the wafer in which they are fabricated so that the light propagates along the active region. Fabry-Perot (FP) and Distributed Feedback (DFB) lasers are examples of edge-emitting lasers that are widely employed in fibre-optic links.

FP lasers are the simplest type of semiconductor lasers. The structure of an FP laser is such that the optical cavity allows multiple lasing modes (longitudinal modes), and the output spectrum, therefore, consists of all the corresponding wavelengths [13]. This poses problems in long distance transmission over optical fibres or in applications involving wavelength division multiplexing techniques [13].

The structure of a DFB laser is essentially a modification of the FP laser structure with the addition of an optical grating. By acting as an internal filter, the periodic optical grating enables the laser to operate at a fixed wavelength (determined by the grating pitch) [2], [13], [22] and [23]. An important feature of a DFB laser is thus single-longitudinal mode operation.

DFB lasers are popular sources for long-distance data communication links due to single mode output and a narrow optical linewidth [24], [25]. Such long-distance links employ single-mode fibre with lengths greater than 20 km and for such lengths, dispersion and loss in optical fibre are of major concern. Therefore, the wavelength of operation is chosen to be either 1300 nm, where chromatic dispersion is zero (for silica fibres), or 1550 nm, where loss is minimum for (silica fibres). For fibre-optic links of lengths between 500 m and 20 km (known as metropolitan fibre-optic links), dispersion, laser wavelength and linewidth requirements are more relaxed thereby allowing the use of FP lasers operating at 1300 nm as optical transmitters [24].

2.3.2 Vertical-Cavity Surface-Emitting Lasers

In vertical-cavity surface-emitting lasers, the optical cavity is perpendicular to the surface of the wafer. The light, therefore, travels vertically within the laser structure and is emitted from the surface of the substrate [13], [23], [24], [26] and [27]. In recent years, short wavelength VCSELs operating in the near infrared region (850 nm) have become extremely popular sources for use in short-haul links. This is mainly due to a number of advantages offered by these VCSELs over edge-emitting lasers [24], [28]. These will be discussed in Section 2.3.3.

The cost advantages offered by VCSELs (compared to edge-emitting lasers) have prompted researchers to investigate the performance of long-wavelength VCSELs (1300 nm ([29]) and 1500 nm ([30], [31])) for use in long-distance analogue communication links [28]. These VCSELs have not seen as rapid a progress as short-wavelength VCSELs mainly due to the difficulty in fabrication, alignment and packaging of these devices [25]. However, recent advances in this area have seen successful utilisation of 1550 nm VCSELs in high-speed fibre-optic links employing either SMF [32] or a combination of SMF and MMF [33], [34].

2.3.3 Advantages of Short Wavelength VCSELs over Edge-Emitting Lasers

This section presents some of the performance and cost advantages offered by short-wavelength VCSELs over DFB and FP lasers. The performance advantages include lower threshold current, single longitudinal-mode operation and better fibre-coupling efficiencies. Easier testing and packaging methods compared to edge-emitting lasers bring down the cost of VCSELs.

Smaller active region volumes in VCSELs result in threshold currents of the order of a few mA compared to tens of mA required for edge-emitting lasers [28]. The short cavity length results in a wide longitudinal mode spacing ensuring single longitudinal mode operation (as in the case of DFB lasers) [13]. However, unlike edge-emitting lasers, VCSELs can additionally operate with multiple transverse modes, depending on the transverse dimensions of the device. VCSELs operating with multiple transverse modes have been reported to provide increased immunity to modal noise when used with multimode fibre [35], [36].

Another advantage offered by VCSELs is that the output beam is circular in cross-section, unlike the elliptical output beam of edge-emitting lasers [13]. A circular cross-section enhances coupling efficiency of the laser light into the optical fibre. Coupling efficiencies as high as 90% into a 50 μm-core graded-index MMF have been reported [37].

In the case of DFB and FP lasers, individual lasers can only be tested once the wafer has been cleaved at the end of the fabrication process. The perpendicular cavity in VCSELs facilitates on-wafer testing which can be carried out simultaneously on a number of VCSEL chips. The serial testing involved in the case of DFB and FP lasers increases their manufacturing costs compared to VCSELs. Additionally, the elliptical output beam of edge-emitting lasers reduces alignment tolerances and introduces the need for a lens element in the final packaged device for better fibre-coupling efficiency [28], [25]. This increases the overall price of the device due to the added costs involved in the packaging. VCSELs, on the other hand, have much lower alignment and packaging costs due to their circular output beam [25].

Short-wavelength VCSELs are therefore the best choice for premises links as they combine the low-cost feature of LEDs and performance features (such as high speed modulation) of edge-emitting lasers. Moreover, in premises links where fibre lengths are less than 500 m, MMF is preferred (as discussed in Section 2.2.2)[3], therefore further bringing down the overall cost. This is the basis for the research presented in this thesis. A review of previous work involving the use of VCSELs operating at 850 nm and MMF in RF fibre-optic links is presented in Chapter 3.

2.4 Photodetector

The final component of an optical link is the photodetector which converts the received optical signal into an electrical signal. The most common semiconductor photodetector used in fibre-optic communications is the p-i-n photodiode [1], [2]. P-i-n photodiodes are characterised by a large intrinsic region which produces a large depletion region; this facilitates maximum absorption of incoming light which results in high responsivity [1], [2].

[3] Note that for high data-rate applications, intermodal dispersion will affect short-range (premises) links. This, in turn, would impose a restriction on the length of the MMF that can be employed in such links.

2.5 Performance Metrics for Radio-over-Fibre Links

Two parameters for assessing the performance of radio-over-fibre links will be discussed in this section: spurious-free dynamic range (SFDR) and error vector magnitude (EVM).

2.5.1 Spurious-Free Dynamic Range

One of the major limitations in analogue fibre-optic links is the distortion caused due to device non-linearities. Signal distortion leads to the creation of new frequencies in the form of harmonics and intermodulation products [13]. The transfer of RF signal power to these new frequencies not only reduces the efficiency of the fibre-optic link but also causes interference with other RF signals in multi-channel systems.

For narrowband systems, the most important form of distortion is the third-order intermodulation distortion [38]. This distortion arises when two or more signals at different frequencies are used to modulate the optical source. For example, using f_1 and f_2 as the input tones, the third-order intermodulation (IM3) products generated at $(2f_1 - f_2)$ and $(2f_2 - f_1)$ lie within the usable bandwidth around the input frequencies and therefore require the most attention. This is illustrated in Figure 2.2; apart from the third-order intermodulation terms at $(2f_1 - f_2)$ and $(2f_2 - f_1)$, all other harmonic frequencies and intermodulation terms can be easily filtered.

For a direct modulation analogue link, the primary source of distortion is the laser itself [39]. A deviation from linearity in the P-I characteristics of the laser results in the generation of harmonics when a single frequency is used to modulate the laser and in the generation of intermodulation products when two or more frequencies are applied to the laser.

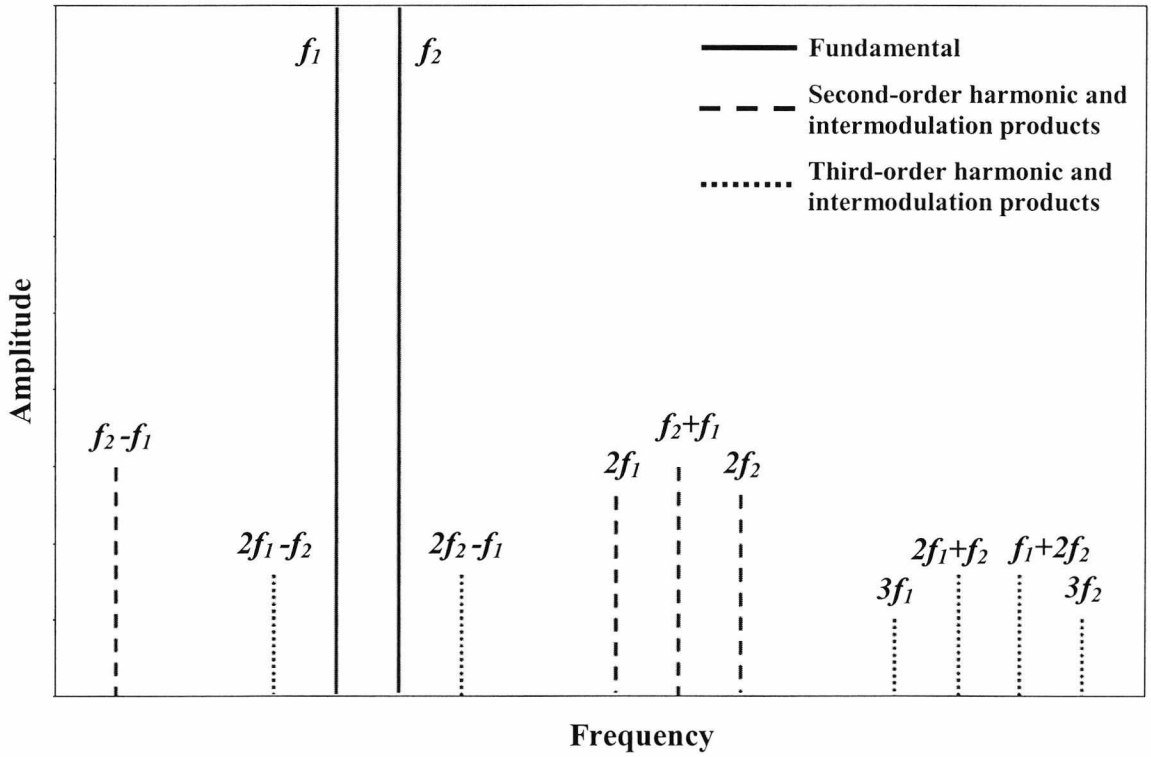

Figure 2.2. Plot illustrating harmonic and intermodulation products (adapted from [13])

A common way to represent the effects of distortion is shown in Figure 2.3, where the output RF signal power (P_{out}) is plotted against the input RF signal power (P_{in}) for one of the fundamental tones and one of the third-order intermodulation products. As the values are plotted in logarithmic units, the slope of the graph represents the exponent of the term being plotted [13]. The output power for the fundamental tone varies linearly (slope = 1) with the input power, while the output power for the IM3 terms varies with the cube of the input power (slope = 3) [13], [38]. Two important parameters may be noted from the graph: the third-order intercept point (IP3) and the SFDR.

The lines for the fundamental tones and for the third-order intermodulation products can be extrapolated to intersect one another. This point of intersection is called the third-order intercept point. The IP3 can be measured either from the input power axis (third-order input intercept point, IIP3) or from the output power axis (third-order output intercept point, OIP3).

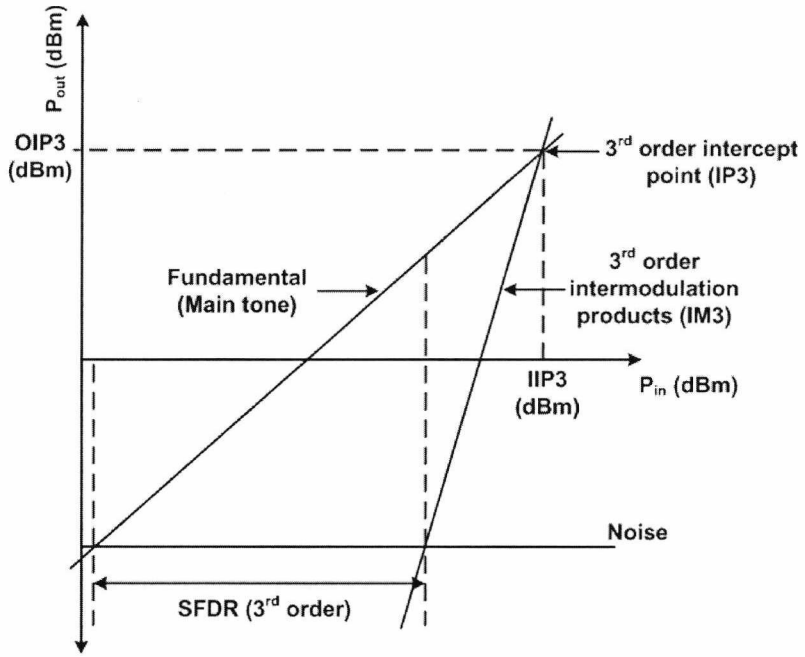

Figure 2.3. Representation of third-order intermodulation distortion effects in analogue fibre-optic links –intercept point and SFDR (adapted from [39])

From Figure 2.3, it is clear that for the range of values between the input power value at which the fundamental tone output power crosses the noise floor, and the input power value where the output power of the intermodulation products crosses the noise floor, the output is completely free of distortion. The difference between these two input power values gives the SFDR for the device/fibre-optic link. As in the case of IP3, SFDR can also be measured from the output power axis. However, the input and output SFDR values are equal unlike the IP3 case where the IIP3 and OIP3 differ by an amount equal to the gain of the device/link. Another important point to note about SFDR is its dependence on the noise floor of the device/link, which in turn makes it dependent on the bandwidth of the device/link (as noise is bandwidth dependent). Like noise, the SFDR values are also quoted in a 1-Hz bandwidth. The SFDR for a given system bandwidth (or for a resolution bandwidth used in a measurement) can then be calculated by scaling the 1-Hz SFDR value using the appropriate scaling law [13]. The scaling law differs for each order of intermodulation products. As an example, to calculate the SFDR value in a resolution bandwidth (or system bandwidth) of Δf Hz from the SFDR value in a 1 Hz bandwidth for the third-order intermodulation, the following equation may be used ([13]):

$$SFDR(\Delta f) = SFDR(1Hz) + \frac{2}{3}10\log\left(\frac{1}{\Delta f}\right) \qquad (2.1)$$

2.5.2 Error Vector Magnitude

Error vector magnitude can be used to measure the transmission performance of digitally modulated RF signals (as in the case of current wireless standards) over an RoF link. Each of the different wireless standards specifies a maximum allowed EVM value and it is important that the measured EVM of the demodulated signal lies below this value. Table 2.1 lists some of the popular wireless standards and a few individual parameters including the maximum allowed EVM limit. EVM measurements are considered to be more useful than the normally-used bit error rate (BER) measurements as they provide information about both amplitude and phase error in the signals [40].

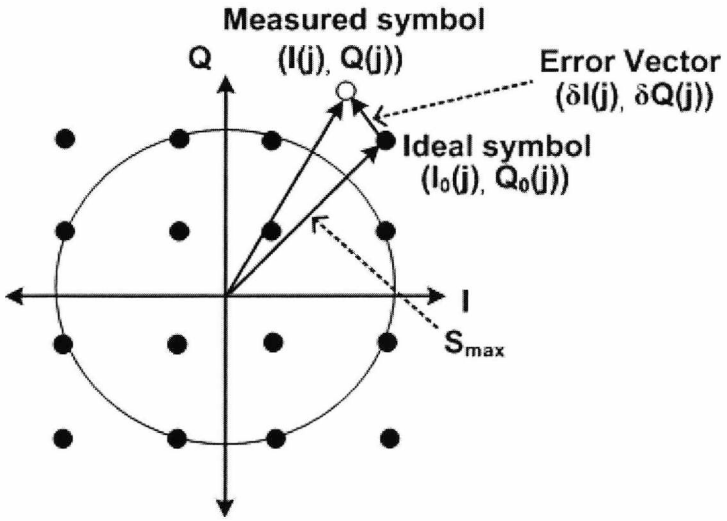

Figure 2.4. Constellation diagram for 16-QAM showing the error vector magnitude for one of the measured symbols (adapted from [41])

EVM may be defined using a constellation diagram as illustrated in Figure 2.4. The 16-QAM constellation diagram contains all the ideal symbols (also called the reference symbols) as well as one of the measured symbols for illustration. At a given time, the distance between the specified ideal constellation point and the measured constellation point gives the error vector (Figure 2.4) and the magnitude of this error vector is called the error vector magnitude. EVM is calculated as a root mean squared value (EVM_{rms}) and is often expressed as a percentage of the peak signal level. The equation for the calculation of EVM_{rms} is given as [42]:

$$EVM_{rms} = \sqrt{\frac{\frac{1}{N}\sum_{j=1}^{N}\left(\delta I^2(j) + \delta Q^2(j)\right)}{S_{\max}^2}} \times 100\% \qquad (2.2)$$

where, N = number of data points for a measurement,

δI, δQ = errors in the received data point,

S_{max} = peak signal level measured as the magnitude of the vector to the outermost constellation point (as shown in Figure 2.4).

2.6 Summary

This chapter has discussed some of the basic components used in fibre-optic links. The attractiveness of utilising 850 nm VCSELs and MMF in premises links (primarily because of the cost advantages offered) has been emphasised. A brief discussion on the use of SFDR and EVM as figures-of-merit for radio-over-fibre links has also been presented. The next chapter focuses on some of the important research that has been conducted in the field of low-cost radio-over-fibre links.

References

[1] J.M. Senior, "*Optical Fiber Communications: Principles and Practice*," Prentice Hall International (UK) Ltd., 1992.

[2] G. Keiser, "*Optical Fiber Communications*," McGraw-Hill Companies, Inc., 2000.

[3] P.F. Kolesar and D.J. Mazzarese, "Understanding multimode bandwidth and differential mode delay measurements and their applications," *Proceedings of the 51st International* Wire and Cable Symposium (IWCS), Lake Buena Vista, FL, pp. 453-460, 2002.

[4] D. Gloge, "Weakly Guiding Fibers," *Applied Optics*, vol. 10, pp. 2252-2258, October 1971.

[5] D. Gloge and E.A.J. Marcatili, "Multimode Theory of Graded-Core Fibers," *Bell System Technical Journal*, Vol. 52, pp. 1563-1578, November 1973.

[6] P. Bell, "Multimode Fiber Standards Overview," *Optical Fiber Communication Conference and Exposition and the National Fiber Optic Engineers Conference (OFC/NFOEC) 2005*, Arnheim, C.A., March 2005.

[7] J.B. Schlager, M.J. Hackert, P. Pepeljugoski and J. Gwinn, "Measurements for enhanced bandwidth performance over 62.5-μm multimode fiber in short-wavelength local area networks," *Journal of Lightwave Technology*, Vol. 21, No. 5, pp. 1276 – 1285, May 2003.

[8] Y.L. Peng and M. Lopez, "50 μm optical fiber Q&A," *White paper*, Corning Incorporated (www.corning.com), May 2006.

[9] D.N. Koon, "The importance of modal bandwidth in Gigabit Ethernet systems," *International Journal of Network Management*, Vol. 11, Issue 3, pp. 139-146, May 2001.

[10] P. Pepeljugoski, S.E. Golowich, A.J. Ritger, P. Kolesar, and A. Risteski, "Modeling and simulation of next-generation multimode fiber links," *Journal of Lightwave Technology*, Vol. 21, No. 5, pp. 1242 – 1255, May 2003.

[11] A. Flatman, "In-premises optical fibre installed base analysis to 2007," *presented to IEEE 802.310GBE over FDDI grade fibre study group*, Orlando, FL, March 2004.

[12] J.E. George, "50 μm or 62.5 μm? Choosing the right multimode fiber for data communications", OFS Optics White Paper, January 2005.

[13] C.H. Cox III, "*Analog Optical Links: Theory and Practice*," Cambridge University Press, 2004.

[14] E.I. Ackerman and C.H. Cox III, "RF-Fiber Optic Link Performance," *IEEE Microwave Magazine*, Vol. 2, Part 4, pp. 50-58, December 2001.

[15] A.J. Seeds, "Microwave Photonics," *IEEE Transactions on Microwave Theory and Techniques*, Vol. 50, No. 3, pp. 877-887, March 2002.

[16] E.L. Wooten, K.M. Kissa, A. Yi-Yan, E.J. Murphy, D.A. Lafaw, P.F. Hallemeier, D. Maack, D.V. Attanasio, D.J. Fritz, G.J. McBrien, and D.E. Bossi, "A Review of Lithium Niobate Modulators for Fiber-Optic Communications Systems," *IEEE Journal of Selected Topics in Quantum Electronics*, Vol. 6, No. 1, pp. 69-82, January/February 2000.

[17] K. Noguchi, O. Mitomi, and H. Miyazawa, "Millimeter-Wave Ti:$LiNbO_3$ Optical Modulators," *Journal of Lightwave Technology*, Vol. 16, No. 4, pp. 615-619, April 1998.

[18] C.H. Cox III, E.I. Ackerman, G.E. Betts, and J.L. Prince, "Limits on the Performance of RF-Over-Fiber Links and Their Impact on Device Design," *IEEE Transactions on Microwave Theory and Techniques*, Vol. 54, No. 2, pp. 906-920, February 2006.

[19] R.N. Hall, G.E. Fenner, J.D. Kingsley, T.J. Soltys, and R.O. Carlson, "Coherent Light Emission from GaAs Junctions," *Physical Review Letters*, Vol. 9, No. 9, pp. 366-368, November 1962.

[20] M.I. Nathan, W.P. Dumke, G. Burns, F.H. Dill, Jr., and G. Lasher, "Stimulated Emission of Radiation from GaAs *p-n* Junctions," *Applied Physics Letters*, Vol. 1, No. 3, pp. 62-64, November 1962.

[21] A. Yariv, *Optical Electronics*, Saunders College Publishing (A Division of Holt, Rinehart and Winston, Inc.), 1991.

[22] H. Kogelnik and C.V. Shank, "Coupled-Wave Theory of Distributed Feedback," *Journal of Applied Physics*, Vol. 43, No. 5, pp. 2327-2335, May 1972.

[23] R.L. Freeman, "*Fiber-Optic Systems for Telecommunications*," John Wiley and Sons, Inc., 2002.

[24] C.W. Wilmsen, H. Temkin, and L.A. Coldren (Editors), "*Vertical-Cavity Surface-Emitting Lasers: Design, Fabrication, Characterization, and Applications*," Cambridge University Press, 1999.

[25] P. Ronco, "Trends in optical transceivers: light sources for premises networks," *2006 BICSI Winter Conference*, Orlando, Florida, January 2006.

[26] K. Iga, F. Koyama, and S. Kinoshita, "Surface Emitting Semiconductor Lasers," *IEEE Journal of Quantum Electronics*, Vol. 24, No. 9, pp. 1845-1855, September 1988.

[27] J.L. Jewell, J.P. Harbison, A. Scherer, Y.H. Lee, and L.T. Florez, "Vertical-Cavity Surface Emitting Lasers: Design, Growth, Fabrication, Characterization," *IEEE Journal of Quantum Electronics*, Vol. 27, No. 6, pp. 1332-1346, June 1991.

[28] N.M. Margalit, S.Z. Zhang, and J.E. Bowers, "Vertical Cavity Lasers for Telecom Applications," *IEEE Communications Magazine*, Vol. 35, Issue 5, pp. 164-170, May 1997.

[29] J. Piprek, M. Mehta, and V. Jayaraman, "Design and optimization of high-performance 1.3 μm VCSELs," *Physics and Simulation of Optoelectronic Devices XII, SPIE Proceedings*, Vol. 5349, pp. 375-384, 2004.

[30] J. Piprek, K. Takiguchi, A. Black, P. Abraham, A. Keating, V. Kaman , S. Zhang, and J.E. Bowers, "Analog Modulation of 1.55-micron Vertical-Cavity Lasers," *Vertical-Cavity Surface-Emitting Lasers III, SPIE Proceedings*, Vol. 3627, pp. 119-127, 1999.

[31] K.A. Black, E.S. Bjorlin, J. Piprek, E.L. Hu, and J.E. Bowers, "Small-signal Frequency Response of Long-Wavelength Vertical-Cavity Lasers," *IEEE Photonics Technology Letters*, Vol. 13, No. 10, pp. 1049-1051, October 2001.

[32] S.Z. Zhang, N.M. Margalit, T.E. Reynolds, and J.E. Bowers, "1.54-μm Vertical-Cavity Surface-Emitting Laser Transmission at 2.5 GB/s," *IEEE Photonics Technology Letters*, Vol. 9, No. 3, pp. 374-376, March 1997.

[33] J.J. Kim, K.H. Kim, M. Lee, H.S. Lee, E. Lee, O. Kwon, J. Roh, and B. Yoo, "2.5-Gb/s Hybrid Single-Mode and Multimode Fiber Transmission of 1.5-μm Wavelength VCSEL," *IEEE Photonics Technology Letters*, Vol. 19, No. 5, pp. 297-299, March 2007.

[34] A. Nkansah, A. Das, N.J. Gomes, and P. Shen, "Multilevel modulated signal transmission over serial single-mode and multimode fiber links using vertical-cavity surface-emitting lasers for millimeter-wave wireless communications," *IEEE Transactions on Microwave Theory and Techniques*, Vol. 55, No. 6, pp. 1219-1228, June 2007.

[35] K.H. Hahn, M.R. Tan, Y.M. Young, and S.Y. Wang, "Large area multitransverse-mode VCSELs for modal noise reduction in multimode fibre systems," *Electronics Letters*, Vol. 29, No. 16, pp. 1482-1483, August 1993.

[36] D.G. Cunningham, M.C. Nowell, P. Dowd, L. Raddatz, and I.H. White, "Modal noise penalties for data communication links employing large area VCSELs," *Electronics Letters*, Vol. 31, No. 25, pp. 2147-2149, December 1995.

[37] J. Heinrich, E. Zeeb, and K.J. Ebeling, "Butt-Coupling efficiency of VCSEL's into multimode fibre," *IEEE Photonics Technology Letters*, Vol. 9, No. 12, pp. 1555-1557, Dec. 1997.

[38] H. Al-Raweshidy and S. Komaki (Editors), *Radio over Fiber Technologies for Mobile Communications Networks*, Artech House, Inc., 2002.

[39] W.S.C. Chang (Editor), *RF Photonic Technology in Optical Fiber Links*, Cambridge University Press, 2002.

[40] M.D. McKinley, K.A. Remley, M. Myslinski, J. S. Kenney, D. Schreurs, and B. Nauwelaers, "EVM Calculation for Broadband Modulated Signals," *64th ARFTG Conference Digest*, Orlando, FL, pp. 45-52, December 2004.

[41] IEEE Standard 802.11a – 1999 (R2003), *Supplement to IEEE Standard for Information technology - Telecommunications and information exchange between systems - Local and metropolitan area networks - Specific requirements Part 11: Wireless LAN Medium Access Control (MAC) and Physical Layer (PHY) specifications: High-speed Physical Layer in the 5 GHz Band*, Reaffirmed June 2003.

[42] *ETSI TR 101 290 version 1.2.1, Digital Video Broadcasting (DVB); Measurement Guidelines for DVB systems*, May 2005.

CHAPTER 3
REVIEW OF PREVIOUS RESEARCH ON RADIO-OVER-FIBRE SYSTEMS

3.1 Introduction

This chapter presents a review of the past research conducted in the field of radio-over-fibre systems. Since this thesis is concerned with the design and implementation of a WLAN RoF system, the discussion focuses primarily on microwave RoF systems, although for completeness, a brief discussion about millimetre-wave RoF systems is also presented.

The chapter begins with a review on the use of 850 nm VCSELs as optical sources in low-cost RoF links. Section 3.3 focuses on past research in the field of RF transmission over multimode fibre. The sub-sections include discussions on the following topics: the different launch techniques that can be used for improving the bandwidth-distance product in MMF, examples of using the passband region in MMF for RF transmission, the use of high-bandwidth MMF in high-performance RoF links, and some examples of experimental demonstrations of wireless system transmission over MMF along with a performance comparison of some of these examples. Section 3.4 presents a discussion on the use of optical transceivers in radio-over-fibre links. Finally, Section 3.5 presents a brief outline of the generation and transportation techniques used in millimetre-wave RoF systems.

3.2 850 nm VCSELs as Sources for Low-Cost RoF Links

In recent years, VCSELs operating at 850 nm have been investigated as potential low-cost sources for analogue fibre-optic communications. In [1], the microwave modulation characteristics of VCSELs operating at 840 nm have been studied. VCSELs with oxide aperture diameters between 2 and 10 μm were used, with single transverse mode operation being achieved only for the 2 μm oxide aperture VCSEL. All VCSELs were found to satisfy the performance requirements for RF fibre-optic links used in fibre-fed microcellular systems and indoor GSM systems. However, the 2 μm single-transverse mode VCSEL displayed an inferior performance compared to the larger

oxide-aperture VCSELs. A single-mode VCSEL (operating at 850 nm) using a new surface relief structure etched on top of a large aperture oxide-confined VCSEL is discussed in [2]. An improvement in the electrical-to-optical conversion efficiency and fibre coupling efficiency is observed. The study also showed that such VCSELs used with multimode fibres performed as well as links using FP lasers and single-mode fibres. In practical analogue fibre-optic systems, VCSELs used as optical sources must be available in packaged form. 850 nm multimode VCSELs mounted on a TO-46 header are demonstrated for the first time as efficient low-cost sources for RF fibre-optic links in [3].

Using a single-transverse mode VCSEL operating at 850 nm as the optical transmitter and a 9/125 μm SMF as the transmission medium, radio-over-fibre transmission has been demonstrated in [4]. The VCSEL used was in a TO-46 package with a pigtail to connect to the SMF. For fibre lengths up to 2 km, the SFDR of the RoF link was measured to be above 90 dB.Hz$^{2/3}$ for the transmission of RF signals at 900 MHz, 1800 MHz and 2.4 GHz.

Short-wavelength VCSELs operating at 980 nm have been shown to provide low distortion performance comparable to Fabry-Perot and DFB lasers in analogue links [5]. SFDR values as high as 104 dB.Hz$^{2/3}$ at 102 MHz and 98 dB.Hz$^{2/3}$ at 1 GHz were reported.

3.3 RF Transmission over Multimode Fibre

It is known that the use of multimode fibre in short-haul links is more attractive as it continues to be deployed in significant quantities inside buildings compared to single-mode fibre. Therefore, in-building RoF systems using distributed antennas to provide coverage and capacity need to make use of this pre-installed legacy MMF. However, modal dispersion in MMF results in limited bandwidth which is affected not only by the length of fibre used but also by the type of laser and the launch condition.

3.3.1 Launch Techniques for Multimode Fibre

Early examples of fibre-optic communication links with data transmission rates of a few hundred Mbps used low-cost LEDs as optical transmitters [6], [7], [8]. With modulation

speeds rapidly increasing to Gbps rates, it became important to use semiconductor lasers as optical sources instead. However, when using laser transmitters, the expected performance in terms of the OFL bandwidth specification of MMF was not achieved in some cases. The reasons for this are stated below.

LEDs with their large numerical aperture and large area essentially flood the MMF core with light. LED launches, therefore, are able to excite many modes supported by the MMF resulting in a bandwidth which closely approximates to the OFL bandwidth specification [9]. Compared to an LED, a laser-based transmitter produces a spectrally narrow and highly collimated beam of light. Due to the collimated beam output, it is difficult to know what modes will be excited and the relative power in each mode when the laser is coupled into an MMF [10]. Moreover, laser sources operating at 1300 nm which are ideal for use with SMF for long-distance communication links are packaged with an SMF pigtail. Using such sources with MMF results in an underfilled launch, with only a few of the lower-order modes being excited. In [11], the effect of underfilled launch condition was studied using 13 MMF samples from different manufacturers. The fibre samples used were all 62.5 μm-core MMFs of different lengths ranging between 300 m and 2200 m. Each fibre sample had its own OFL bandwidth specification. The underfilled launch condition was created by directly connecting the SMF pigtail of a 1300 nm FP laser module to each MMF sample. Under this launch condition, of the 13 fibre samples tested, 8 fibre samples exhibited bandwidth-distance products much lower than the corresponding OFL bandwidth specifications.

The centre-launch technique is a type of underfilled launch in which the beam is launched exactly at the centre of the MMF core allowing the excitation of only the lowest order mode [11], [12]. In [11], the centre launch condition is seen to give the maximum bandwidth-distance product (as shown in the top frame of Figure 3.1) which is much higher than the OFL bandwidth specification for the 500 m long 62.5 μm-core MMF. However, in conventional fibre links, accurate centre launch is difficult to achieve as the connectors used in these links normally have an offset close to 5 μm [13].

An underfilled launch technique considered to increase the bandwidth performance of MMF links using laser transmitters is the offset launch technique [11], [12]. The technique involves introducing light into the MMF from an SMF which is radially offset from the axis of the MMF. In [12], the offset launch technique is discussed for the first

time. In this work, using offset launching, a bandwidth-distance product of 7.5 Gbps.km was achieved which was approximately four times better than the specified OFL bandwidth for the employed 50 μm-core MMF. In [11], the offset launch technique was employed for a 500 m long 62.5 μm-core MMF (OFL bandwidth specification of 480 MHz.km) to investigate the improvement in the fibre's bandwidth performance. Bandwidth-distance products measured for different offset values from the centre of the MMF are depicted in the top frame of Figure 3.1. For an offset of 8 μm, Figure 3.1 (top frame) shows that the measured bandwidth for the MMF is much lower than its OFL bandwidth specification (depicted by the dotted line in the figure). Figure 3.1 (top frame) also shows that only for radial offsets beyond 15 μm was the bandwidth performance of the MMF either equal to or greater than the OFL bandwidth specification. The frequency response of the MMF, shown in the two bottom frames in Figure 3.1, at offsets of 8 µm and 18 µm confirm the bandwidth-distance product values shown in the top frame of Figure 3.1.

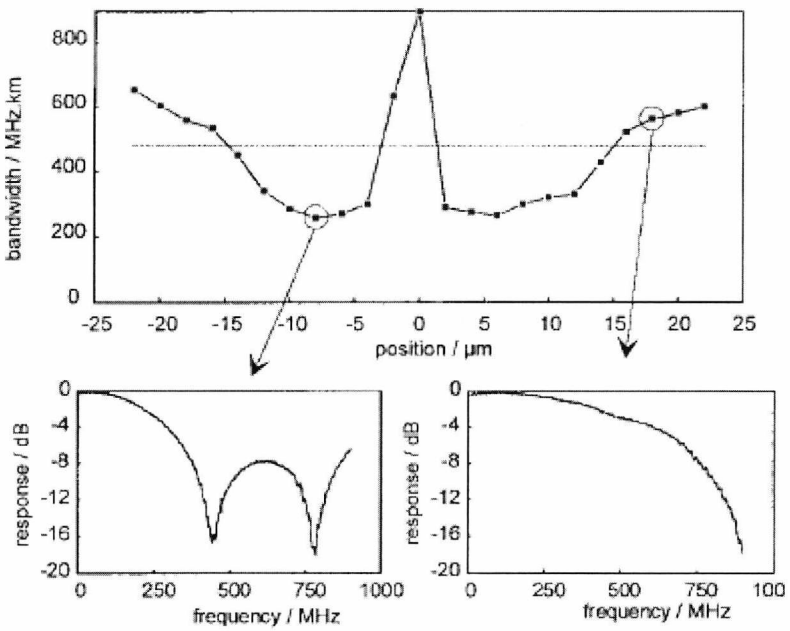

Figure 3.1. Bandwidth-distance product measured for a 500 m long, 62.5 μm-core MMF for different launch offsets from the centre of the fibre (top). The dotted line in the figure denotes the OFL bandwidth for the MMF. Frequency response of the MMF measured at offsets of 8 μm (bottom left) and 18 μm (bottom right) (reproduced from [11])

In practical multimode fibre links (for Gigabit Ethernet), offset launching is provided by using a mode conditioning patchcord (MCP) which is compliant with the IEEE 802.3z Gigabit Ethernet standard [14] - [16]. An MCP is a duplex patchcord and one of its legs consists of a single-mode fibre section connected to a multimode fibre section with a

pre-defined offset. The laser light is launched into the single-mode fibre section of the MCP. An MCP is designed for use in long-wavelength multimode applications of Gigabit Ethernet [15].

A much simpler launch technique was used for the work described in this thesis. The large area, multi-transverse mode 850 nm VCSEL manufactured by ULM Photonics provides an annular farfield emission pattern (doughnut-shaped)[1]. Connecting this VCSEL directly to an MMF will not launch light close to the centre of the MMF, resulting in the excitation of only the higher-order mode groups.

3.3.2 Transmission in the Passband Region of Multimode Fibre

Even though the offset launch technique (discussed in sub-section 3.3.1) has been shown to increase the bandwidth performance of MMF, its use has primarily been demonstrated for baseband transmission as shown in [12]. For transmission of higher frequencies, it has been established that passband regions exist beyond the 3-dB bandwidth of the MMF [17], [18]. This is illustrated in Figure 3.2, which shows the frequency response of a 62.5 μm-core MMF of length 1 km (using an 850 nm VCSEL) used for measurements in [17]. The response shows peaks in amplitude at certain frequencies beyond the -3 dB frequency of 180 MHz, thus creating passband regions. Using this concept, transmission of 200 Mbps sub-carrier multiplexed channels over the above fibre at RF frequencies as high as 3.8 GHz has been demonstrated in [17].

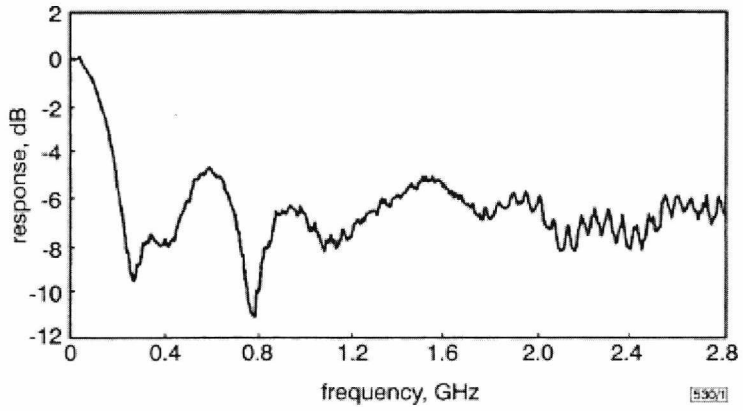

Figure 3.2. Frequency response of a 62.5 μm-core MMF of length 1 km using an 850 nm VCSEL. Note the relatively flat response at high frequencies, approximately 7 dB below the response at low frequencies (reproduced from [17])

[1] Private communication with ULM Photonics, 2005.

A comparison between baseband and passband modulation techniques has been performed in [18]. An 850 nm VCSEL and a 500 m long 62.5 μm-core MMF with a bandwidth-distance product of 190 MHz.km was used for the measurements. Transmission of a single 1.25 Gbps channel using digital baseband modulation and of two binary phase shift keyed (BPSK) channels at 625 Mbps using SCM were demonstrated separately. For the 1.25 Gbps transmission, the eye-diagram in Figure 3.3a shows a closed eye indicating that the transmission over the 500 m MMF was not successful. For the two-channel multiplexed transmission at sub-carrier frequencies of 1.0 GHz and 3.0 GHz, the open eyes in the eye-diagrams (Figure 3.3b) indicate successful transmission. The sub-carrier frequencies were chosen based on the relatively flat frequency response of the MMF observed at these frequencies. A few other examples of higher frequency RF transmission over MMF using the SCM technique may be found in [19]-[22].

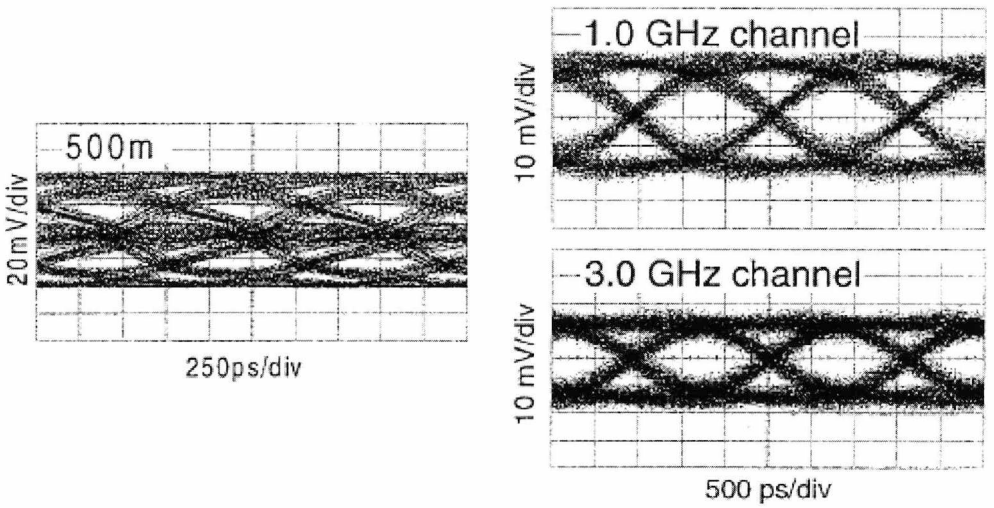

Figure 3.3. Eye-diagrams for the transmission of a) single 1.25 Gbps baseband channel and b) two multiplexed BPSK 625 Mbps channels at sub-carrier frequencies of 1.0 GHz (top) and 3.0 GHz (bottom) over a 62.5 μm-core diameter MMF of length 500 m (reproduced from [18])

Transmission of 1 Gbps (BPSK) data, using a sub-carrier at 2.5 GHz, over a 62.5 μm-core MMF of length 1 km was successfully demonstrated in [19]. A further improvement in data rate is shown in [20], where the SCM transmission of 2.5 Gbps BPSK data at 5.1 GHz is demonstrated over 300 m long 62.5 μm-core MMF with a bandwidth-distance product of 300 MHz.km. More recently, much higher data transmission capacities over standard MMF have been demonstrated in [21] and [22]. Transmission of 40 dense wavelength division multiplexed channels using 2.55 Gb/s

subcarrier signals (total capacity of 204 Gb/s) over standard 50 μm-core MMF of length 3 km has been successfully demonstrated in [21]. The authors in [22] have also demonstrated transmission of data capacity greater than 200 Gb/s (40 channels at 5.1 Gb/s each) over both 62.5 μm-core MMF (worst-case fibre) of length 300 m and 50 μm-core MMF of length 3 km, with the combined use of SCM and dense wavelength-division multiplexing. Initial results also indicate the possibility of 1 Tb/s data transmission capacity over 3 km of 50 μm-core MMF provided that the wavelength division multiplexed channel spacing is scaled appropriately.

In order to utilize MMF passband transmission capabilities in DAS applications, it is important to investigate the possibility of the transmission of RF signals modulated using complex digital modulation schemes (as in the case of 2G and 3G wireless systems) over MMF. In this respect, one of the first demonstrations of RF signal transmission over MMF for DAS applications is discussed in [23]. To test the fibre performance, EVM measurements for the transmission of 32-QAM signals at 10 Mbps were carried out using a DFB laser and an FP laser (both operating at 1300 nm and with SMF pigtails). Separate transmissions over a reference coaxial cable, a short SMF patchcord, a 1.1 km long SMF reel and a 50 μm-core MMF of length 1 km were performed. Two RF transmission frequencies were selected: 1.5 GHz, as the 1 km long MMF recorded the maximum electrical loss (of 7 dB) at this frequency (worst-case scenario), and 2.0 GHz to represent a 3G system. For the transmission of the 1.5 GHz signal over the 1 km MMF, EVM values of 1.2% for the DFB laser and 3.3% for the FP laser were recorded. Slightly better EVM values of 0.7% for the DFB laser and 1.8% for the FP laser were recorded for the transmission of the 2.0 GHz signal over the 1 km long MMF. For both frequencies, however, these values were only slightly higher than the EVM values recorded for the coaxial cable reference, the SMF patchcord and the 1.1 km SMF reel. The constellation and eye-diagrams for the 32-QAM transmission at 2 GHz over the coaxial reference cable and the 1 km MMF using the DFB source are shown in Figure 3.4.

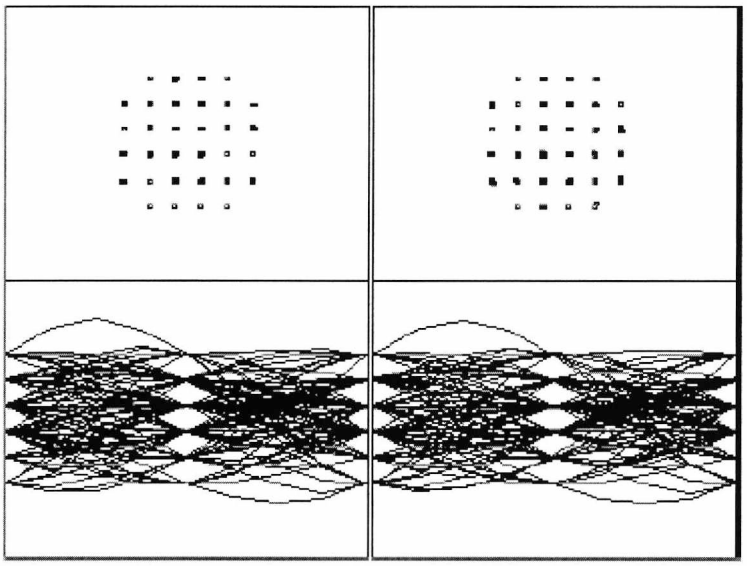

Figure 3.4. Constellation (top) and eye-diagrams (bottom) for the transmission of 32 QAM modulated signals at 2 GHz over a reference coaxial cable (left) and over a 50 μm-core MMF of length 1 km (right) using a DFB optical source operating at 1300 nm. (reproduced from) [23]

Further investigation in [24] characterised the RF transmission performance of two 62.5 μm-core MMF samples of length 1.1 km and a 50 μm-core MMF sample of length 1 km. The lasers used were 1300 nm DFB and FP lasers with SMF pigtails. The fibre response measured using an MMF pigtailed photodetector was seen to be very stable over a measurement period of 30 minutes, with a maximum detected power variation of 1 dB for the DFB laser and 0.5 dB for the FP laser. For a 10 Mbps 32-QAM transmission at 2.0 GHz, EVM values of 0.5% were measured for all three fibre reels when used with a DFB laser. With the FP laser, the EVM values varied between 1% and 1.5% for the different fibres.

The maximum EVM limit for 32-QAM transmission according to [23] and [24] is 17% and all EVM values measured were much lower than this limit. These results, therefore, show that RF transmission over MMF is possible at frequencies beyond the 3 dB bandwidth of the MMF with negligible penalty compared to using SMF, even when using the complex 32-QAM modulation scheme. This further suggests that the use of pre-installed MMF in building backbones is practical for fibre-based distributed antenna systems. Using pre-installed MMF obviously results in a reduction in the overall costs of the RoF system. Moreover, due to better alignment tolerances and its ease of handling (compared to SMF), MMF can be easily used with low-cost lasers like

VCSELs at 850 nm and even edge-emitting lasers without their expensive fibre-alignment packaging, consequently further bringing down system costs.

3.3.3 Use of High-Bandwidth MMF for RF Signal Transmission

Laser-optimised 50 μm-core MMF was developed mainly for Gigabit Ethernet applications [25]. This MMF has a high bandwidth-distance product of 2000 MHz.km and is specifically designed for efficient use with 850 nm VCSELs. This section discusses the research that has been carried out in recent years to characterise the RF transmission performance of this high-bandwidth (or OM3) multimode fibre.

Link characterisation measurements, especially the enhancement in the link SFDR, have been discussed in [26] and [27]. In [26], SFDR values as high as 100 dB.Hz$^{2/3}$ were obtained at 6 GHz using an 850 nm multimode VCSEL and the laser-optimised MMF. For all frequencies measured (1–8 GHz), the SFDR values obtained were always greater than 94 dB.Hz$^{2/3}$, even in the case of the longest fibre length of 300 m.

A similar investigation, comparing the performance of standard (400 MHz.km) and high-bandwidth (2000 MHz.km) MMF, at an operating wavelength of 840 nm has been carried out in [27]. For a multimode VCSEL biased at 5 mA and modulated at 2 GHz, as the fibre length was increased from 100 m to 500 m, SFDR values ranging between 104 dB.Hz$^{2/3}$ and 102 dB.Hz$^{2/3}$ were recorded for the high-bandwidth fibre. Corresponding SFDR values between 103 dB.Hz$^{2/3}$ and 99 dB.Hz$^{2/3}$ were recorded for the standard fibre. Additionally, a study of the influence of the VCSEL-fibre misalignment on the link performance showed that the optimised high-bandwidth MMF was more tolerant to the lateral offset allowing a misalignment as high as +/- 12 μm with an SFDR variation of only 3 dB.

RoF links using directly modulated DFB laser diodes and MMF and supporting RF frequency transmission up to 20 GHz are demonstrated in [28]. Two types of MMF were used for the measurements: a low-bandwidth MMF (62.5/125 μm) with an OFL bandwidth specification of 595 MHz.km, and a high-bandwidth MMF (50/125 μm typically designed for laser launches) with a bandwidth-distance specification of 2000 MHz.km. For both the MMFs, the passband region was measured to extend up to RF frequencies as high as 25 GHz, with the limit being imposed by the measurement

equipment. Uncooled DFB laser diodes operating at 1300 nm (discussed in [29]) were used as optical transmitters. Transmission of a 10 Mbps QPSK modulated signal and a 54 Mbps OFDM signal using 64-QAM modulation was demonstrated over three separate fibres for an RF frequency range of 1–25 GHz: an SMF of length 2 m, a low-bandwidth MMF of length 575 m and high-bandwidth MMF of length 1000 m. For the 2 m SMF, EVM values less than 2% for the QPSK signal and 4.6% for the 64-QAM OFDM signal were recorded for RF frequencies up to 20 GHz. Inserting the 575 m MMF results in an excess EVM of only 1% up to a frequency of 20 GHz for both the QPSK and OFDM 64-QAM signals compared to the 2 m SMF link. With the 1000 m MMF, the maximum excess EVM compared to the SMF link was recorded to be 1.08% for both modulation schemes over the 1–20 GHz frequency range.

3.3.4 Experimental Demonstrations of Wireless System Transmission over MMF

For DAS applications, the distribution of wireless systems such as GSM, UMTS and WLAN (IEEE 802.11b and IEEE 802.11g) over multimode fibre has been investigated in recent years. Table 3.1 lists some of the parameters of the wireless systems discussed in this section. As most of the examples discussed here use EVM (discussed in Section 2.5.2, Chapter 2) for characterising system transmission, Table 3.1 also includes the maximum allowed EVM values for the transmitted wireless standard.

TABLE 3.1 SYSTEM PARAMETERS OF THE DIFFERENT WIRELESS STANDARDS

Systems	Frequency (GHz)	Modulation format	Data rate	Maximum rms EVM (%)
GSM900	0.9	GMSK	270.833 ksym/s	7.0
GSM1800	1.8	GMSK	270.833 ksym/s	7.0
DPRS	1.88	64 QAM	1.152 Msym/s	
UMTS	2.0	QPSK	3.84 Msym/s	12.5
IEEE 802.11a	5.0	64 QAM (OFDM)	54 Mbit/s	5.6
IEEE 802.11b	2.4	CCK (DSSS)	11 Mbit/s	35
IEEE 802.11g	2.4	64 QAM (OFDM)	54 Mbit/s	5.6

Individual transmission of GSM 1800 (generated using a GSM 1800 base station, *Ericsson RBS 2202*) and UMTS signals at 2.0 GHz (emulated using an *Agilent* Vector Signal Generator (VSG) *ESG-DP*) using an 850 nm VCSEL and 50/125 μm MMF of

length 600 m has been shown in [30]. BER measurements for the GSM signal and EVM measurements for the UMTS transmission were carried out at the end of the optical link. For both signal transmissions, no penalty was observed for transmission over the fibre compared to a coaxial back-to-back link.

A recent study [31] demonstrated the transmission of emulated UMTS signals using a high-performance single-mode VCSEL [2] operating at 850 nm. The optical fibre used for the transmission was a high-bandwidth (2000 MHz.km) 50 μm-core diameter MMF of length 500 m. For RF input power values of up to more than -5 dBm, EVM values measured at the output of the optical link were below the required maximum limit of 12.5 % (Table 3.1).

The authors in [32] have analysed the transmission performance of WLAN signals over a low-cost VCSEL-MMF-based RoF link. IEEE 802.11g (2.4 GHz) using OFDM modulation with 64-QAM at a data rate of 54 Mbps and IEEE 802.11b using DSSS with DPSK modulation at 11 Mbps were emulated using an *Agilent E4438C* VSG. For IEEE 802.11b, the EVM values measured are much lower than the maximum limit (of 35% as shown in Table 3.1), even for an MMF of length 1.5 km. As with the IEEE 802.11b, the IEEE 802.11g measurements also satisfy the EVM requirements up to an MMF transmission length of 1.5 km.

In [33], a radio-over-multimode fibre link (using a 1550 nm single-mode VCSEL) based on an external light-injection technique is demonstrated. The wavelength of an external VCSEL is tuned relative to the wavelength of the VCSEL modulated by a 2.4 GHz signal. An optimum detuning (0.14 nm in this case) between the two laser wavelengths results in the modulated VCSEL being stably injection-locked. The external injection-locking technique is shown to improve the frequency response, IP3 and output optical power of the injection-locked laser. Based on these improvements, the transmission of 11 Mbps IEEE 802.11b signals at 2.4 GHz was successfully demonstrated with the measured EVM and BER performances indicating good signal quality up to MMF lengths of 2 km.

EVM measurements for individual transmission of different wireless systems over high bandwidth 50 μm-core MMF (1550 MHz.km and 2000 MHz.km) and standard 50 μm-core and 62.5 μm-core MMF (500 MHz.km), have been carried out using 850 nm

VCSELs in [34], [35]. In both studies, EVM values increased with increase in optical fibre length. In [34], the wireless systems transmitted include emulated GSM (900 MHz), UMTS (2 GHz), DPRS (1.88 GHz) and WLAN (IEEE 802.11a at 5 GHz, IEEE 802.11b and IEEE 802.11g at 2.4 GHz). The EVM measurements for these systems were carried out only for the downlink optical path i.e., wireless path transmission was not evaluated. EVM values were below the required maximum limits for all system transmissions over the 50 μm-core standard and high-bandwidth MMF of lengths up to 300 m. IEEE 802.11a was, however, an exception allowing only a 100 m fibre link before the signal quality degraded. Using 62.5μm-core standard MMF, link lengths below 300 m gave acceptable EVM values for signal transmissions below 2 GHz. In [35], transmission of emulated GSM (900 MHz), EDGE (900 MHz) and UMTS (2 GHz) wireless systems was studied. Note that despite using the same frequency (900 MHz), GSM and EDGE utilise different modulation schemes: GSM uses GMSK modulation while EDGE uses 8-PSK modulation. Even though EVM values were recorded for the combined optical and wireless downlink path, the wireless distance between the transmit and receive antennas has not been specified. The results indicated that for all the transmitted wireless systems, EVM values were much below the required maximum limits over optical link lengths of up to 600 m for the 50 μm-core MMF (both standard and high-bandwidth) and up to 300 m for the standard 62.5 μm-core MMF.

Research carried out in [36] investigates the EVM performance of a low-cost MMF-based DAS capable of simultaneously transporting multiple standards in the 1.5–6.4 GHz frequency range. Uncooled DFB laser diodes operating at 1300 nm [29] were used as the optical transmitters and 62.5 μm-core MMF (bandwidth of 500 MHz.km at 1300 nm) was used as the optical link. The DAS was analysed for the transmission of IEEE 802.11 a/b/g signals, with the optimum bias current and input RF power to the laser being carefully chosen based on EVM measurements. For the transmission of a 54 Mbps 64-QAM OFDM signal, EVM values less than 1% were obtained for the 1.5–6.4 GHz frequency range. For the simultaneous transmission of IEEE 802.11a and IEEE 802.11g signals (generated using two different access points), MMF lengths up to 1375 m were possible before EVM values reached the maximum allowed limit of 5.6% (Table 3.1).

Another example of a low-cost distributed antenna system for the transmission of WLAN signals, in particular, IEEE 802.11b signals, is presented in [37]. For this

WLAN demonstrator as well, uncooled DFB lasers operating at 1300 nm [29] and OM1 MMF (62.5 μm-core MMF with a bandwidth specification of 500 MHz.km at 1300 nm) were used. In addition to reporting the EVM performance of the link for different fibre lengths, the authors also demonstrate the transmission of 'real' video signals over the designed link. For an MMF length of 1 km, EVM values of 1.21% and 2.19% were measured for the 2.41 GHz IEEE 802.11b signal (at 11 Mbps) and 5.35 GHz IEEE 802.11a signal (at 54 Mbps) respectively. These values are much below the maximum allowed EVM values of 35% and 5.6% for the IEEE 802.11b and IEEE 802.11a standards respectively (shown in Table 3.1). For the transmission of video signals over the IEEE 802.11b WLAN demonstrator, an average transmission rate exceeding 1 Mbps was recorded.

A very recent demonstration of wireless system transmission is discussed in [38]. In this work, the bi-directional transmission of UMTS (FDD) and WLAN systems over a radio-over-fibre link has been demonstrated. Two separate versions of the link were designed: one employing SMF of length less than 5 km and another employing MMF of length less than 300 m. For the MMF-based RoF link, high-quality FP lasers operating at 1310 nm were used at the central unit and two VCSELs operating at 840 nm and 810 nm were used at the RAU to avoid the crosstalk between the received UMTS and WLAN signals. For the downlink simultaneous system (UMTS and WLAN) transmission, EVM values were measured for the back-to-back link (without MMF) as well as after transmission over the MMF. For the UMTS signal (using 16-QAM modulation), EVM values of 5.58% and 6.48% were recorded for the back-to-back and MMF transmissions respectively. The corresponding values for the WLAN signal (using 64-QAM modulation) were 2.24% and 4.06%. Both systems satisfied the maximum EVM specifications (12.5% for UMTS and 5.6% for WLAN, as shown in Table 3.1) even after transmission over MMF. For the uplink transmission, the dynamic range was measured to be 26 dB for the UMTS signal. The dynamic range measurement results for the WLAN signal were, however, not specified.

3.3.4.1 Performance Comparison of Wireless System Transmission over RoF Links

In order to provide a context to the research carried out in the thesis, this section presents a comparison of the different wireless system transmissions over RoF links that have been demonstrated previously (brief details of the experiments have already been

discussed in Section 3.3.4). The microwave RoF systems that are being compared are listed in Table 3.2 and have been confined to wireless systems up to 5 GHz.

The various experiments have been conducted for wireless system transmission over all three types of MMF: OM1 ([34]-[37]), OM2 ([30], [34], [35]) and OM3 ([31], [32], [34], [35]). Note that as the measurements in all these examples have been carried out for available lengths of MMF (rather than maximum achievable lengths), a direct comparison of performance in terms of fibre type is not possible.

Almost all the example demonstrations achieve error-free transmission for MMF lengths of at least 300 m (as mentioned in Section 2.2.2, for in-building backbones, MMF link lengths up to 300 m are the most widely deployed). The exception to this is the EVM result obtained in [34] for the transmission of IEEE 802.11a signals over MMF. The EVM value of 11.5% quoted was recorded for transmission over 62.5 μm-core MMF of length 300 m. This well exceeds the maximum EVM specification of 5.6%. This result, however, seems specific to the measurements carried out in [34]. For the other IEEE 802.11a transmissions over standard 62.5 μm-core MMF ([36] and [37]), error-free transmission has been achieved for MMFs of lengths up to 1375 m. It should be noted, however, that a direct comparison between these results is difficult as they use different laser and RF sources. For example, the laser source used in [34] is an 850 nm VCSEL while [36] and [37] use 1300 nm uncooled DFB lasers. Additionally, the IEEE 802.11a signal in [34] is emulated using a signal generator while a WLAN access point is used in [36] for signal generation.

For the majority of the examples listed in Table 3.2 ([30]-[36] and [38]), wireless system transmission over only the optical link has been characterised. The exception is the demonstration carried out in [37] where video transmission over the complete optical and wireless paths has been shown. However, the wireless distance over which such a transmission was carried out has not been stated. Undoubtedly, optical path characterisation (e.g. in terms of EVM measurements) is important as it gives an idea about the maximum length of fibre that may be used for antenna remoting without degrading signal quality. However, as multipath signal fading in the wireless path further degrades the signal, it is important to measure signal quality at the mobile receiver (after transmission over the wireless path). Characterising the wireless path transmission performance has an impact on the complete RoF link performance and also

helps in measuring the wireless coverage of the RoF system. In the work presented in this thesis, the performance of both the optical and wireless paths of an RoF link transmitting different wireless systems (particularly, WLAN) has been characterised using EVM and throughput measurements. Furthermore, most of the examples presented in Table 3.1 are for signal transmission in one direction (downlink) [30]-[36]. Bi-directional operation of the RoF link has been demonstrated only in [37] and [38]. This is another important aspect of the research presented in the thesis, where not only has bi-directional transmission of WLAN signals been demonstrated, but this has been done for a link design optimised using a detailed link budget analysis.

TABLE 3.2 COMPARISON OF PREVIOUS RESEARCH ON WIRELESS SYSTEM TRANSMISSIONS OVER RoF LINKS

Wireless system	RF source used	Multimode fibre used		Laser source used	Link performance	rms EVM (%)
		Type	Length (m)			
GSM 1800	GSM base station (*Ericsson RBS 2202*)	*Corning® Infinicor® 600* 50/125 μm MMF	600	850 nm VCSEL	Downlink optical path only	N/A
UMTS [30]	*Agilent* VSG *ESG-DP*					Approx. 3.6
UMTS [31]	*Agilent* VSG *E4436B*	High-bandwidth 50/125 μm MMF (2000 MHz.km)	500	850 nm VCSEL	Downlink optical path only	Approx. < 4
IEEE 802.11a 54 Mbps	*Agilent* VSG *E4438C*	High-bandwidth 50/125 μm MMF (2000 MHz.km)	1000	850 nm VCSEL	Downlink optical path only	Approx. 5.6
IEEE 802.11b 11 Mbps			1500			Approx. 3.3
IEEE 802.11g rate not specified [32]						Approx. 4
IEEE 802.11b 11 Mbps [33]	Signal generator	50/125 μm MMF (bandwidth not specified)	2000	1550 nm VCSEL	Downlink optical path only	Approx. 3.5

Wireless system	RF source used	Multimode fibre used		Laser source used	Link performance	rms EVM (%)
		Type	Length (m)			
GSM 900	*Agilent* VSG *E4438C*	*Corning® Infinicor® Sxi* 50/125 μm MMF *Corning® Infinicor® Sx+* 50/125 μm MMF *Corning® Infinicor® Sx* standard 50/125 μm MMF *Corning® Infinicor® Sx* standard 62.5/125 μm MMF	100 300 600 (600 m N/A for 62.5 μm MMF)	850 nm VCSEL	Downlink optical path only	Approx. < 1.2
UMTS						Approx. < 8
DPRS (64 QAM)						Approx. < 1
IEEE 802.11g 54 Mbps						Approx. < 8
IEEE 802.11a 54 Mbps [34][2]						Approx. < 11.5
GSM 900	*WinQSim* PC software + *Rhode & Schwarz* modulator (*AMIQ02*) + *Rhode & Schwarz* vector generator (*SMIQ03*)	*Corning® Infinicor® Sxi* 50/125 μm MMF *Corning® Infinicor® Sx+* 50/125 μm MMF *Corning® Infinicor® Sx* standard 50/125 μm MMF *Corning® Infinicor® Sx* standard 62.5/125 μm MMF	100 300 600 (600 m N/A for 62.5 μm MMF)	850 nm VCSEL	Downlink optical path only	Approx. < 3.5
EDGE						Approx. < 3
UMTS [35][2]						Approx. < 5.5
IEEE 802.11a with IEEE 802.11g present	WLAN access point	Standard 62.5/125 μm MMF (500 MHz.km)	Up to 1375	1300 nm uncooled DFB laser diodes	Downlink optical path only	Approx. 5.5
IEEE 802.11a without IEEE 802.11g present [36]						Approx. 5.6

[2] Note that each of the wireless systems were transmitted over 100 m, 300 m and 600 m for all the types of MMF specified. Also, the rms EVM values listed here refer to the maximum of all the rms values measured using the different MMFs for the corresponding wireless system transmission.

Wireless system	RF source used	Multimode fibre used		Laser source used	Link performance	rms EVM (%)
		Type	Length (m)			
IEEE 802.11b	EVM measurements: RF source not specified	Standard 62.5/125 μm MMF (500 MHz.km)	Up to 1000	1300 nm uncooled DFB laser diodes	EVM measured at the end of optical link only	1.21
IEEE 802.11a [37]	Video signal transmission: IEEE 802.11b access point				Video transmission demonstrated but wireless distance not specified	2.19
UMTS	*Agilent* VSG *E4438C*	Standard MMF (360 MHz.km)	300	CU source: 1310 nm FP laser	Bi-directional transmission demonstrated but only optical path characterised	6.48
IEEE 802.11g [38]	WLAN access point			RAU source: 810 nm VCSEL, 840 nm VCSEL		4.06

As the work presented in the thesis focuses on WLAN (2.4 GHz) signal transmission over RoF links, Figure 3.5 presents a comparison of the EVM performances for IEEE 802.11b and IEEE 802.11g signal transmissions carried out by various research groups for different lengths of MMF. The maximum MMF length over which IEEE 802.11b transmission has been demonstrated is 2 km (in [33]), while that for IEEE 802.11g is 1.5 km (in [32]). The EVM values reported in [34], indicate that IEEE 802.11g signals may be transmitted over longer lengths of 50 μm-core MMF compared to 62.5 μm-core MMF. The results in [34] also show that the EVM value (8%) for the transmission of IEEE 802.11g signals over standard 62.5 μm-core MMF of length 300 m is higher than the maximum specification of 5.6%. In [38], however, successful IEEE 802.11g transmission is achieved over standard MMF (bandwidth-distance product 360 MHz.km, as shown in Table 3.2) with a measured rms EVM of 4%. A direct comparison of the two performances is not possible as each uses different optical sources and possibly different RF transmission powers. As mentioned earlier, all the measurements presented in this section have been carried out for WLAN signal transmission only over the optical path. Furthermore, these examples only state the physical WLAN data rates transmitted over the RoF link (i.e., 11 Mbps for IEEE 802.11b and 54 Mbps for IEEE 802.11g and IEEE 802.11a) without any indication of the actual data throughput achieved. In this research, therefore, WLAN signal

transmission performance over the designed RoF link has also been characterised by means of throughput measurements. Additionally, the throughput performance has been investigated in terms of the IEEE 802.11 MAC protocol.

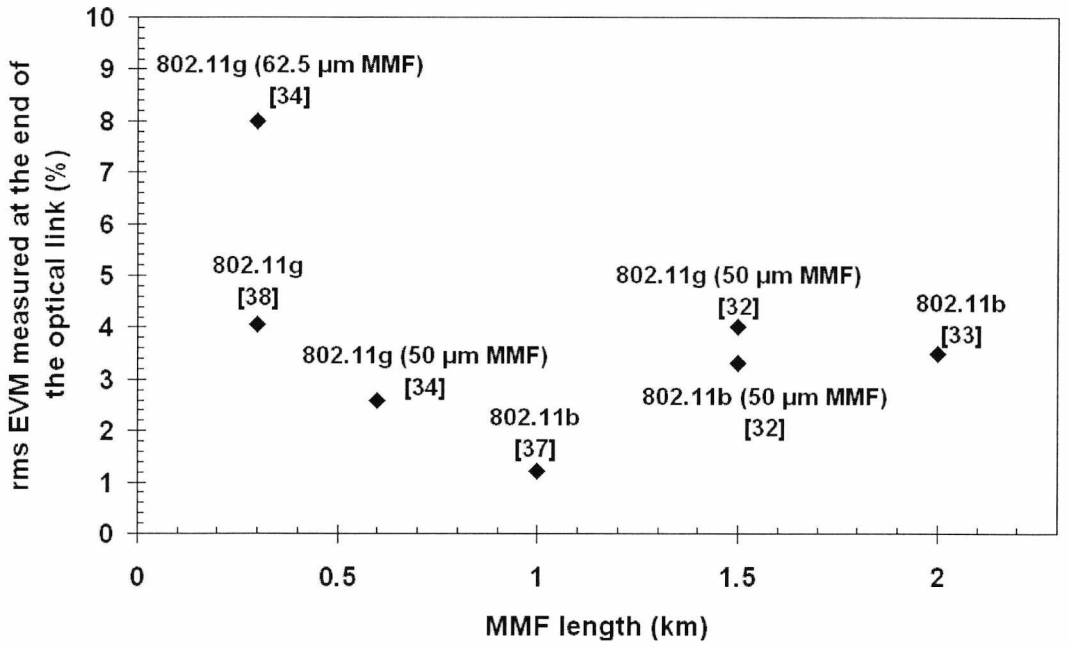

Figure 3.5. Comparison of the rms EVM performance for WLAN (2.4 GHz) signal transmission over different lengths of MMF conducted by various research groups (Note: maximum data rates for IEEE 802.11b = 11 Mbps and for IEEE 802.11g = 54 Mbps)

3.4 Use of Optical Transceivers

In an attempt to further simplify the design of remote antenna units and thereby reduce the overall system cost, the use of electroabsorption modulators (EAM) at the RAU has been investigated over the years [39] – [44]. Utilising an EAM as a modulator at the RAU, results in there being no laser source at the RAU which would reduce power consumption and simplify bias control [39], [40]. The central unit would then have a laser (the one that will be modulated) for the downlink path and a continuous-wave (CW) laser source for the EAM. The advantage of such an arrangement is that the laser source is now in a more controlled environment with easier access to power supply outlets. Another advantage of using an EAM at the RAU is that both the modulation and detection functions can be performed in one device. Brief descriptions of the operation of an EAM transceiver can be found in [39] and [44].

In [40], the use of an electroabsorption device as a simultaneous detector and modulator was demonstrated for the first time in a full-duplex bi-directional analogue fibre-optic link. The full-duplex operation of the link (at an operating wavelength of 1.55 μm) was achieved by using a frequency division multiplexed arrangement. The measured RF insertion loss for the EAM link (approximately 42 dB at a reverse bias of -1.4 V) was comparable to the loss measured for a commercial laser-detector module (approximately 39 dB) used by the authors. The intermodulation distortion between the downlink and uplink signals during full-duplex operation was measured to be at an acceptable level demonstrating the feasibility of such an arrangement.

In [41], a wideband, full-duplex, bi-directional analogue fibre-optic link using an electroabsorption modulator transceiver at the RAU has been demonstrated with a data transmission rate of up to 120 Mbps over 25 km of optical fibre. BER measurements were carried out for the simultaneous transmission of two 120 Mbps QPSK modem signals (one upconverted to 1.347 GHz and the other centered at 140 MHz) over the downlink path. The results showed that, compared to the back-to-back electrical measurement for the modem, no power penalty due to the use of an EAM was observed in the link.

A further reduction in installation and maintenance costs can be achieved by using a passive transceiver having zero power consumption at the RAU as demonstrated in [42] - [44]. This concept is introduced for the first time in [42] where an EAM is used as the only component connected to the antenna in the RAU without any amplifiers or power supply, as shown in Figure 3.6. In this setup, the RF output from the access point (operating range of 2.4 – 2.48 GHz) was fed to the laser at the central unit. The modulated optical signal was sent over the optical link to the EAM located in the picocell. The EAM acts as a photodiode for the downlink and the converted RF power is then transmitted over the wireless path via an antenna. For the uplink path, the EAM acts as a modulator and the received RF signal modulates the remaining optical power in the EAM (this is the light from the downlink laser). The result is that the uplink modulated optical signal has both the downlink and uplink RF signal components. This is then dealt with by the receiver at the central unit (the access point, in this case) by

either TDD (as in the case of WLAN signals) or FDD (as in the case of GSM or UMTS signals)[3].

The only disadvantage of operating the EAM at zero bias was that the uplink RF insertion loss was greater than that of the downlink. It has been shown in [40] that the two losses can be made equal by choosing an appropriate bias. This imbalance in the link was overcome by using different antenna gains (transmit and receive) at the mobile unit. Using this configuration, complete coverage of a 6 m picocell at 2.4 GHz and a transmission rate of 3 Mbps with a 6 dB power margin were achieved. For a transmission rate of 1 Mbps, the power margin increased to 24 dB. Based on these values (and assuming a fibre loss of 0.2 dB/km), optical link lengths of 7.5 km for 3 Mbps and up to 30 km for 1 Mbps are predicted.

Radio range predictions for RoF links using electroabsorption transceivers at the RAU have been carried out in [44]. Using typical values of loss, noise figure and transmit power for the available electroabsorption modulator transceiver, a range of 7 m has been predicted for the transmission of IEEE 802.11b signals. A further optimistion of device and circuit parameters is suggested which could increase the range to approximately 20 m.

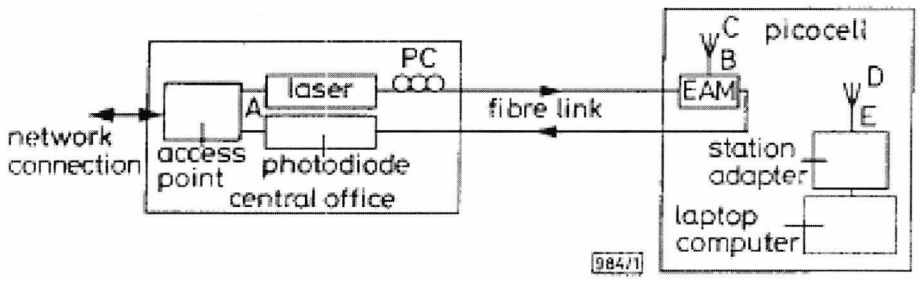

Figure 3.6. Experimental layout of a passive picocell demonstrating the use of an electroabsorption modulator in the remote antenna unit (reproduced from [42])

A recent study in [45] investigated the use of dual-purpose VCSELs operating at 850 nm to construct a half-duplex bi-directional RoF link with transmission over a single MMF cable. These dual-purpose VCSELs can be switched between operating as laser sources or as resonant cavity enhanced avalanche photodetectors. Error-free transmission of 1.25 Gbps of binary data over 500 m of 50 μm-core MMF was demonstrated. Additionally, the transmission of 32-QAM modulated signals at 2 GHz

[3] Private communication with the author.

over 300 m and 600 m of 62.5 μm-core MMF was achieved, for which EVM values as low as 1% (for the 300 m fibre link) and 1.3% (for the 600 m fibre link) were recorded.

3.5 Millimetre-Wave Radio-over-Fibre Techniques

To meet the increasing demand for higher data rates and to combat the congestion at microwave frequencies, transmission in the millimetre-wave frequency band (26–70 GHz) has been considered. However, due to increased path loss at such high frequencies and problems such as high attenuation (due to oxygen absorption) at 60 GHz [46], the cell coverage size becomes restricted. While this is advantageous in terms of short frequency reuse distances, it also means that larger number of antenna units will be required to cover a given area. In order to reduce the cost of infrastructure, radio-over-fibre techniques for the distribution of millimetre-wave signals have been investigated [47], [48].

The discussion of millimetre-wave RoF systems presented in this section focuses primarily on transportation techniques. As has been mentioned in Section 1.1.1, the signal may be transported from the central office to the RAU at the millimetre-wave frequency (RF-over-fibre), at an intermediate frequency (IF-over-fibre), or as a baseband signal (baseband-over-fibre) [49]. All the examples of microwave RoF systems discussed in this chapter have used the RF-over-fibre transportation technique. With respect to millimetre-wave RoF systems, the RF-over-fibre technique has been employed in [50], [51] and [52]. However, the main problem with transmission at the high millimetre-wave frequencies is the chromatic dispersion-induced penalty introduced by the optical fibre [49], [53]. The fibre dispersion effects are significantly reduced by using IF-over-fibre and baseband-over-fibre techniques. These techniques are therefore more widely employed in millimetre-wave RoF systems compared to the RF-over-fibre technique.

IF-over-fibre and baseband-over-fibre millimetre-wave RoF systems may be further classified based on the delivery of the millimetre-wave reference signal required for the up/down-conversion at the RAU. For such systems, the millimetre-wave reference signal may be either provided using an electrical millimetre-wave local oscillator (and a mixer) at the RAU [54], or it can be generated at the central office and optically delivered to the RAU [55], [56], [57], [58]. The remote delivery of the local oscillator

signal removes the need for expensive millimetre-wave generation equipment at the RAU simplifying its design and reducing the overall cost of the system. Further reduction in the cost of the system may be achieved by using an optical transceiver at the RAU as discussed in [52] and [59] (and as discussed in Section 3.4 for microwave RoF systems).

References

[1] C. Carlsson, H. Martinsson, R. Schatz, J. Halonen, and A. Larsson, "Analog Modulation Properties of Oxide Confined VCSELs at Microwave Frequencies," *Journal of Lightwave Technology*, Vol. 20, No. 9, pp. 1740-1749, September 2002.

[2] C. Carlsson, A. Haglund, P. Modh, J. Gustavsson, J. Vukusic, and A. Larsson, "New Single Mode VCSELs for High Performance Fiber Optic RF Links," *Proceedings of International Topical Meeting on Microwave Photonics*, Budapest, Hungary, September 2003.

[3] D. Vez, S. Hunziker, S. Eitel, U. Lott, M. Moser, R. Hoevel, H. Gauggel, A. Hold, and K. Gulden, "Packaged 850 nm vertical-cavity surface-emitting lasers as low-cost optical sources for transparent fibre-optic," *Proceedings of the 33rd European Microwave Conference 2003*, Vol. 2, pp. 611-614, October 2003.

[4] D. Vez, S.G. Hunziker, R. Kohler, P. Royo, M. Moser, and W. Bachtold, "850 nm vertical-cavity laser pigtailed to standard singlemode fibre for radio over fibre transmission," *Electronics Letters*, Vol. 40, No. 19, pp. 1210-1211, September 2004.

[5] R.V. Dalal, R.J. Ram, R. Helkey, H. Roussell, and K.D. Choquette, "Low distortion analogue signal transmission using vertical cavity lasers," *Electronics Letters*, Vol. 34, No. 16, pp. 1590-1591, August 1998.

[6] R.W. Berry, D.J. Brace, and I.A. Ravenscroft, "Optical fiber system trials at 8 Mbits/s and 140 Mbits/s," *IEEE Transactions on Communications*, Vol. Com-26, pp. 1020-1027, July 1978.

[7] K. Okura and M. Ejiri, "Optical fiber system applications aspects in future NTT networks," *IEEE Transactions on Communications*, Vol. Com-26, pp. 968-976, July 1978.

[8] S.D. Miller, T. Li, and E.A.J. Marcatili, "Research toward optical-fiber transmission systems – part II: devices and systems considerations," *Proceedings of the IEEE*, Vol. 61, pp. 1726-1751, December 1973.

[9] P.F. Kolesar and D.J. Mazzarese, "Understanding multimode bandwidth and differential mode delay measurements and their applications," *Proceedings of the 51st International* Wire and Cable Symposium (IWCS), Lake Buena Vista, FL, pp. 453-460, 2002.

[10] J.B. Schlager, M.J. Hackert, P. Pepeljugoski, and J. Gwinn, "Measurements for Enhanced Bandwidth Performance Over 62.5-μm Multimode Fiber in Short-Wavelength Local Area Networks," *Journal of Lightwave Technology*, Vol. 21, No. 5, pp. 1276-1285, May 2003.

[11] L. Raddatz, I.H. White, D.G. Cunningham, and M.C. Nowell, "Influence of restricted mode excitation on bandwidth of multimode fiber links," *IEEE Photonics Technology Letters*, Vol. 10, No. 4, pp. 534-536, April 1998.

[12] L. Raddatz, I.H. White, D.G. Cunningham, and M.C. Nowell, "Increasing the bandwidth-distance product of multimode fibre using offset launch," *Electronics Letters*, Vol. 33, No. 3, January 1997.

[13] M. Wegmuller, S. Golowich, G. Giaretta, and M. Nuss, "Evolution of the beam diameter in a multimode fiber link through offset connectors," *IEEE Photonics Technology Letters*, Vol. 13, No. 6, pp. 574-576, June 2001.

[14] Mode conditioning patchcord application note AN3015 (rev. a), FibreDyne Labs, www. fiberdyne.com.

[15] Mode conditioning patchcord datasheet, LANScape Solutions, Corning Cable Systems LLC, USA, www. corning.com/cablesystems, July 2007.

[16] Mode conditioning patchcord datasheet, iFiber Optix Inc., USA, www.ifiberoptix.com.

[17] L. Raddatz, D. Hardacre, I.H. White, R.V. Penty, D.G. Cunningham, M.R.T. Tan, and S.-Y. Wang, "High bandwidth data transmission in multimode fibre links using subcarrier multiplexing with VCSELs," *Electron. Letters*, Vol. 34, No.7, pp. 686 – 688, April 1998.

[18] L. Raddatz and I.H. White, "Overcoming the modal bandwidth limitation of multimode fiber by using passband modulation," *IEEE Photonics Technology Letters*, Vol. 11, No. 2, pp. 266-268, February 1999.

[19] T.K. Woodward, S. Hunsche, A.J. Ritger, and J.B. Stark, "1 Gb/s BPSK transmission over 1 km of 62.5-μm-core multimode fiber using a single 2.5 GHz subcarrier," *IEEE Photonics Technology Letters*, Vol. 11, No. 3, pp. 382-384, March 1999.

[20] E.J. Tyler, M. Webster, R.V. Penty, and I.H. White, "Subcarrier modulated transmission of 2.5Gb/s over of 62.5-μm-core diameter multimode fiber," *IEEE Photonics Technology Letters*, Vol. 14, No. 12, pp. 1743 – 1745, December 2002.

[21] P. Kourtessis, T. Quinlan, E. Rochat, S.D. Walker, M. Webster, I.H. White, R.V. Penty and M.C. Parker, "0.6 Tbit/s/km multimode fibre feasibility experiment using 40 channel DWDM over quadrature-subcarrier transmission," *Electronics Letters*, Vol. 38, No. 15, pp. 813-815, July 2002.

[22] E.J. Tyler, P. Kourtessis, M. Webster, E. Rochat, T. Quinlan, S.E.M. Dudley, S.D. Walker, , R.V. Penty and I.H. White, "Toward terabit-per-second capacities over multimode fiber links using SCM/WDM techniques," *IEEE Journal of Lightwave Technology*, Vol. 21, No.12, pp. 3237-3243, December 2003.

[23] D. Wake, S. Dupont, C. Lethien, J-P. Vilcot, and D. Decoster, "Radiofrequency transmission of 32-QAM signals over multimode fibre for distributed antenna system applications," *Electronics Letters*, Vol. 37, No. 17, pp. 1087-1089, August 2001.

[24] D. Wake, S. Dupont, J-P. Vilcot, and A.J. Seeds, "32-QAM radio transmission over multimode fibre beyond the fibre bandwidth," *Proceedings of the*

International Topical Meeting on Microwave Photonics (MWP '01), Volume supplement 4, January 2002.

[25] P. Pepeljugoski, S.E. Golowich, A.J. Ritger, P. Kolesar, and A. Risteski, "Modeling and simulation of next-generation multimode fiber links," *Journal of Lightwave Technology*, Vol. 21, No. 5, pp. 1242 – 1255, May 2003.

[26] C. Carlsson, H. Martinsson, and A. Larsson, "High performance microwave link using a multimode VCSEL and high-bandwidth multimode fiber," *International Topical Meeting on Microwave Photonics (MWP '01), Technical Digest*, pp. 81-84, January 2002.

[27] C. Carlsson, A. Larsson, and A. Alping, "RF transmission over multimode fibers using VCSELs – comparing standard and high-bandwidth multimode fibers," *Journal of Lightwave Technology*, Vol. 22, No. 7, pp. 1694-1700, July 2004.

[28] P. Hartmann, X. Qian, A. Wonfor, R.V. Penty, and I.H. White, "1-20 GHz directly modulated radio over MMF link," *Proceedings of the IEEE International Topical Meeting on Microwave Photonics (MWP '05)*, pp. 95-98, October 2005.

[29] J.K. White, C. Blaauw, P. Firth, and P. Aukland, "85°C investigation of uncooled 10-Gb/s directly modulated InGaAsP RWG GC-DFB lasers," *IEEE Photonics Technology Letters*, Vol. 13, No. 8, pp. 773-775, August 2001.

[30] R.E. Schuh, A. Alping, and E. Sundberg, "Penalty-free GSM-1800 and WCDMA radio-over fibre transmission using multimode fibre and 850 nm VCSEL," *Electronics Letters*, Vol. 39, No. 6, pp. 512-514, March 2003.

[31] K.-A. Persson, C. Carlsson, A. Alping, A. Haglund, J.S. Gustavsson, P. Modh, and A. Larsson, "WCDMA radio-over-fibre transmission experiment using singlemode VCSEL and multimode fibre," *Electronics Letters*, Vol. 42, No. 6, pp. 372-374, March 2006.

[32] M.Y.W. Chia, B. Luo, M.L. Yee, and E.J.Z. Hao, "Radio over multimode fibre transmission for wireless LAN using VCSELs," *Electronics Letters*, Vol. 39, No. 15, pp. 1143-1144, July 2003.

[33] H.-H. Lu, P.-C. Lai, and W.-S. Tsai, "Radio-on- multimode fiber systems based on VCSELs and External Light Injection Technique," *IEEE Photonics Technology Letters*, Vol. 16, No. 4, pp. 1215-1217, April 2004.

[34] C. Lethien, C. Loyez, and J-P. Vilcot, "Potentials of Radio over Multimode Fiber Systems for the In-Buildings Coverage of Mobile and Wireless LAN Applications," *IEEE Photonics Technology Letters*, Vol. 17, No. 12, pp. 2793-2795, December 2005.

[35] I. Dayoub, A. Zaouche, J.M. Rouvaen, C. Lethien, J.-P. Vilcot, and D. Decoster, "Radio-optic demonstrator for distributed antenna system indoor wireless applications using low-cost VCSELs," *European Transactions on Telecommunications (in press)*, Published online by Wiley Interscience, 2007.

[36] P. Hartmann, X. Qian, R.V. Penty, and I.H. White, "Broadband multimode fibre (MMF) based IEEE 802.11a/b/g WLAN distribution system," *Proceedings of the IEEE International Topical Meeting on Microwave Photonics (MWP '04)*, pp. 173-176, October 2004.

[37] P. Hartmann, M. Webster, A. Wonfor, J.D. Ingham, R.V. Penty, I.H. White, D. Wake, and A.J. Seeds, "Low-cost multimode fibre-based wireless LAN distribution system using uncooled, directly modulated DFB laser diodes," *29th European Conference on Optical Communication (ECOC-ICOC '03)*, Italy, Vol. 3, pp. 804-805, September 2003.

[38] S. Hwang, H. Kim, B. Kim, S.K. Kim, J. Lee, H. Lee, Y. Kim, G. Lee, S. Kim, and Y. Oh, "RoF technologies for in-building wireless systems," *IEICE Transactions in Electronics*, Invited paper, *Special section on Evolution of Microwave and Millimeter-Wave Photonics Technology*, Vol. E90-C, No. 2, pp. 345-350, February 2007.

[39] P.P. Smyth, "Optical radio – a review of a radical new technology for wireless access infrastructure," *BT Technology Journal*, Vol. 21, No. 3, pp. 22-31, July 2003.

[40] L.D. Westbrook and D.G. Moodie, "Simultaneous bi-directional analogue fibre-optic transmission using an electroabsorption modulator," *Electronics Letters*, Vol. 32, No. 19, pp. 1806-1807, September 1996.

[41] L.D. Westbrook, L. Noel, and D.G. Moodie, "Full-duplex, 25 km analogue fibre transmission at 120 Mbit/s with simultaneous modulation and detection in an electroabsorption modulator," *Electronics Letters*, Vol. 33, No. 8, pp. 694-695, April 1997.

[42] D. Wake, D. Johansson, and D.G. Moodie, "Passive picocell: a new concept in wireless network infrastructure," *Electronics Letters*, Vol. 33, No. 5, pp. 404-406, February 1997.

[43] D. Wake and D.G. Moodie, "Passive picocell – an unpowered remote transceiver for short range, high capacity radio systems," *IEE Colloquium on Fibre Optics and Microwave Systems (IEE Digest 1997/131)*, pp. 14/1-14/4, June 1997.

[44] D. Wake and K. Beacham, "Passive electroabsorption tranceivers for broadband wireless access," *Proceedings of the IEEE International Topical Meeting on Microwave Photonics (MWP '02)*, pp. 21-24, November 2002.

[45] J.D. Ingham, R.V. Penty, and I.H. White, "Bi-directional multimode-fiber communication links using dual-purpose vertical-cavity devices," *Journal of Lightwave Technology*, Vol. 24, No. 3, pp. 1283-1294, March 2006.

[46] J.J. O'Reilly, P.M. Lane, J. Attard, and R. Griffin, "Broadband wireless systems and networks: an enabling role for radio-over-fibre," *Philosophical Transactions of the Royal Society of London (A)*, Vol. 358, pp. 2297-2308, 2000.

[47] H. Ogawa, D. Polifko, and S. Banba, "Millimeter-Wave fiber optics systems for personal radio communication," *IEEE Trans. Microwave Theory Tech.*, vol. 40, no. 12, pp. 2285.2293, December 1992.

[48] L. Noel, D. Wake, D.G. Moodie, D.D. Marcenac, L.D. Westbrook, and D. Nesset, "Novel techniques for high-capacity 60-GHz fiber-radio transmission systems," *IEEE Transactions on Microwave Theory and Techniques*, Vol. 45, No. 8, pp. 1416-1423, August 1997.

[49] D. Novak, A. Nirmalathas, C. Lim, C. Marra, and R.B. Waterhouse, "Fibre-radio – challenges and possible solutions," *Proceedings of the International Topical Meeting on Microwave Photonics (MWP '03)*, pp. 49-56, September 2003.

[50] T. Kuri, K. Kitayama, A. Stohr, and Y. Ogawa, "Fiber-Optic millimeter-wave downlink system using 60 GHz-band external modulation," *Journal of Lightwave Technology*, Vol. 17, No. 5, pp. 799-806, May 1999.

[51] G.H. Smith, D. Novak, and C. Lim, "A millimeter-wave full-duplex fiber-radio star-tree architecture incorporating WDM and SCM," *IEEE Photonics Technology Letters*, Vol. 10, No.11, pp. 1650-1652, November 1998.

[52] K. Kitayama, A. Stohr, T. Kuri, R. Heinzelmann, D. Jager, and Y. Takahashi, "An approach to single optical component antenna base stations for broadband millimeter-wave fiber-radio access systems," *IEEE Transactions on Microwave Theory and Techniques*, Vol. 48, No. 12, pp. 2588-2595, December 2000.

[53] U. Gliese, S. Norskov, and T.N. Nielsen, "Chromatic dispersion in fiber-optic microwave and millimeter-wave links," *IEEE Transactions on Microwave Theory and Techniques*, Vol. 44, No. 10, pp. 1716-1724, October 1996.

[54] C. Loyez, C. Lethien, R. Kassi, J.-P. Vilcot, D. Decoster, N. Rolland, and P.A. Rolland, "Subcarrier radio signal transmission over multimode fibre for 60 GHz WLAN using a phase noise cancellation technique," *Electronics Letters*, Vol. 41, pp. 91–92, January 2005.

[55] T. Kuri, K. Kitayama, and Y. Ogawa, "Fiber-Optic millimeter-wave uplink system incorporating remotely fed 60-GHz-band optical pilot tone," *IEEE Transactions on Microwave Theory and Techniques*, Vol. 47, No. 7, pp. 1332-1337, July 1999.

[56] A. Nkansah, A. Das, N.J. Gomes, and P. Shen, "Multilevel modulated signal transmission over serial single-mode and multimode fiber links using vertical-cavity surface-emitting lasers for millimeter-wave wireless communications," *IEEE Transactions on Microwave Theory and Techniques*, Vol. 55, No. 6, pp. 1219-1228, June 2007.

[57] T. Ismail, C. P. Liu, J. E. Mitchell, A. J. Seeds, X. Qian, A. Wonfor, R.V. Penty, and I.H. White, "Transmission of 37.6-GHz QPSK wireless data over 12.8-km fiber with remote millimeter-wave local oscillator delivery using a bi-directional SOAin a full-duplex system with 2.2-km CWDM fiber ring architecture," *IEEE Photonics Technology Letters*, Vol. 17, No. 9, pp. 1989–1991, September 2005.

[58] C. Lim, A. Nirmalathas, D. Novak, R. Waterhouse, and G. Yoffe, "Millimeter-wave broad-band fiber-wireless system incorporating baseband data transmission over fiber and remote LO delivery," *Journal of Lightwave Technology*, Vol. 18, No. 10, pp. 1355-1363, October 2000.

[59] K. Kitayama and R.A. Griffin, "Optical downconversion from millimeter-wave to IF-Band over 50-km-long optical fiber link using an electroabsorption modulator," *IEEE Photonics Technology Letters*, Vol. 11, No. 2, pp. 287-289, February 1999.

CHAPTER 4
RADIO-OVER-FIBRE LINK COMPONENT CHARACTERISATION

4.1 Introduction

This chapter deals with the first stage in the design of a low-cost radio-over-fibre link: characterization of the various components.

A review of the current research in the field of radio-over-fibre systems in Chapter 3 shows that RoF-based distributed antenna systems can provide high quality mobile/wireless coverage for high density in-building user populations. It has been discussed in Chapter 1 that the simplicity and cost-effectiveness of IMDD using direct modulation of the laser makes it a popular choice as the transmission method in low-cost RoF links. For these reasons, the RoF-based distributed antenna system analysed in this thesis employs direct modulation of the laser combined with direct detection using a photodiode.

A basic DAS may be divided into four main parts: the central unit, the optical link, the remote antenna unit and the mobile unit (MU) as shown in Figure 4.1. The RF signal fed to the downlink (DL) path modulates the CU laser; the RF modulated optical signal is sent over the optical link to the RAU. At the RAU, the incoming downlink signal is detected by a photodiode and the retrieved RF signal is amplified and transmitted over the wireless path. In the uplink (UL), the RF signal from the mobile unit reaches the antenna at the RAU, is amplified and modulates the RAU laser. This modulated signal is sent over the optical link to the CU where it is detected by the CU PD.

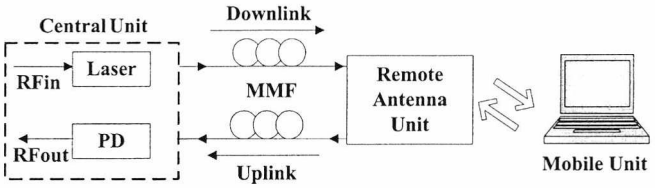

Figure 4.1. Basic fibre-fed distributed antenna system

For the RAU, a two-antenna design and a single-antenna design, as shown in Figures 4.2a and 4.2b respectively, are considered. The two-antenna RAU uses separate transmit and receive antennas. Figure 4.3 is a photograph of the two-antenna RAU utilised for measurements in this research.

The single-antenna RAU employs the same RF antenna for both transmission and reception with a power-splitter/combiner separating the downlink and uplink signals. Normally, at the antenna end of the RAU, a circulator is more commonly used than a power-splitter/combiner. This is mainly because inserting a power-splitter/combiner incurs an additional 3-dB splitter loss (for a two-way splitter). As the received (uplink) signal may already have low signal strength, using a power-splitter/combiner instead of a circulator may result in a reduction of the uplink maximum achievable range. The impact of inserting an isolator and power-splitter/combiner in the designed RoF link using a single-antenna RAU (as shown in Figure 4.2b) on the maximum achievable range is further discussed in Section 6.2.1, Chapter 6. However, the isolation values (approximately 25 dB, as stated on the datasheet) of the commercially available circulators were much lower than the isolation value (approximately 40 dB, as stated on the datasheet) of the power-splitter/combiner. It should be mentioned here that the datasheet isolation values were specified for a load impedance of 50 Ω. However, as the antenna utilised did not meet the 50 Ω impedance requirement, the isolation value of the power-splitter/combiner measured during the experiments was much lower (only 12 dB).

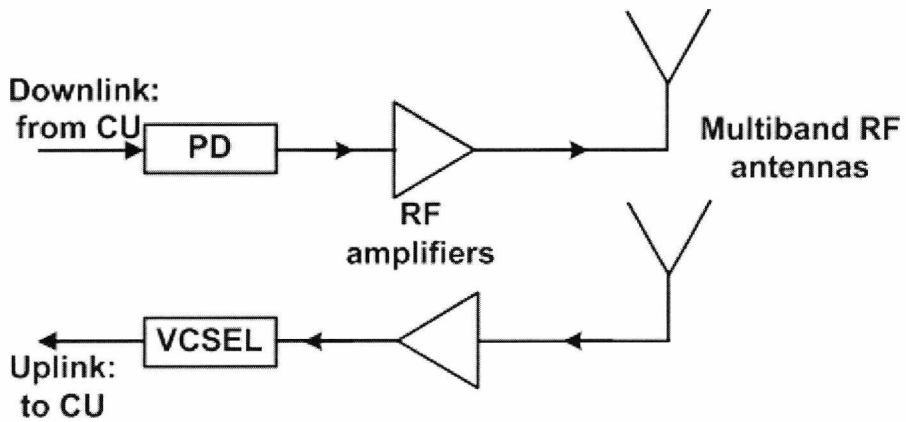

Figure 4.2a. Two-antenna RAU design

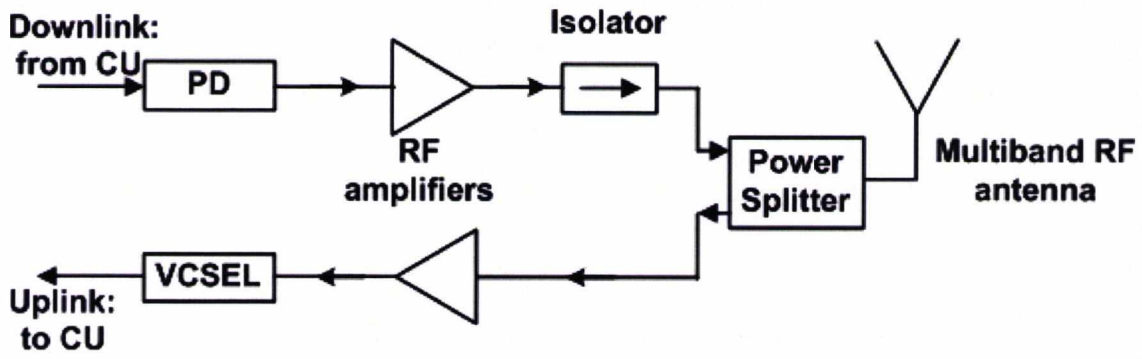

(b)

Figure 4.2b. Single-antenna RAU design

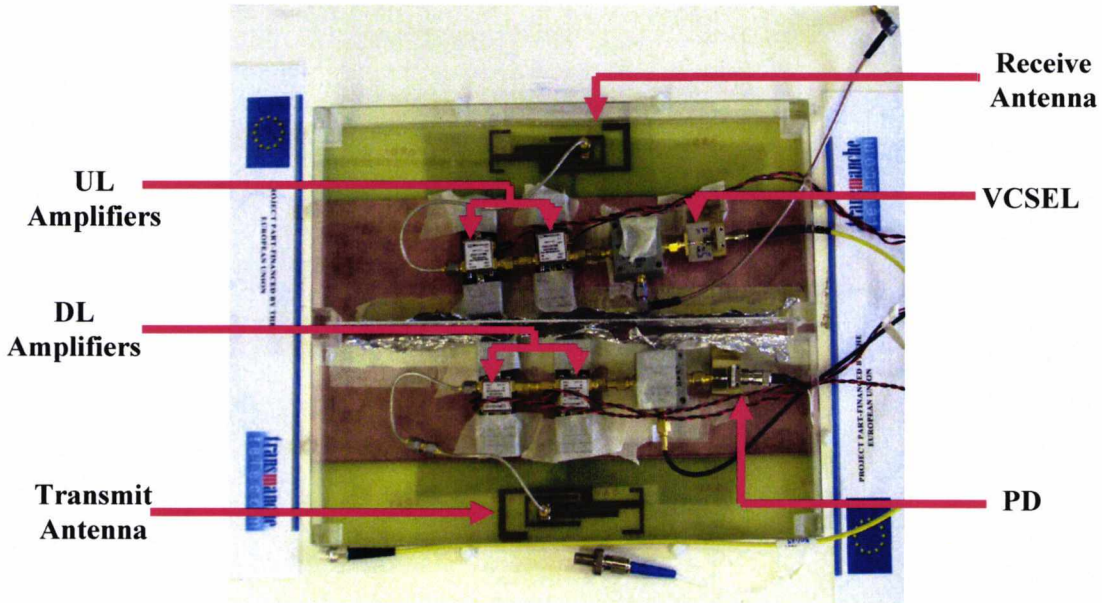

Figure 4.3. Photograph (top-view) of the two-antenna RAU used in the measurements

The first stage in the design of any link is the characterisation of the different components. In order to implement the DAS, VCSELs operating at 850 nm were used as optical transmitters at both the CU and the RAU, and multimode fibre was used as the optical link. The advantage of using VCSELs operating at 850 nm and MMFs in low-cost distributed antenna systems has already been discussed in Chapters 2 and 3.

For the VCSELs, characteristics such as output power, noise and intermodulation distortion are investigated. As the noise and intermodulation distortion depend on the frequency being used, these measurements were carried out at specific frequencies corresponding to different wireless systems: GSM 900, GSM 1800, UMTS and in particular, WLAN. Additionally, the frequency responses of VCSELs and multimode

fibre are determined over the frequency range covering the above mentioned wireless systems.

4.2 P-I Characteristics

The 850 nm multimode *ULM* VCSEL (datasheet [1] included in Appendix A) used for the measurements was packaged with an SMA receptacle for optical output. An MMF patchcord (both 62.5/125 μm and 50/125 μm versions were available) with an SMA connector at one end and an ST connector at the other end was used to couple light from the VCSEL into a photodiode or an MMF of longer length. The VCSEL had an aperture size of 20 μm and an annular far-field emission pattern[1].

An annular (or doughnut-shaped) emission pattern of the laser when launched into an MMF can be considered to produce a response which is a combination of multiple offset launches into the MMF. The offset launch technique involves the introduction of light into the MMF from an SMF which is radially offset from the axis of the MMF (Section 3.3.1, Chapter 3). Simultaneous offset launches at different radial offsets from the axis of the MMF should produce an annular pattern in the MMF. As the light is being launched away from the centre of the MMF for an offset launch and therefore for an annular launch, this results in a majority of the higher order modes of the fibre being excited (this has also been discussed in Section 3.3.1, Chapter 3).

The first step in evaluating the VCSEL performance was to measure the static (or continuous wave) characteristics, mainly the P-I characteristics. For this, the bias current to the VCSEL was provided by a precision current source (*ILX Lightwave LDX-3412*). The VCSEL was connected to an *Appointech* PD (datasheet [2] included in Appendix A) via the MMF patchcord. The PD was biased using a 5 V voltage supply and an ammeter to record the DC photocurrent.

For most of the PDs, responsivity values sent by the manufacturer were used for the power measurements. The accuracy of the manufacturer-supplied responsivity values was determined by checking the output optical power measured using the photodiode against power measurements using an optical power-meter.

[1] Private communication, *ULM Photonics*, 2005

For the P-I measurements, using the VCSEL-patchcord-PD experimental set-up, the VCSEL bias current was varied between 0.5 mA and 11 mA (with a 0.5 mA increment) and the corresponding DC photocurrent was recorded. The output optical power for each bias current was calculated by normalising the measured DC photocurrent value using the photodiode responsivity. The P-I characteristics were measured for different VCSELs and the results are displayed in Figure 4.4.

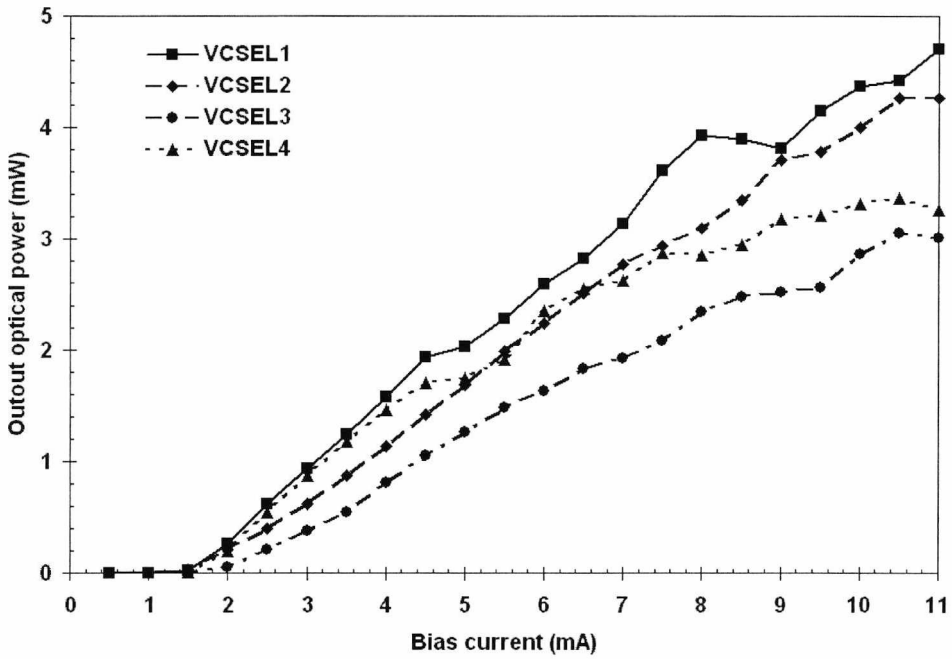

Figure 4.4. Continuous wave P-I characteristics for different VCSELs

It should be noted that the above experiments were carried out at room temperature and no temperature-control mechanism was implemented. The threshold currents for three of the VCSELs (VCSEL1, VCSEL2 and VCSEL 4) were recorded to be 1.5 mA while for VCSEL3, it was recorded as 2 mA. Another parameter that can be calculated from the P-I curves is the fibre-coupled slope efficiency of the VCSEL, which is an important contributor to the RoF link gain (as shown in Chapter 5). At a bias current of 7 mA, slope efficiencies of 0.57 W/A, 0.5 W/A, 0.38 W/A and 0.48 W/A were obtained from the above characteristics for VCSELs 1, 2, 3 and 4 respectively.

4.3 Frequency Response Measurements

Frequency response measurements were carried out both for the VCSELs and the MMFs used in the link. The corresponding results gave an indication of the power loss due to each of the components at different frequencies.

For the VCSEL frequency response measurements, the VCSEL-PD link used in the P-I experiments was connected to an *HP8722ES* network analyser. The RF frequency range (on the network analyser) was set between 0.5 GHz and 3 GHz (to cover the frequencies corresponding to the wireless systems) and the input power was set to be -10 dBm. S21 and S11 measurements were carried out over the RF frequency range for different bias currents to the VCSEL. The network analyser was calibrated at the end of its input/output cables to remove the loss from the cables. To further remove the effect of reflection, the S21 response was normalized and the power gain was calculated as [3]:

$$G_p = \frac{|S_{21}|^2}{1-|S_{11}|^2} \tag{4.1}$$

As the photodiode response was not decoupled from the measured frequency response, Figure 4.5 shows the results for the combined frequency response of one of the VCSEL-PD links, for different bias currents.

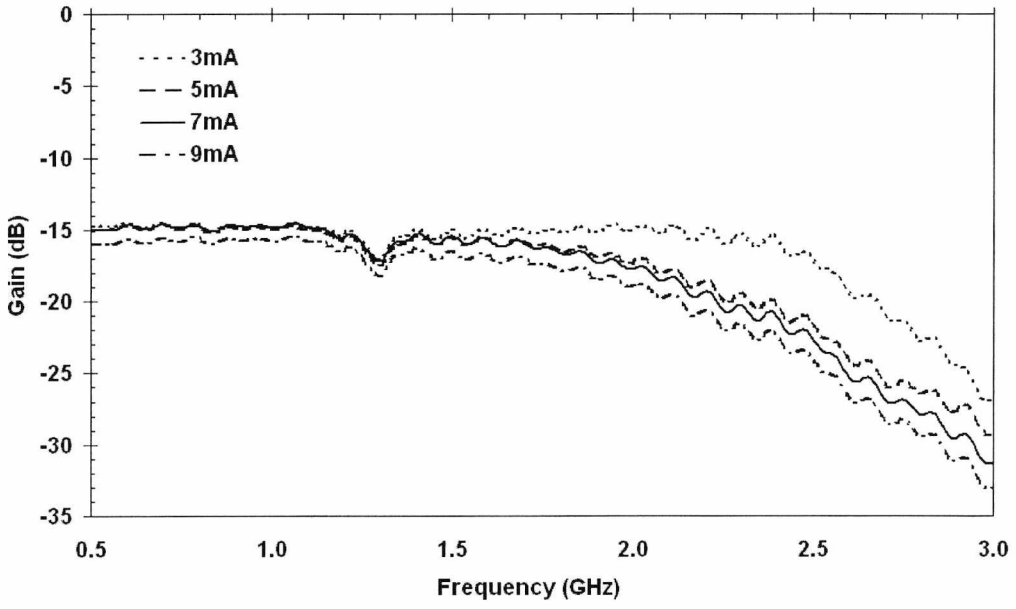

Figure 4.5. Frequency response of the combined VCSEL (at 850 nm) -PD link for different bias currents

At a given frequency, a slight decrease in the power gain is observed with an increase in bias current in Figure 4.5. 3 dB modulation bandwidths of 2.04 GHz for bias currents 5 mA, 7 mA and 9 mA, and 2.56 GHz for a bias current of 3 mA, are measured from the above frequency response (note that a 3 dB modulation bandwidth specification of 3 GHz is given in the VCSEL manufacturer datasheet). The *Appointech* photodiode

used for the measurements had a modulation bandwidth of 1.5 GHz [2]. This could be one of the reasons for the early roll-off in power seen in Figure 4.5 resulting in such low modulation bandwidths for the VCSEL. According to measurements carried out in [4] and [5], VCSEL modulation bandwidths may also be affected by either parasitic capacitances or heating effects in the VCSEL [4], or a combination of these two effects and damping [5]. The ripples observed in the above frequency response are most likely to be due to calibration errors of the network analyser. Another reason, as stated in [6], might be the use of longer pins on the VCSEL. It was experimentally demonstrated in [6] that the frequency response of the VCSEL (1550 nm) was much more 'smooth' on cutting the pins on the VCSEL as short as possible.

For measuring the frequency response of the fibre, different lengths of MMF were inserted between the VCSEL patchcord and the PD. Standard 50 μm-core (OM2) and 62.5 μm-core (OM1) multimode fibres were used for all measurements. For measuring the frequency response of the MMF, the RF frequency range of the network analyser was set to be in the range 0.05 GHz – 6.0 GHz. The effect of the frequency-dependent VCSEL response was eliminated by calibrating the network analyser with the VCSEL-patchcord-PD link connected. The frequency response measurements were carried out for both 50/125 μm and 62.5/125 μm fibres of lengths 100 m, 300 m and 600 m using the 850 nm *ULM* VCSEL. The frequency response measurement results for both the 50/125 μm and 62.5/125 μm MMF for different fibre lengths are shown in Figures 4.6a and 4.6b, respectively.

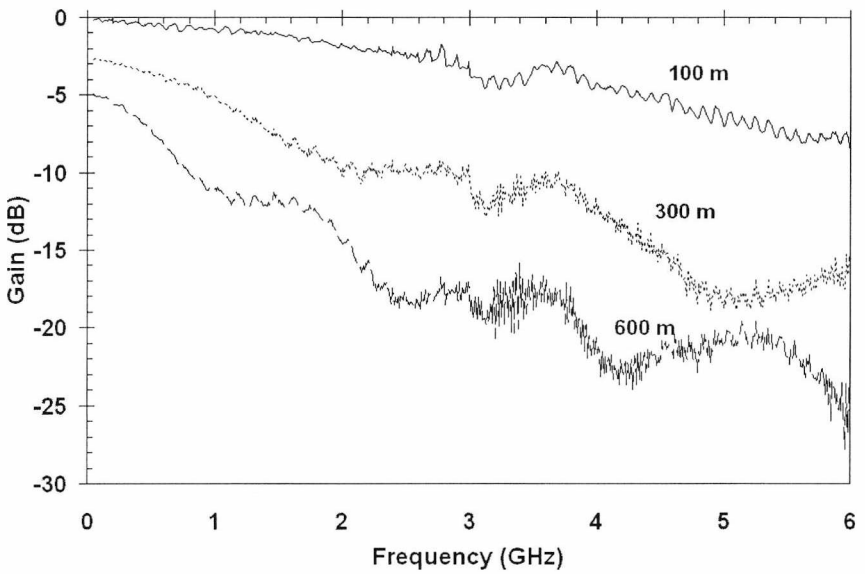

Figure 4.6a. Frequency response of a 62.5 μm-core MMF using an 850 nm VCSEL

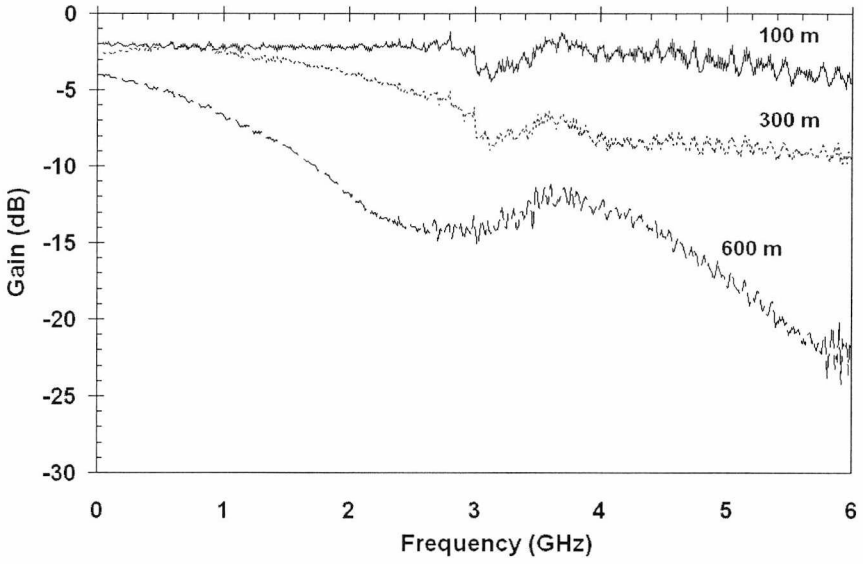

(b)

Figure 4.6b. Frequency response of a 50 μm-core MMF using an 850 nm VCSEL

As can be seen from Figures 4.6a and 4.6b, the fibre RF insertion loss is dependent on both frequency and the length of fibre used. The dips in the responses shown above (for the 300 m and 600 m MMF) have also been reported in [7] and [8] and are attributed to the interference between the different mode groups with different propagation delays.

The frequency response of the above 62.5/125 μm MMF has been simulated using the VPIphotonics™ simulation package in [9]. A good match was obtained between the simulated and measured impulse and frequency responses of the 62.5/125 μm MMF (of lengths 300 m and 600 m, measured using a Honeywell VCSEL source).

In particular, for the wireless frequency range of interest (0.9 GHz – 2.5 GHz), RF losses ranging between 16 dB (at 0.9 GHz) and 30 dB (at 2.5 GHz) at a bias current of 7 mA were obtained for the VCSEL-patchcord-PD link. For the same frequency range, additional RF loss values of 2 dB for the 100 m length, between 2 dB and 5 dB for the 300 m length and between 6 dB and 14 dB for the 600 m length were obtained from the MMF frequency response curves.

4.4 Relative Intensity Noise (RIN) Measurements

For these measurements, the VCSEL and PD were again connected by means of the MMF patchcord used for the P-I and frequency response measurements. The RF input of the bias-tee for the VCSEL was terminated using a 50 Ω load. The bias current to the

VCSEL was provided using the precision current source (*ILX Lightwave LDX-3412*) and the PD was connected to a 5 V supply and an ammeter to record the DC photocurrent. The PD was followed by an RF amplifier (*Mini-Circuits ZX60-2522M*) to amplify the signal beyond the noise floor of the RF spectrum analyser (*Agilent E4407B*). For the final RIN calculation, the output noise power was normalised using the amplifier gain values to remove the effect of the amplifier. All the noise measurements were carried out in a 1 Hz bandwidth. It should be noted here that the noise powers were measured with a unit of dBm/Hz but were converted to linear values for use in the calculations (discussed below).

The output noise power at a particular frequency was recorded on the spectrum analyzer, first with the VCSEL bias on (N_{on}) and then with the VCSEL bias turned off (N_{off}). With the VCSEL bias on, the total noise power measured consisted of the RIN noise power (N_{rin}), shot noise power (N_{sh}) and thermal noise power (N_{th}), while with the VCSEL bias turned off, only the thermal noise contributed to the total noise power. Therefore, the difference between the two noise powers (N_{diff}) gives a sum of just the RIN noise power and the shot noise power. These powers may be written as:

$$N_{on} = N_{rin} + N_{sh} + N_{th} \tag{4.2}$$

$$N_{off} = N_{th} \tag{4.3}$$

$$N_{diff} = N_{on} - N_{off} = N_{rin} + N_{sh} \tag{4.4}$$

Using the measured DC photocurrent (I_{ph}), the shot noise power is calculated as [10]:

$$N_{sh} = 2qZ_{pd}I_{ph} \tag{4.5}$$

where, q is the electronic charge and Z_{pd} is the PD impedance. N_{rin} may be calculated by substituting Equation 4.5 in Equation 4.4. Finally, using the calculated value of N_{rin}, the RIN of the VCSEL may be calculated from the following expression [10]:

$$RIN = 10\log\left(\frac{N_{rin}}{I_{ph}^2 Z_{pd}}\right) \tag{4.6}$$

As the measurements were done manually, VCSEL RIN was measured only at frequencies corresponding to certain wireless systems such as GSM 900, GSM 1800, UMTS (TDD and FDD) and WLAN. Table 4.1 contains example RIN values ranging between -139 dB/Hz and -146 dB/Hz measured for one of the VCSELs (used in the RoF link) biased at 7 mA. It should be noted that for the FDD systems (GSM 900, GSM 1800 and UMTS FDD), the frequencies used for the measurements correspond to the downlink frequencies (defined as base transmit frequencies in the corresponding standards) for the different systems.

TABLE 4.1 MEASURED NOISE VALUES AT DIFFERENT WIRELESS FREQUENCIES FOR A VCSEL BIASED AT 7 mA

Frequency (GHz)	N_{on} (dBm/Hz)	N_{off} (dBm/Hz)	I_{ph} (μA)	N_{diff} (dBm/Hz)	N_{sh} (dBm/Hz)	N_{rin} (dBm/Hz)	RIN (dB/Hz)
0.95 GSM 900	-156.1	-160.8	594	-157.9	-170.9	-158.2	-140.6
1.84 GSM 1800	-155.6	-164.1	593	-156.3	-170.2	-156.4	-138.9
2.01 UMTS TDD	-155.7	-163.7	594	-156.5	-170.2	-156.6	-139.1
2.14 UMTS FDD	-157.6	-164.1	592	-158.7	-170.2	-159	-141.5
2.4 WLAN	-159	-162.4	614	-161.7	-170.1	-162.3	-145.1

For the other VCSELs used in the measurements, RIN values ranging between -119 dB/Hz and -144 dB/Hz were measured for the different wireless systems.

4.5 Third-Order Intermodulation Measurements: IP3 and SFDR

As a figure of merit of the RoF link performance, third-order intercept point (IP3) and spurious-free dynamic range (SFDR) measurements were carried out (IP3 and SFDR have been defined in Section 2.5.1, Chapter 2). For determining the IP3 and SFDR values of the RoF link, standard two-tone intermodulation measurements were carried out (as performed in [5]). The experimental set-up is shown in Figure 4.7. RF signals from two signal generators (*Agilent E4438C* and *HP83640L*) were combined using an RF combiner and fed to the *ULM* VCSEL. The output power from the VCSEL was fed into the PD via a 50 μm or 62.5 μm core MMF. The output of the PD was connected to the RF spectrum analyser (*Agilent* E4407B).

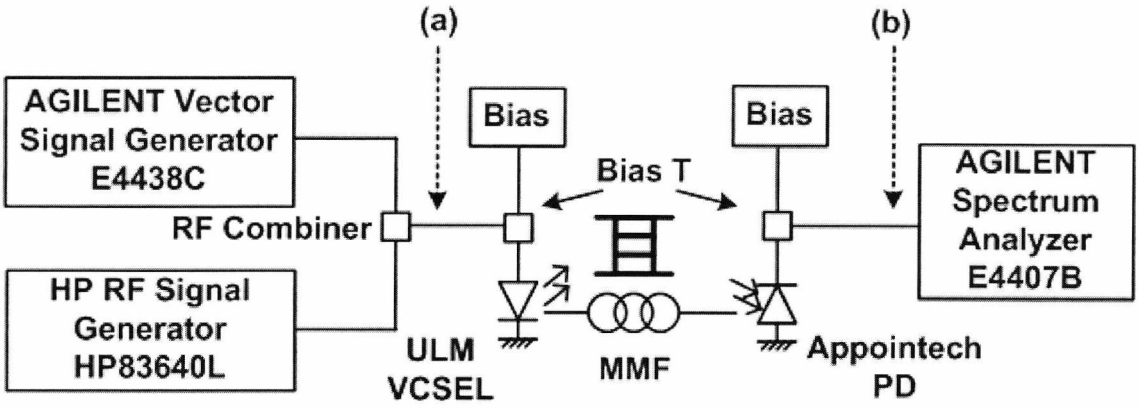

Figure 4.7. Two-tone measurements: experimental set-up

Using the WLAN frequency (2.4 GHz) as an example for two-tone measurements (measurement results at other wireless frequencies are presented later), the two RF signal frequencies were chosen as 2.4 GHz and 2.401 GHz (set to be 1 MHz apart as required for two-tone measurements [5]). Before being fed into the VCSEL, the combined RF signal from the two generators (at point (a) in Figure 4.7) was first directly fed into the spectrum analyzer (at point (b) in Figure 4.7) and the source power values were adjusted so that the power was equal at the two signal frequencies. Once the powers from the two signal generators were made equal, two-tone measurements were carried out for the RF combiner and bias tee combination in order to verify that these passive components were not contributing to the third-order intermodulation distortion of the link. The third-order input intercept point (IIP3) for these measurements was recorded to be 28 dBm, which was much higher than the IIP3 measured for the link (as will be seen later). It should be noted that even at the maximum input power of 14 dBm allowed by the signal generators, no compression in the output was observed.

The VCSEL-MMF-PD link was then inserted and two-tone measurements carried out for the RoF link. The input RF power to the VCSEL was varied between -23 dBm and 4 dBm and the corresponding output RF power was recorded at the two main tones (2.400 GHz (f_1) and 2.401 GHz (f_2)) and at the third-order intermodulation frequencies ($2f_1 - f_2$: 2.399 GHz and $2f_2 - f_1$: 2.402 GHz). Third-order intermodulation measurement results for the transmission of a 2.4 GHz signal over a link using an MMF of length 100 m are shown in Figure 4.8. Note that as the output RF power values at the two main tones were approximately equal to one another (similarly for the third-order intermodulation products), RF power values recorded at only one of the main tones (2.4 GHz) and one of the third-order intermodulation frequencies (2.399 GHz) were used for

plotting the graph. For calculating the SFDR, the noise floor for the measurements was noted for a resolution bandwidth of 1 Hz and is also indicated in Figure 4.8. The IIP3 and SFDR for the link were measured to be 14.5 dBm and 91 dB.Hz$^{2/3}$ respectively.

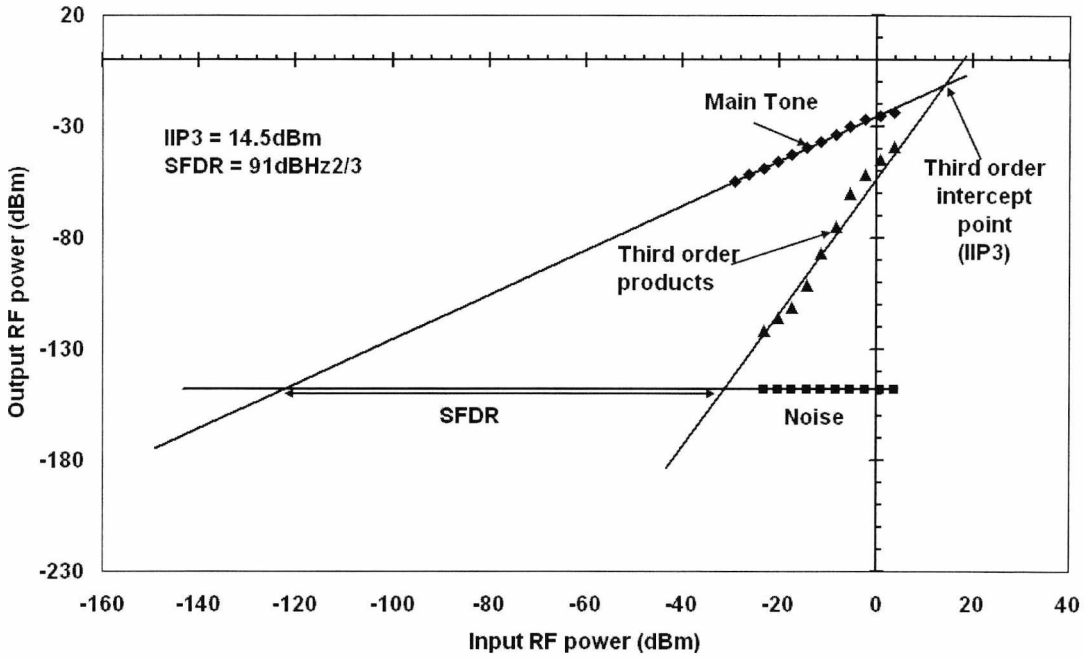

Figure 4.8. Third-order intermodulation measurements for the RoF link using an MMF of length 100 m

The IIP3 and SFDR values for the above link were also measured at frequencies (mobile transmit frequencies for the FDD systems) corresponding to certain wireless systems (as in the case of the VCSEL RIN measurements) and the corresponding results have been tabulated in Table 4.2. The table also shows the IIP3 and SFDR values for an RoF link using a different VCSEL and PD, and an MMF of length 300 m (note that both MMFs are of the 62.5/125 μm specification). SFDR values ranging between 91 dB.Hz$^{2/3}$ and 97 dB.Hz$^{2/3}$ for the RoF link using the 100 m MMF and between 86 dB.Hz$^{2/3}$ and 91 dB.Hz$^{2/3}$ for the RoF link using the 300 m MMF were measured for the different wireless frequencies.

TABLE 4.2 MEASURED IIP3 AND SFDR VALUES AT DIFFERENT WIRELESS FREQUENCIES FOR THE ROF LINK USING TWO DIFFERENT FIBRE LENGTHS

Frequency (GHz)	IIP3 (dBm)		SFDR (dB.Hz$^{2/3}$)	
	100 m MMF	300 m MMF	100 m MMF	300 m MMF
0.9 GSM 900	11.6	9	96.8	91
1.75 GSM 1800	14.3	10.5	95	88
1.95 UMTS FDD	18.8	9.3	92.5	87
2.01 UMTS TDD	16.5	11.4	95	89
2.4 WLAN	14.5	11.2	91	86

4.6. Effect of VCSEL Non-Linearity on the Transmission of Different Digital Modulation Schemes

As the wireless systems being transmitted over the RoF link are digitally modulated, it is important to assess the distortion introduced by VCSEL non-linearity on the modulation scheme. Error vector magnitude was used as the measure of this distortion. These measurements aid in determining the maximum input RF power that can be fed to the VCSEL without inducing distortion. The transmitted wireless systems include GSM (1.8 GHz), DPRS (1.88 GHz) and UMTS (2.0 GHz).

The experimental set-up for the non-linearity measurements is shown in Figure 4.9. An *Agilent* vector signal generator (VSG) *E4438C* was used to emulate the different wireless systems based on the properties listed in Table 4.3. An *Agilent* spectrum analyzer connected to a laptop installed with *Agilent* vector signal analyser (VSA) software was used as the receiver. The VSA software had the capability of decoding the RF signal and measuring its EVM. Measurements for the transmission of WLAN signals over the RoF link, however, could not be carried out as the *Agilent* VSG/VSA did not have OFDM modulation/demodulation capabilities. Moreover, the WLAN channel bandwidth is 22 MHz whereas the receiver (VSA) had a bandwidth of only 10 MHz.

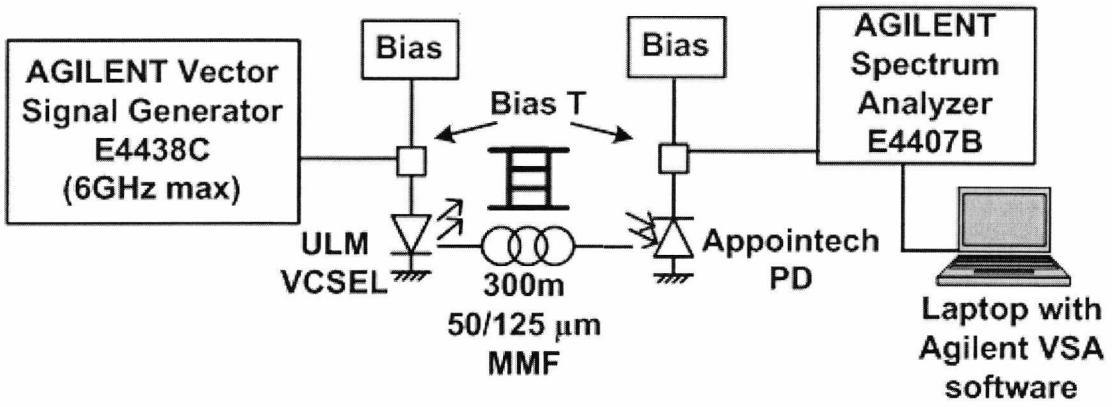

Figure 4.9. Experimental set-up for VCSEL non-linearity measurements

TABLE 4.3 PROPERTIES OF THE EMULATED WIRELESS SYSTEMS: GSM, DPRS AND UMTS

Systems	Frequency (GHz)	Modulation	Data rate	Filter type	Maximum rms EVM (%)
GSM	1.8	GMSK	270.833 ksym/s	Gaussian BT = 0.3	7.0
DPRS	1.88	64 QAM	1.152 Msym/s	RRC $\alpha = 0.5$	2.6
UMTS	2.0	QPSK	3.84 Msym/s	RRC $\alpha = 0.22$	12.5

For the measurements, the input powers driving the *ULM* VCSEL were varied and the EVM was measured first at the output of the signal generator (for each of the systems), then for the VCSEL-PD (back-to-back) link, and finally for the complete VCSEL-MMF-PD link. For the VCSEL-PD link measurements, the 50 μm-core MMF patchcord was used instead of the MMF. The results for transmission of UMTS signals are shown in Figure 4.10. It should be noted that the input power to the VCSEL incorporates the RF losses due to cables and connectors i.e., it is measured at the VCSEL after cable losses.

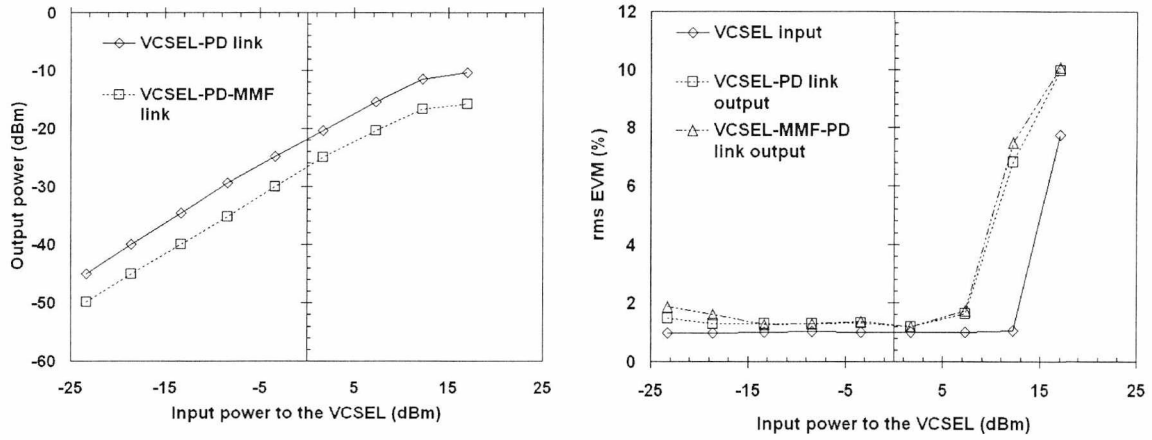

(a) (b)

Figure 4.10. VCSEL distortion performance for the transmission of UMTS signals (a) Output power (b) Measured rms EVM

The optical link response (Figure 4.10a) was measured with and without the MMF in the experimental set-up and the measurements show that the VCSEL response is linear up to about 12 dBm input RF power; beyond this, it saturates. The only effect of introducing the 300 m long 50 μm-core MMF is that an additional 5 dB loss is incurred in the link.

The EVM measurement results for UMTS (Figure 4.10b) show that for input powers between -23 dBm and 12 dBm, the rms EVM of the signal fed to the VCSEL remains constant at approximately 1%. On introducing the VCSEL-PD link, the rms EVM recorded at the output of the link increases only slightly for low input powers, as can be seen from Figure 4.10b. This increase is seen to be insignificant compared to the input UMTS signal. However, for input powers greater than 2 dBm, the signal suffers considerable distortion from the VCSEL, as is seen by the sudden rise in the measured rms EVM readings. At the saturation input power of 12 dBm to the VCSEL, the rms EVM recorded at the output of the VCSEL-PD link was 6.81% compared to 1.06% recorded for the input UMTS signal. Figure 4.10b also shows that insertion of the 300 m long MMF results in only a small degradation in the rms EVM compared to the VCSEL-PD back-to-back link.

For comparison, the EVM results for all three systems (GSM, DPRS and UMTS) are shown in Figure 4.11a (EVM measurements at the output of the VCSEL-PD link) and Figure 4.11b (EVM measurements at the output of the VCSEL-MMF-PD link).

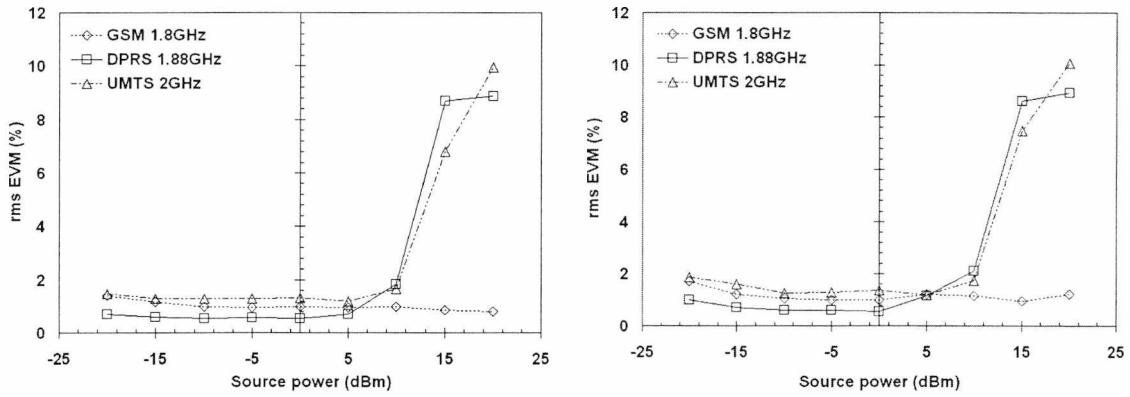

Figure 4.11. rms EVM performances for the GSM, DPRS and UMTS systems at the output of the (a) VCSEL-PD link and (b) VCSEL-MMF-PD link

For a given power setting on the signal generator, the input power being fed to the VCSEL (after taking into account the different cable and connector losses) was recorded to have different values for the different transmission frequencies. For example, at a source power setting of -10 dBm, the VCSEL input power value was measured to be -12.5 dBm, -13 dBm and -13.3 dBm for GSM, DPRS and UMTS systems, respectively. As the difference in the VCSEL input power values for the three systems is not significant, common source power values (same for all three systems) were used as the x-axis values in Figure 4.11.

For the VCSEL-PD link (Figure 4.11a), when the source power is between -20 dBm and 5 dBm (which corresponds approximately to the laser input power range of -23 dBm and 2 dBm for all the systems), the DPRS system has the best rms EVM performance among the three systems. Beyond 5 dBm source power, the rms EVM values for DPRS and UMTS signals are seen to increase suddenly. The rms EVM value for the GSM system, however, remains constant at approximately 0.9% for source power values greater than 5 dBm.

For the VCSEL-MMF-PD link in Figure 4.11b, again DPRS gives the best rms EVM performance but for source power values between -20 dBm and 0 dBm. As for the VCSEL-PD case (Figure 4.11a), the rms EVM values for DPRS and UMTS signals increase rapidly beyond source powers of 5 dBm while the GSM signal suffers very little distortion (average rms EVM of 1.1%). The measurement results indicate that for the transmission of narrowband signals such as GSM, DPRS and UMTS, the effect of

inserting the 300 m long MMF in the VCSEL-PD link on the EVM is insignificant compared to the EVM measured for the VCSEL-PD link.

The superior EVM performance of the GSM system compared to the DPRS and UMTS systems at high input powers may be attributed to the GMSK modulation scheme used in GSM. GMSK belongs to a class of signals called constant envelope signals, which are less prone to distortion when passed through non-linear devices being operated closer to saturation [11], [12]. Using a Gaussian filtering method, GMSK is able to considerably suppress power in the sidebands unlike the case of QPSK used with root-raised cosine filtering (implemented in UMTS). QAM modulation, as used by DPRS, is a non-constant envelope modulation scheme known to be much less tolerant to phase distortion (in particular) introduced by non-linear devices operating near their saturation point [11].

On comparing the measured EVM results (Figures 4.11a and 4.11b) and the acceptable maximum rms EVM values for each of the systems (listed in Table 4.3), it is possible to decide the range of VCSEL input power values for which the rms EVM values, recorded at the output of the VCSEL-MMF-PD link, are much lower than the acceptable maximum values. It is important to ensure this in order to achieve a reasonable wireless range. For the GSM system, VCSEL input power values between -12.5 dBm and 17.2 dBm resulted in an average rms EVM value of 1.1% which is much lower than the maximum 7% rms EVM value (Table 4.3). Note that, in this case, the limit on the maximum input power to the VCSEL is imposed by the signal generator. For the UMTS and DPRS systems, input power values between -23.3 dBm and 7.3 dBm and between -18 dBm and -3 dBm respectively, should be used to operate the VCSEL. Such a limited VCSEL driving power range for the DPRS signal is expected since the maximum allowed rms EVM for it is only 2.6% (Table 4.3).

4.7 Conclusion

This chapter discusses some of the preliminary component characterisation measurements carried out for the design of a low-cost RoF link. Keeping in mind the low-cost approach to the design of the RoF link, 850 nm VCSELs and MMFs were used as the optical transmitter and the optical link respectively.

The main aim of carrying out these characterisation measurements was to obtain specific component parameter values that could be used as inputs to the link budget spreadsheet (discussed in Chapter 5) in order to predict the performance of the designed RoF link (discussed in Chapter 6).

Furthermore, transmission of digitally modulated signals (emulated GSM, DPRS and UMTS) over the VCSEL-MMF-PD link was also carried out. EVM measurements were used to analyse the effect of VCSEL non-linearity on the modulation scheme used for the transmitted signals. Additionally, these measurements aided in the determination of the range of input powers that could be fed to the VCSEL such that the EVM values for the complete optical link (VCSEL-MMF-PD link) were much lower than the maximum values (specified in the respective wireless standards) for the transmitted signals.

References

[1] ULM-850-00-TT-HSMAPP VCSEL (850 nm VCSEL with an SMA receptacle) datasheet as supplied by the manufacturer *ULM Photonics Inc.* (datasheet also available on *www.ulmphotonics.com*).

[2] PD1G5G-RO-M2-X-B1 1.5 GHz PIN photodiode module datasheet, *Appointech Inc.* (*www.appointech.com*).

[3] M. Sobhy, "Microwave circuits I," EL662 Course Notes (B.Eng. third year), University of Kent, 2000-2001.

[4] L.A. Coldren and E.R. Hegblom, "*Vertical-Cavity Surface-Emitting Lasers – Design, Fabrication, Characterization, and Applications*," Edited by C. Wilmsen, H. Temkin and L.A. Coldren, published by Cambridge University Press, 1999, Chapter 2, pp. 60-65.

[5] C. Carlsson, H. Martinsson, R. Schatz, J. Halonen, and A. Larsson, "Analog modulation properties of oxide confined VCSELs at microwave frequencies", *Journal of Lightwave Technology*, Vol. 20, No. 9, pp. 1740-1749, September 2002.

[6] S. Galt, A. Larsson, J. Gustavsson, P. Westbergh, E. Söderberg, S. Constant, and B. Cabon, "Report on the performance of the integration of VCSELs in low-cost radio-over-fibre systems," ISIS Deliverable 2.3 (www.isis-ist.org), June 2007.

[7] C. Carlsson, A. Larsson, and A. Alping, "RF transmission over multimode fibers using VCSELs – comparing standard and high-bandwidth multimode fibers," *Journal of Lightwave Technology*, Vol. 22, No. 7, pp. 1694-1700, July 2004.

[8] D. Wake, S. Dupont, C. Lethien, J-P. Vilcot, and D. Decoster, "Radiofrequency transmission of 32-QAM signals over multimode fibre for distributed antenna system applications," *Electronics Letters*, Vol. 37, No. 17 pp. 1087-1089, August 2001.

[9] K.A.G. Nkansah, "Millimetre-Wave Over Fibre System for Pico-Cellular Networks", Ph.D. Thesis, University of Kent, 2007.

[10] C. Cox III, E. Ackerman, R. Helkey, and G. E. Betts, "Techniques and performance of intensity-modulation direct-detection analog optical links," *IEEE Transactions on Microwave Theory and Techniques*, Vol. 45, No. 8, pp. 1375-1383, August 1997.

[11] S. Haykin and M. Moher, "*Modern wireless communications*," International edition published by Pearson Education, Inc., 2005.

[12] P. M. Shankar, "*Introduction to wireless systems*," published by John Wiley & Sons, Inc., 2002.

CHAPTER 5

SYSTEM LINK BUDGET THEORY

5.1 Introduction

The RAU designs and the choice of components for the RoF link have been discussed in the previous chapter. In order to achieve maximum coverage, it is important that the values of the component parameters be optimised. It is also important to ensure that the component parameter values (particularly the RAU amplifier gain values) obtained for the maximum achievable range do not make the system unstable. Therefore, to estimate the feasibility of the link and to understand the design trade-offs, a link budget analysis was carried out.

The link budget analysis allows radio range predictions for the designed RAUs. The analysis can be divided into wireless path, downlink optical path and uplink optical path calculations.

The block diagrams for the RoF links are shown in Figures 5.1 and 5.2, for the two-antenna RAU and the single-antenna RAU respectively. The parameters used for the link budget analysis have been labelled for each component and will be defined in the subsequent sections.

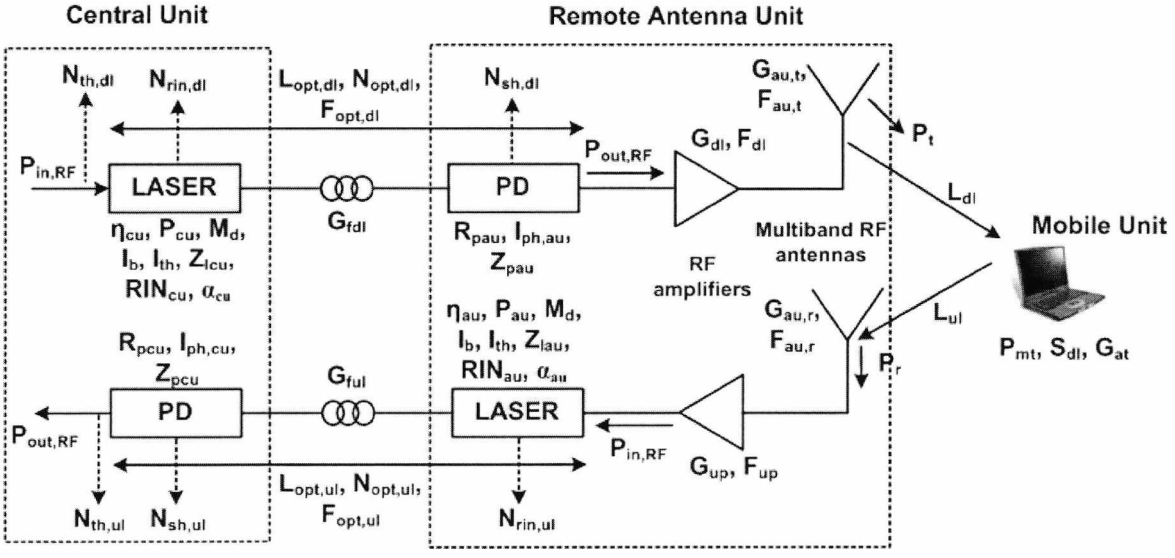

Figure 5.1. Block diagram of the RoF link using a two-antenna RAU

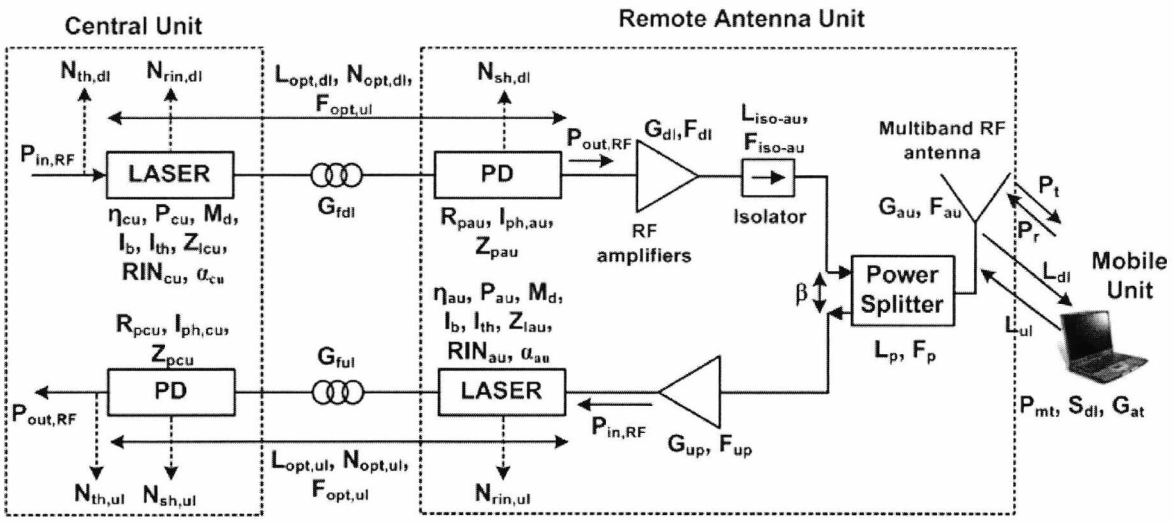

Figure 5.2. Block diagram of the RoF link using a single-antenna RAU

5.2 Wireless Path

The Keenan-Motley propagation model [1] is frequently used for calculating path loss (*PL*) in indoor environments. This model primarily explains radio coverage and propagation within buildings. It, therefore, models a complicated environment, also taking into account the loss when the signal passes through walls and floors, in addition to the loss due to free-space propagation. A simple interpretation of the Keenan-Motley model is given by the following path loss equation [1]:

$$PL = \left(\frac{4\pi f}{c}\right)^2 d^n (10^{kF})(10^{pw}) \tag{5.1}$$

Here, f is the frequency of the RF signal, c is the velocity of light, d is the distance between the transmitter and receiver, k is the floor factor in dB (attenuation per floor), F is the number of floors between the transmitter and receiver, p is the wall factor in dB (attenuation per wall) and w is the number of walls between the transmitter and receiver. The path loss exponent n is a characteristic of the propagation environment and typically takes on values of 3 to 4 for indoor environments.

However, as all the measurements are to be carried out in a single room with line of sight (LOS) condition between the transmitter and receiver, the effects of transmission

loss through walls and floors can be ignored. Using this assumption, the Keenan-Motley equation reduces to the open-space path loss equation, with a modified path loss exponent n [2] (n=2 for open-space environment):

$$PL = \left(\frac{4\pi f}{c}\right)^2 d^n \tag{5.2}$$

where the parameters are as defined for Equation 5.1.

5.2.1 Determining the Path Loss Exponent

To correctly model the target environment, the path loss exponent was empirically determined for the office room where the measurements were to be conducted. For this purpose, the floor of the target room was divided into squares of $1m^2$ area and RF signal coverage measurements were carried out. A 2.5 GHz signal was generated using an RF signal generator (*Agilent E4438C*) and fed into the transmit antenna (in the RAU) mounted at one end of the ceiling, at approximately equal distances from the side walls (It must be noted that since the primary aim was to design a WLAN system demonstrator, a frequency of 2.5 GHz was utilised in these measurements. In order to determine the path loss exponents for the transmission of other wireless systems such as GSM and UMTS, the corresponding frequencies must be used in the measurements). The room was modelled as a 2-D surface with the x-axis along the width of the room and the y-axis along the length of the room. The 3rd dimension along the z-axis is constant as all the measurements were made at a constant table-top height (i.e. the distance between the ceiling and the measurement points is constant). Finally, the received signal strength was measured at 30 different points in the room, for which the signal intensity distribution is shown in Figure 5.3:

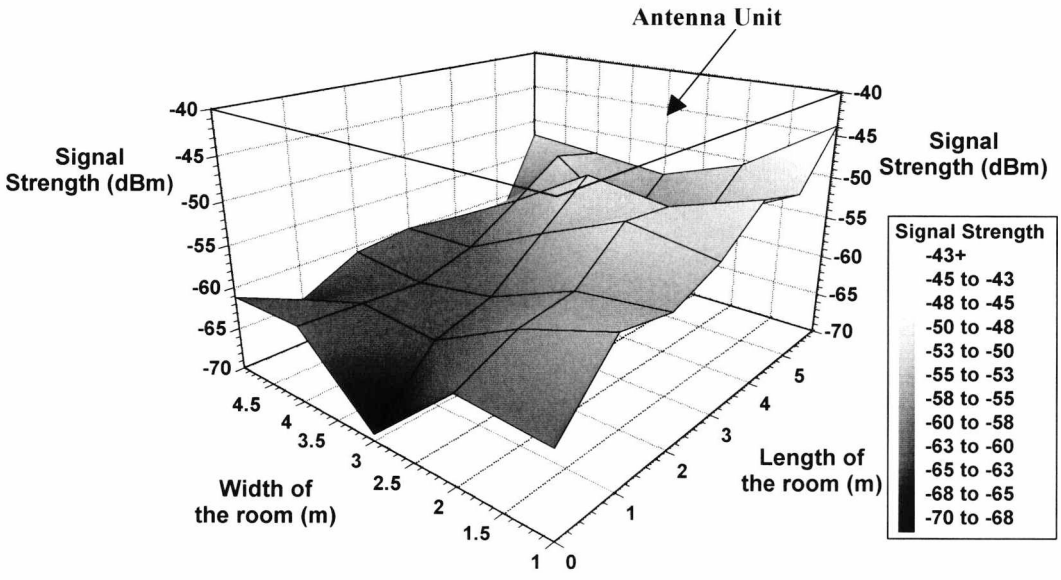

Figure 5.3. Signal intensity variation in the target room

As expected, the signal strength decreases as we move away from the RAU. Path loss was calculated from the received signal strength and plotted as a function of distance. The RF path loss was also calculated using Equation 5.2 and n for the room was determined by varying n in Equation 5.2 to best fit the measured path loss. For instance, based on the measurements illustrated in Figure 5.3, n was calculated to be equal to 3.2. Finally, the path loss exponent calculated using this method was substituted in Equation 5.2 and implemented in the link budget for estimating the path loss in the target room, for increasing distances from the RAU.

5.3 Downlink Optical Path

The input RF power ($P_{in,RF}$) to the central unit laser needs to be chosen such that distortion is avoided. A high $P_{in,RF}$ results in a high modulation index (M_d), which has been reported to result in a high EVM, especially important for systems using OFDM modulation (e.g. IEEE 802.11g at 54 Mbps) [3]. The modulation index may be calculated from $P_{in,RF}$ using the following equation:

$$M_d = \frac{\sqrt{2P_{in,RF}/Z_{lcu}}}{(I_b - I_{th})} \tag{5.3}$$

where, Z_{lcu} is the CU laser impedance, I_b is the laser bias current and I_{th} is the laser threshold current.

Using $P_{in,RF}$ and M_d, the RF power at the output of the laser-fibre-PD link ($P_{out,RF}$) may be calculated as:

$$P_{out,RF} = \frac{(P_{cu} M_d \alpha_{cu} G_{fdl} R_{pau})^2 Z_{pau}}{2} \tag{5.4}$$

where, P_{cu} is the optical output power from the CU laser, R_{pau} is the responsivity of the RAU photodiode, Z_{pau} is the RAU PD impedance, α_{cu} is the frequency response factor of the CU laser and G_{fdl} is the gain[1] of the downlink fibre measured at a particular frequency.

For a given I_b and I_{th}, the optical output power from the laser, P_{cu}, may be calculated as:

$$P_{cu} = \eta_{cu}(I_b - I_{th}) \tag{5.5}$$

where, η_{cu} is the slope efficiency of the CU laser and can be calculated from the P-I characteristic curve of the laser (discussed in Section 4.2, Chapter 4). Note that the above equation is applicable only to the linear region of the P-I characteristics.

Due to packaging effects and laser resonance frequency, the RF modulation response of the laser becomes frequency dependent. In order to incorporate this frequency dependence, the frequency response factor, α_{cu}, is included in Equation 5.4 for the CU laser. α takes into account laser frequency response variations that would not be modelled using the static slope efficiency. It is calculated as the ratio of the measured gain of the laser-PD link at a particular frequency (found from the frequency response curve of the laser shown in Section 4.3, Chapter 4) and the calculated gain of the laser-PD link. The gain of the laser-PD link depends on the RF output power of the back-to-back laser-PD link, $P_{l,RF}$, which may be calculated as:

$$P_{l,RF} = \frac{(P_{cu} M_d R_{pau})^2 Z_{pau}}{2} \tag{5.6}$$

[1] Note that G_{fdl} is the optical gain of the fibre. Optical gain = (RF gain)$^{1/2}$.

Substituting the values of M_d and P_{cu}, from Equations 5.3 and 5.5 respectively, into Equation 5.4, $P_{out,RF}$ may be written as:

$$P_{out,RF} = P_{in,RF}(\eta_{cu}\alpha_{cu}G_{fdl}R_{pau})^2\left(\frac{Z_{pau}}{Z_{lcu}}\right) \tag{5.7}$$

Once $P_{in,RF}$ has been set and $P_{out,RF}$ has been calculated, the downlink (DL) optical insertion loss, $L_{opt,dl}$, can then be evaluated as:

$$L_{opt,dl} = \frac{P_{in,RF}}{P_{out,RF}} = \left(\frac{1}{(\eta_{cu}\alpha_{cu}G_{fdl}R_{pau})^2}\right)\left(\frac{Z_{lcu}}{Z_{pau}}\right) \tag{5.8}$$

In terms of $P_{in,RF}$ and $L_{opt,dl}$, the effective isotropic radiated power (P_t) for a two-antenna RAU can be written as:

$$P_t = \left(\frac{P_{in,RF}}{L_{opt,dl}}\right)G_{dl}G_{au,t} \tag{5.9}$$

where, G_{dl} is the DL amplifier gain and $G_{au,t}$ is the two-antenna RAU transmit antenna gain.

For a single-antenna RAU, P_t is further reduced by the insertion losses of the isolator ($L_{iso\text{-}au}$) and the power divider (L_p), and may therefore be expressed as:

$$P_t = \frac{(P_{in,RF}/L_{opt,dl})G_{dl}G_{au}}{L_{iso-au}L_p} \tag{5.10}$$

where, G_{au} is the single-antenna RAU antenna gain.

Finally, using P_t, the maximum tolerable DL propagation loss (L_{dl}) may be calculated as:

$$L_{dl} = \frac{P_t G_{at}}{S_{dl}} \tag{5.11}$$

where, S_{dl} is the DL receiver (i.e. the mobile unit) sensitivity specified for each standard and G_{at} is the mobile terminal antenna gain.

The above calculated loss was matched against the propagation loss values calculated using Equation 5.2 for the different distances and the range for which the closest match (calculated loss value equal to or less than the propagation loss value for that range) was obtained was quoted to be the maximum achievable range for the DL.

5.4 Uplink Optical Path

The uplink radio range calculations depend ultimately on the receiver equipment sensitivity at the CU, that is defined in terms of a minimum detectable signal ($S_{ul,s}$). The value of $S_{ul,s}$ is obtained from the standards or may be specified by the equipment manufacturer. This leads to a minimum RF power required to drive the UL laser, and a minimum UL power at the receive antenna (P_r). However, additional noise from the optical link increases the total uplink noise floor which in turn, causes an increase in $S_{ul,s}$. The final value of the uplink minimum detectable signal (S_{ul}) may then be written as:

$$S_{ul} = S_{ul,s} + (C/N)N_{tot,ul} \tag{5.12}$$

where, C/N is the required carrier to noise ratio at the receiver specified in the relevant documents for each standard and $N_{tot,ul}$ is the total output UL noise power.

$N_{tot,ul}$ is defined as:

$$N_{tot,ul} = F_{tot,ul}kTG_{tot,ul} \tag{5.13}$$

where, k is Boltzmann's constant, T is the ambient room temperature (290K). $G_{tot,ul}$ and $F_{tot,ul}$ are the cascaded gain and the cascaded noise factor of the overall uplink subsystem respectively, and may be calculated using the standard cascade relationships [4]. For the two-antenna RAU, $F_{tot,ul}$ and $G_{tot,ul}$ may be written as:

$$F_{tot,ul} = F_{au,r} + \frac{F_{up} - 1}{G_{au,r}} + \frac{F_{opt,ul} - 1}{G_{au,r} G_{up}} + \frac{(F_{cu} - 1) L_{opt,ul}}{G_{au,r} G_{up}} \tag{5.14a}$$

$$G_{tot,ul} = \frac{G_{au,r} G_{up} G_{cu}}{L_{opt,ul}} \tag{5.14b}$$

where, $F_{au,r}$, F_{up} and $F_{opt,ul}$ are the noise factors for the receive antenna, uplink amplifier and uplink optical path respectively and $L_{opt,ul}$ is the UL optical insertion loss; $G_{au,r}$ is the gain of the receive antenna for the two-antenna RAU and G_{up} is the UL amplifier gain. In order to account for any new components[2] that may be added after the photodiode at the CU, F_{cu} and G_{cu} represent the additional noise factor and gain respectively. Similar cascaded equations may be written for calculating $F_{tot,ul}$ and $G_{tot,ul}$ for the single-antenna RAU:

$$F_{tot,ul} = F_{au} + \frac{F_p - 1}{G_{au}} + \frac{(F_{up} - 1) L_p}{G_{au}} + \frac{(F_{opt,ul} - 1) L_p}{G_{au} G_{up}} + \frac{(F_{cu} - 1) L_p L_{opt,ul}}{G_{au} G_{up}} \tag{5.15a}$$

$$G_{tot,ul} = \frac{G_{au} G_{up} G_{cu}}{L_p L_{opt,ul}} \tag{5.15b}$$

where, F_p (= L_p) is the noise factor for the power-splitter/combiner.

For calculating $F_{tot,ul}$, the noise factor of the uplink optical path needs to be determined as:

$$F_{opt,ul} = \frac{N_{opt,ul} L_{opt,ul}}{kT} \tag{5.16}$$

where $N_{opt,ul}$ is the total noise power at the output of the optical link. $N_{opt,ul}$, is calculated as the sum of the individual noise powers contributed by the components. It is written as:

$$N_{opt,ul} = N_{rin,ul} + N_{sh,ul} + N_{th,ul} \tag{5.17}$$

[2] As will be seen in Chapter 6, the designed RoF link for the transmission of WLAN signals uses an additional isolator and circulator at the CU.

where, $N_{rin,ul}$ is the RIN noise power of the uplink VCSEL, $N_{sh,ul}$ is the shot noise power of the photodiode at the CU and $N_{th,ul}$ is the thermal noise power measured at the output of the CU PD.

As stated in Chapter 4 (Equations 4.5 - 4.6), $N_{sh,ul}$ and $N_{rin,ul}$ are calculated as:

$$N_{sh,ul} = 2qZ_{pcu}I_{ph,cu} \tag{5.18}$$

$$N_{rin,ul} = \{10\text{^}(RIN_{au}/10)\}I_{ph,cu}^2 Z_{pcu} \tag{5.19}$$

where, q is the electronic charge, Z_{pcu} is the CU PD impedance, $I_{ph,cu}$ is the measured dc photocurrent and RIN_{au} is the relative intensity noise (in dB/Hz) of the RAU laser. Both $N_{th,ul}$ and RIN_{au} demonstrate frequency dependence and were therefore experimentally determined for each of the standards (using measurement methods discussed in Chapter 4, Section 4.4).

As the UL and DL paths are similar, $L_{opt,ul}$ may be calculated in the same way as $L_{opt,dl}$ as shown in Equation 5.8:

$$L_{opt,ul} = \left(\frac{1}{(\eta_{au}\alpha_{au}G_{ful}R_{pcu})^2}\right)\left(\frac{Z_{pcu}}{Z_{lau}}\right) \tag{5.20}$$

where, η_{au} is the RAU laser slope efficiency, α_{au} is the frequency factor of the RAU laser, G_{ful} is the gain of the UL fibre (determined from the frequency response of the fibre), R_{pcu} is the CU PD Responsivity and Z_{lau} is the RAU laser impedance.

Once $N_{tot,ul}$ is calculated and S_{ul} determined, P_r for the two-antenna RAU is calculated as:

$$P_r = \frac{S_{ul}L_{opt,ul}}{G_{au,r}G_{up}} \tag{5.21}$$

For a single-antenna RAU, the splitter ratio of the power-splitter (β) also contributes to the value of P_r. Therefore, P_r for the single-antenna RAU may be written as:

$$P_r = \frac{S_{ul} L_{opt,ul} \beta}{G_{au} G_{up}} \tag{5.22}$$

The maximum tolerable UL propagation loss (L_{ul}) is then calculated as:

$$L_{ul} = \frac{P_{mt}}{P_r} \tag{5.23}$$

where, P_{mt} is the mobile transmit power (and includes G_{at}) specified in the ETSI documents for each standard. Using L_{ul}, the maximum achievable UL range may be determined by comparison with Equation 5.2, in the same way as for the DL.

5.5 Additional Restrictions

Although the above equations represent the link budget for each direction of operation, further restrictions are posed in a real system.

5.5.1 Loop Gain

The RAU subsystem forms a loop with its DL and UL branches as shown in Figures 5.4 and 5.5.

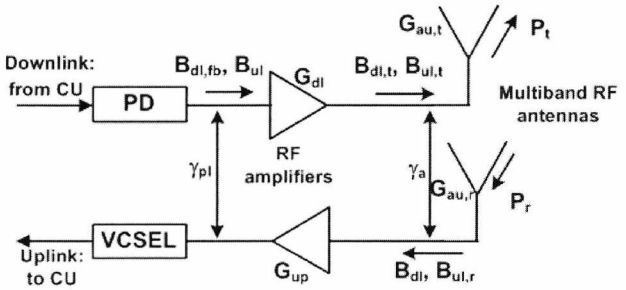

Figure 5.4. Two-antenna RAU with the bleed signals labelled

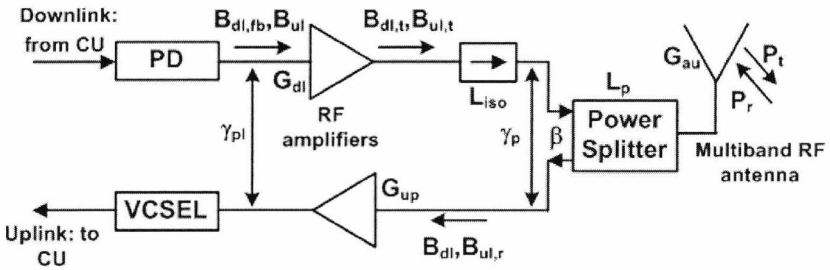

Figure 5.5. Single-antenna RAU with the bleed signals labelled

In this loop, DL bleed occurs when a part of the downlink signal, before reaching the antenna (transmit antenna, in the case of a two-antenna RAU), is coupled into the uplink due to imperfect isolation between the two RAU antennas or the power-splitter/combiner (for the single-antenna RAU). The DL bleed for the two-antenna RAU may be written as:

$$B_{dl} = \frac{P_t}{G_{au,t}\gamma_a} \tag{5.24a}$$

where, γ_a is the isolation between the two antennas. For the single-antenna RAU, this DL bleed may be written as:

$$B_{dl} = \frac{P_t L_p}{G_{au}\gamma_p} \tag{5.24b}$$

where, γ_p is the isolation between the two ports of the power-splitter.

As can be seen from Figures 5.4 and 5.5, due to insufficient isolation (γ_{pl}) between the DL and UL paths at the laser-PD end of the RAU, B_{dl} is coupled back to the downlink path. This fed-back DL bleed signal ($B_{dl,fb}$) for both the RAUs may be written as:

$$B_{dl,fb} = \frac{B_{dl} G_{up}}{\gamma_{pl}} \tag{5.25}$$

$B_{dl,fb}$, after amplification (by the DL amplifier), reaches the antenna (transmit antenna in the case of the two-antenna RAU) and may cause interference with the transmitted DL signal (P_t). If the amplifier gains are high enough, this can also cause oscillation in the

circuit. The DL bleed signal just before the transmit antenna ($B_{dl,t}$) for the two-antenna RAU may be written as:

$$B_{dl,t} = B_{dl,fb} G_{dl} \tag{5.26}$$

Substituting the values of $B_{dl,fb}$ (from Equation 5.25) and B_{dl} (from Equation 5.24a) in Equation 5.26, $B_{dl,t}$ for the two-antenna RAU may then be written as:

$$B_{dl,t} = \frac{P_t G_{up} G_{dl}}{G_{au,t} \gamma_a \gamma_{pl}} \tag{5.27}$$

For the single-antenna RAU, after amplification at the DL amplifier, $B_{dl,fb}$ suffers a loss at the isolator before arriving at the power-splitter (as shown in Figure 5.5). Therefore, for the single-antenna RAU, $B_{dl,t}$ may be written as:

$$B_{dl,t} = \frac{B_{dl,fb} G_{dl}}{L_{iso-au}} \tag{5.28}$$

Again, substituting the values of $B_{dl,fb}$ (from Equation 5.25) and B_{dl} (from Equation 5.24b) in Equation 5.28, $B_{dl,t}$ may then be written as:

$$B_{dl,t} = \frac{P_t L_p G_{up} G_{dl}}{G_{au} \gamma_p \gamma_{pl} L_{iso-au}} \tag{5.29}$$

Similarly, for the UL path in the two-antenna RAU, a part of the received signal (P_r) (after being amplified by the UL amplifier) is coupled to the DL path (B_{ul}) again due to inadequate isolation between the DL and UL paths at the laser-PD end of the RAU. This UL bleed, B_{ul}, after amplification (by the DL amplifier) arrives at the transmit antenna as $B_{ul,t}$. This is then coupled again to the UL path as $B_{ul,r}$, as shown in Figure 5.4. Applying the same principles as for the DL bleed, $B_{ul,r}$ may be written as:

$$B_{ul,r} = \frac{P_r G_{au,r} G_{up} G_{dl}}{\gamma_{pl} \gamma_a} \tag{5.30}$$

For the single-antenna RAU, additional parameters such as β and $L_{iso\text{-}au}$ affect $B_{ul,r}$ and it may be therefore written as:

$$B_{ul,r} = \frac{P_r G_{au} G_{up} G_{dl}}{\beta \gamma_{pl} L_{iso-au} \gamma_p} \tag{5.31}$$

This fed-back UL bleed signal may cause interference with the received uplink signal. For high amplifier gains, this can not only cause an oscillation in the link (as in the case of DL bleed) but can also lead to an additional drive to the UL laser.

For the two-antenna RAU, the loop gain for the downlink and uplink paths may be written as:

$$G_{loop,dl} = \frac{B_{dl,t}}{(P_t / G_{au,t})} \tag{5.32a}$$

$$G_{loop,ul} = \frac{B_{ul,r}}{P_r G_{au,r}} \tag{5.32b}$$

In order to avoid oscillation (with some margin) the maximum loop gain was set to be less than -10 dB (0.1). Substituting values of $B_{dl,t}$ (from Equation 5.27) and $B_{ul,r}$ (from Equation 5.30) in Equations 5.32a and 5.32b respectively, the loop gain condition for the two-antenna RAU may be written as:

$$\frac{G_{up} G_{dl}}{\gamma_a \gamma_{pl}} \leq 0.1 \tag{5.33}$$

For the single-antenna RAU, the loop gain for the downlink and uplink paths may be written as:

$$G_{loop,dl} = \frac{B_{dl,t}}{(P_t L_p / G_{au})} \tag{5.34a}$$

$$G_{loop,ul} = \frac{B_{ul,r}}{(P_r G_{au} / \beta)} \tag{5.34b}$$

Again for a loop gain less than -10 dB (0.1), substituting the values of $B_{dl,t}$ (from Equation 5.29) and $B_{ul,r}$ (from Equation 5.31) in Equations 5.34a and 5.34b respectively, the loop gain condition for the single-antenna RAU may be written as:

$$\frac{G_{up}G_{dl}}{\gamma_p \gamma_{pl} L_{iso-au}} \leq 0.1 \tag{5.35}$$

With such a margin for the loop gain it has been calculated that the signal coupled back into the downlink causes little interference to the actual downlink signal, and that the total signal level for the uplink (the signal applied to the RAU laser) is not increased significantly, so having little effect on the uplink capping limit (discussed in the following sub-section).

5.5.2 Uplink Capping

As discussed in Section 5.4, the uplink receiver sensitivity (S_{ul}) sets a limit on the minimum RF power that is required to drive the uplink VCSEL. This requirement defines the lower limit for the uplink amplifier gain values which should be high enough to allow distant mobile units to communicate with the receiver at the CU. Similarly, it is equally important take into consideration the RF power that will be received at the RAU antenna from mobile units that are very close to the RAU. The upper limit on the uplink amplifier gain values is, therefore, set by the maximum amplified RF power that can be fed to the RAU laser ($P_{r,max}$) without causing distortion. $P_{r,max}$ is calculated as the RF power that reaches the RAU laser when the mobile unit is at a minimum distance (d_{min}) from the RAU. Figures 5.6 and 5.7 show the uplink paths for the two-antenna RAU and the single-antenna RAU respectively.

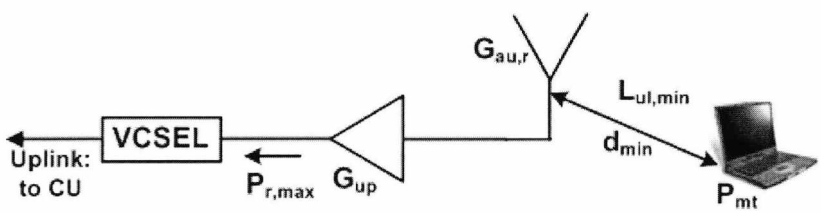

Figure 5.6. Determining the capping condition for the two-antenna RAU

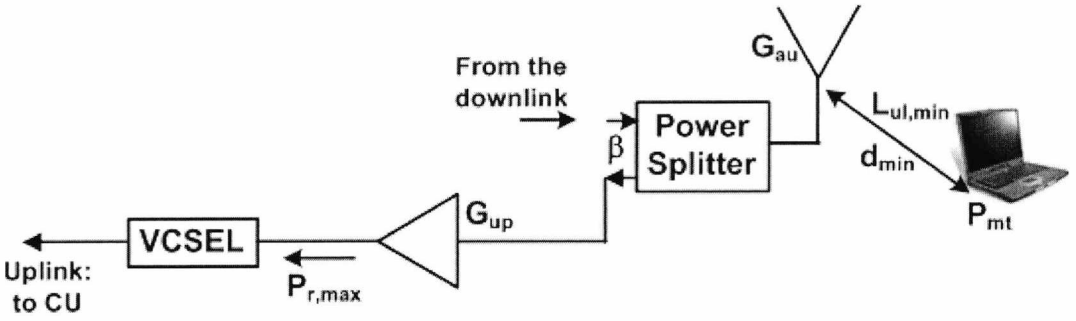

Figure 5.7. Determining the capping condition for the single-antenna RAU

From Figure 5.6, $P_{r,max}$ for the two-antenna RAU may be calculated as:

$$P_{r,\max} = \frac{P_{mt} G_{au,r} G_{up}}{L_{ul,\min}} \tag{5.36}$$

where, $L_{ul,min}$ is the path loss at d_{min}. For the single-antenna RAU, $P_{r,max}$ is reduced further due to β of the power-splitter (as shown in Figure 5.7) and may be written as:

$$P_{r,\max} = \frac{P_{mt} G_{au} G_{up}}{L_{ul,\min} \beta} \tag{5.37}$$

For the calculations, $P_{r,max}$ was set to be equal to $P_{in,RF}$ (for the CU laser). d_{min} was calculated as the distance between the mobile unit and the RAU when the mobile unit was directly below the RAU. For example, the majority of measurements carried out in this research have been targeted at the transmission of WLAN signals over the designed RoF link. In this case, assuming the height of the ceiling (where the RAU is mounted) to be 2.6 m and the height of the table on which the mobile unit (e.g. laptop) is placed to be 0.9 m, d_{min} will be equal to 1.7 m.

5.5.3 Transmitted Noise

Equations similar to Equations 5.13 – 5.19 were used to calculate the total transmitted (downlink) noise power ($N_{tot,dl}$) components. The amplifier gains were calculated such that $N_{tot,dl}$ was within acceptable limits as defined by IEEE or ETSI standards. These limits for the different wireless standards (GSM, UMTS and WLAN) along with the spreadsheet-calculated downlink transmitted noise powers have been listed in Chapter 6 (Section 6.3).

As for the uplink (Equation 5.13), $N_{tot,dl}$ is defined as:

$$N_{tot,dl} = F_{tot,dl} kTG_{tot,dl} \tag{5.38}$$

where, $G_{tot,dl}$ and $F_{tot,dl}$ are the cascaded gain and the cascaded noise factor of the overall downlink subsystem respectively.

Based on Equations 5.14a and 5.14b, $F_{tot,dl}$ and $G_{tot,dl}$ for the two-antenna RAU may be written as:

$$F_{tot,dl} = F_{cu} + \frac{F_{opt,dl} - 1}{G_{cu}} + \frac{(F_{dl} - 1)L_{opt,dl}}{G_{cu}} + \frac{(F_{au,t} - 1)L_{opt,dl}}{G_{cu}G_{dl}} \tag{5.39a}$$

$$G_{tot,dl} = \frac{G_{au,t}G_{dl}G_{cu}}{L_{opt,dl}} \tag{5.39b}$$

where, $F_{au,t}$, F_{dl} and $F_{opt,dl}$ are the noise factors for the transmit antenna, downlink amplifier and downlink optical path, respectively. From Equations 5.15a and 5.15b, $F_{tot,dl}$ and $G_{tot,dl}$ for the single-antenna RAU may be written as:

$$F_{tot,dl} = F_{cu} + \frac{F_{opt,dl} - 1}{G_{cu}} + \frac{(F_{dl} - 1)L_{opt,dl}}{G_{cu}} + \frac{(F_{iso-au} - 1)L_{opt,dl}}{G_{cu}G_{dl}} + \frac{(F_{au} - 1)L_{iso-au}L_{opt,dl}}{G_{cu}G_{dl}} \tag{5.40a}$$

$$G_{tot,dl} = \frac{G_{au}G_{dl}G_{cu}}{L_{iso-au}L_{opt,dl}} \tag{5.40b}$$

where, $F_{iso\text{-}au}$ ($L_{iso\text{-}au}$) is the noise factor for the isolator used in the single-antenna RAU.

For calculating $F_{tot,dl}$, the noise factor of the downlink optical path ($F_{opt,dl}$) needs to be determined as:

$$F_{opt,dl} = \frac{N_{opt,dl}L_{opt,dl}}{kT} \tag{5.41}$$

where $N_{opt,dl}$ is the total noise power at the output of the downlink optical path.

$N_{opt,dl}$ is calculated as the sum of the individual noise powers contributed by the downlink optical components (as for the uplink). It is written as:

$$N_{opt,dl} = N_{rin,dl} + N_{sh,dl} + N_{th,dl} \tag{5.42}$$

where, $N_{rin,dl}$ is the RIN noise power of the downlink VCSEL, $N_{sh,dl}$ is the shot noise power of the photodiode at the RAU and $N_{th,dl}$ is the thermal noise power measured at the output of the photodiode at the RAU.

Again, using Equations 4.5 - 4.6 from Chapter 4, $N_{sh,dl}$ and $N_{rin,dl}$ are calculated as:

$$N_{sh,dl} = 2qZ_{pau}I_{ph,au} \tag{5.43}$$

$$N_{rin,dl} = \{10\text{^}(RIN_{cu}/10)\}I_{ph,au}^2 Z_{pau} \tag{5.44}$$

where, $I_{ph,au}$ is the measured dc photocurrent for the RAU PD and RIN_{cu} is the relative intensity noise (in dB/Hz) of the CU laser. As in the case of uplink, $N_{th,dl}$ and RIN_{cu} were experimentally determined for each of the standards (using the measurement methods discussed in Chapter 4).

5.6 Link Budget Spreadsheet Implementation

The relevant equations were implemented using a Microsoft Excel spreadsheet to calculate the maximum achievable ranges for both the two-antenna RAU and the single-antenna RAU, for the transmission of different wireless systems. Figure 5.8 is a screen-shot of the range calculation being carried out in the spreadsheet, with the highlighted cell (cell K15) showing the calculation of the UL optical insertion loss (Equation 5.20).

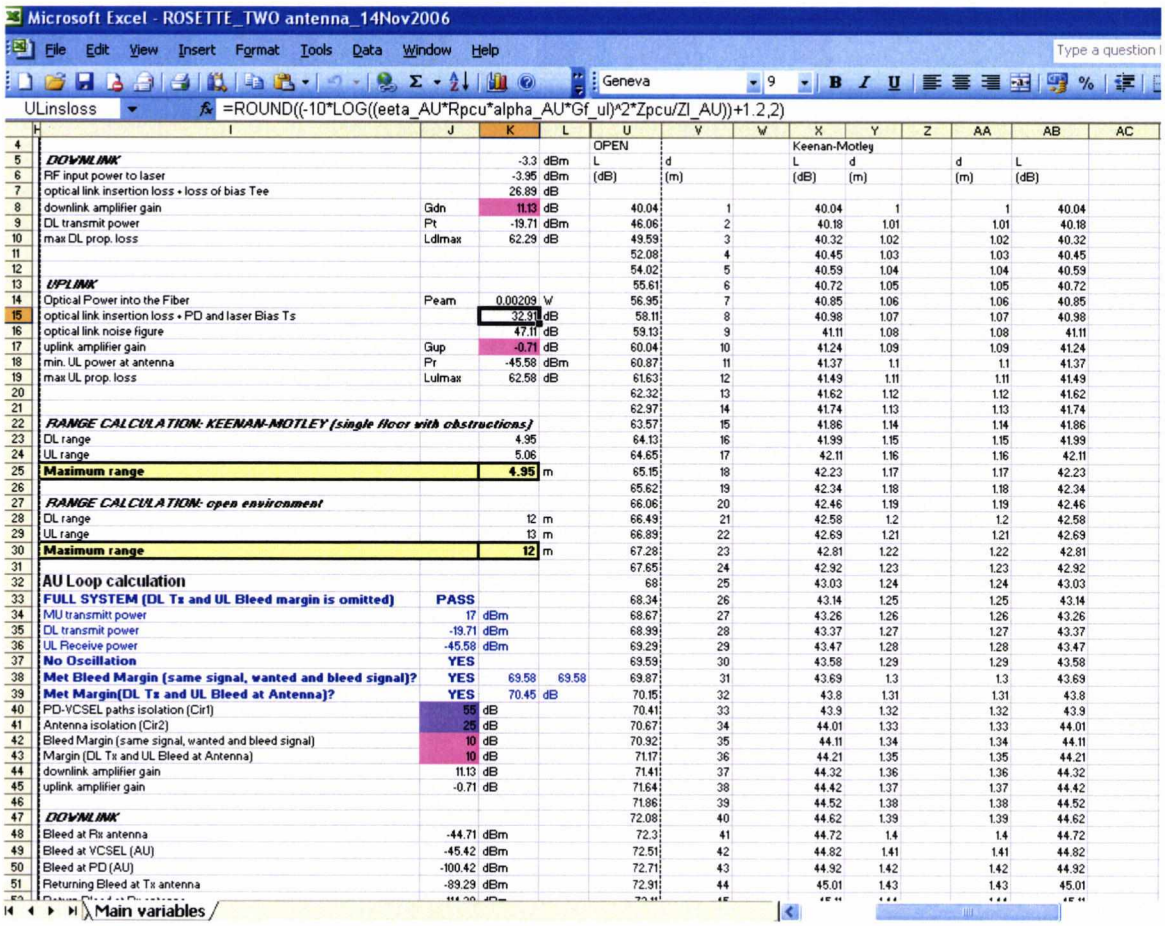

Figure 5.8. Screen-shot of the spreadsheet showing the range calculation

The different component parameter values obtained using the characterisation measurements described in the previous chapter (Chapter 4) were used as inputs to the link budget spreadsheet. The parameter list in the spreadsheet is shown in Figure 5.9.

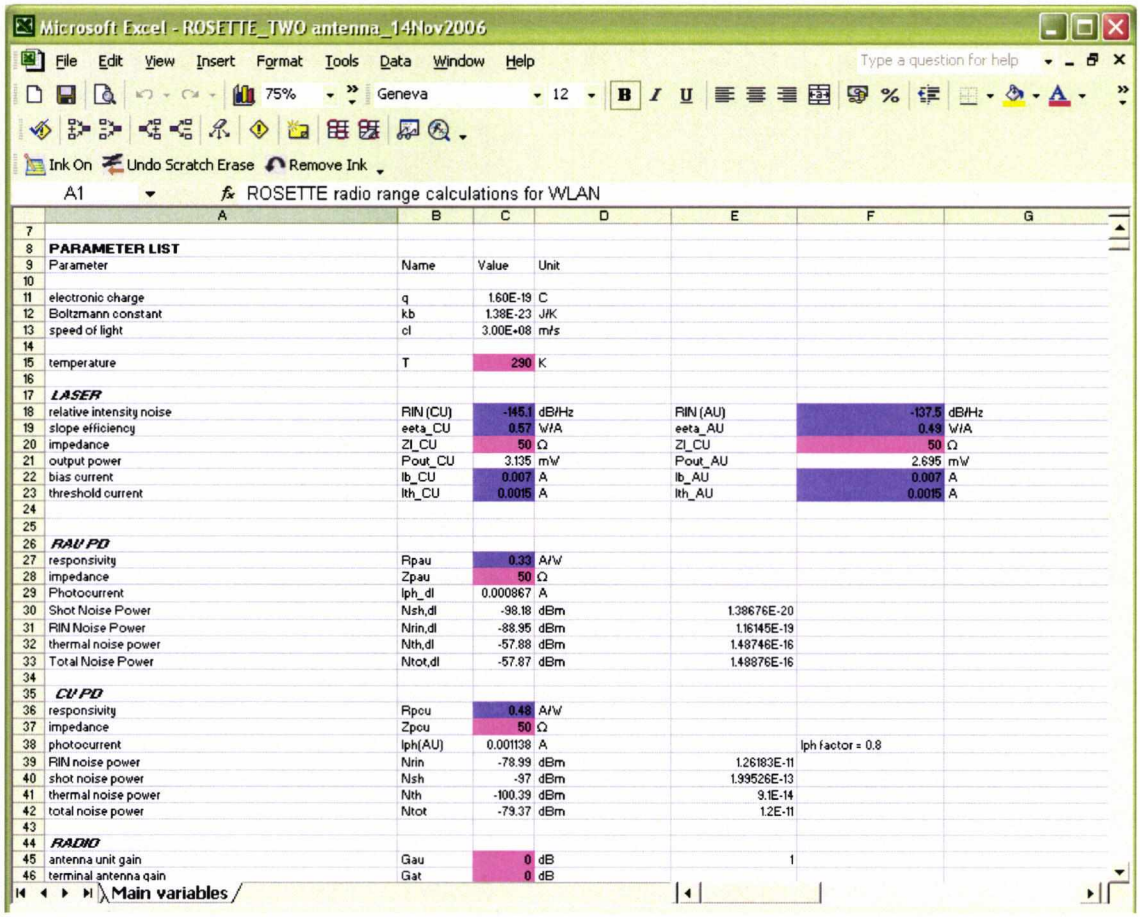

	A	B	C	D	E	F	G
7							
8	**PARAMETER LIST**						
9	Parameter	Name	Value	Unit			
10							
11	electronic charge	q	1.60E-19	C			
12	Boltzmann constant	kb	1.38E-23	J/K			
13	speed of light	cl	3.00E+08	m/s			
14							
15	temperature	T	290	K			
16							
17	***LASER***						
18	relative intensity noise	RIN (CU)	-145.1	dB/Hz	RIN (AU)	-137.5	dB/Hz
19	slope efficiency	eeta_CU	0.57	W/A	eeta_AU	0.43	W/A
20	impedance	ZI_CU	50	Ω	ZI_CU	50	Ω
21	output power	Pout_CU	3.135	mW	Pout_AU	2.695	mW
22	bias current	Ib_CU	0.007	A	Ib_AU	0.007	A
23	threshold current	Ith_CU	0.0015	A	Ith_AU	0.0015	A
24							
25							
26	***PAU PD***						
27	responsivity	Rpau	0.33	A/W			
28	impedance	Zpau	50	Ω			
29	Photocurrent	Iph_dl	0.000867	A			
30	Shot Noise Power	Nsh,dl	-98.18	dBm	1.38676E-20		
31	RIN Noise Power	Nrin,dl	-88.95	dBm	1.16145E-19		
32	thermal noise power	Nth,dl	-57.88	dBm	1.48746E-16		
33	Total Noise Power	Ntot,dl	-57.87	dBm	1.48876E-16		
34							
35	***CU PD***						
36	responsivity	Rpcu	0.48	A/W			
37	impedance	Zpcu	50	Ω			
38	photocurrent	Iph(AU)	0.001138	A		Iph factor = 0.8	
39	RIN noise power	Nrin	-78.99	dBm	1.26183E-11		
40	shot noise power	Nsh	-97	dBm	1.99526E-13		
41	thermal noise power	Nth	-100.39	dBm	9.1E-14		
42	total noise power	Ntot	-79.37	dBm	1.2E-11		
43							
44	***RADIO***						
45	antenna unit gain	Gau	0	dB	1		
46	terminal antenna gain	Gat	0	dB			

Figure 5.9. Screen-shot of the spreadsheet showing the parameter list

The calculations were automated and carried out iteratively such that the restrictions (discussed in Section 5.5) posed limits on the amplifier gains. Figure 5.10 shows a screen-shot of a part of the macro program used to automate the range calculation. In particular, the code implemented to incorporate the loop gain restriction discussed in Section 5.5.1 is depicted.

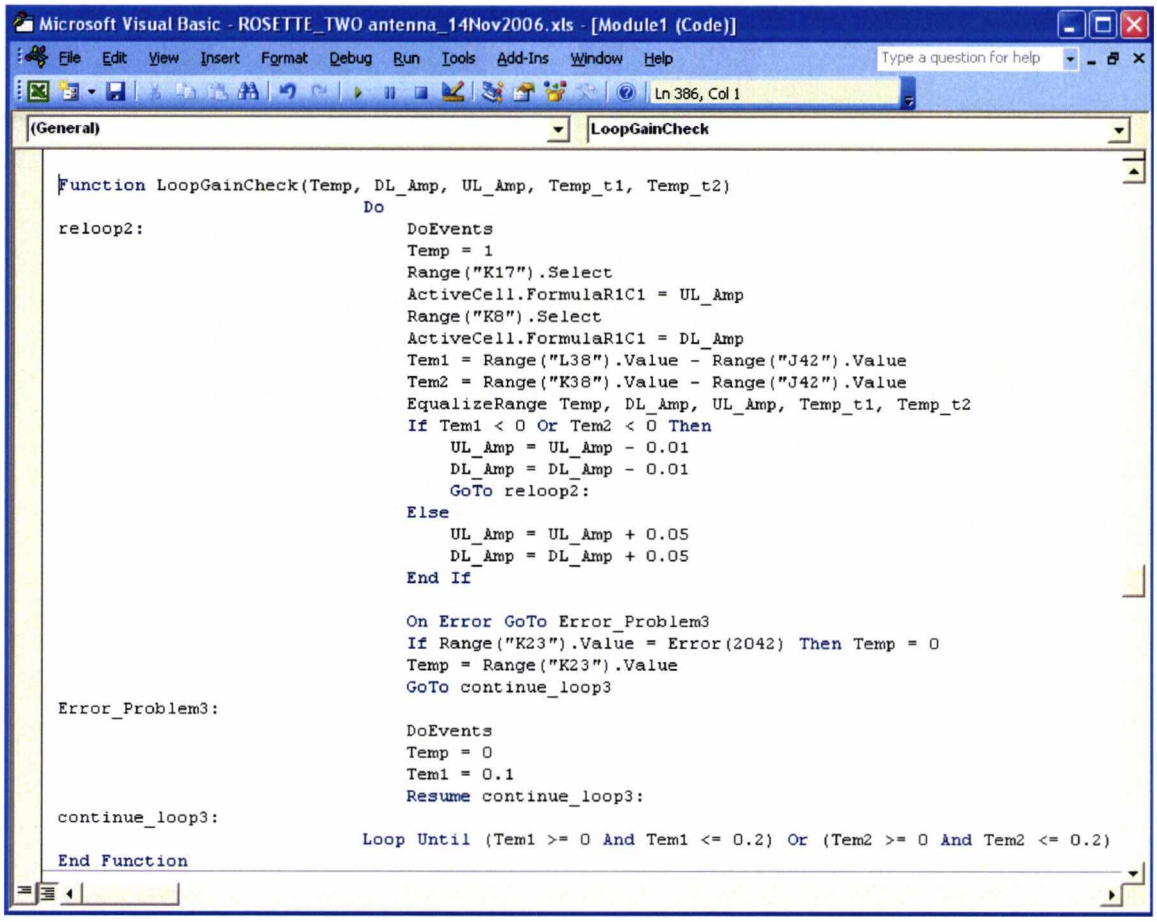

Figure 5.10. Screen-shot of the macro program used to automate the spreadsheet range calculation

5.7 Conclusion

In this chapter, a link budget analysis has been developed for the bi-directional operation of a fibre-fed indoor wireless network. The analysis allows for the optimisation of component values to obtain the best possible range, while taking into account restrictions such as crosstalk and noise emissions.

The next chapter discusses the deployment of a WLAN system demonstrator for a typical office environment based on the results of the link budget analysis. The performance of the system demonstrator is characterised using signal strength and throughput measurements.

References

[1] T.S. Rapapport and S. Sandhu, "Radio-Wave propagation for emerging wireless personal-communication systems," *IEEE Antennas and Propagation Magazine*, Vol. 36, pp. 14-23, October 1994.

[2] RF Monolithic Inc. (RFM), "ASH Transceiver Designer's Guide," Dallas, Texas, pp. 51, May 2004.

[3] H. Sasai, T. Niiho, K. Tanaka, and K. Utsumi, "Radio over fibre transmission performance of OFDM signal for dual-band wireless LAN systems," *2003 International Topical Meeting on Microwave Photonics*, Budapest, Hungary, pp. 139–142, September 2003.

[4] T.S. Rappaport, "*Wireless Communications – Principles and Practice*," Appendix B, Prentice Hall PTR, Upper Saddle River, New Jersey, pp. 565-568, 1996.

CHAPTER 6
EXPERIMENTAL DEMONSTRATION OF THE TRANSMISSION OF WIRELESS SYSTEMS OVER A RADIO-OVER-MULTIMODE FIBRE LINK

6.1 Introduction

Chapter 5 presented the theory behind the link budget equations. Using the component parameter values obtained either from experimental data or from component data sheets, the link budget spreadsheet enabled the calculation of maximum achievable ranges and the corresponding amplifier gains. These calculations can be used for estimating the coverage performance of different wireless systems such as GSM, DCS, UMTS and WLAN.

In this chapter, the link budget range predictions are first verified for the transmission of WLAN signals over the radio-over-fibre link using a system demonstrator. Signal strength and throughput measurements are carried out to evaluate the performance of the demonstrator. The performance of both the two-antenna RAU and the single-antenna RAU has been investigated. Range calculations for other systems (GSM, DCS and UMTS) using component values better than what have been measured are then presented. Finally, the transmission of different combinations of systems – DPRS, UMTS, GSM and IEEE 802.11g (54 Mbps) – in a dual-band configuration over an MMF-fed indoor wireless network is demonstrated.

6.2 System Demonstrator for WLAN

A WLAN system demonstrator was set up using both the two-antenna RAU and the single-antenna RAU. For the operational demonstration, the two-antenna RAU was set up in a room of size 5 m x 6 m (room A), while a room of size 6 m x 3 m (room B) was used for the single-antenna RAU. Both rooms contained typical office furniture. The path loss exponents were determined for each room (3.2 for room A and 2.6 for room B), using the method discussed in Chapter 5, Section 5.2.1. Separate transmissions of 'real' WLAN signals (IEEE 802.11b and IEEE 802.11g generated using an access

point) over the two RAU sub-systems were carried out. In order to achieve complete coverage of the rooms in which the respective RAUs were placed, the link budget analysis (discussed in Chapter 5) was used to optimise the component parameters.

The following sub-section presents the link budget calculation results for the transmission of WLAN signals and also provides a brief analytical comparison of the two RAU designs. The experimental set-ups for the WLAN system demonstrator using each RAU design are presented in sub-sections 6.2.2–6.2.3; the corresponding measurements are presented in sub-sections 6.2.5–6.2.6. Sub-section 6.2.4 presents a brief review of some of the past research in the field of conventional (non-fibre) WLAN networks.

6.2.1 Link Budget Calculation Results

The component parameters for the two-antenna RAU and the single-antenna RAU used in the link budget calculations are listed in Table 6.1a and 6.1b respectively. The parameter values for the VCSEL, PD and MMF have been obtained using the characterisation measurements discussed in Chapter 4.

It should be noted that for the link budget calculations, two different sets of component parameter values were used for the two RAU system designs. The use of different sets of components and obtaining separate range predictions for the RoF link using the two RAUs was important as simultaneous implementation of the two RAU systems (discussed in Chapter 7, Section 7.7) was being considered for investigation.

TABLE 6.1A INPUT PARAMETERS TO THE LINK BUDGET: TWO-ANTENNA RAU

Downlink		
Component	**Parameter**	**Measured/Used**
VCSEL	Threshold current (I_{th})	1.5 mA
	Bias current (I_b)	7 mA
	Slope efficiency (η_{cu})	0.5 W/A
	RIN (RIN_{cu})	-128 dB/Hz
	Impedance (Z_{lcu})	50 ohms
	Frequency factor (α_{cu})	0.575 (-2.4 dB)
	Input RF Power ($P_{in,RF}$)	0.41 mW (-3.9 dBm)
PD	Responsivity (R_{pau})	0.42 A/W
	Impedance (Z_{pau})	50 ohms
MMF 50/125μm	Gain (G_{fdl})	0.43 (-3.7 dB)
Uplink		
Component	**Parameter**	**Measured/Used**
VCSEL	Threshold current (I_{th})	1.5 mA
	Bias current (I_b)	7 mA
	Slope efficiency (η_{au})	0.38 W/A
	RIN (RIN_{au})	-144 dB/Hz
	Impedance (Z_{lau})	50 ohms
	Frequency factor (α_{au})	0.575 (-2.4 dB)
	Max. input RF power ($P_{r,max}$)	0.41 mW (-3.9 dBm)
PD	Responsivity (R_{pcu})	0.44 A/W
	Impedance (Z_{pcu})	50 ohms
MMF 62.5/125μm	Gain (G_{ful})	0.27 (-5.7 dB)
Wireless Path		
Component	**Parameter**	**Measured/Used**
Antenna (MU)	Gain (G_{at})	1 (0 dB)
Antenna (RAU)	Gain ($G_{au,t}$)	1 (0 dB)
	Gain ($G_{au,r}$)	1 (0 dB)
	Path loss exponent (n)	3.2
Two-Antenna RAU		
Component	**Parameter**	**Measured/Used**
	Antenna isolation (γ_a)	316.23 (25 dB)
	Isolation at PD-VCSEL end (γ_{pl})	316.23e3 (55 dB)
Central Unit		
Component	**Parameter**	**Measured/Used**
Circulator	Insertion loss (L_{cir})	1.12 (0.5 dB)
Isolator	Insertion loss ($L_{iso\text{-}cu}$)	1.12 (0.5 dB)

TABLE 6.1B INPUT PARAMETERS TO THE LINK BUDGET: SINGLE-ANTENNA RAU

Downlink		
Component	**Parameter**	**Measured/Used**
VCSEL	Threshold current (I_{th})	1.5 mA
	Bias current (I_b)	7 mA
	Slope efficiency (η_{cu})	0.57 W/A
	RIN (RIN_{cu})	-145.1 dB/Hz
	Impedance (Z_{lcu})	50 ohms
	Frequency factor (α_{cu})	0.525 (-2.8 dB)
	Input RF Power ($P_{in,RF}$)	0.3 mW (-5.23 dBm)
PD	Responsivity (R_{pau})	0.33 A/W
	Impedance (Z_{pau})	50 ohms
MMF 50/125μm	Gain (G_{fdl})	0.56 (-2.6dB)
Uplink		
Component	**Parameter**	**Measured/Used**
VCSEL	Threshold current (I_{th})	1.5 mA
	Bias current (I_b)	7 mA
	Slope efficiency (η_{au})	0.49 W/A
	RIN (RIN_{au})	-137.5 dB/Hz
	Impedance (Z_{lau})	50 ohms
	Frequency factor (α_{au})	0.38 (-4.2 dB)
	Max. input RF power ($P_{r,max}$)	0.3 mW (-5.23 dBm)
PD	Responsivity (R_{pcu})	0.48 A/W
	Impedance (Z_{pcu})	50 ohms
MMF 62.5/125μm	Gain (G_{ful})	0.42 (-3.8 dB)
Wireless Path		
Component	**Parameter**	**Measured/Used**
Antenna (MU)	Gain (G_{at})	1 (0 dB)
Antenna (RAU)	Gain (G_{au})	1 (0 dB)
	Path loss exponent (n)	2.6
Single-Antenna RAU		
Component	**Parameter**	**Measured/Used**
Isolator	Insertion loss ($L_{iso\text{-}au}$)	1.06 (0.27 dB)
Power-Splitter/Combiner	Insertion loss (L_p)	2.08 (3.19 dB)
	Splitter ratio (β)	2.18 (3.38 dB)
	Isolation between port 1 and 2 (γ_p)	15.85 (12 dB)
-	Isolation at PD-VCSEL end (γ_{pl})	1.58e6 (62 dB)
Central Unit		
Component	**Parameter**	**Measured/Used**
Circulator	Insertion loss (L_{cir})	1.33 (0.25 dB)
Isolator	Insertion loss ($L_{iso\text{-}cu}$)	1.33 (0.25 dB)

Based on the component parameter values listed in Tables 6.1a and 6.1b, the maximum achievable ranges (both uplink and downlink) and the corresponding amplifier gain values for the transmission of IEEE 802.11b (at 11 Mbps) and IEEE 802.11g (at

54 Mbps) signals were calculated using the link budget spreadsheet (discussed in Chapter 5), for each RAU design. IEEE 802.11b/g system parameters (taken from or calculated using [1] and [2] respectively) used for the link budget calculations are listed in Table 6.2. The link budget calculation results are presented in Table 6.3. The table also shows the amplifier gains required for the WLAN system demonstrator to cover the two target rooms (where each RAU was placed). For these calculations, the maximum achievable radio range was set to be 5 m for the two-antenna RAU and 6 m for the single-antenna RAU.

TABLE 6.2 WLAN SYSTEM PARAMETERS

System	Frequency (GHz)		Receiver Sensitivity (dBm)		P_{mt} (dBm)	B (MHz)	CNR (dB)
	DL	UL	DL	UL			
IEEE 802.11b	2.4	2.4	-82	-82	17	11	7
IEEE 802.11g	2.4	2.4	-68	-68	17	11	24.8

P_{mt} = Mobile transmit power, B = Bandwidth, CNR = Carrier-to-noise ratio

TABLE 6.3 CALCULATIONS FOR THE SYSTEM DEMONSTRATOR

RAU	System	Range (m)	Amplifier Gain (dB)		P_t (dBm)	DL Transmitted Noise Power (dBm)
			DL	UL		
Two-antenna	802.11b	32 maximum	38.4	26.7	6.1	-33.6
		5 target room	12.5	1.2	-19.7	-59.4
	802.11g	9.3 maximum	35.4	26.7	3.1	-36.6
		5 target room	26.5	17.9	-5.7	-45.4
Single-antenna	802.11b	45.2 maximum	36.1	27.3	1.1	-51.9
		6 target room	13.2	4.6	-21.8	-74.8
	802.11g	9.5 maximum	32.5	27.3	-2.6	-55.6
		6 target room	27.2	22	-7.8	-60.8

P_t = Downlink transmit power of the RAU

The results in Table 6.3 show that reasonable ranges (sufficient for indoor coverage) may be achieved for transmission of IEEE 802.11b and IEEE 802.11g via both the two-antenna RAU and the single-antenna RAU. The difference in calculated ranges for

IEEE 802.11b and IEEE 802.11g is expected since the IEEE 802.11g has a much higher required CNR compared to IEEE 802.11b (as can be seen from Table 6.2). It should be noted that all the maximum achievable range values and the corresponding amplifier gain values, listed in Table 6.3, are limited by UL capping (Section 5.5.2, Chapter 5). As discussed in Section 5.5.2, Chapter 5, this means that the calculated amplifier gain values (for the maximum achievable range) are the maximum amplifier gain values that will be allowed by the link such that the received RF power from the mobile units at the minimum distance from the RAU (d_{min}) do not exceed the maximum amplified RF power that can be fed to the uplink VCSEL ($P_{r,max}$) without causing distortion.

However, since the results for the single-antenna RAU and two-antenna RAU (shown in Table 6.3) come from two different link budget spreadsheet calculations each of which use different component parameter values (listed in Tables 6.1a and 6.1b), apart from simply providing an indication of the relative theoretical performance of the two systems, a direct comparison of the results is not possible. In order to realistically compare the theoretical performance of the two RAUs, identical component parameter values were input to both spreadsheets. Table 6.4 contains the maximum achievable ranges and corresponding amplifier gains calculated using the same component parameter values (from Table 6.1b) for the transmission of both IEEE 802.11b and IEEE 802.11g via each of the two RAUs.

TABLE 6.4 PERFORMANCE COMPARISON OF THE TWO RAU SYSTEMS FOR THE TRANSMISSION OF IEEE 802.11B AND IEEE 802.11G SIGNALS

Case	Isolation (dB)		RAU	Standard	Range (m)	Amplifier Gain (dB)		Limitation
	γ_{pl}	γ_p/γ_a				DL	UL	
1	62	12	Two-antenna	802.11b	45.4	32.7	23.9	UL capping
				802.11g	9.5	29	23.9	
			Single-antenna	802.11b	45.2	36.1	27.3	
				802.11g	9.5	32.5	27.3	
2	50	12	Two-antenna	802.11b	37	30.4	21.6	Loop gain
				802.11g	9.1	28.5	23.5	
			Single-antenna	802.11b	27.7	30.6	21.7	
				802.11g	6.8	28.7	23.5	

The results for case 1 in Table 6.4 show that both the RAU systems give similar range performance for each transmitted standard. However, greater amplifier gains (both DL and UL) are needed in the single-antenna RAU to achieve the same range as the two-antenna RAU. Such a performance is obtained mainly because the restriction being

imposed on the range and amplifier gain calculations in this case is due to UL capping (Section 5.5.2, Chapter 5). This behaviour has been proved by means of a detailed derivation presented in Section B.1 Appendix B. Looking at Equation B.3 (Section B.1 Appendix B), it is clear that the difference between the uplink amplifier gains for the single-antenna RAU and the two-antenna RAU is due to the additional loss introduced by the splitting ratio (β) of the power-splitter/combiner in the single-antenna RAU. Considering IEEE 802.11b results for case 1 from Table 6.4 as an example, the difference between the uplink amplifier gains for the two RAU systems is 3.4 dB (27.3 dB – 23.9 dB). This is equal to the splitting ratio (β in dB) of the power-splitter/ combiner given in Table 6.1b. Similarly, Equation B.12 shows that the combined insertion losses of the isolator ($L_{iso\text{-}au}$) and the power-splitter/combiner (L_p) result in the difference in downlink amplifier gains for the two RAU systems. The calculations also show that the maximum tolerable path losses (both uplink and downlink) were equal for the two RAU systems resulting in equal maximum achievable ranges. Another important point to note is that as long as the range calculations are limited by UL capping, the isolation values have no effect on the calculated maximum achievable range.

A reduction in the isolation values would result in the link budget calculations (range and amplifier gain) being limited by loop gain. This is observed in case 2 in Table 6.4, where lower (but identical) isolation values have been input to the two spreadsheets. A loop gain limitation (Section 5.5.1, Chapter 5) results in a reduction of the calculated maximum achievable range for the transmission of both IEEE 802.11b and IEEE 802.11g over both the RAU systems (compared to case 1 in Table 6.4). For example, for the transmission of IEEE 802.11b via the two-antenna RAU, the range reduces from 45.4 m in case 1 to 37 m in case 2. Moreover, the calculated maximum achievable range is different for the two RAU systems (for example, two-antenna maximum achievable range = 37 m and single-antenna maximum achievable range = 27.7 m). The relation between the calculated ranges for the two RAU systems is discussed in detail in Section B.2, Appendix B. From this discussion, it is seen that the maximum tolerable propagation losses (both uplink and downlink) for the two RAU systems are no longer equal (unlike for case 1) under a loop gain limitation (as shown in Equations B.15 and B.17). This, in turn, results in a difference in the calculated maximum achievable ranges. According to Equation B.20, the difference in ranges depends on the path loss exponent, the splitter ratio (β) and the insertion loss (L_p) of the power-splitter/combiner.

The amplifier gains calculated for the two systems, on the other hand, are almost equal to one another as can be seen from Table 6.4. According to Equation B.14, the slight difference between the total amplifier gain (sum of the uplink and downlink amplifier gains (in dB)) for the two systems is due to the additional insertion loss of the isolator ($L_{iso\text{-}au}$) in the single-antenna RAU system.

It is evident from this analysis that the performance of both the single-antenna RAU system as well as the two-antenna RAU system depends not only on the component parameter values, the path loss exponent and the isolation values, but also on the type of limitation being imposed on the calculated maximum range.

6.2.2 Experimental Set-Up: Two-Antenna RAU

The complete experimental set-up for the performance analysis of the WLAN-over-fibre link using the two-antenna RAU system is shown in Figure 6.1.

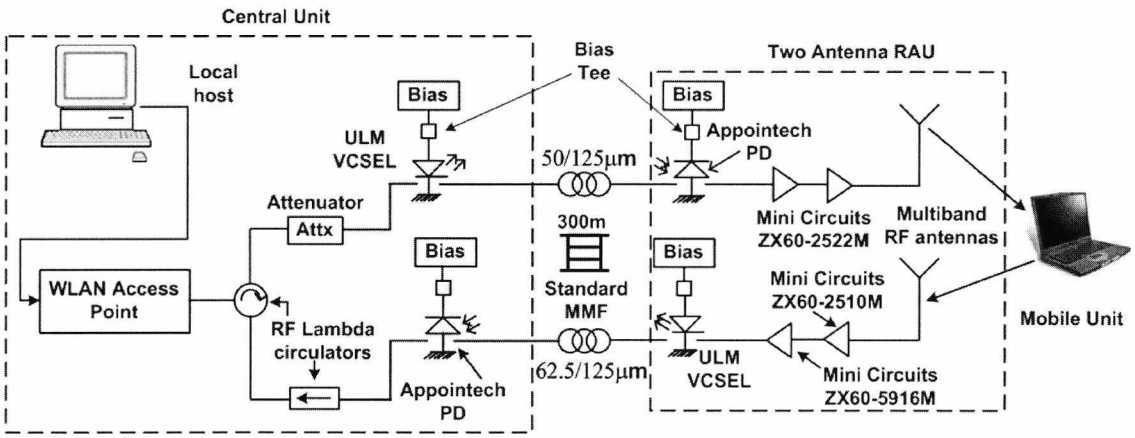

Figure 6.1. Complete experimental set-up for performance analysis of the WLAN-over-fibre link using the two-antenna RAU

The central unit and the remote antenna unit were placed in separate rooms connected by a 300 m MMF. A WLAN signal was generated using a commercial access point (AP) - *D-Link DWL-AP2000+*. The access point was able to provide IEEE 802.11b signals at 1, 2, 5.5 and 11 Mbps and IEEE 802.11g signals at 6, 9, 12, 18, 24, 36, 48 and 54 Mbps. The RF output power from the AP was measured (using an *Agilent E4407B* RF spectrum analyser) to be approximately 17 dBm. The AP uses an external detachable antenna with 1 dB gain. For the measurements, the external antenna was removed and the RF output port of the AP was connected to port 1 of an *RFLambda*

circulator (*RFLC-3000-1*, frequency range: 2.4–2.4835 GHz). Port 2 of the circulator sends the WLAN signal from the access point over the downlink path while port 3 receives the signal over the uplink path to be fed back to the access point.

ULM VCSELs (characterization results presented in Chapter 4) operating at 850 nm were used as optical transmitters for both the downlink and uplink paths. The current to the VCSEL is provided by a precision current source (*ILX Lightwave LDX-3412*). In order to avoid distortion, an RF attenuator was used to attenuate the output power from the access point before feeding it to the downlink VCSEL. The RF attenuator setting was varied (incremented by 1 dB) and for each power level fed to the downlink VCSEL, the corresponding downlink throughput was recorded. It was observed that the throughput deteriorated for an RF power greater than -3.9 dBm (achieved using 21 dB attenuation) into the VCSEL. This was therefore, set as the input RF power to the VCSEL. Using the same argument, the input RF power for the uplink VCSEL was also set so as to not exceed -3.9 dBm. This has been discussed in detail in Chapter 5 (Section 5.5.2).

The light from the VCSEL was coupled into fibre via an MMF patchcord. Standard 50/125 μm (OM1) and 62.5/125 μm (OM2) MMF, with lengths of 300 m, were used for the downlink and uplink paths respectively. The incoming downlink signal on the MMF was detected by a photodiode (the same as that used for the characterisation measurements presented in Chapter 4) and the retrieved RF signal was amplified and then transmitted using a multiband, omni-directional RF antenna. For the uplink, the received WLAN signal was first amplified and then fed to a VCSEL operating at 850 nm. The modulated optical signal was transmitted over the 300 m MMF and was converted back into an RF signal by a photodiode (similar to the one used at the RAU) at the CU and transmitted over to the AP. For both the downlink and uplink, *ZX60* series, SMA connectorized, coaxial amplifiers, from *Mini-Circuits* were used. The amplifier gains were adjusted to the values given in Table 6.3 through bias control. Separate (but co-located) multiband transmit and receive antennas, designed by the University of Kent Antennas group [3] were used at the RAU.

For all the experiments, unless otherwise stated, the mobile unit was a laptop installed with a *D-Link AirPlus G+ DWL-G650+* external wireless card.

6.2.3 Experimental Set-Up: Single-Antenna RAU

The complete experimental set-up for the performance analysis of the WLAN-over-fibre link using the single-antenna RAU is illustrated in Figure 6.2.

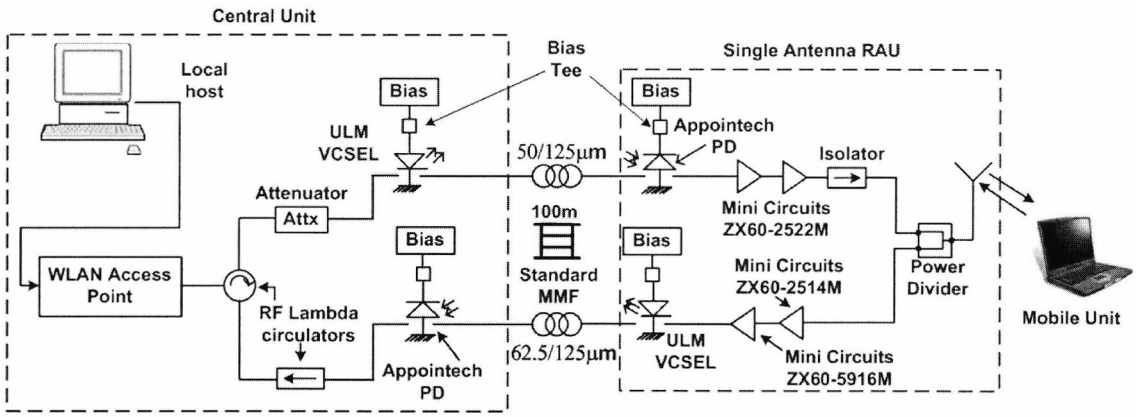

Figure 6.2. Complete experimental set-up for performance analysis of the WLAN-over-fibre link using the single-antenna RAU

The setup for the CU in Figure 6.2 is similar to the one used in Figure 6.1 (experimental set-up using the two-antenna RAU). The same types of MMF (as used for the WLAN-over-fibre link employing the two-antenna RAU) were used except that their lengths were 100 m for the UL and DL. As has been mentioned earlier in Section 6.2.1, simultaneous implementation of the two RAUs was being considered (discussed later in Section 7.7, Chapter 7). For this reason, separate pairs of MMFs would be needed to feed the two RAUs. However, as only one pair of 300 m MMFs was available during these measurements and was used for the two-antenna RAU, a pair of MMFs of length 100 m (for both UL and DL) was used for the single-antenna RAU measurements. At the RAU, a 2-port power divider (*RFLambda FLT-2-3-2700,* frequency range: 1.6–2.7 GHz) was used to separate the downlink and uplink signals. An imperfect impedance matching between the power-divider and the antenna would result in part of the downlink signal being fed back. In order to avoid this reflected downlink signal from damaging the downlink amplifiers, and isolator was employed in the downlink path (at the RAU). A multiband antenna, designed by the University of Kent Antennas group, was used at the RAU.

Once the links were set up using the amplifier gain values listed in Table 6.3, signal strength and throughput measurements were carried out to characterise the performance

of both RAU systems. These results have been discussed in Sections 6.2.5 and 6.2.6. However, before discussing the throughput results for the transmission of WLAN signals over the designed radio-over-fibre link, a brief review on the throughput performance of conventional (non-fibre) WLAN networks is presented in the next section (Section 6.2.4) .

6.2.4 Throughput Performance of Conventional WLAN Networks

One of the parameters used to characterise the performance of a WLAN network is its throughput. Though very little research has been conducted to characterise the throughput performance of WLAN-over-fibre networks, the performance of conventional WLAN networks can be used as a basis to analyse and perhaps predict the performance of WLAN-over-fibre networks.

According to the IEEE 802.11 standard and as most WLAN access point manufacturers specify, the maximum data rates achievable by IEEE 802.11b and IEEE 802.11g are 11 Mbps and 54 Mbps respectively. However, these values refer to the raw data rates at the physical (PHY) layer. Factors such as the medium access control (MAC) protocol (more information on the MAC protocol is included in Chapter 7) overhead, distance between the client and the access point and propagation conditions (LOS or non-LOS) degrade the PHY layer data rates [4] and the actual throughput measured is the TCP-to-TCP protocol throughput [5]. As an example, an IEEE 802.11b network's maximum throughput taking into account only the protocol overheads was calculated to be 6.27 Mbps [4]. According to [6], the approximate throughput value for IEEE 802.11b should be 6 Mbps; for IEEE 802.11g, the throughput values should be 22 Mbps in a g-only environment with the throughput dropping to 8 Mbps in the presence of 802.11b clients. In [7], the theoretical maximum throughput (TMT) for IEEE 802.11b was calculated to be 6 Mbps for the carrier-sense multiple access/collision avoidance (CSMA/CA) MAC scheme, which dropped to 4.5 Mbps when the request-to-send/clear-to-send (RTS/CTS) mechanism was utilised (RTS/CTS and other MAC related mechanisms are examined in detail in Chapter 7).

An important contributing factor to the improvement in the throughput performance of an IEEE 802.11 network is the signal-to-noise ratio (SNR) of the received signal. It has been shown in [8] that for IEEE 802.11b the calculated throughput reaches a maximum

value only beyond a certain SNR known as the critical SNR value. As expected, both the critical SNR and maximum throughput values depend on the data rate used. The calculations in [8] illustrate that the higher the data rate, the higher is the value of critical SNR and consequently the higher is the value of the maximum achievable throughput. A similar result is observed in the case of IEEE 802.11g as well [9]; in this study, an experimental investigation was carried out to determine the network performance. Additionally, IEEE 802.11g throughput has also been observed to be affected by a number of other factors such as: the presence of other users contending for the channel [9], interference from 802.11b access points located in the measurement area [10], and by the type of chipset used in the access points [9].

Studies comparing the performance of IEEE 802.11b and IEEE 802.11g networks show that IEEE 802.11b provides a better quality of service compared to IEEE 802.11g [11], [12]. For the transmission of real-time audio traffic between two mobile stations, it has been experimentally verified in [11] that IEEE 802.11b provides lower packet loss rates compared to IEEE 802.11g. Based on simulation results, it has been shown in [12] that IEEE 802.11b has a more stable performance in terms of throughput and network utilization in the presence of hidden nodes (the hidden node scenario is discussed in Section 7.7.2, Chapter 7), compared to IEEE 802.11g.

6.2.5 Measurements and Results: Two-Antenna RAU

For the measurements, the two-antenna RAU was mounted on the ceiling at one end of room A. As mentioned earlier, the room represents a standard office environment with computers, chairs and tables placed in different parts of the room. For a basic transmission scenario, the mobile unit could, at all times, see the ceiling-mounted RAU (i.e., line of sight). Although LOS propagation was maintained at all times during the measurements, multipath effects were also very evident.

The received signal strength at the MU was measured using commercial software (*Wireless Network Ignition*), which itself was checked against measurements with an electrical spectrum analyzer (*Agilent E4407B*) and a known antenna (the external antenna of the *D-Link* access point). As the optimum component parameter values for the WLAN system demonstrator were calculated using the link budget spreadsheet, signal strength measurements were a means of verifying the link budget predictions.

Such verification will help in utilising the link budget spreadsheet in predicting the range performance of other wireless systems when transmitted over the designed RoF link.

The variation of signal strength with distance from the RAU for IEEE 802.11b and IEEE 802.11g signals is shown in Figures 6.3a and 6.3b respectively. As expected, the received signal strength generally decreases as the MU moves away from the RAU. The predicted signal strength from the link budget calculations has also been plotted in the figures. For both transmitted standards, the graphs show a close match between the measured and predicted signal strength values.

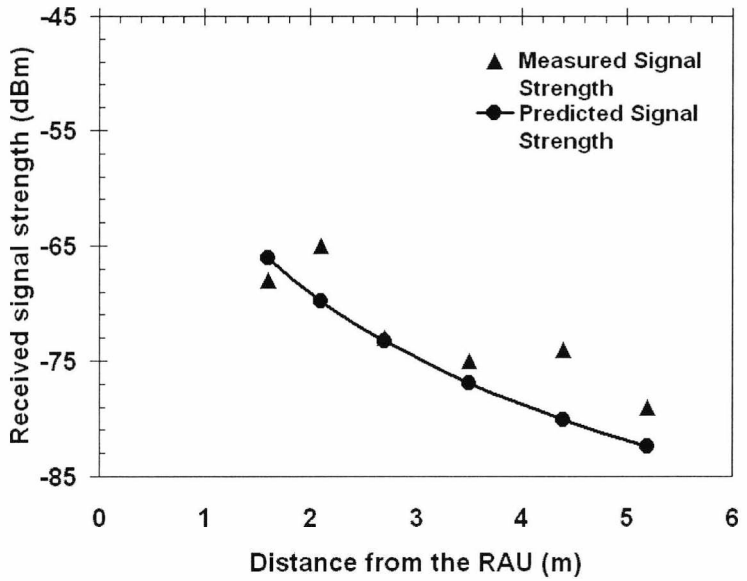

Figure 6.3a. Received signal strength for IEEE 802.11b using the two-antenna RAU

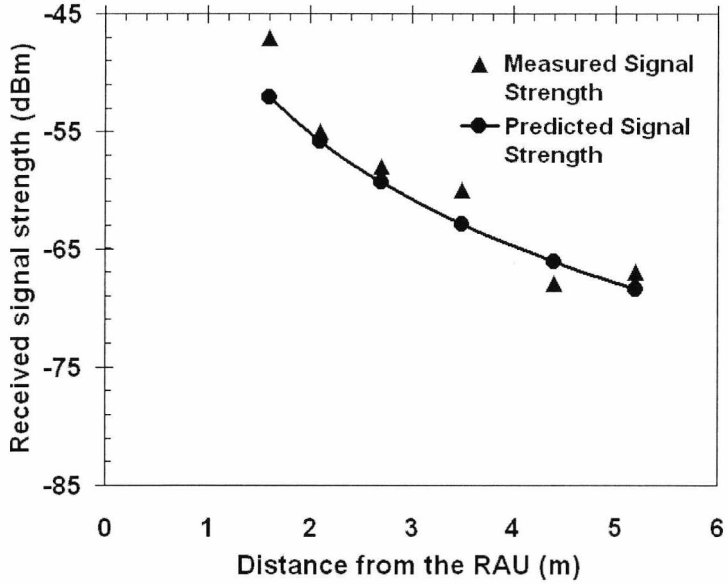

Figure 6.3b. Received signal strength for IEEE 802.11g using the two-antenna RAU

The link quality was tested by streaming a video signal over the link. It was possible to obtain high quality signal reception throughout the room. In order to quantify the link performance, throughput measurements were carried out using a commercial software package called *Networx* during the transfer of a large data file (700 MB) over the link. The variation of average throughput (for the UL and DL) with distance from the RAU is plotted in Figures 6.4a and 6.4b for the 802.11b and 802.11g standards respectively.

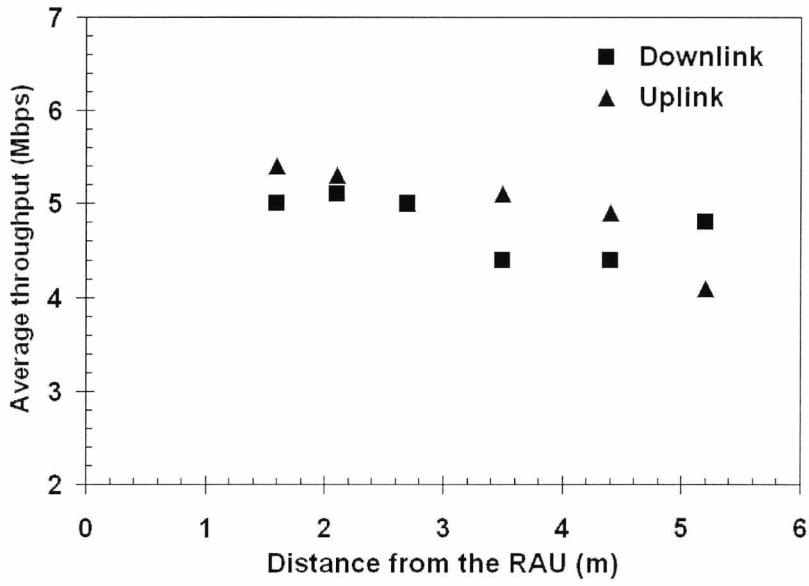

Figure 6.4a. Throughput performance for IEEE 802.11b using the two-antenna RAU

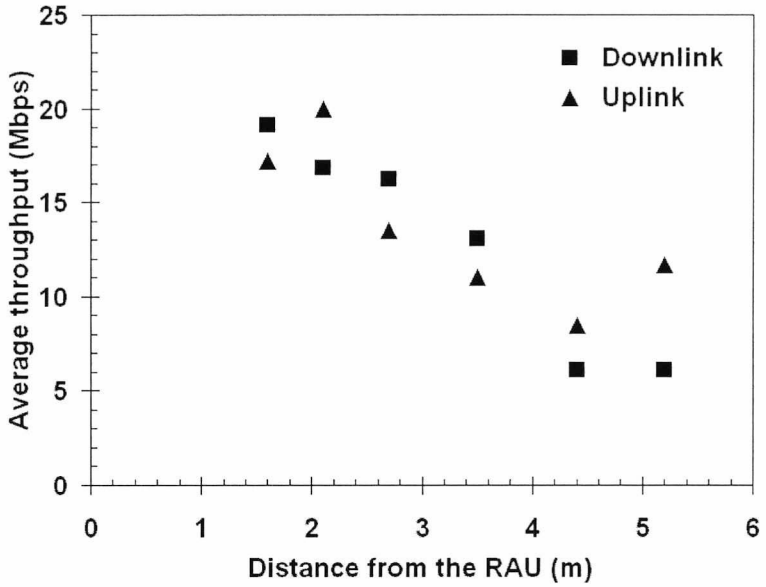

Figure 6.4b. Throughput performance for IEEE 802.11g using the two-antenna RAU

Throughputs as high as 5.2 Mbps for IEEE 802.11b and 20 Mbps for IEEE 802.11g (at 54 Mbps) were achieved closer to the RAU. These values were very close to the approximate maximum throughput values of 6 Mbps for IEEE 802.11b and 22 Mbps for IEEE 802.11g (at 54 Mbps) reported in the literature for conventional WLAN networks [6]. For IEEE 802.11b (Figure 6.4a), the throughput values were relatively stable over the 5 m range. However, during the measurements for the IEEE 802.11g system, it was observed that on approaching the edge of the 5 m range the data rate of the signal varied between 54 Mbps and 36 Mbps, due to fluctuations in signal strength (Figure 6.3b shows average values). This leads to the decrease in the average throughput, even though the measured average signal strengths match predictions.

6.2.6 Measurements and Results: Single-Antenna RAU

Similar signal strength and throughput performance measurements were also carried out using the single-antenna RAU. The RAU was mounted on the ceiling of another office room (room B), which was adjacent to room A. As mentioned in Section 6.2, path loss measurements were carried out for room B and the path loss exponent was determined to be equal to 2.6. LOS propagation conditions, similar to the two-antenna RAU case, were maintained at all times.

The received signal strength at the MU was measured using a software package called *WirelessMon*. In order to ensure the validity of the measurements, the signal strength

values obtained using *WirelessMon* were matched against the values measured using *Wireless Network Ignition* for the same measurement points. The results for the signal strength measurements (carried out using *WirelessMon*) using the single-antenna RAU are depicted in Figures 6.5a and 6.5b for IEEE 802.11b and IEEE 802.11g respectively. As for the two-antenna RAU case, the signal strength values obtained using the link budget spreadsheet have also been plotted for both the wireless systems.

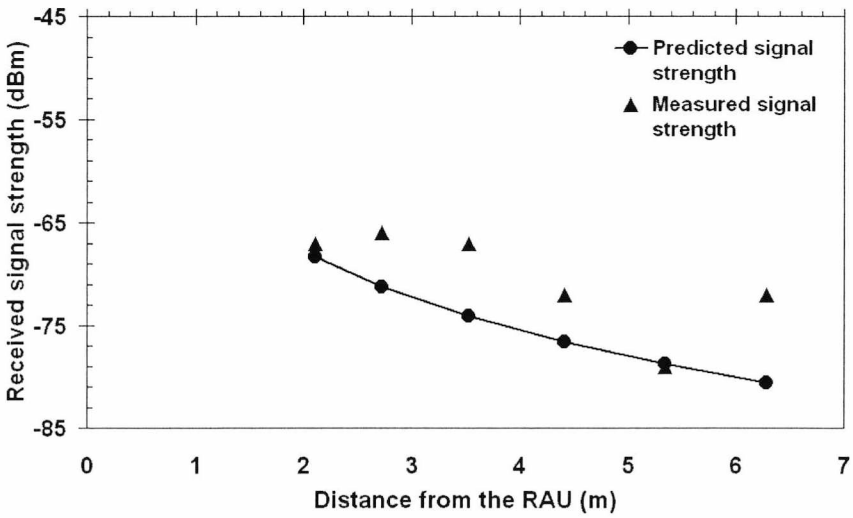

Figure 6.5a. Received signal strength for IEEE 802.11b using the single-antenna RAU

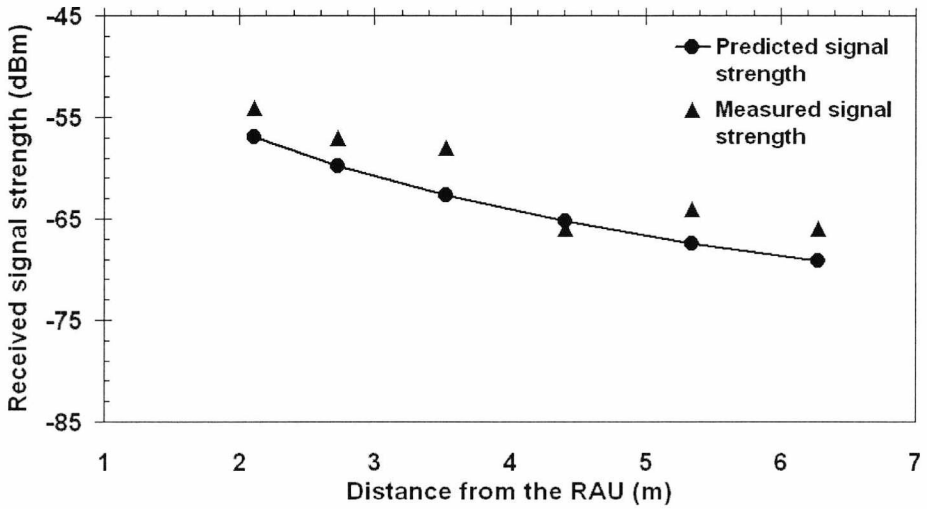

Figure 6.5b. Received signal strength for IEEE 802.11g using the single-antenna RAU

The measured signal strength values are reasonably close to the predicted values for both the standards (and as expected, the signal strength decreases with increasing distance from the RAU). It should however be noted that for both the RAU cases, the signal strength and throughput values depend on the measurement instant and achieving exactly the same values for another measurement instant may not be possible.

WirelessMon was preferred for the measurements as it also plotted the variation of signal strength with time over the measurement period (4 minutes). Figure 6.6 depicts an example screen-shot of the signal strength variation with time for the transmission of IEEE 802.11g signal at a distance of 3.53 m from the RAU.

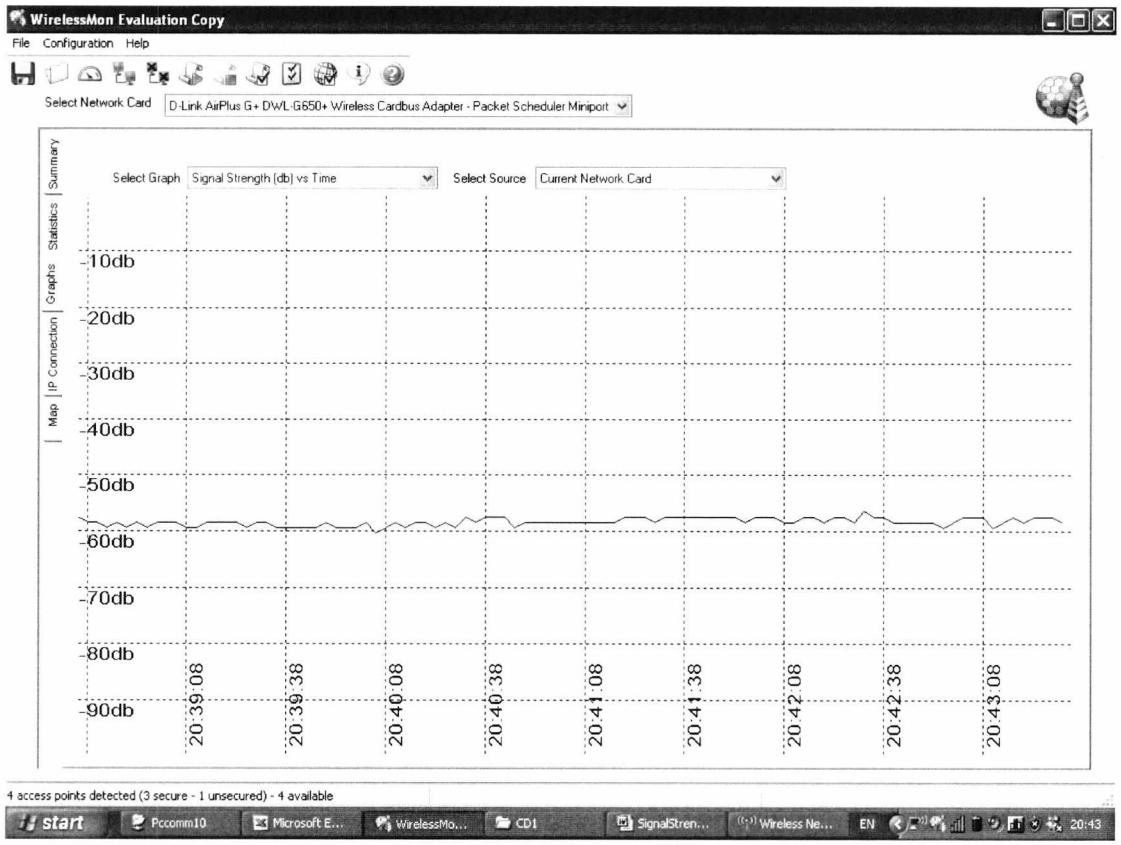

Figure 6.6. Received signal strength variation with time for IEEE 802.11g

The signal strength is very stable over the measurement period.

The average throughput as a function of the distance from the RAU for the transmission of IEEE 802.11b and IEEE 802.11g signals is presented in Figures 6.7a and 6.7b respectively. The measurements were carried out again using the *Networx* software.

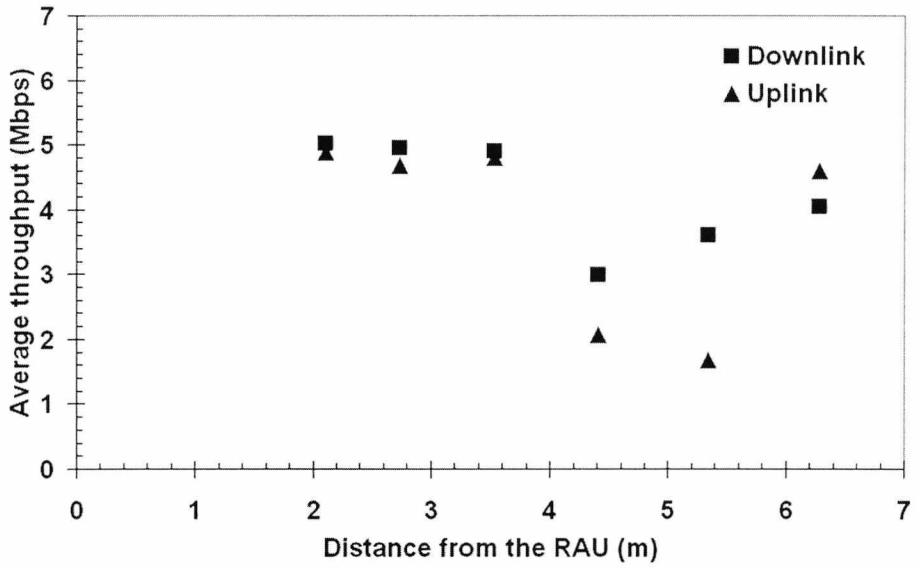

Figure 6.7a. Throughput performance for IEEE 802.11b using the single-antenna RAU

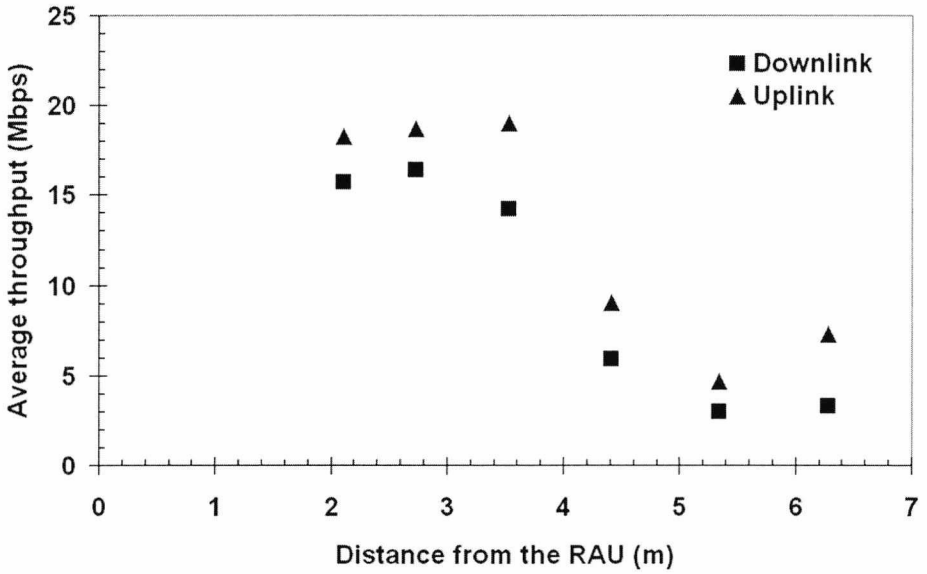

Figure 6.7b. Throughput performance for IEEE 802.11g using the single-antenna RAU

The throughput performance for both the standards is seen to be reasonably stable for the first three metres away from the RAU. Beyond this, the throughput variation does not follow a definite pattern, particularly in the case of IEEE 802.11b. It should be noted that beyond three metres, the measurement points were located within a partially enclosed cubicle housing a computer monitor. Even though the screen-board converting the area into a partially enclosed space was not high enough to cut-off LOS propagation, it appears to have had an impact on the signal strength and throughput results.

Finally, photographs depicting the various sub-systems of the complete WLAN system demonstrator, along with an example screen-shot of a throughput measurement (carried out using *Networx* software) are presented in Figure 6.8.

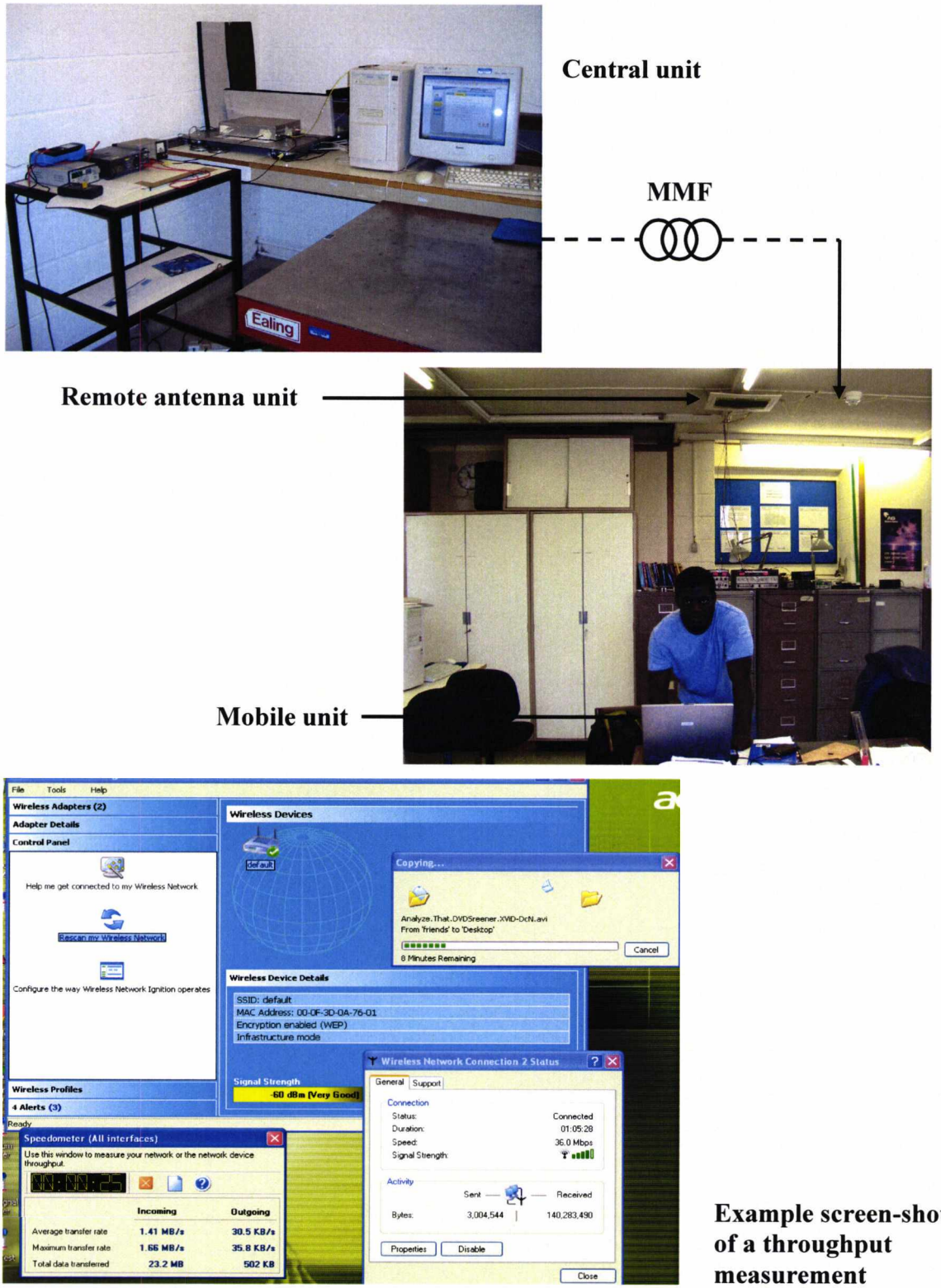

Figure 6.8. Photographs depicting the various sub-systems of the complete WLAN system demonstrator, along with an example screen-shot of a throughput measurement

6.3 Future System Optimisation

The previous section dealt with the transmission of WLAN signals over the designed RoF link. However, the range calculations presented thus far and the system demonstrator performance are limited by the available component specifications. As both the RAUs did not incorporate filters and both used multiband antennas, the transmission of other standards could be considered. This section discusses the improvement in the maximum achievable range possible when using available system components with better characteristics. In addition to the range calculations for the transmission of WLAN standards, the maximum achievable ranges for the transmission of standards such as GSM 900, GSM 1800 and UMTS are also presented.

The parameters of the evaluated standards are listed in Table 6.5. These system parameters have been taken from or calculated using 3GPP standards for GSM 900 [13], GSM 1800 (DCS) [13], and UMTS [14] - [17] standards. Data rates of 54 Mbps and 11 Mbps for have been used for IEEE 802.11g and IEEE 802.11b respectively and 12.2 kbps users have been assumed for UMTS.

TABLE 6.5 SYSTEM PARAMETERS FOR THE DIFFERENT WIRELESS STANDARDS

System	Frequency (GHz)		Receiver Sensitivity (dBm)		P_{mt} (dBm)	B (MHz)	CNR (dB)
	DL	UL	DL	UL			
GSM 900	0.93	0.89	-102	-88	33	0.2	9
GSM 1800	1.8	1.71	-100	-95	30	0.2	9
UMTS (FDD)	2.11	1.92	-107	-107	27	3.84	15.1
UMTS (TDD)	2.01	2.01	-105	-95	24	3.84	15.1
IEEE 802.11b	2.4	2.4	-82	-82	17	11	7
IEEE 802.11g	2.4	2.4	-68	-68	17	11	24.8

P_{mt} = Mobile transmit power, B = Bandwidth, CNR = Carrier-to-noise ratio

Referring to Table 6.1A, it is assumed that the lower RIN laser (with 0.38 W/A slope efficiency), the higher 0.44 A/W responsivity PD, and the 300 m OM1 MMF with gain -3.67 dB are available for both the UL and DL. The remaining parameters are assumed to be the same as in Table 6.1A. The resulting radio range predictions for the different systems are listed in Table 6.6. The range predictions are based only on the assumed

system parameters of Table 6.5. Within each system's bandwidth, the respective access protocol may be used to support multiple mobile units (or clients) depending on the service requirements.

TABLE 6.6 POTENTIAL RANGE CALCULATIONS FOR THE TRANSMISSION OF DIFFERENT WIRELESS SYSTEMS USING THE TWO-ANTENNA RAU

System	Range (m)	Amplifier Gain (dB)		P_t (dBm)	DL Transmitted Noise Power (dBm/Hz)	
		DL	UL		Required	Calculated
GSM 900	64	21.9	2.1	-12.4	-95	-152
GSM 1800	74	31.7	10.6	-2.6	-95	-142.2
UMTS (FDD)	23	9.6	10.7	-24.7	-90	-163.9
UMTS (TDD)	22	12.6	19.7	-21.8	-90	-134
IEEE 802.11b	40	43.6	26.4	9.2	-100.4[1]	-114.5
IEEE 802.11g	12.4	38.4	26.7	4	-100.4	-119.5

P_t = Transmit power at the RAU

The results in Table 6.6 indicate that reasonable ranges can be obtained for all the systems that have been considered. It is unlikely that 30+ m radius cells would be required for indoor coverage when the fibre link lengths are themselves typically no more than 300 m. System architectures can be envisaged where many RAUs provide the coverage for high-speed WLANs (such a configuration will be discussed in Chapter 7), whereas only subsets of these (with simultaneous transmission, as will be discussed in Section 6.4) provide coverage for the less demanding systems.

The DL transmitted noise power was found to be in accordance with the spurious emission limit stated in each of the standards (the required DL transmitted noise power column in Table 6.6 gives this value). However, the standards impose a much stricter limit on the spurious emission from a base station in another base-station's frequency band when co-locating different types of base stations or, in other words, where there is simultaneous transmission of different systems. In such a case, band-pass filters may be employed to further attenuate the noise power outside the wanted frequency band.

[1] The required transmitted noise power values for IEEE 802.11b and IEEE 802.11g signals have been calculated based on the information given in [18].

6.4 Simultaneous Dual-Band Transmission over a Radio-over-Fibre Link

The main advantage of radio-over-fibre links is that they can be employed to provide multiple wireless services over the same link. This section, therefore, discusses the transmission of different combinations of wireless signals in dual-band configuration over an RoF link. In a dual-band configuration, two wireless systems are simultaneously transmitted over the RoF link. The different wireless signals used for the measurements include DECT packet radio service (DPRS) at 1.88 GHz, GSM 1800 at 1.8 GHz, UMTS at 2.0 GHz and IEEE 802.11g (data rate of 54 Mbps) at 2.412 GHz. It should be noted that the uplink and downlink path transmissions were not carried out simultaneously. The transmitted signals were emulated using signal generators. The EVM performance of the link was measured and the maximum achievable range was determined by comparing the measured EVM with the maximum EVM values allowed by the respective standards. The measurements were carried out in a laboratory with dimensions 10 m x 10 m.

6.4.1 Experimental Set-Up: Downlink

The downlink set-up for the dual-band transmission experiments is shown in Figure 6.9. The central unit transmitter has two independent signal sources: *Agilent VSG E4438C* (capable of emulating GSM, UMTS and DPRS systems) and *Agilent VSG E8267C* (capable of emulating GSM, UMTS and DPRS and WLAN signals). The system properties, used in the emulation, are shown in Table 6.7.

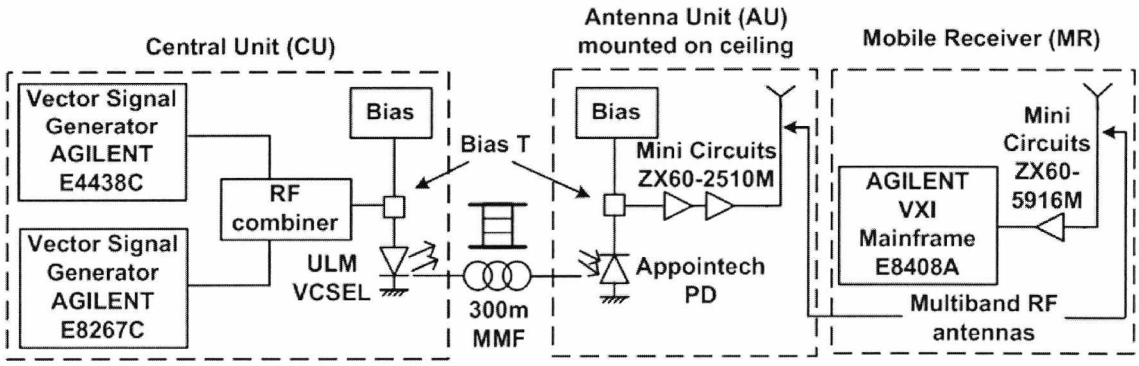

Figure 6.9. Experimental set-up for the simultaneous dual-band downlink radio transmission

The RF signals from the two signal sources were combined using an RF combiner and the combined signal was used to modulate the drive current of a *ULM-Photonics* multimode VCSEL operating at 850 nm (similar to the one used for the measurements discussed in Section 6.2). The modulated optical signal was then transported to the antenna unit (AU) via *Corning SXi* 50 μm-core MMF (similar to the one used in [19]) with a length of 300 m. The AU was mounted on the ceiling in the centre of the room. At the AU, an *Appointech* photodiode (similar to the one used for the measurements discussed in Section 6.2) was connected to amplifiers (*Mini-Circuits ZX-2510M*) with a total gain of 24 dB. An omni-directional multiband planar antenna [3] was used at the antenna unit. The mobile receiver (MR) consisted of an omni-directional perpendicular antenna, a *Mini-Circuits ZX-2510M* amplifier with a gain of 16 dB, and *Agilent* EVM measuring equipment (*Agilent VXI mainframe* (*E8408A*) connected to a laptop with *Agilent VSA* software).

TABLE 6.7 PROPERTIES OF THE EMULATED WIRELESS SYSTEMS: GSM, DPRS, UMTS AND IEEE 802.11G

System	Frequency (GHz)	Modulation	Data Rate	Filter Type	Maximum rms EVM (%)
GSM	1.8	GMSK	270.833 ksym/s	Gaussian BT = 0.3	7
DPRS	1.88	64 QAM	1.152 Msym/s	RRC $\alpha = 0.5$	2.6
UMTS	2.0	QPSK	3.84 Msym/s	RRC $\alpha = 0.22$	12.5
IEEE 802.11g	2.412	64 QAM - OFDM	54 Mbps	Gaussian BT = 0.5	5.6

It should be noted that the signal power levels from the two sources were not optimised, but set to equal levels, 2 dBm in this case, which was the maximum available for the WLAN OFDM signals. After taking into account cable/combiner losses, this corresponds to a combined drive power to the VCSEL of approximately -2.5 dBm. However, EVM measurements carried out at a different measurement facility (discussed in Chapter 4, Section 4.6) for the transmission of GSM 1800, DPRS and UMTS wireless systems suggested that higher input powers could be tolerated by the VCSEL before EVM degradation due to laser non-linearity was observed. The results for VCSEL non-linearity measurements (discussed in Chapter 4, Section 4.6) show that for the transmission of GSM 1800 system over the VCSEL-MMF-PD link, input power values as high as 17 dBm could be fed to the VCSEL. It should be noted that even at

17 dBm input RF power, the EVM recorded was only 1.1 %, and therefore this limit on the input power was imposed by the measuring equipment. For the transmission of UMTS and DPRS systems, maximum input power values that could be fed to the VCSEL were recorded to be 7.3 dBm and -3 dBm, respectively. Thus, significant improvement in the link performances, especially for the GSM 1800 and UMTS systems, than those obtained here could be expected.

6.4.2 Measurements and Results: Downlink

For the downlink transmission, signal power and rms EVM values for each system in the dual-band configuration were first recorded at the input of the AU antenna. These values are listed in Table 6.8. For the measurements at the input of the AU antenna, 100 rms EVM values were recorded for each dual-band transmission and the mean of these values was quoted as the final rms EVM shown in Table 6.8. It is important to ensure that these rms EVM values are much lower than the maximum rms EVM values (Table 6.7) specified in each of the standards, as the signal quality will be considerably degraded by the wireless channel. A poor rms EVM value at the AU antenna would therefore mean shorter wireless ranges.

TABLE 6.8 DOWNLINK: EVM MEASUREMENTS AT THE INPUT OF THE AU ANTENNA

System	Measured Signal	Antenna Unit		
		Peak Power (dBm)	Inband Power (dBm)	Mean rms EVM (%)
DPRS and IEEE 802.11g	DPRS	-30	-3.5	1
	IEEE 802.11g	-30	-4.9	2.5
GSM and IEEE 802.11g	GSM	-25	-2.5	2.7
	IEEE 802.11g	-35	-4.9	1.9
UMTS and IEEE 802.11g	UMTS 2.0 GHz	-35	-5	1.8
	IEEE 802.11g	-30	-5	1.8
UMTS and GSM	UMTS 2.00 GHz	-30	-4.1	0.9
	GSM	-25	-3.4	2.4
UMTS 2.00 GHz and UMTS 2.01GHz	UMTS 2.00 GHz	-25	-3.2	0.9
	UMTS 2.01 GHz	-25	-3.4	1.1

After transmission over the wireless path, EVM measurements were again carried out at the mobile receiver to determine the quality of the received signals. During the measurements, it was observed that the ability of the receiver to decode the transmitted wireless system depended on the orientation of the mobile receiver antenna. This was mainly due to multipath effects in the wireless channel caused by metallic objects in the

experimental room. Therefore, for each dual-band transmission, the mobile receiver was moved to a position which resulted in rms EVM values as close to the maximum allowed EVM values for each transmitted system. The multipath effects also resulted in unstable rms EVM readings at the mobile receiver. In order to obtain more accurate rms EVM measurements, six sets of 100 rms EVM readings with an interval of 10 seconds between each set were recorded for each dual-band system transmission. The mean of the rms EVM and the standard deviation (σ) of the readings were calculated from these 600 rms EVM readings and are listed in Table 6.9. The reported rms EVM values give an indication of the quality of transmission over both the optical and wireless links while the standard deviation values signify the stability of the measurements, and the reliability of the EVM values quoted. The radius quoted in Table 6.9 is the distance at table-top level from a position directly below the AU.

TABLE 6.9 DOWNLINK: EVM MEASUREMENTS AT THE MOBILE RECEIVER

System	Measured Signal	Mobile Receiver	
		Mean rms EVM (%)	σ
DPRS and IEEE 802.11g	DPRS	2	0.2
		(at 1 m radius)	
	IEEE 802.11g	3.8	0.3
		(at 4.2 m radius)	
GSM and IEEE 802.11g	GSM	4. 6	0.6
		(at 5 m radius)	
	IEEE 802.11g	4.4	0.5
		(at 3.2 m radius)	
UMTS and IEEE 802.11g	UMTS	10.4	1.4
		(at 5 m radius)	
	IEEE 802.11g	4	0.9
		(at 3.5 m radius)	
UMTS and GSM	UMTS	9.3	1.2
		(at 3.8 m radius)	
	GSM	3.7	0.9
		(at 5 m radius)	
UMTS 2.00 GHz and UMTS 2.01 GHz	UMTS 2.00 GHz	10.6	0.3
		(at 2.4 m radius)	
	UMTS 2.01 GHz	11.6	0.5
		(at 2.8 m radius)	

6.4.3 Experimental Set-Up: Uplink

The set-up for the uplink dual-band transmission experiment is shown in Figure 6.10. The uplink setup is divided into a mobile transmitter (MT), an antenna unit (again mounted on the ceiling) and a central unit. In this case, the same two signal sources

(*Agilent VSG E4438C* and *Agilent VSG E8267C*) and RF combiner that were utilised for the downlink (in the central unit) were used as the mobile transmitter. An omni-directional perpendicular antenna (same as the one used for the downlink measurements) was employed to emit the wireless signals to the AU. The AU consisted of the planar antenna [3], *Mini-Circuits ZX60-2510M* amplifiers (with a total gain of 24 dB) and the 850 nm *ULM* VCSEL. As the uplink and downlink transmissions were not carried out simultaneously, the same MMF used for downlink transmissions (*Corning SXi* 50 μm-core MMF of length 300 m) was used to carry the modulated optical signal to the central unit receiver. Finally, the receiver at the central unit consisted of the *Appointech* PD followed by a *Mini-Circuits ZX60-5916M* amplifier with a gain of 16 dB, and the *Agilent* EVM measuring equipment (*Agilent VXI mainframe* (*E8408A*) connected to a laptop with *Agilent VSA* software).

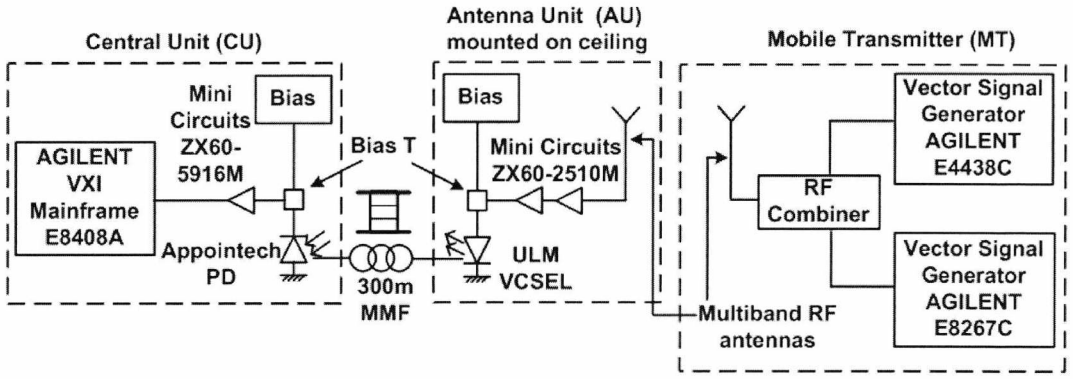

Figure 6.10. Experimental set-up for the simultaneous dual-band uplink radio transmission

6.4.4 Measurements and Results: Uplink

For the uplink, the simultaneous dual-band transmission of only UMTS and IEEE 802.11g systems was carried out. As for the downlink transmission, the signal power and rms EVM values of the transmitted systems were first measured at the mobile transmitter (just before the transmit antenna) before wireless transmission. These values are depicted in Table 6.10. Again, the mean of 100 rms EVM readings has been reported as the final rms EVM value. As can be seen from the table the rms EVM values for both the transmitted systems was much lower than the maximum rms EVM values (shown in Table 6.7).

TABLE 6.10 UPLINK: EVM MEASUREMENTS AT THE MOBILE TRANSMITTER

System	Measured Signal	Antenna Unit		
		Peak Power (dBm)	Inband Power (dBm)	Mean rms EVM (%)
UMTS and IEEE 802.11g	UMTS 2.0 GHz	-25	-3.4	0.9
	IEEE 802.11g	-25	-4.3	1.8

Table 6.11 shows the EVM measurements at the central unit (computed in a similar manner to those of Table 6.9) for the signal transmission over both the wireless and optical links. The radius values quoted in Table 6.11 for each of the wireless systems are the distances at table-top level from a position directly below the AU. As can be seen from the results, the uplink range values for both systems, especially IEEE 802.11g, are lower than that obtained for the downlink. One reason for this could be the low transmitted signal powers used for both systems. For example, transmitted signal power of -4.3 dBm used for IEEE 802.11g was relatively low with respect to the maximum transmit power of typical mobile equipment which is 17-20 dBm for IEEE 802.11g [2]. Such low transmit powers were mainly used to ensure that the transmitted signals did not interfere with commercial radio systems outside the experimental room.

TABLE 6.11 UPLINK: EVM MEASUREMENTS AT THE CENTRAL UNIT RECEIVER

System	Measured Signal	Mobile Receiver	
		Mean rms EVM (%)	σ
UMTS and IEEE 802.11g	UMTS 2.0 GHz	8.8	2.6
		(at 4.3 m radius)	
	IEEE 802.11g	4.7	0.5
		(at 1.2 m radius)	

The results presented in Tables 6.9 and 6.11 indicate that the signal quality for the systems were within the maximum allowed rms EVM values for each system (shown in Table 6.7). Although for some systems, only small distances were achievable, it should be noted that the system experiments did not involve optimisation for radio range. Additionally, for these measurements, equal powers were always used for both the systems transmitted in the dual-band configuration. In a practical scenario, allowance could be made for the system with the more demanding requirements.

6.5 Conclusion

A WLAN system demonstrator using low-cost components (VCSELs, OM1/OM2 MMF) has been set up for the transmission of IEEE 802.11b signals at 11 Mbps and IEEE 802.11g signals at 54 Mbps via two different types of RAUs. The aim was to achieve complete coverage of a standard office room. For this, the link budget analysis (discussed in the Chapter 5) has been used to optimise the component parameter values used in the demonstrator design. A brief theoretical comparison of the performance of the two RAU designs has also been carried out using the link budget. Signal strength measurements carried out using the system demonstrator helps in verifying the range predictions carried out using the link budget analysis. The demonstrator also verifies the operation of the whole fiber-fed WLAN system, giving throughput values similar to those normally expected.

Theoretical range predictions for different radio systems such as GSM900, GSM1800, UMTS (both FDD and TDD) as well as WLANs have been carried out for a system using better component parameters. The results show that reasonable cell sizes may be achieved for all systems.

Additionally, it has been shown that different combinations of DPRS, GSM, UMTS and 802.11g (54Mbps) signals in a dual-band configuration, can be transmitted over an indoor wireless network fed by a low-cost 850 nm VCSEL-MMF optical link, with EVM measurements within the required limits.

References

[1] *Supplement to IEEE Standard for Information Technology—Telecommunications and Information Exchange Between Systems—Local and Metropolitan Area Networks Specific Requirements—Part 11: Wireless LAN Medium Access Control (MAC) and Physical Layer (PHY) Specifications: Higher-Speed Physical Layer Extension in the 2.4 GHz Band*, IEEE Standard 802.11b-1999, 1999.

[2] *Supplement to IEEE Standard for Information Technology—Telecommunications and Information Exchange Between Systems—Local and Metropolitan Area Networks—Specific Requirements Part 11: Wireless LAN Medium Access Control (MAC) and Physical Layer (PHY) Specifications Amendment 4: Further Higher Data Rate Extension in the 2.4 GHz Band*, IEEE Standard 802.11g-2003, 2003.

[3] B. Sanz-Izquierdo, J. Batchelor, and R. Langley, "Broadband multi-function planar PIFA antenna," *Loughborough Antennas Propagation Conference (LAPC)*, Loughborough, pp. 209-212, April 2005.

[4] I. Pellejero, F. Andreu, A. Barbero, and A. Lesta, "Compatibility between IEEE 802.11b and IEEE 802.11g networks: Impact on throughput," Paper 012, *Third International Working Conference on Performance Modelling and Evaluation of Heterogenous Networks*, West Yorkshire, U. K., pp. P12/1-P12/9, July 2005.

[5] D. Dobkin, "The correlation of data throughput with link loss for commercial WLAN devices," *High Frequency Electronics*, published by Summit Technical Media LLC, pp. 22-28, January 2003.

[6] R. Seide, "Capacity, coverage, and deployment considerations for IEEE 802.11g", *Cisco Systems white paper*, San Jose, CA, October 2003.

[7] J. Jun, P. Peddabachagari, and M. Sichitiu, "Theoretical maximum throughput of IEEE 802.11 and its applications," *Proceedings of the 2nd IEEE International Symposium on Network Computing and Applications (NCA '03)*, Cambridge, MA, pp. 249-256, April 2003.

[8] Javier del Prado Pavon, and Sunghyun Choi, "Link adaptation strategy for IEEE 802.11 WLAN via received signal strength measurement," *Proceedings of the IEEE International Conference on Communications (ICC'03)*, Alaska, USA, Vol. 2, pp. 1108-1113, May 2003.

[9] T. Wang and H.H. Refai, "Empirical network performance analysis on IEEE 802.11g with different protocols and signal to noise ratio values," *Proceedings of the 2nd IFIP International Conference on Wireless and Optical Communication Networks*, pp. 29-33, March 2005.

[10] M. Boulmalf, H. El-Sayed, and A. Soufyane, "Measured throughput and SNR of IEEE 802.11g in a small enterprise environment," *Proceedings of the 61st IEEE Vehicular Technology Conference*, Vol. 2, pp. 1333-1337, May/June 2005.

[11] A. Bazzi, M. Diolati, and G. Pasolini, "Measured performance of real time traffic over IEEE 802.11b/g infrastructured networks," *Proceedings of the IEEE 61st Vehicular Technology Conference*, Vol. 5, pp. 2885-2889, May/June 2005.

[12] A. Athanasopoulos, E. Topalis, C. Antonopoulos, and S. Koubias, "Evaluation analysis of the performance of IEEE 802.11b and IEEE 802.11g standards," *Proceedings of the 5th International Conference on Networking, International Conference on Systems and International Conference on Mobile Communications and Learning Technologies (ICNICONSMCL'06)*, pp. 141-147, April 2006.

[13] *3rd Generation Partnership Project; Technical Specification Group GSM/EDGE Radio Access Network; Radio Transmission and Reception*, 3GPP TS 45.005, 2004-11, version 6.7.0.

[14] *Universal Mobile Telecommunications System (UMTS); User Equipment (UE) Radio Transmission and Reception (FDD)*, 3GPP TS 25.101, 2003-03, version 6.7.0, release 6.

[15] *Universal Mobile Telecommunications system (UMTS); User Equipment (UE) Radio Transmission and Reception (TDD)*, 3GPP TS 25.102, 2003-12, version 6.0.0, release 6.

[16] *Universal Mobile Telecommunications system (UMTS); Base Station (BS) Radio Transmission and Reception (FDD)*, 3GPP TS 25.104, 2004-12, version 6.8.0, release 6.

[17] *Universal Mobile Telecommunications system (UMTS); Base Station(BS) Radio Transmission and Reception (TDD)*, 3GPP TS 25.105, 2004-12, version 6.2.0, release 6.

[18] *Radio Equipment and Systems (RES); Wideband Transmission Systems; Technical Characteristics and Test Conditions for Data Transmission Equipment Operating in the 2,4 GHz ISM Band and Using Spread Spectrum Modulation Techniques*, ETSI 300 328, November 1996.

[19] C. Lethien, C. Loyez, and J-P. Vilcot, "Potentials of Radio over Multimode Fiber Systems for the In-Buildings Coverage of Mobile and Wireless LAN Applications," *IEEE Photonics Technology Letters*, Vol. 17, No. 12, pp. 2793-2795, December 2005.

CHAPTER 7

INFLUENCE OF THE IEEE 802.11 MAC PROTOCOL ON THE RADIO-OVER-FIBRE LINK PERFORMANCE

7.1 Introduction

The previous chapters (Chapters 5 and 6) focussed on developing a link budget analysis for a WLAN system demonstrator and on its deployment. The experiments carried out in Chapter 6 mainly concentrated on verifying the link design in terms of range coverage by using signal strength and throughput measurements. However, it is equally important to estimate the impact of inserting an optical fibre path in a wireless system on the timing boundaries imposed by the wireless network's protocol. This chapter, therefore, discusses the performance of the designed WLAN-over-fibre link in terms of the WLAN MAC protocol.

To begin with, a brief introduction to the IEEE 802.11 WLAN system and the IEEE 802.11 MAC is provided. MAC protocol features such as fragmentation and the use of RTS/CTS (which are seen to improve performance in conventional wireless networks) have been experimentally investigated for WLAN-over-fibre networks and the effects are discussed. The effects on throughputs of multiple clients accessing the AP via a single RAU, and of clients simultaneously accessing the AP via two RAUs, are also analysed experimentally.

7.2 IEEE 802.11 WLAN

The IEEE initiated a project for the development of an international WLAN standard in 1990 and it adopted the first standard (IEEE Std. 802.11-1997) for WLANs in 1997 [1], [2], with a revised version coming in 1999 [3]. Quoting from the IEEE Std 802.11-1999 [3]:

"*The scope of this standard is to develop a channel access control (MAC) and physical layer (PHY) specification for wireless connectivity for fixed, portable, and moving stations within a local area. The purpose of this standard is to provide wireless connectivity to automatic machinery, equipment, or stations that require rapid*

deployment, which may be portable or hand-held, or which may be mounted on moving vehicles within a local area. This standard also offers regulatory bodies a means of standardizing access to one or more frequency bands for the purpose of local area communication."

The initial version of IEEE 802.11 defines a channel access control sublayer (called the MAC layer), MAC management protocols and services, and three PHY layers [2]. The MAC layer deals with the access to the wireless channel and the sending of data over it, while the PHY layer is responsible for the actual transmission and reception [4]. IEEE 802.11 PHY and MAC layers are discussed in Sections 7.3 and 7.4 respectively.

The main component in the IEEE 802.11 architecture is called a basic service set (BSS). The BSS is defined as a group of stations that can all communicate with each other. If in a BSS, all the stations are mobile units it is called an independent BSS (IBSS), also known as an adhoc network. In an adhoc network, all the stations communicate directly with one another implying that they should be within direct communication range of each other. The other type of WLAN network configuration is an infrastructure network (infrastructure BSS or simply BSS), where an access point controls the communication between the mobile units. An AP in a wireless network is analogous to a base station in a cellular network. In an infrastructure network, if an MU has to communicate with another MU, it needs to send the information first to the AP and then the AP sends it to the destination MU. This configuration utilises double the bandwidth compared to an adhoc network, but using an AP provides benefits such as range extension [1], [2]. Using range extension, two BSSs can communicate with each other via their APs, thus forming an extended service set (ESS). This communication is performed using a channel called the distribution system (DS), which determines whether the data received from a BSS needs to be sent back to another station in the same BSS, to an AP in another BSS via the DS, or to a destination outside the ESS [2]. The IEEE 802.11 standard does not impose any restriction on the implementation of a DS which means that it may be a wired network (Ethernet, fibre) or another wireless network. The DS is in charge of the MAC-level transport of MAC service data units (MSDUs) [1]. IEEE 802.11 MAC accepts these MSDUs from higher layers and adds information as headers and trailers to these to create MAC protocol data units (MPDUs) [2]. The MPDU, also called a MAC frame or packet, is then passed to the physical layer to be sent over the wireless channel.

7.3 IEEE 802.11 PHY

The three PHY layers defined in the IEEE 802.11 standard are [3]: infrared (IR), frequency hopping spread spectrum (FHSS) and direct sequence spread spectrum (DSSS). All three PHY layers support the mandatory 1 Mbps data rate with an optional support for the 2 Mbps rate. In 1999, two new standards, IEEE 802.11a [5] and IEEE 802.11b [6] were introduced. IEEE 802.11a operates in the 5 GHz band and uses orthogonal frequency division multiplexing (OFDM) to achieve data rates as high as 54 Mbps. The IEEE 802.11b standard is an extension to the DSSS PHY. It works in the 2.4 GHz band and supports data rates up to 11 Mbps.

In 2003, a new standard called IEEE 802.11g [7] operating in the 2.4 GHz band was introduced in order to provide the same high data rates offered by IEEE 802.11a. IEEE 802.11g offers data rates of up to 54 Mbps by introducing four different physical layers together known as the extended rate PHY (ERP) [7], [8]. The ERP in IEEE 802.11g enables the combined use of DSSS (used by IEEE 802.11b) and OFDM (used by IEEE 802.11a). The sender and the receiver can choose which layer to use as long as they both support it. The four physical layers defined in the standard are:

1) ERP-DSSS/CCK – This is the same physical layer used by IEEE 802.11b. It uses DSSS with complementary code keying (CCK) modulation to provide the IEEE 802.11b data rates of 1, 2, 5.5 and 11 Mbps.
2) ERP-OFDM – This layer uses OFDM to provide IEEE 802.11a data rates between 6 and 54 Mbps.
3) ERP-DSSS/PBCC – This is an optional layer which was introduced in IEEE 802.11b. It uses DSSS with the packet binary convolutional code (PBCC) algorithm but provides the same data rates as DSSS/CCK layer. For IEEE 802.11g additional data rates of 22 Mbps and 33 Mbps have been added.
4) DSSS-OFDM – This is also an optional layer which combines DSSS and OFDM.

Another feature introduced in the IEEE 802.11g standard is the use of a short preamble in order to reduce the IEEE 802.11 packet overhead and thereby improve performance [8]. The ERP-OFDM physical layer uses only a short preamble while the other physical layers allow the use of both long and short preamble options depending on what the

sender and receiver support. It should be noted that older IEEE 802.11 devices (1 and 2 Mbps) support only the long preamble option unless their firmware is upgraded to work with the short preamble. While IEEE 802.11b has both long and short preamble options, its short preamble is longer than that of IEEE 802.11g.

IEEE 802.11g also offers the advantage of a shorter slot-time (defined in Section 7.4) of 9 μs compared to the 20 μs slot-time used in IEEE 802.11b [8], [9]. This feature, combined with the use of a short preamble, further improves the network performance. However, the short slot-time can be used only when all the stations in the BSS transmit using the ERP-OFDM physical layer i.e., all the devices in the network support the IEEE 802.11g standard.

7.4 IEEE 802.11 MAC

The IEEE 802.11 MAC sublayer primarily has three functions: ensuring a reliable delivery of user data over the unpredictable wireless channel, providing a fair access to the wireless channel and security i.e., protecting the data [2].

Once data has been sent over the wireless channel, a station has no way of ensuring that the data has reached the destination, unlike in the case of a wired channel. For this purpose, the IEEE 802.11 MAC employs a basic frame exchange protocol in which a frame (MPDU) is sent from the source to the destination and another frame called the acknowledgement (ACK) frame is sent back by the destination acknowledging the correct receipt of the MPDU. If the acknowledgement does not come back, either due to a frame transmission error or channel error, a retransmission of the frame is allowed; this, however, reduces the performance of the network. This is known as the two-way handshaking technique. In addition to this, an optional four-way handshaking technique, known as request-to-send/clear-to-send, has also been defined. Using RTS/CTS, before transmitting an MPDU, a station sends an RTS frame as an attempt to essentially reserve the wireless channel. The destination (either a station or an AP) sends back a CTS frame to acknowledge the receipt of the RTS frame, if it is not busy with another transmission. Once the CTS frame is received, the basic frame exchange protocol is implemented. The ACK, RTS and CTS frames are known as control frames in the IEEE 802.11 MAC.

In the IEEE 802.11 MAC, two schemes for accessing the channel are defined: distributed coordination function (DCF) and point coordination function (PCF). DCF is defined as the fundamental method to access the wireless channel [1] and is based on the principle of CSMA/CA. PCF, which is not very widely implemented, is a centralized access control method based on polling and is designed to provide contention-free transfer.

This section mainly focuses on the DCF access method. PCF and its co-existence with DCF are discussed in detail in [1] – [4] and the performance of an infrastructure network with both DCF and PCF operating is additionally investigated (using simulations) in [1].

7.4.1 Distributed Coordination Function

A short description of the DCF access method is presented in this section. Comprehensive treatments of the various aspects of the DCF access have been given in [2] – [4] and [10].

The carrier sensing function of the CSMA/CA feature of DCF is performed both at the air interface, using a physical carrier sense mechanism, as well as at the MAC layer, using a virtual carrier sense mechanism. Using physical carrier sensing, the channel activity is detected by the relative level of signal strength from other stations [1]. Virtual carrier sensing is carried out based on the duration information contained either in the data or control (RTS and CTS) frames. When a station transmits a frame, the duration field in the frame indicates the amount of time after the end of the transmission of the current frame, for which the channel will be utilized for completing the transmission successfully. The other stations then set their network allocation vector (NAV) accordingly to indicate the amount of time that the channel will be busy with the current transmission. Each station will therefore wait for this duration before checking the channel again. It should be noted that the channel is sensed busy if either the physical or the virtual carrier sense mechanisms indicate that the channel is busy.

Figure 7.1 illustrates the basic access method (two-way handshaking) of the DCF. As shown in the figure, when a station (Tx station A) has a frame to transmit, it listens to the channel before beginning transmission. If the channel is idle for an interval of time

equal to or greater than the distributed inter frame space (DIFS), the station will transmit. If, however, the channel becomes busy during the DIFS (as in the case of Tx station B), the station continues listening until the channel is again sensed idle for a DIFS. The station then generates a random number called the backoff value from a time interval defined as the contention window [10]. The time period after a DIFS is slotted and the backoff value is equal to a certain number of time slots. The duration of each time slot depends on the physical layer implementation. For example, for the DSSS PHY, the value of the slot time parameter given in the IEEE 802.11 standard is 20 μs [3]. A station is allowed to transmit only at the beginning of each slot time. After a DIFS for which the channel is sensed idle, the backoff counter is decremented until either the channel is sensed to be busy again or the counter reaches zero. If the channel is sensed busy during this countdown, the timer is frozen and it starts counting down again when the channel is sensed idle for a DIFS period (as for Tx station A in Figure 7.1). The random backoff procedure implementation is the collision avoidance feature of the CSMA/CA.

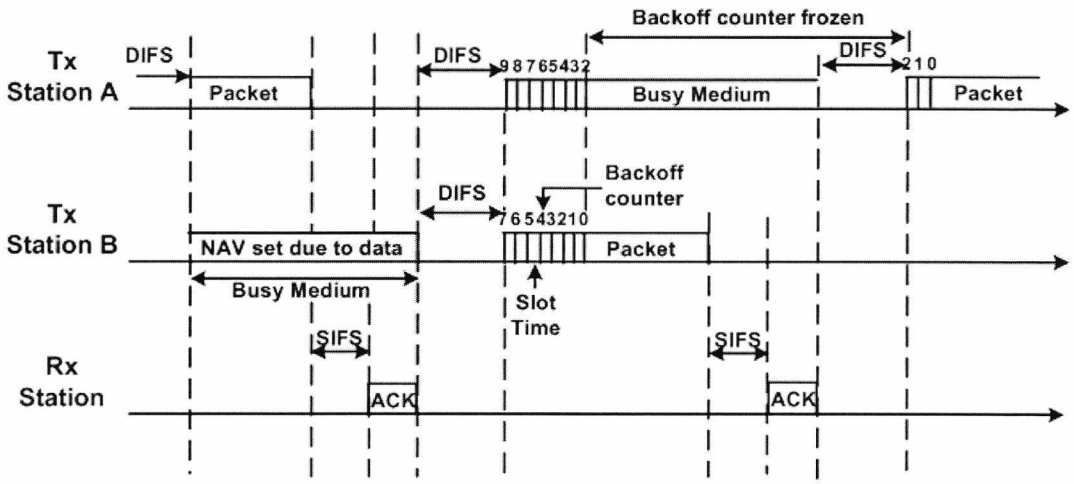

Figure 7.1. DCF: Basic access mechanism

In the event of a collision, the contention window size of the stations for which the collision has occurred is doubled and the backoff procedure is again implemented for a retransmission of frames. Another collision would result in further doubling of the contention window size and this continues until a maximum value (as specified by the standard) is reached. Once this happens, the frame is dropped and the contention window size is reset back to its minimum value as defined by the standard. The size of the contention window also depends on the PHY being implemented.

Once the frame is correctly received at the destination station or AP (Rx station in Figure 7.1), it waits for a short inter frame space (SIFS) interval and then transmits an ACK frame back to the source. The value of the DIFS is larger than the SIFS and therefore the channel cannot be sensed idle until the receipt of the ACK frame.

For the four-way handshaking technique, as depicted in Figure 7.2, the transmitting station contends for the channel in the same manner as described previously (i.e., for the basic access technique). However, before transmitting the queued MPDU, it transmits a short RTS frame (20 bytes). The aim of the RTS frame transmission is to reserve the channel by informing the neighbouring stations in the BSS of the duration of the transmission that is to follow. The information is contained in the duration field of the RTS frame and its value is equal to the amount of time needed to transmit a CTS frame, a SIFS, the data frame, another SIFS and an ACK frame (as can be seen from Figure 7.2). On receiving the RTS frame, the other stations set their NAV according to its duration field. When the destination station (whose MAC address is specified in the receiver address field of the RTS frame) receives the RTS it waits for an SIFS and then responds by sending a CTS frame (14 bytes). Again the other stations update their NAV after reading the duration field of the CTS frame.

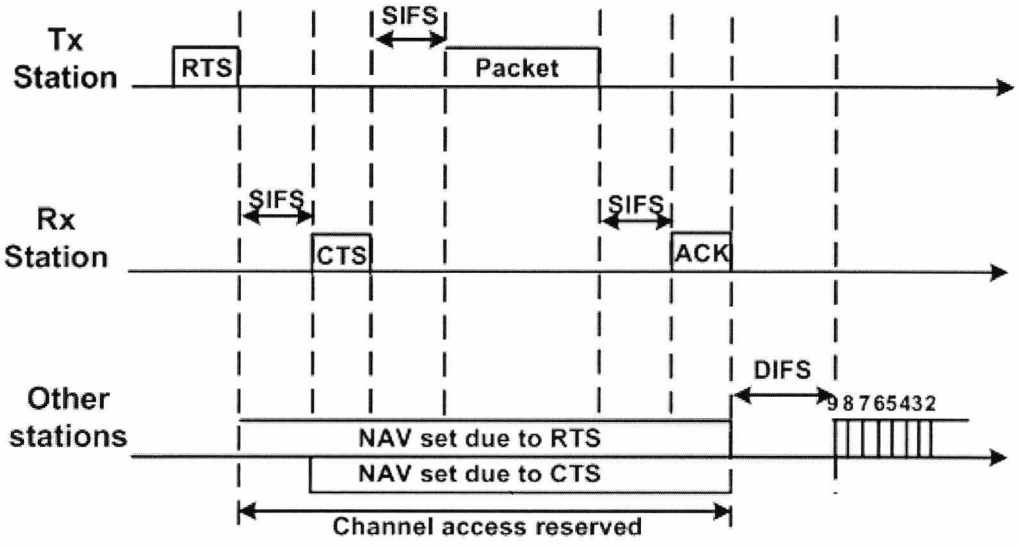

Figure 7.2. DCF access using RTS/CTS

This exchange of RTS and CTS frames is beneficial both during the transmission of large frames and to combat the hidden node problem. The maximum MPDU size specified in the IEEE 802.11 standard is 2346 bytes [3] and if a collision occurs during the transmission of such large frames, unnecessary wastage of channel bandwidth will

result. IEEE 802.11 defines a RTS threshold parameter (defined as the *dot11RTSThreshold* parameter in the standard) and the RTS/CTS mechanism can be switched on by varying the value of this parameter. This parameter can be set on each of the stations as well as at the AP. The stations can choose to use the RTS/CTS always, never or only for cases when frames with a size greater than the RTS threshold value exist. It should, however, be noted that when the network is lightly loaded or the size of the MPDU is not too large, switching on the RTS/CTS mechanism might add extra overhead and therefore result in a reduction in throughput. The hidden terminal problem and the effect of changing the value of the RTS threshold parameter in such a scenario has been experimentally investigated in sub-section 7.7.2.

7.5 Fragmentation

The IEEE 802.11 MAC employs the process of fragmentation, which involves the partitioning of the large data frames received from higher layers (MSDUs) into smaller MAC level frames, MPDUs. This increases reliability when the radio environment adversely affects the reception of longer frames [3].

The size of the fragment is decided by the fragmentation threshold parameter (defined as *aFragmentationThreshold* in [3]). The MPDU is compared to the fragmentation threshold value and if its size exceeds the threshold value, the MSDU received by the MAC is broken down into fragments, each the size of the fragmentation threshold value. The last fragment, however, is generally an exception with a size less than the threshold value. Once the fragmentation is carried out and the station is ready to transmit, it contends for the channel as described earlier in Section 7.4. On acquiring access to the channel, all the fragments are transmitted sequentially and the channel is not released until the complete MSDU has been transmitted. IEEE 802.11 labels this continuous transmission of fragments as a fragment burst. The destination station, after receiving a correct fragment, waits for an SIFS interval and sends an acknowledgement back to the source. After receiving the acknowledgement, the source waits for an SIFS interval and then sends the next fragment out. If the source does not receive the corresponding acknowledgment for a transmitted fragment, it will not send out the next fragment and the transmission is stopped. In such a case, the access to the channel will have to be given up and the source station will have to contend for the channel to transmit again.

Once access to the channel is regained, the source starts transmission with the last unacknowledged fragment.

If RTS/CTS mechanism is used with fragmentation, the RTS frame is sent out only once before the first fragment. Normally, for a data frame, the duration value is calculated from the end of that frame to the end of the ACK frame that is sent by the destination. The duration value of each fragment, however, is calculated from the end of that fragment to the end of the subsequent fragment and therefore includes the ACK frame that is supposed to follow. For the last fragment, though, the duration calculation reverts back to that for a normal data frame. Thus, when fragments are transmitted over the channel, the NAVs for the other stations in the BSS are updated based on the duration value in each fragment. The transmission of a fragmented MSDU is illustrated in Figure 7.3.

The fragmentation threshold value may be changed both for the AP and for the wireless cards being used in the stations. The default setting however is such that no frame will be fragmented. Thus, fragmentation is only useful in noisy environments where transmission of shorter fragments has been shown to be beneficial in conventional WLANs [11] due to the decrease in the time wasted when frames are corrupted. However, when such a situation does not exist, fragmentation will probably result in a fall in throughput as each fragment carries an overhead. The next sub-section (Section 7.5.1) deals with the effect of fragmentation on the performance of the designed WLAN-over-fibre network.

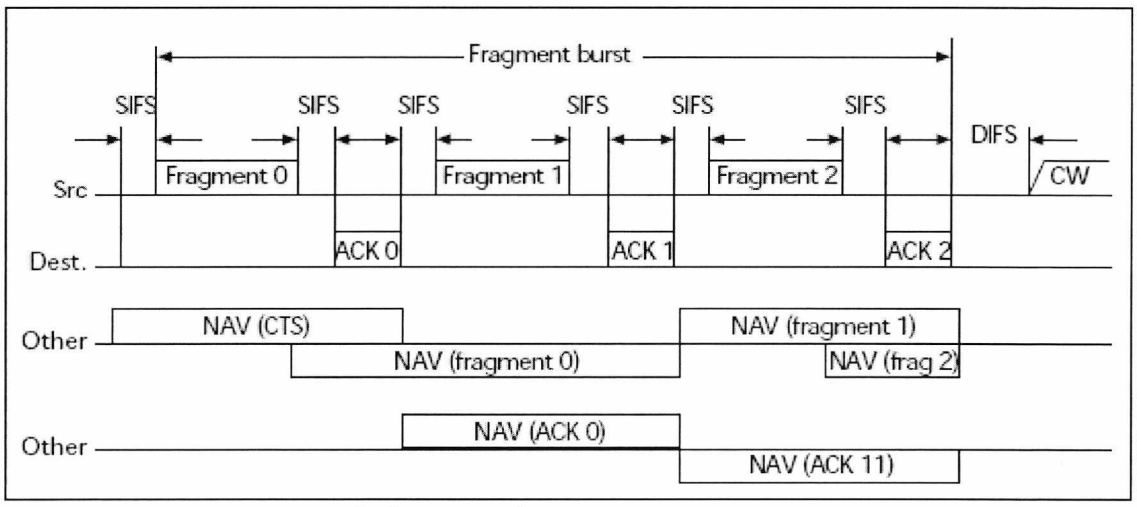

Figure 7.3. Transmission of a fragmented MSDU (reproduced from [1])

7.5.1 Experimental Results

This sub-section discusses the experimental investigation (supported by simulation results) carried out for the transmission of IEEE 802.11b and IEEE 802.11g signals, in order to analyze the effect of fragmentation threshold on the throughput performance of the WLAN-over-fibre links employing the two RAUs.

The first set of measurements was carried out for the transmission of both IEEE 802.11b and IEEE 802.11g signals via the single-antenna RAU. For these measurements, the experimental set-up is similar to the one shown in Figure 6.2 in Chapter 6 where the CU and the RAU are placed in separate rooms and connected by MMF of length 100 m. The WLAN signal was generated using the *D-Link* AP (*D-Link DWL AP2000+*). The RAU was mounted on the ceiling of a room of dimensions 6 m x 3 m x 2.7 m and a single MU was placed at a distance of approximately 3 m from the RAU. The MU used was a laptop with a *D-Link AirPlus G+ DWL-G650+* external wireless card installed. The amplifier gains were set to be equal to the values calculated using the link budget spreadsheet (DL amplifier gain: 13.2 dB and UL amplifier gain: 4.6 dB for IEEE 802.11b and DL amplifier gain: 27.2 dB and UL amplifier gain: 22 dB for IEEE 802.11g), as shown in Table 6.3, Chapter 6. For these measurements, the values of fragmentation threshold are varied both at the AP as well as the MU.

The effect of fragmentation threshold on a conventional WLAN (non-fibre based) compared to a WLAN-over-fibre system (for a fibre length of 900 m) has been discussed in [12], by means of OPNET simulations. The results show that when fragmentation is used, the throughput of the system does not change significantly when a fibre link is inserted. An MSDU size of 1500 bytes was used for the simulations and the results illustrated that a step increment in throughput occurred whenever the number of MPDU fragments obtained from a single MSDU was decreased by one. Between these thresholds, however, the throughput was seen to remain constant.

The experimental results confirming the above effect of fragmentation threshold on the throughput performance of IEEE 802.11b and IEEE 802.11g are shown in Figures 7.4a and 7.4b respectively. The two figures also depict the supporting simulation results obtained using OPNET, for different frame error rates (FER), which account for higher layer transmission errors [12]. Both Figures 7.4a and 7.4b depict that with the increase

in the fragmentation threshold, the throughput performance of both the downlink and the uplink improves. For lower fragmentation thresholds (i.e., for values less than the size of the packets being sent) more overhead is added on fragmentation and consequently results in lower throughput values. OPNET simulation results discussed in [13] also confirm the increase in throughput with an increase in fragmentation threshold for a given fibre length.

As the fragmentation threshold increases (Figures 7.4a and 7.4b), there is a point where the threshold exceeds the packet size being transmitted. For the simulations, a packet size of 1500 bytes was used but for the experiments the packet size could not be ascertained. However, for both IEEE 802.11b and 802.11g, experimental and simulation results show that the throughput becomes stable for fragmentation thresholds larger than 1500 bytes suggesting that the packets being sent are no longer fragmented. A throughput of approximately 5 Mbps for IEEE 802.11b (Figure 7.4a) and 20 Mbps for IEEE 802.11g (Figure 7.4b) is reached when the fragmentation threshold exceeds 1500 bytes.

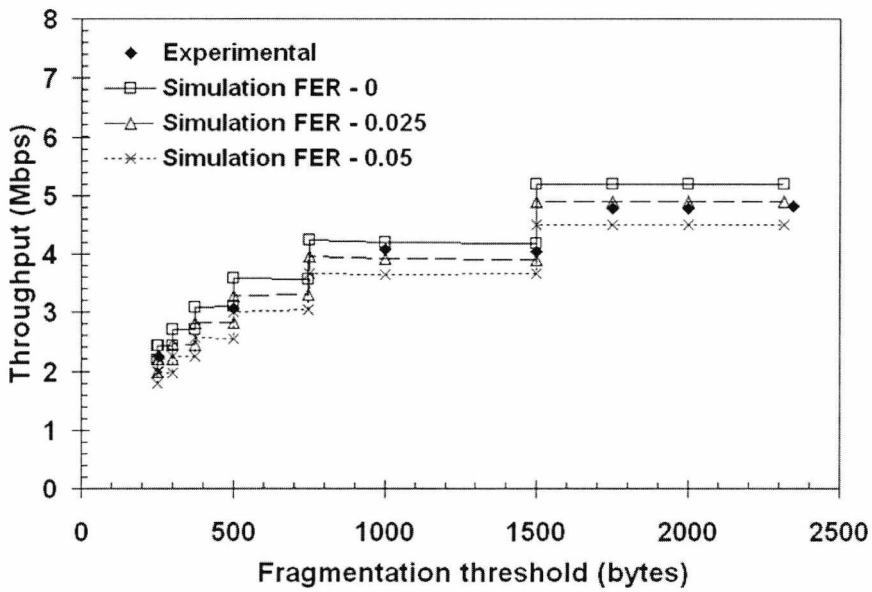

Figure 7.4a. Effect of fragmentation threshold on the downlink throughput performance for the transmission of IEEE 802.11b signals via the single-antenna RAU

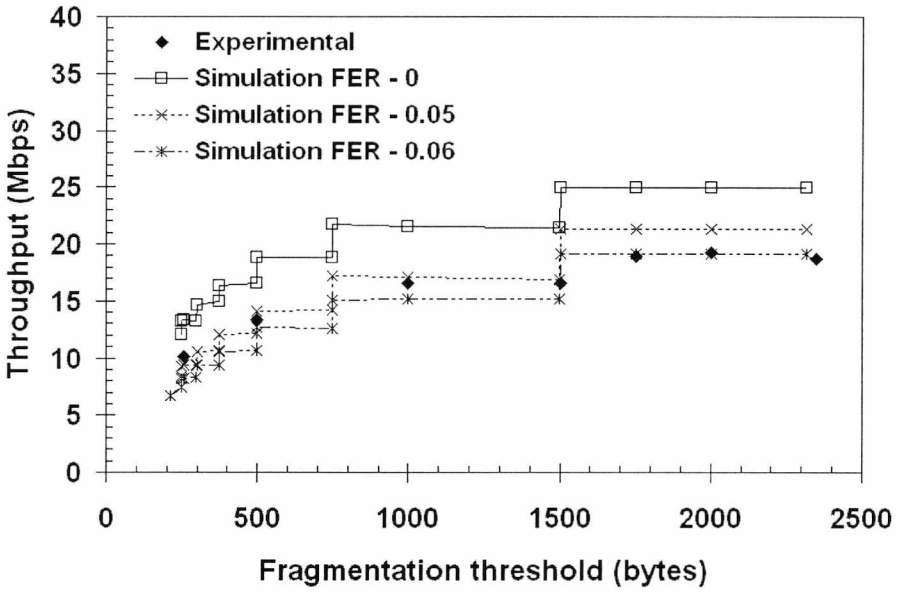

Figure 7.4b. Effect of fragmentation threshold on the downlink throughput performance for the transmission of IEEE 802.11g signals via the single-antenna RAU

Figure 7.4b also indicates that the frame error rate can be estimated to be higher in the 802.11g system as the transmissions are more susceptible to noise (compared to IEEE 802.11b). Finally, for both system transmissions, the effect of fragmentation threshold on the uplink throughput performance was observed to be very similar to that of the downlink.

The next set of measurements involved the transmission of IEEE 802.11g signals from two different access points (*D-Link DWL AP2000+* and *Netgear PROSAFE WG102*) via the two-antenna RAU. The main aim was to see if the throughput performance of the link was dependent on the type of access point being used in the network. The experimental set-up was the same as that used in Figure 6.1 in Chapter 6 with the two-antenna RAU being fed by an MMF of length 300m. The RAU was mounted on the ceiling of a room of dimensions 5 m x 6 m x 2.7 m and a single MU (the same as that used with the single-antenna RAU) was placed at a distance of approximately 3 m from the RAU. The amplifier gains were set to be equal to the values calculated using the link budget spreadsheet (DL amplifier gain: 26.5 dB and UL amplifier gain: 17.9 dB), as shown in Table 6.3, Chapter 6.

The experimental and simulation [12] results for the downlink transmission of IEEE 802.11g signals using the *D-Link* and *Netgear* access points are shown in Figure 7.5.

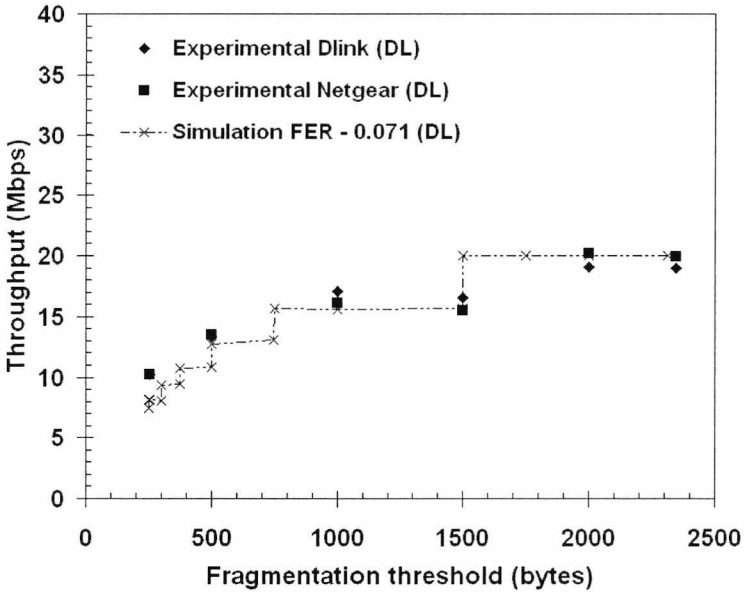

Figure 7.5. Throughput vs. fragmentation threshold for the downlink transmission of IEEE 802.11g signals from two different access points via the two-antenna RAU

As before, the graph shows an improvement in the throughput performance with increasing fragmentation threshold values. For both the access points, the fragmentation threshold ceases to have an effect on the throughput after attaining a value of 1500 bytes. Both access points are seen to give similar performances and a match with simulation results is achieved for an FER of 0.071 [12]. Fragmentation threshold was seen to have a similar effect on the uplink throughput as well.

These results suggest that the type of access point being used does not heavily influence the throughput performance. However, testing the performance of access points from other manufacturers would be helpful.

7.5.2 Influence of Fibre Propagation Delay

The insertion of an optical fibre between a WLAN AP and the wireless channel is expected to increase the delay experienced by the WLAN packets being sent over the WLAN-over-fibre networks [13] – [16].

Fibre delay is directly proportional to the length of the fibre and may be calculated by the following equation:

$$\tau = \frac{l}{c} \times 1.5 \tag{7.1}$$

where, τ = fibre delay in s

l = length of fibre in m

c = speed of light in m/s

The above formula may be derived from Snell's law, assuming a refractive index of 1.5 for the fibre. Therefore, a fibre of length 100 m would introduce a delay of 0.5 μs and a fibre of length 300 m would introduce a delay of 1.5 μs.

As has been mentioned earlier, WLAN transmission works on the principle of packets being sent from the transmitter and an acknowledgement being sent by the receiver to confirm the correct receipt of the packet. It is important that the fibre delay does not exceed the acknowledgement timeout (ACK_TIMEOUT) parameter of the transmitter [14]. If the acknowledgement is not received within the ACK_TIMEOUT, a retransmission would occur, resulting in a degradation of throughput. Unfortunately, ACK_TIMEOUT does not have a constant value specified in the IEEE 802.11 standard but depends on the chipset (of both the AP and the wireless card) manufacturer. This means that the maximum tolerable delay in a particular WLAN-over-fibre network (i.e., the maximum length of fibre that can be used in the network) depends on the access point and/or on the wireless card being used. Simulations involving varying fibre propagation delays and their effect on the throughput performance have been carried out using OPNET and the results are discussed in [13]. Their simulation results show that for a given value of ACK_TIMEOUT, there is a maximum length of fibre supported by the WLAN-over-fibre network.

Experiments were carried out using the single-antenna RAU by varying the fibre lengths to the RAU for the transmission of IEEE 802.11g signals, generated using the *D-Link* AP. As different lengths were unavailable for MMF, the measurements were carried out using SMF. Furthermore, due to the limited choice of fibre lengths available, only three different fibre lengths (1.2 km, 1.7 km and 21.2 km) could be used. As SMF was being

used, instead of 850 nm multimode VCSELs, prototype 1.5 μm single-mode VCSELs were used both at the CU and at the RAU.

Figure 7.6 shows the effect of varying the fibre length between the RAU and CU, on the throughput performance of the RoF link using the single-antenna RAU. After recording the throughput values for 1.2 km and 1.7 km fibre lengths, in the absence of more fibre lengths at the time of the measurements and to verify if the wireless card supported very long fibre lengths (as have been simulated in [13]), a 20 km fibre was inserted in the uplink path. The total fibre propagation delays for the 1.2 km (600 m fibre for uplink and 600 m for downlink), 1.7 km (500 m + 600 m fibre for uplink and 600 m for downlink) and 21.2 km (20 km + 600 m fibre for uplink and 600 m for downlink) fibre lengths were calculated (using Equation 7.1) to be 6 µs, 8.5 µs and 106 µs respectively. The fibre propagation delay calculated is the round trip delay i.e., the sum of the delay encountered by the data packets sent and the delay encountered by the acknowledgement packet sent in return. It may be noted that no fragmentation (fragmentation threshold value = 2346 bytes) was used for these measurements.

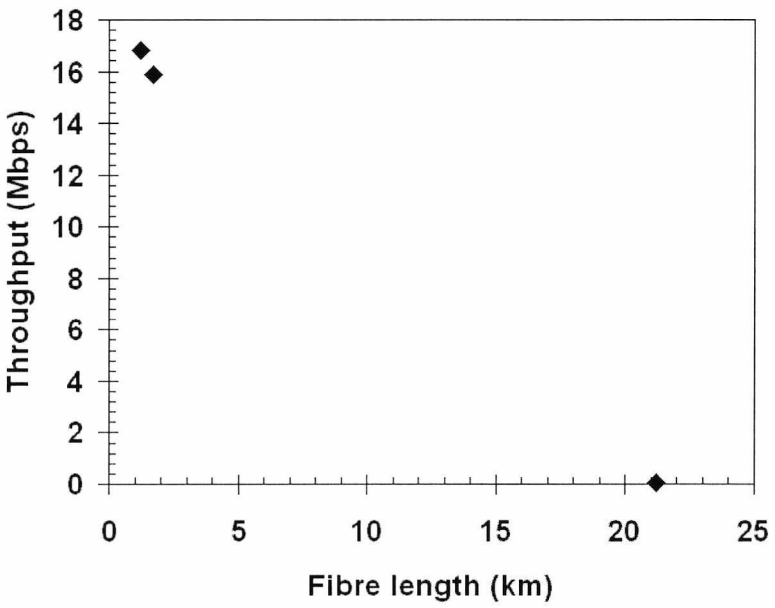

Figure 7.6. Effect of fibre length on the throughput performance of the RoF link using the single-antenna RAU

In Figure 7.6, as the fibre length increases from 1.2 km to 1.7 km, the total throughput falls from 16.8 Mbps to 15.9 Mbps. For the 21.2 km fibre, the throughput is seen to drop to 62 Kbps. Moreover, for this length, it was seen that during data transmission it was difficult to maintain the connection between the AP and the MU. This illustrates

that the propagation delay introduced by the 21.2 km fibre causes the total propagation time (between the transmission of packets and the receipt of acknowledgements) to exceed the ACK_TIMEOUT value of the transmitter. Therefore, at least for the *D-Link* AP and wireless card, fibre lengths equal to or greater than 21.2 km cannot be used for transmission.

For completion, the graph in Figure 7.7 shows the uplink throughput performance for the transmission of IEEE 802.11g signals via the single-antenna RAU fed by the 1.2 km and 1.7 km SMF, for different fragmentation threshold values.

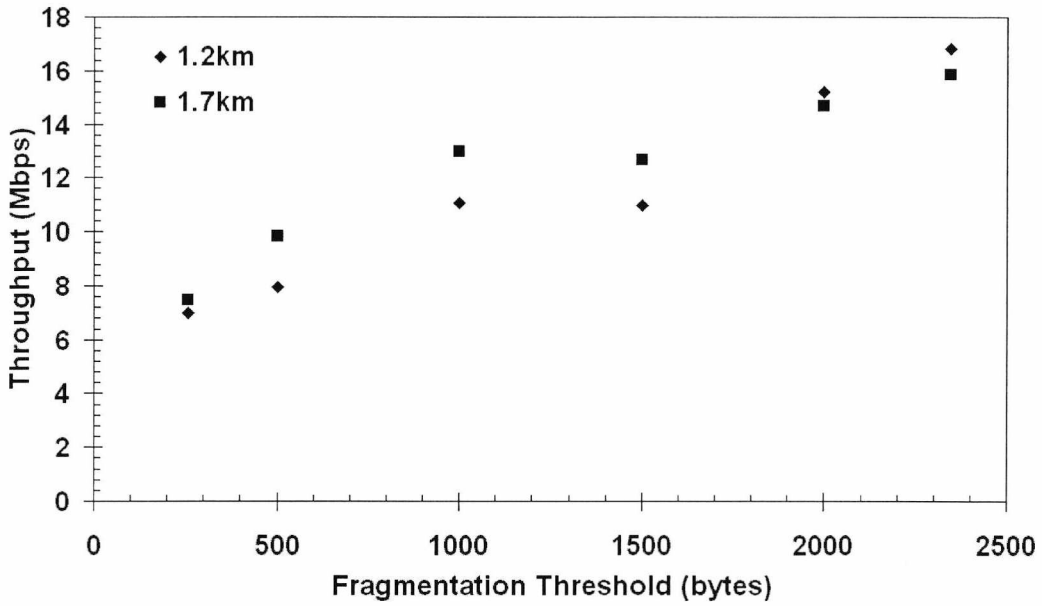

Figure 7.7. Throughput vs. fragmentation threshold for the transmission of IEEE 802.11g signals via the single-antenna RAU fed by two different lengths of SMF

As the difference in the fibre lengths was only 500 m, the throughput is seen to be close for both the fibre lengths, for the different fragmentation threshold values.

In general, the graphs in Figures 7.6 and 7.7 show that the uplink throughput recorded for the single-antenna RAU fed with SMF is lower than for the earlier cases when it is fed with an MMF (Figure 7.4b). One of the reasons for this may be the lower received signal strength recorded at the MU, even when the MU was placed very close to the RAU. The 1550 nm VCSELs used at the CU and the RAU were from different manufacturers (*RayCan RT3xxx1-F* 1550 nm VCSEL and *Vertilas VL-1550* 1550 nm VCSEL respectively) and therefore had different output optical power values. The *RayCan RT3xxx1-F* 1550 nm VCSEL, used at the CU, had a very low output optical

power compared to the 850 nm VCSEL (used for the results shown in Figures 7.4 and 7.5) resulting in a high downlink optical path loss. This loss could not be compensated by increasing the downlink amplifier gains as the isolation between the uplink and downlink paths at the RAU was not high and any increase in the amplifier gains was seen to cause interference between the two paths. This resulted in a lower downlink transmit power and the MU had to be placed very close to the RAU (approximately 1.5 m away) to obtain a 54 Mbps data rate. Even at this distance the signal strength recorded at the MU was only -67 dBm compared to the signal strength of -54 dBm recorded when the single-antenna RAU was fed by a 100m long MMF (Section 6.2.6, Chapter 6).

It must be noted that a better understanding of the influence of fibre propagation delay on the throughput performance of WLAN-over-fibre networks would have been possible if a greater number of fibre lengths were available for the measurements. Nevertheless, the results presented in this section do emphasize the importance of the ACK_TIMEOUT parameter in the context of WLAN-over-fibre networks, as the length of the fibre used will depend on this value. Another interesting variation to the experiment might have been the use of an AP and a wireless card from another manufacturer or mixing access points and wireless cards each from different vendors.

7.6 Multiple Clients Accessing a Single RAU

In the previous chapter, the throughput performances of RoF links using the two-antenna RAU and the single-antenna RAU were analysed in the context of a single MU. In a practical situation, however, the number of clients accessing the RAU, and therefore accessing the AP will, most probably, be more than one. Therefore, it is important to know how the increase in the number of clients affects throughput. This section thus examines the effect of multiple clients accessing the RAU.

7.6.1 Experimental Set-Up

The experimental configuration used for the two RAUs is similar to that discussed in Section 7.5, except that the two-antenna RAU was fed by an MMF of length 600 m (50/125 μm for downlink and 62.5/125 μm for uplink). Again for these measurements, the transmission of both IEEE 802.11b and IEEE 802.11g signals via each RAU is

discussed. A maximum of four clients (denoted as MU1, MU2, MU3 and MU4) for the two-antenna RAU and a maximum of two clients (MU1 and MU2) for the single-antenna RAU were used for the measurements. Client MU1 used an external *D-Link* wireless card, MU2 used an internal *Acer* card, MU3 also used an internal *Acer* card and MU4 used an external *Linksys* wireless card. An attempt was made to transfer a 700 MB file and the throughput performance was measured using the *Networx* commercial software (that was also utilised in some of the experiments described in Chapter 6). For all the measurements, the throughput was always measured at the receiver. The fragmentation threshold value was set to 2346 bytes at the AP and the MUs (i.e., no fragmentation was used).

7.6.2 Measurement Results: IEEE 802.11b

The results for the transmission of IEEE 802.11b via the two-antenna RAU are shown in Figure 7.8. The uplink throughput was measured as the total throughput at the AP and the downlink throughputs were measured at each MU.

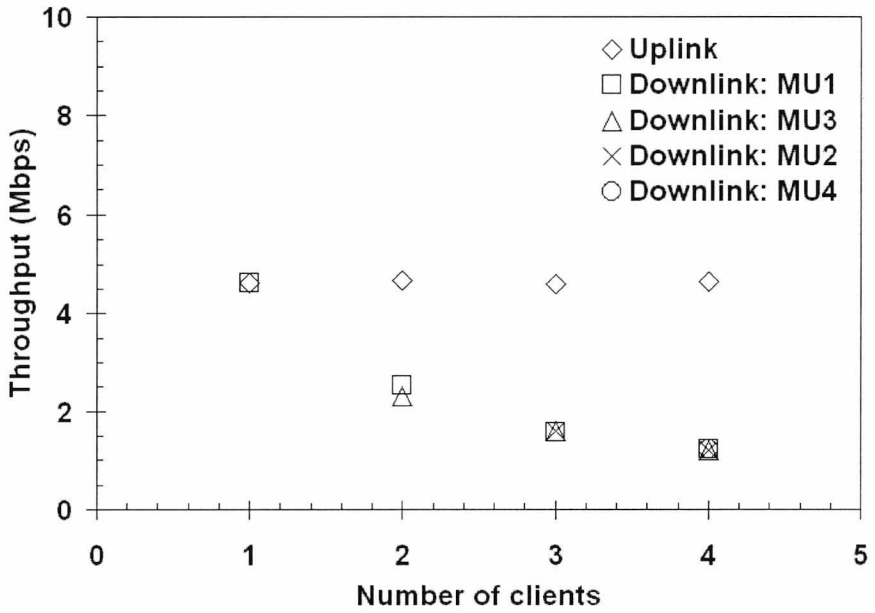

Figure 7.8. Throughput performance for the transmission of IEEE 802.11b signals via the two-antenna RAU when multiple clients are accessing the RAU

The results illustrate that the total uplink and downlink throughputs remain almost constant as the number of MUs is increased. For a single MU (MU1) accessing the RAU, the downlink and uplink throughputs are both equal to 4.6 Mbps. As the number of clients increases, the total downlink throughput which remains close to 4.6 Mbps,

becomes evenly distributed between the contending clients. Each MU receives approximately 50%, 33% and 25% of the total downlink throughput in the two (MU1 and MU4), three (MU1, MU4 and MU2) and four-client (MU1, MU4, MU2 and MU3) cases respectively. This is illustrated in Table 7.1, which lists the individual uplink and downlink throughput values recorded at each of the MUs. For instance, in the three-client case, the downlink throughput at the AP is equal to 4.9 Mbps and the downlink throughput at each of the MUs (MU1, MU4 and MU2) is approximately equal to 33% of this value i.e., 1.6 Mbps.

For the uplink however, a constant throughput (as shown in Figure 7.8) recorded at the receiver (AP) does not mean that each MU contributes equally to the total throughput, as would be the case ideally. For example, looking at the two-client (MU1 and MU4) case in Table 7.1, the uplink throughput recorded at MU1 is 67% of the total throughput at the AP while only 32% of the total throughput is recorded at MU4. A similar non-uniform distribution of throughputs among the different MUs (with MU1 contributing the maximum towards the total throughput) is also observed for the three-client and four-client cases. Such behaviour could be attributed to the type of wireless card being used for each MU.

TABLE 7.1 INDIVIDUAL UPLINK AND DOWNLINK THROUGHPUT VALUES FOR THE TRANSMISSION OF IEEE 802.11B SIGNALS VIA THE TWO-ANTENNA RAU WHEN MULTIPLE CLIENTS ARE ACCESSING THE RAU

No. of clients	Uplink					Downlink				
	MU1	MU2	MU3	MU4	AP	MU1	MU2	MU3	MU4	AP
1	4.6	-	-	-	4.6	4.6	-	-	-	4.6
2	3.2	-	-	1.5	4.7	2.5	-	-	2.3	4.8
3	2.1	1.2	-	1.2	4.6	1.6	1.6	-	1.6	4.9
4	1.6	1.1	1.2	0.8	4.6	1.2	1.2	1.2	1.2	4.8

The wireless cards used for this experiment come from different manufacturers and may be programmed in different ways to contend for the channel. Consequently, a scenario is likely to exist where a single wireless card may dominate the channel. A performance study of six different commercial cards (from different vendors) has been carried out in [17]. Their experimental results show that not all wireless cards implement the MAC protocol as defined by the standard. Variation in the minimum contention window sizes (with one of the cards not performing the backoff procedure at all) along with hardware delays being programmed in certain cards, considerably affects the throughputs achieved by them. The authors in [17] also showed that in case of frame transmission

errors, some cards choose to lower their transmission rates resulting in lower throughputs. This reduction again depends on the manufacturer and is therefore random. The research conducted in [17] therefore concludes that unfairness exists among the wireless cards from different vendors and is mainly due to the different MAC implementations in the cards rather than environmental factors.

The performance of the single-antenna RAU for the transmission of IEEE 802.11b (Figure 7.9) is very similar to the performance of the two-antenna RAU. For the single MU case, the uplink and downlink throughputs are approximately equal at 4.7 and 4.8 Mbps respectively. For the two MU case, the total uplink throughput remains at 4.7 Mbps though the individual MU contributions are recorded as 61% and 39% of the total throughput for MU1 and MU3 respectively. The reasons for this behaviour have been discussed earlier. For the downlink, each MU records similar throughputs of approximately 2.5 Mbps. (It must be noted that at the time of carrying out these measurements only two mobile units were available.)

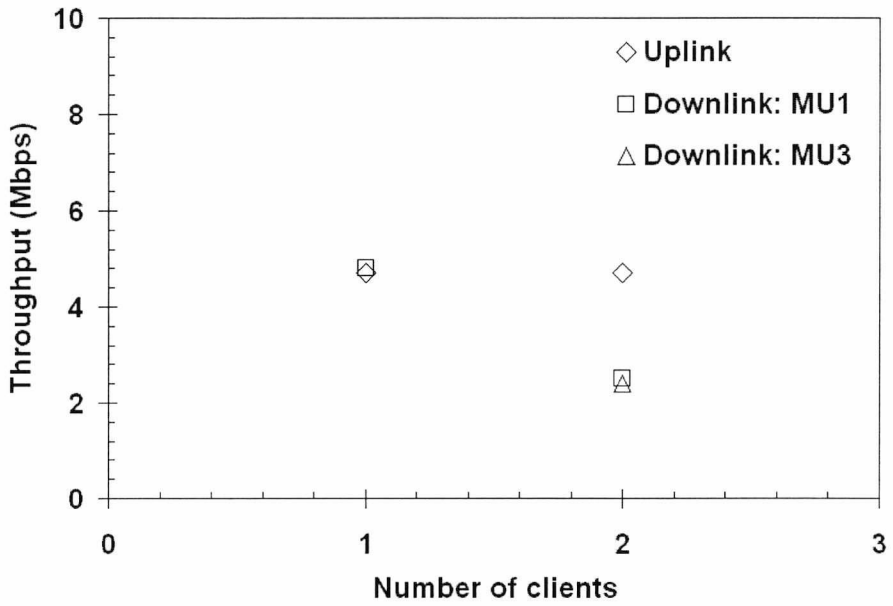

Figure 7.9. Throughput performance for the transmission of IEEE 802.11b signals via the single-antenna RAU when multiple clients are accessing the RAU

OPNET simulations were also carried out for this scenario in order to support the experimental results [12]. For both the two-antenna and single-antenna RAU configurations, the experimental and simulation results were found to agree for an FER = 0.025.

7.6.3 Measurement Results: IEEE 802.11g

For IEEE 802.11g, the results for the uplink and downlink transmission using the two RAUs are shown in Figures 7.10a and 7.10b, together with some comparative simulation results [12]. For these results, the uplink throughput is the total throughput measured at the AP while the total downlink throughput is the sum of individual throughputs at each MU.

For both the RAU configurations, while with up to two MUs the total throughput (both downlink and uplink) is observed to be relatively stable (or even rising), with more than two MUs, the experimental results show a marked decrease in throughput. The simulation results however, suggest that the total throughput should be stable when transmission rates are stable. One of the reasons for this disparity may be the increased channel errors which caused the transmission rates to drop for certain MUs, even though the connection was initially established at 54 Mbps. During the measurements, the transmission rates (and therefore the throughput values) were seen to depend on the location of the MUs in the room and it is possible that a low throughput for one MU would cause a reduction in throughputs for the other contending MUs.

In order to verify the above assumption, a scenario was simulated using OPNET (as discussed in [12]), when one of the three or four MUs transmits at 12 Mbps while the others transmit at 54 Mbps. The throughput values achieved in this case for an FER value of 0.1 were closer to the uplink experimental results (shown in Figure 7.10a). In the case of the downlink, the experimental results for three and four MUs were seen to more closely match the simulations when the AP was simulated to transmit at 12 Mbps, resulting in a lowering of throughput for all MUs (as shown in Figure 7.10b).

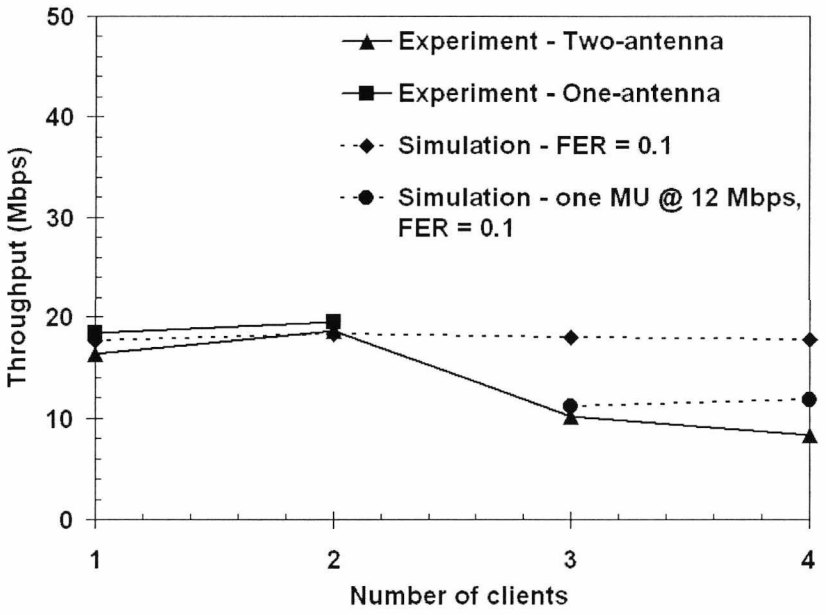

Figure 7.10a. Throughput performance for the uplink transmission of IEEE 802.11g signals via both RAUs when multiple clients are accessing each RAU: experimental and simulation results

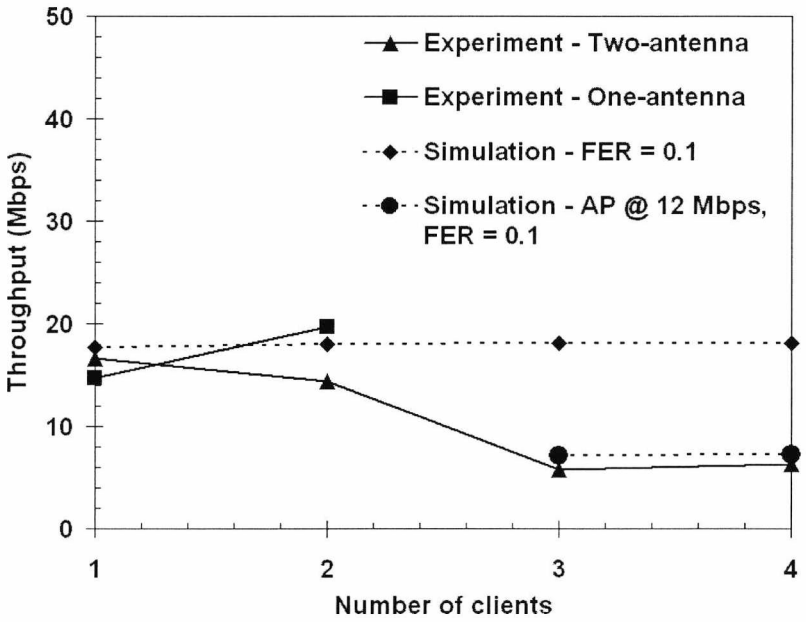

Figure 7.10b. Throughput performance for the downlink transmission of IEEE 802.11g signals via both RAUs when multiple clients are accessing each RAU: experimental and simulation results

7.7 Multiple RAUs: Single Access Point

In the previous chapter (Chapter 6), the signal strength and throughput performance of two different types of RAUs (the two-antenna RAU and the single-antenna RAU) was investigated. In both cases, each RAU was individually connected to the same AP. In

this section, the results for the simultaneous operation of the two RAUs driven by a single AP are presented.

Using multiple RAUs driven by a single AP, two kinds of scenarios have been considered:

(a) where the coverage areas for the two RAUs overlap and therefore, the MUs accessing each RAU can 'hear' each other's transmissions.

(b) where the two RAUs and the mobile units are hidden from each other.

The latter scenario is also referred to as the *hidden node problem* and will be discussed in greater detail in Section 7.7.2.

The experimental set-up used for both scenarios is a modification of the RoF link set-up described in Chapter 6. Figure 7.11 is a schematic arrangement of the experimental set-up used for the two scenarios. For the downlink, the WLAN signal from the AP is fed to a 2-port power divider (*RFLambda FLT-2-3-2700*, frequency range: 1.6–2.7 GHz) via a 3-port RF circulator (*RFLC-3000-1*, frequency range: 2.4–2.4835 GHz) and an attenuator. The divided signals are then used to drive the CU VCSELs for each RAU. For the uplink, the WLAN signals from the two RAUs, after being detected by the respective photodiodes at the CU, are combined using the 2-port power combiner (the power divider works as a combiner in the opposite direction) before being fed to the AP via an isolator and the RF circulator.

It should be noted that for the WLAN-over-fibre link using the single-antenna RAU link, prototype 1550 nm single-mode VCSELs were used as the optical transmitters in the CU and RAU (*RayCan RT3xxx1-F* 1550 nm VCSEL and *Vertilas VL-1550* series respectively). This resulted in lower received signal strength at the MU and therefore a lower throughput, even when the MU was placed close to the RAU. This has been discussed earlier in Section 7.5.2. The components used for the two-antenna RAU link however, were similar to the ones mentioned in Chapter 6 (Section 6.2.2).

7.7.1 RAUs without Hidden Nodes

The first scenario (scenario (a)) is discussed in this section, where the two RAUs were mounted on the ceilings in adjacent rooms with the CU located two rooms away from the two-antenna RAU. The two RAUs were within the range of each other and the MUs accessing each RAU could hear each other's transmissions. The amplifier gains for each RAU were calculated using the link budget spreadsheet such that complete coverage for the respective rooms was achieved. However, as the investigation was mainly in terms of the MAC protocol, it was more important to ensure that the amplifier gains used were sufficient to give good signal strength at the points where the MUs were placed. The experiments were performed for the transmission of both IEEE 802.11b and IEEE 802.11g signals.

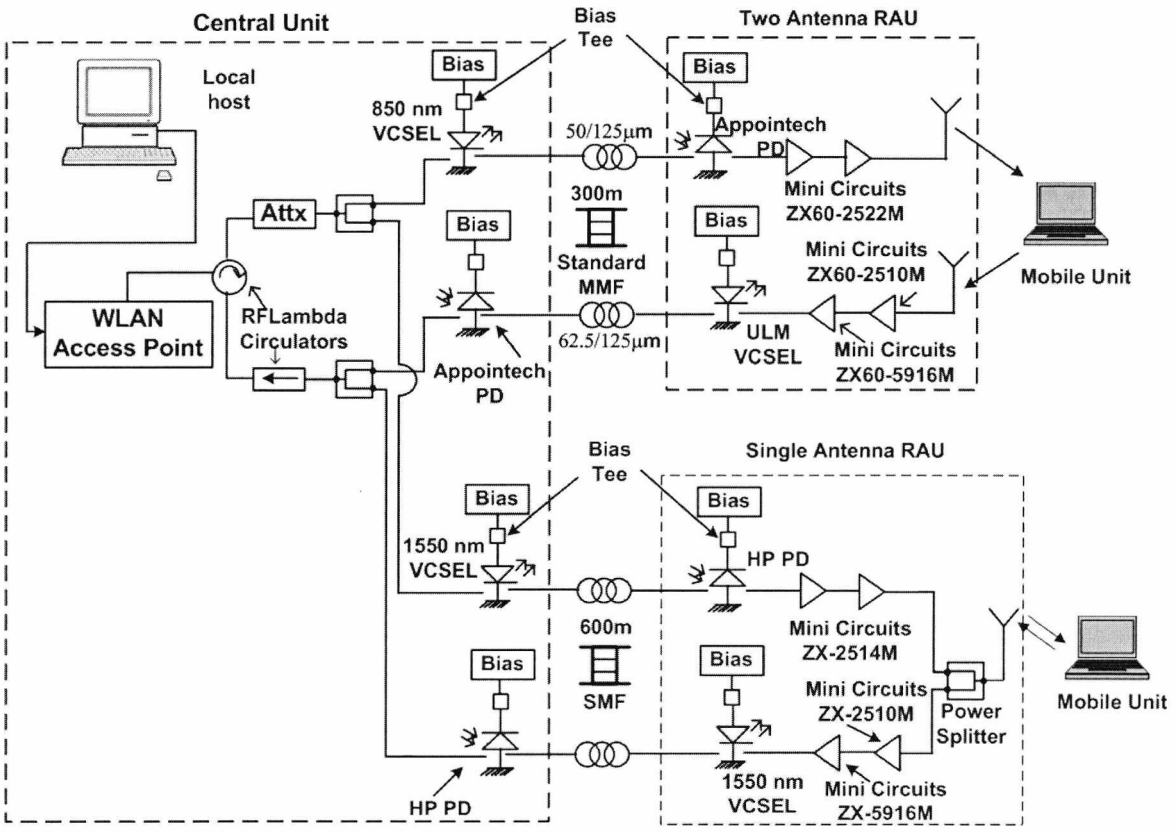

Figure 7.11. Experimental set-up for multiple RAUs driven by a single access point

7.7.1.1 RAUs without Hidden Nodes: IEEE 802.11g

Two different sets of fibre lengths were used for the experiments. For the first set, the two-antenna RAU used the same components as specified in Figure 7.11 but the single-antenna RAU was fed by a 100 m long MMF (50/125 μm for the downlink and

62.5/125 μm for the uplink). For the second set, the single-antenna RAU used the same components as specified in Figure 7.11, but the two-antenna RAU was fed by a 600 m long MMF (50/125 μm for the downlink and 62.5/125 μm for the uplink).

Two mobile units (MU1 and MU2) were used, with MU1 in the same room as the single-antenna RAU and MU2 in the same room as the two-antenna RAU, as shown in Figure 7.12. For these measurements, only the uplink transmission of IEEE 802.11g at a data rate of 54 Mbps was considered. The performance of the set-up was characterized by throughput measurements, using the *Networx* commercial software. Different configurations for accessing the AP are listed in Table 7.2 and have been discussed below.

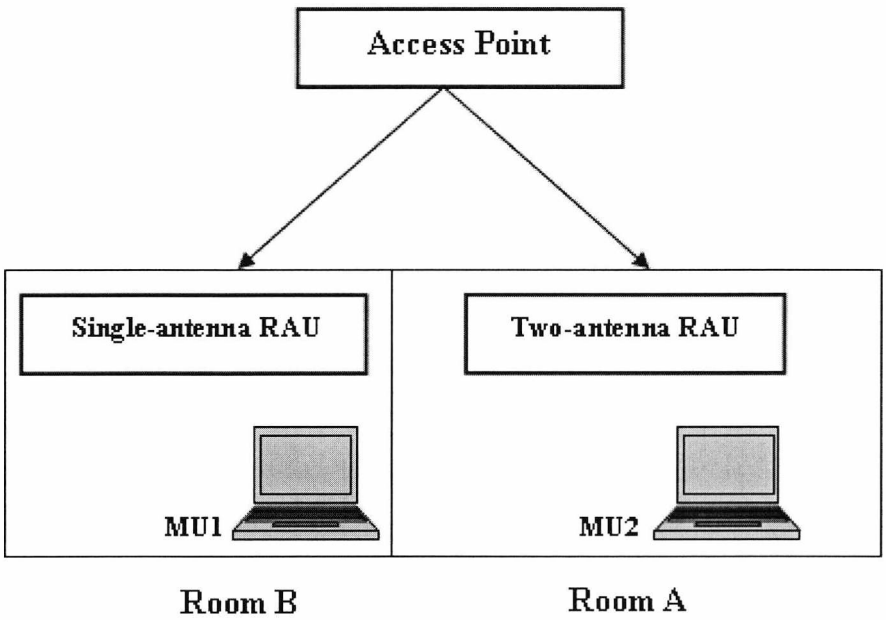

Figure 7.12. Multiple RAUs driven by a single AP: non-hidden node scenario

It should be noted that due to the high transmit power of the MU (17 dBm), each MU was seen to be able to access the AP via both the RAUs. Some of the configurations discussed involve one of the RAUs being switched off while the other continues working. In order to 'switch off' an RAU, the uplink VCSEL and amplifiers for the particular RAU were switched off. However, due to the low transmit powers of the RAUs, the downlink for each RAU was always working.

a) *Case 1*: The RAU and the MU in the neighbouring room were switched off so that each MU accessed the AP via the RAU which was nearer to it. For example, as stated for case 1a in Table 7.2, the two-antenna RAU and MU2 in room A

were switched off and MU1 in room B communicated with the AP via the single-antenna RAU also placed in room B (and hence nearer to MU1).

b) *Case 2*: The RAU nearer to an MU was switched off and the MU accessed the AP via the neighbouring RAU. For example, as stated for case 2b, the two-antenna RAU in room A and MU1 in room B were switched off and MU2 in room A accessed the AP via the single-antenna RAU. Due to the high transmit power of the mobile unit, the transmitted signal from MU2 was able to reach the single-antenna RAU located in the adjacent room. However, due to the low transmit power of the RAU, the acknowledgement from the AP was received via the two-antenna RAU which was nearer to MU2. This was verified by the observation that when the two-antenna RAU was switched off completely (both downlink and uplink), the connection between MU2 and the AP was lost.

c) *Case 3*: In this case, both the MUs accessed the AP only via one of the RAUs i.e, at any time only one of the RAUs was working. The uplink transmission (from MU to AP) was via the working RAU but the acknowledgement from the AP was always received via the nearer RAU i.e, the single-antenna RAU for MU1 and the two-antenna RAU for MU2.

d) *Case 4*: In this case, both the RAUs were working with only one MU accessing the AP at a time.

e) *Case 5*: Both RAUs and both MUs were working simultaneously.

The throughput results obtained for the above cases (corresponding to both the sets of fibre lengths) are shown in Table 7.2.

TABLE 7.2 THROUGHPUT RESULTS FOR THE UPLINK TRANSMISSION OF IEEE 802.11G SIGNALS USING MULTIPLE RAUS (WITHOUT HIDDEN NODES) FED BY TWO SETS OF FIBRE LENGTHS

Case No.	Accessing the AP – cases considered	Total uplink throughput at the AP (Mbps)	
		300 m MMF for two-antenna RAU/100 m MMF for single-antenna RAU	600 m MMF for two-antenna RAU/600 m SMF for single-antenna RAU
1a	Neighbouring (two-antenna) RAU off, only MU1 working	21.8	11.6
1b	Neighbouring (single-antenna) RAU off, MU2 working	10.2	5.1
2a	Own (single-antenna) RAU off, only MU1 working	10.6	5.8
2b	Own (two-antenna) RAU off, only MU2 working	4.5	5.6
3a	Both MUs working, single-antenna RAU working	16.7	8
3b	Both MUs working, two-antenna RAU working	12.7	5.9
4a	Both RAUs working, only MU1 working	6.4	11.3
4b	Both RAUs working, only MU2 working	11.3	5.7
5	Both RAUs working, both MUs working	7.6	8.4

The following observations may be made from the table:

a) For the 300 m/100 m MMF set, when MU1 is operating alone and the nearer RAU, i.e., the single antenna RAU, is working, the throughput achieved is close to 22 Mbps (case 1a). However, when both RAUs are working simultaneously, as in case 4a, the throughput of MU1 drops by approximately 71% to 6.4 Mbps. For MU2, however, the throughput for case 1b (10.2 Mbps) is approximately 10% lower than for case 4b (11.3 Mbps). As the throughput values were seen to vary with time (or measurement instant) for each MU, the latter variation in throughput is relatively insignificant. The marked decrease in throughput for MU1 may be explained by the difference in the fibre delay encountered by frames sent via the two RAUs. The two-antenna RAU uses a 300 m MMF with a total round-trip fibre delay of 3 μs while the single-antenna RAU uses a 100 m MMF with a total round-trip fibre delay of only 1 μs. It is assumed that a frame from MU1 arriving at the AP after the two different delays can interfere with itself, causing the reduction in throughput. This assumption is verified by the results when approximately equal fiber lengths are

used - 600 m MMF for the two-antenna RAU and 600 m SMF for the single-antenna RAU. Comparing cases 1a (11.6 Mbps) and 4a (11.3 Mbps) for this set, the fall in throughput for MU1 is only 2.5%. Note that the higher optical path loss for the single-antenna RAU (as discussed in Section 7.5.2) causes the reduction in the throughput, as does the increased delay (total round-trip delay of 6 μs) introduced by the 600 m long fibre. For MU2, on the other hand, the throughput for case 1b (5.1 Mbps) is 10.5% lower than that of case 4b (5.7 Mbps). The difference in the throughputs for MU2, despite the fibre lengths for the two RAUs being the same, may be again attributed to the fact that the throughput values are seen to vary with time (or measurement instant) for each MU.

Results from OPNET simulations for a scenario where up to two MUs transmit via different fibre lengths to the AP, with the MUs within transmission range of each other but only in the receiving range of one RAU, conclude that the interference apparent in the experiment will not occur [12]. The simulations show a stable throughput of 20 Mbps irrespective of the fibre lengths. Therefore, based on the measurements and simulations, it may be concluded that the difference in the length of the fibre being used for each RAU affects the throughput only in cases when MUs are in the receiving range of more than one RAU. In such situations, the throughput is more stable if equal lengths of fibre are used for each RAU. It can also be stated that this is a PHY layer effect which might be alleviated by employing some form of MU transmit power control.

b) For the 300 m/100 m MMF set, in cases 2a (10.6 Mbps) and 2b (4.5 Mbps), when the RAU closer to a mobile unit is off (discussed as case 2, earlier), the throughputs for MU1 and MU2 decrease by approximately 51% and 56% compared to cases 1a (21.8 Mbps) and 1b (10.2 Mbps) respectively. For the 600 m/600 m fibre set, however, the throughput for MU1 decreases by 50% (from 11.6 Mbps for case 1a to 5.8 Mbps for case 2a) while there is a relatively insignificant change in throughput for MU2 (from 5.1 Mbps for case 1a to 5.6 Mbps for case 2a). Due to the greater distance between the transmitting MU and the working RAU in this case (they are located in different rooms, as shown in Figure 7.12), the received signal strength at the RAU can be expected to be low, resulting in a lower throughput.

c) For both the fibre sets, in cases 3a and 3b, when both the mobile units are using only one RAU to access the AP, it would be expected that the total uplink throughput recorded at the AP equals the sum of the individual uplink throughputs recorded for each MU accessing the particular RAU in the previous cases. For example, in case 3a for the 300 m /100 m MMF set, when the single-antenna RAU is working, the total uplink throughput at the AP should be equal to the sum of the individual MU throughputs in cases 1a (21.8 Mbps) and 2b (4.5 Mbps) i.e., 26.3 Mbps. Similarly, for case 3b, the total uplink throughput at the AP should be equal to the sum of the throughputs in cases 1b (10.2 Mbps) and 2a (10.6 Mbps) i.e., 20.8 Mbps. The throughputs recorded, however, are 36.5% and 38.9% lower than the expected values for cases 3a (16.7 Mbps) and 3b (12.7 Mbps) respectively. This behaviour may be explained by considering the individual throughputs recorded at each MU in the above cases. It should be noted that these throughput values have not been quoted in Table 7.2, as all the throughput values reported till now have been the ones recorded at the receiver (i.e., for the uplink, throughput was measured at the AP and for the downlink, throughput was measured at the individual MUs).

In case 3a (single-antenna RAU working), individual uplink throughputs of 10.9 Mbps and 4.9 Mbps were recorded at MU1 and MU2 respectively. Comparing these values with the throughputs in cases 1a and 2b respectively, the throughput for MU1 falls by 50% (from 21.8 Mbps in case 1a to 10.9 Mbps) while there is a relatively insignificant change in throughput for MU2 (from 4.5 Mbps in case 2b to 4.9 Mbps). In case 3b (two-antenna RAU working), individual uplink throughputs of 2.8 Mbps and 8.8 Mbps were recorded at MU2 and MU1 respectively. Comparing these with the throughput values for cases 1b and 2a respectively, it is seen that the throughput for MU2 falls by approximately 72% (from 10.2 Mbps in case 1a to 2.8 Mbps) and the throughput for MU1 falls by 17% (from 10.6 Mbps in case 2a to 8.8 Mbps). The fall in throughput for MU1, in case 3a, and for MU2, in case 3b, is mainly due to the additional client (i.e., MU2 or MU1 respectively) now contending for the channel via its 'own' RAU (i.e., the nearer RAU). In an ideal situation the throughput drop should be equal for both mobile stations, but practically, this is seen to depend on the how the wireless cards used in the stations are programmed to contend for the wireless channel (as has been discussed earlier in Section 7.6). During the measurements, it was again observed that some wireless cards dominate

the channel usage thereby decreasing the throughput of the other contending stations to extremely low values.

d) For case 5, when both RAUs and both MUs are working, the situation is far more complex, with the throughput being affected both by the different fibre delays and by the other MU contending for the channel. This results in a very low overall uplink throughput. Comparing cases 4 and 5, for the 300 m/100 m MMF set, the throughput for MU2 drops by 84% (from 11.3 Mbps in case 4b to 1.8 Mbps in case 5) while the throughput of MU1 drops by only 6% (from 6.4 Mbps in case 4a to 6 Mbps in case 5). For the 600 m/600 m fibre set, however, the throughput for MU2 drops only by 65% (from 5.7 Mbps in case 4b to 2 Mbps in case 5), while the throughput for MU1 falls by 47% (from 11.3 Mbps in case 4a to 6 Mbps in case 5). Therefore, the fall in throughput is much more uniform for equal fibre lengths. It should be noted that for these comparisons, individual uplink throughputs for the MUs have been considered in case 5. These throughput values are not presented in Table 7.2 due to reasons discussed earlier (in observation (c)).

These results, thus, demonstrate that it is possible to have a scenario in which multiple RAUs are being fed by a single AP for the transmission of IEEE 802.11g signals. The results also show that improved throughput performance is achieved when equal lengths of fibre are used for the two RAUs. The discussion based on the simulation results presented in [12] however indicates that such an improvement is possible only when the MUs are in the receiving range of more than one RAU. The effect of a particular wireless card dominating the wireless channel is again observed from the results for cases 3 and 5. Finally, the throughput performance when multiple RAUs and multiple MUs are operating simultaneously (case 5) is not satisfactory, compared to the throughput performance achieved when multiple MUs access the AP via one RAU (as discussed in Section 7.6.3). The overall decrease in throughput for the 600 m/600 m fibre set compared to the 300 m/100 m fibre set for all the cases can be attributed to the higher optical path loss (for the single-antenna RAU link) and to the increased fibre delay (for both RAU links).

7.7.1.2 RAUs without Hidden Nodes: IEEE 802.11b

To verify if the throughput degradation in the case of IEEE 802.11g was a result of the multiple RAU configuration, the transmission of a lesser demanding system like IEEE 802.11b (at 11 Mbps) over the same experimental set-up was considered. As it has been established previously that a more stable throughput performance may be achieved by using equal lengths of fibre for the two RAUs, the following measurements have been performed using only the 600 m (MMF, for the two-antenna RAU)/600 m (SMF, for the single-antenna RAU) fibre set. The resultant throughputs for the transmission of IEEE 802.11b for the various configurations (both downlink and uplink) are listed in Table 7.3. For the measurements, the uplink throughput was recorded at the AP and the downlink throughputs were recorded at each mobile unit.

TABLE 7.3 THROUGHPUT RESULTS FOR THE TRANSMISSION OF IEEE 802.11B SIGNALS USING MULTIPLE RAUs (WITHOUT HIDDEN NODES)

Case No.	Accessing the AP – cases considered	Uplink	Downlink	
		Throughput measured at the AP (Mbps)	Throughput measured at MU1 (Mbps)	Throughput measured at MU2 (Mbps)
1a	Neighboring (two-antenna) RAU off, only MU1 working	4.6	4.7	-
1b	Neighboring (single-antenna) RAU off, MU2 working	4.8	-	4.8
2a	Own (single-antenna) RAU off, only MU1 working	4.2	4.7	-
2b	Own (two-antenna) RAU off, only MU2 working	4.8	-	4.8
3a	Both MUs working, single-antenna RAU working	4.7	2.5	2.4
3b	Both MUs working, two-antenna RAU working	4.6	2.5	2.4
4a	Both RAUs working, only MU1 working	4.7	4.7	-
4b	Both RAUs working, only MU2 working	4.7	-	4.7
5	Both RAUs working, both MUs working	4.7	2.5	2.3

The following observations may be made from Table 7.3:

a) In all cases, both mobile units exhibit similar throughput performance.

b) Comparing cases 1 and 4 (as discussed in the Section 7.7.1.1), the difference in uplink throughputs for either MU is insignificant, as can be seen from the throughput values in cases 1a (4.6 Mbps) and 4a (4.7 Mbps) for MU1, and cases 1b (4.8 Mbps) and 4b (4.7 Mbps) for MU2. This again shows that the throughput performance of a mobile unit is not affected by the number of RAUs operational within its range provided the fibre lengths between the different RAUs and the AP are equal. Furthermore, as expected the downlink and uplink throughput values for each MU are also very similar to each other.

c) For cases 2a and 2b, when the RAU nearer to a mobile unit is switched off along with the neighbouring MU, the throughput values remain the same as were for cases 1a and 1b. For obtaining such a performance, it is important that the downlink path for each RAU must be working at all times. As has been mentioned while discussing case 2 (Section 7.7.1.1), the MU transfers the uplink data via the neighbouring RAU but receives the acknowledgement packets from the AP via the downlink path of the RAU nearer to it.

d) In cases 3a and 3b, when both MUs are working via a single RAU, the total uplink throughputs recorded at the AP are similar to the other cases (including case 5) when both RAUs and both MUs are working simultaneously. The individual uplink throughputs at the MUs were, however, recorded to be approximately 63% (of 4.7 Mbps) for MU1 and 35% (of 4.7 Mbps) for MU2 in case 3a, 64% (of 4.6 Mbps) for MU1 and 35% (of 4.6 Mbps) for MU2 in case 3b and 64% (of 4.7 Mbps) for MU1 and 34% (of 4.7 Mbps) for MU2 in case 5. It is expected that an increase in the number of clients per RAU would lead to such a drop in throughput for each MU. However, as has been stated earlier, each MU should contribute an equal fraction towards the total uplink throughput in theory, but practically this is never seen to be the case. These throughput values again indicate that the channel is being dominated by a single wireless card. The downlink throughputs for each MU, on the other hand, are approximately 50% of the total downlink throughput recorded at the AP in all three cases (cases 3a, 3b and 5).

Thus, the throughput performance of the WLAN-over-fibre network, for IEEE 802.11b, remains the same whether a single RAU is used or whether multiple RAUs (using equal

fibre lengths for the RAUs) are implemented, which is how it should be in an ideal situation. Also, as is seen from the results, the performance of IEEE 802.11b is better than IEEE 802.11g and most of the results obtained are predictable.

7.7.2 Hidden Node Scenario

It has been discussed earlier (Section 7.4.1) that the DCF access technique of the MAC protocol works on a carrier sense mechanism in which a station will always listen to the channel before transmitting any data. Even when a data frame is transmitted, the other stations in the BSS will set their NAV according to the duration information in the frame and not contend for the channel during that time. In the context of infrastructure networks, the carrier sense feature of the DCF enables each station to 'hear' the transmission from either the AP or a neighbouring station. The situation, however, becomes complicated when there is a station that can hear the AP but not the other stations – this particular situation is described as the hidden node scenario (Figure 7.13).

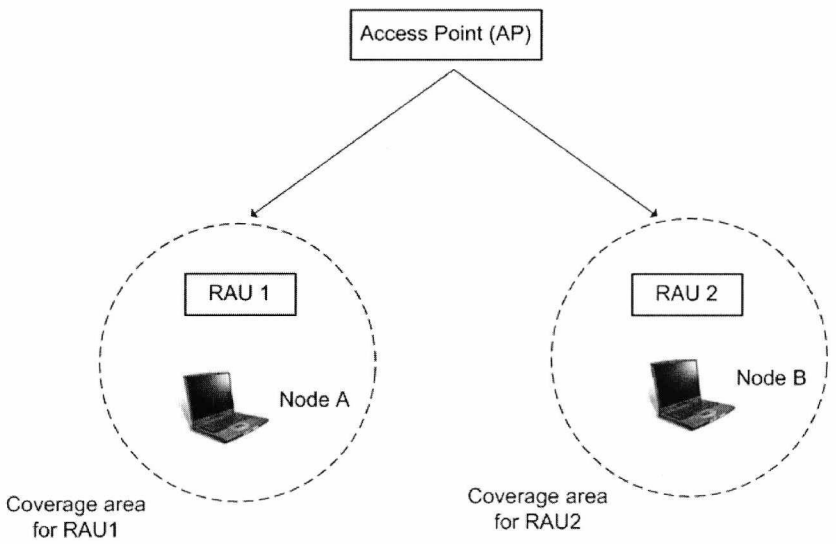

Figure 7.13. Multiple RAUs driven by a single AP: hidden node scenario

As shown in Figure 7.13, both nodes A and B can hear the AP via their own RAUs but cannot hear each other's transmissions as they are out of range (it is also possible that there is an obstacle between them). There may be a situation when node A, sensing that the channel is idle, waits for the DIFS period and then starts a transmission to the AP. During this transmission, node B, which has a queued MPDU, also decides to transmit; and as it cannot hear node A, it also senses the channel to be idle, waits for a DIFS and

starts transmitting. In such a scenario, both the data frames are bound to collide with one another thereby resulting in a drop in throughput.

If the RTS/CTS mechanism is switched on in this case (at both the AP and the two nodes) then node A, before sending out a data frame would send out an RTS request. The AP, upon receiving the RTS frame, would send back a CTS response. Even though node B cannot hear node A's RTS frame, it will be able to hear the CTS frame sent by the AP and will consequently set its NAV based on the duration information contained in the CTS frame. Node B will therefore hold back transmitting. Even if node B sends out an RTS request at the same time as node A, the only collision likely to occur will be that of the RTS frames and therefore the channel bandwidth will not be significantly wasted.

Specifically related to WLAN-over-fibre networks, very little information is available in literature on the use of RTS/CTS as a solution to the hidden node problem. Most research on the hidden node problem has been conducted in the context of conventional WLAN networks and primarily focuses on IEEE 802.11b adhoc networks.

In particular, the throughput performance of high-speed IEEE 802.11b adhoc networks is discussed in [18]. Their results (simulations) indicate that basic access performs better than RTS/CTS when no hidden terminals are present and when the network load is not very high. The effect of different values of the RTS threshold parameter on the performance of the IEEE 802.11 protocol has been analysed by means of simulations in [19]. Their results indicate that choosing an optimal RTS threshold value is very important in improving the throughput performance of the network, especially for longer packet lengths, high packet arrival rates and for larger number of nodes. They conclude that the number of contending stations is the main factor influencing the choice of an optimal RTS threshold.

The effect of hidden terminals and the use of RTS/CTS as a solution for a 1 Mbps IEEE 802.11 adhoc network is discussed in [20]. Their simulation results confirm that the performance of the protocol degrades in the presence of hidden terminals and an acceptable throughput is achieved only when less than 10% of the station pairs are hidden. They also verify that RTS/CTS helps improve network performance in the

presence of hidden terminals and the best throughput for such a scenario is achieved when RTS/CTS is used before the transmission of each frame irrespective of its length.

The results discussed in [18], [19], [20] mainly concentrate on the performance of adhoc low rate IEEE 802.11 networks. The effectiveness of RTS/CTS in current high rate IEEE 802.11b and IEEE 802.11a networks is investigated in [21]. They analyse the performance of an infrastructure network using a basic rate set of 1 and 2 Mbps for IEEE 802.11b, and 6 to 24 Mbps for IEEE 802.11a. The authors state that for lower data rate networks, since the transmission of both data and control frames takes place at the same rate, collisions can be avoided by using RTS/CTS, especially for longer frames. However, in the case of higher data rate networks (like IEEE 802.11b going up to 11 Mbps and IEEE 802.11a up to 54 Mbps), the rate at which data frames are transmitted can be much higher than the control frame rate as the control frames are generally transmitted at one of the rates from the basic rate set or one included in the PHY mandatory set (as defined in the IEEE 802.11 standard), which is supported by all the stations. Thus, the control frames with the additional overheads use as many resources and have transmission times comparable to that of the data frames, making the earlier reason for using the RTS/CTS scheme (i.e., lower collision time) invalid. They also show for IEEE 802.11b networks, by means of simulations, that RTS/CTS performs better than basic access only for heavily loaded networks. For the hidden node scenario, using an 11 Mbps transmission rate, their results indicate that the basic access performs better for a hidden node probability of less than 10%, after which the throughput falls rapidly.

One of the more recent works which investigates (by means of simulations) the effect of RTS/CTS on the performance of WLAN-over-fibre networks is [22]. For a case where no hidden nodes are present, they conclude that for lower fibre delays basic access performs better than RTS/CTS as discussed in [18] for a conventional WLAN network (not WLAN-over-fibre). However, either an increase in the network load with longer frame transmissions or an increase in the fibre delay can change the situation in favour of switching on the RTS/CTS mechanism. Their simulations also suggest determining an optimum RTS threshold value, which depends upon the size of the MPDU frame being transmitted. Additionally, they analyse the effect of transmission rates on the RTS/CTS performance and conclude that the lower the transmission rate to control rate ratio, the better is the RTS/CTS performance compared to the basic access scheme, as in

the case of a conventional WLAN network (as discussed in [21]). In the case of hidden nodes, their simulation results show that RTS/CTS proves very effective in reducing the throughput degradation. For a case of 20 hidden nodes operating in the network, RTS/CTS improves the throughput performance by ten-fold for an MPDU size of 1500 bytes. The worst throughput degradation is identified in a situation where there are equal numbers of hidden station pairs. For simulating such a scenario, they consider 30 stations divided into two groups hidden from each other, with 15 stations in each group. The results show that for a packet size of 2000 bytes, the throughput is approximately 14 times lower than that for a non-hidden node case. In such a situation, switching on the RTS/CTS mechanism results in a 14.4 times increase in throughput. However, the magnitude of the throughput improvement caused by RTS/CTS decreases for increased fibre lengths for the hidden node scenario.

In a more recent investigation [23], the transport of Transmission Control Protocol (TCP) and User Datagram Protocol (UDP) traffic over a fibre-fed IEEE 802.11b network (maximum fibre length: 13.2 km) is both simulated and experimentally verified. It is concluded that the introduction of the fibre delay degrades the TCP performance more than the UDP performance. The results, though, are reported only for a single station case; an increase in the number of stations contending for the common medium might cause significant differences.

7.7.2.1 Experimental Verification

With WLAN-over-fibre networks consisting of several RAUs placed in clearly separated areas, driven by a single AP, the occurrence of groups of MUs hidden from each other becomes more probable [22]. Therefore, the degradation of throughput caused by hidden nodes in a WLAN-over-fibre network and the use of RTS/CTS mechanism to combat this problem is investigated in this sub-section. The RTS/CTS mechanism is used prior to the transmission of a MPDU if the MPDU size is greater than the RTS threshold parameter.

The experimental set-up used for the analysis of the hidden node scenario is the same as the one shown in Figure 7.11. For this situation, however, the single-antenna RAU was moved to an anechoic chamber at a distance where the mobile units accessing the two RAUs were unable to hear each other's transmissions. The anechoic chamber was

mainly utilised to further improve the isolation between the mobile units using each RAU.

Two mobile units – MU1 and MU2 – were used to access the AP via the two RAUs (one MU per RAU). In order to verify that the nodes were completely hidden (i.e., could not hear each other at the chosen distance), an adhoc network was temporarily set up between the two mobile units. The two MUs were first placed close to one another, where they immediately detected each other's presence. Then one of the mobile units was moved away from the other until the anechoic chamber was reached. It was noted that the connection to the adhoc network was lost mid-way. The amplifier gain values for the two RAUs (using the link budget separately for each RAU) were calculated and set for achieving a maximum range of 6 m for each RAU. This implied that the transmit powers of the two RAUs were very low compared to the transmit powers of the mobile units (17–20 dBm). Thus, as the MUs could not hear each other, it could be safely assumed that the two RAUs were also completely isolated.

The measurements were carried out for the uplink transmission of IEEE 802.11g signals at 54 Mbps. For the measurements, MU1 accessed the AP via the single-antenna RAU and MU2 used the two-antenna RAU. The uplink throughputs recorded for MU1 and MU2, when operating alone via their respective RAUs, were 11.7 Mbps and 9.3 Mbps respectively. However, when simultaneous operation was initiated, MU1's performance was seen to be severely affected by the introduction of the hidden node, MU2. This behaviour was seen to occur irrespective of the RAU being accessed. The throughput for MU2 also dropped to a lower value when MU1 started transmitting but it maintained a reasonably constant value with time and did not get completely disconnected. It should be noted that during these preliminary measurements, the RTS/CTS mechanism was turned off.

Experiments were also conducted using four MUs, by creating two groups hidden from one another with each group accessing one RAU at a time. Initially all the MUs were placed in the same room; i.e., there were four MUs in the first group and no MUs in the second. Then the number of MUs in the second group was increased until there were equal numbers of MUs in each group. The measurements were carried out for both basic access (when RTS/CTS was set to its maximum value of 2432 bytes) and for RTS/CTS always on (when set to its minimum value of 256 bytes). Figure 7.14 compares the

effect of the increase in the number of hidden nodes on the throughput performance in the two scenarios.

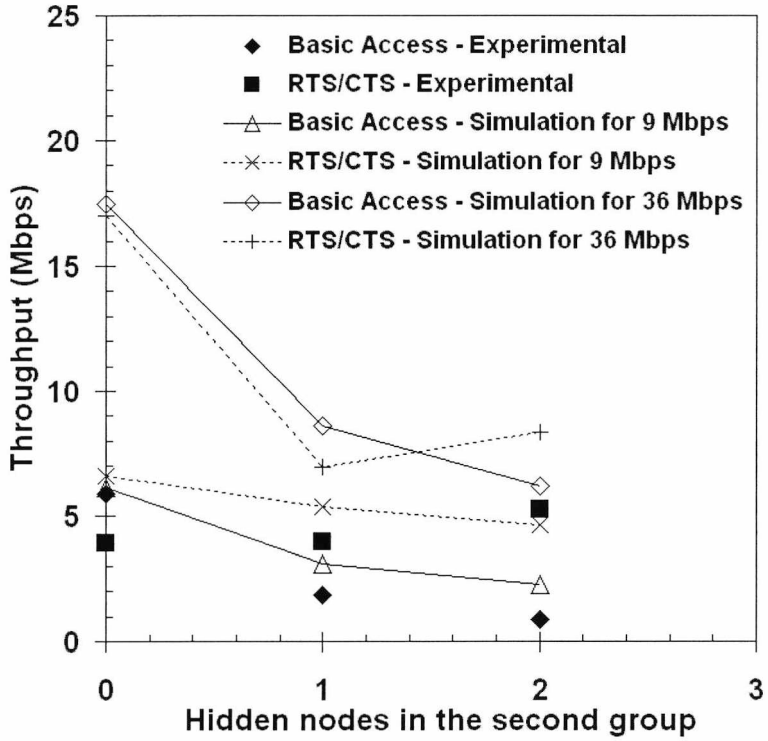

Figure 7.14. RTS/CTS vs. basic access for the hidden node scenario using four mobile units

The experimental results show that basic access performs better than RTS/CTS access when there are no hidden nodes – this is just a simple case of multiple clients accessing the AP. Switching on the RTS/CTS mechanism results in increased overhead due to the additional control frames being sent. RTS/CTS, though, has been shown to help the performance of the network for longer data frames and when the number of stations is high [22].

With an increase in the number of hidden nodes (i.e., an increase in the number of nodes in the second group), RTS/CTS is clearly seen to improve the network's throughput. For the case, when there is one node in the second group, the throughput using RTS/CTS is approximately 2.2 times higher than the throughput using basic access. The worst case scenario is when there are equal numbers of nodes in the two groups and the throughput using RTS/CTS is 6.1 times higher than that using the basic access scheme. As mentioned earlier (Section 7.7.2), such an improvement in throughput by using RTS/CTS is also seen from the results presented in [22] for a hidden node scenario.

In order to support the experimental results, the above hidden node scenario was also modelled using OPNET, as discussed in [12]. As low-power 1550 nm prototype VCSELs were being used for the single-antenna RAU set-up, the received signal strength even at an MU placed very close to the RAU was recorded to be very low. The reasons for this have been discussed in Section 7.5.2. Low signal strengths can lead to low transmission rates and therefore lower throughputs, as can be seen from the simulation results depicted earlier in Figures 7.10a and 7.10b. In order to account for the low signal strengths, different transmission rates (9 Mbps and 36 Mbps) were used in the simulations. The throughput values obtained using a 9 Mbps transmission rate are closer to the experimentally obtained throughput values and show a better RTS/CTS performance in all the cases considered, as can be seen from Figure 7.14. For the higher transmission rate of 36 Mbps, however, RTS/CTS is seen to perform better only when the number of hidden nodes in each group was two.

Measurements were also carried out to determine the effect of varying the RTS threshold value on the throughput. Again, uplink transmission of IEEE 802.11g signals has been considered. Two cases, one using two MUs and the second using four MUs were investigated. As mentioned before, two groups hidden from each other were created. For the two-node case, each group had one MU accessing each RAU while for the four-node case each group had two MUs accessing each RAU. Throughput for the two cases is plotted in Figure 7.15.

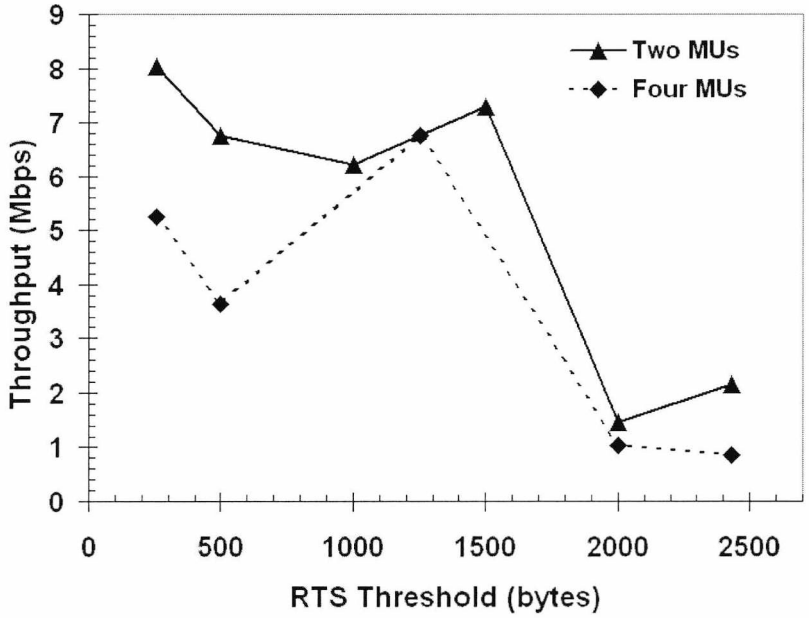

Figure 7.15. Throughput vs. RTS threshold for the hidden node scenario

The general trend for both the two-node case and the four-node case is that the throughput falls with increasing RTS threshold, certainly for higher threshold values, showing that performance improves with increased use of RTS/CTS. This is expected since for smaller RTS thresholds (e.g. 256 bytes) an RTS/CTS message is sent after every 256 bytes of data and this reduces the amount of data lost even if there is a collision. As the RTS threshold increases, there is a chance that it exceeds the size of the packets being transmitted which would then switch off the RTS/CTS mechanism and result in lower throughput. The increase in the throughput for the [1000, 1500] RTS threshold range in the two-MU case and [500, 1250] range for the four-MU case does, however suggest that there exists an optimum RTS threshold value. The difference in the RTS threshold ranges for the two cases shows that this optimum value depends on the network load and on the number of hidden nodes present. This value will also be influenced by the size of the MPDU frame being transmitted [22].

These measurements and results, therefore, confirm that the use of RTS/CTS is beneficial for the hidden node problem, even in the context of WLAN-over-fibre networks.

7.8 Conclusion

The performance of WLAN-over-fibre networks using different MAC mechanisms has been studied in this chapter. In particular, the effect of fragmentation, fibre propagation delay and the use of RTS/CTS when hidden nodes are present have been experimentally investigated. In addition, scenarios where multiple clients access a single AP via a single RAU and where clients access the AP via multiple RAUs have also been discussed. The network performance has been analysed based on throughput measurements for the transmission of IEEE 802.11b (at 11 Mbps) and IEEE 802.11g (at 54 Mbps) signals via two different RAUs (the two-antenna RAU and the single-antenna RAU). The experimental observations have also been supported wherever possible using simulations carried out using the OPNET Modeler software package.

For both RAU set-ups, fragmentation of the transmitted packet is seen to cause a decrease in throughput for the transmission of IEEE 802.11b and IEEE 802.11g signals. Simulations and experiments show that the throughput becomes stable once the fragmentation threshold reaches the transmitted MSDU size of 1500 bytes. Based on the

results for the two access points (*D-Link* and *Netgear*) investigated using the two-antenna RAU, it was also shown that the type of access point being used had very little influence on the throughput performance of the transmitted signal. It is however, important to investigate access points from more manufacturers to draw a more significant conclusion on the influence of the access point hardware on the throughput performance.

Another important parameter investigated was the fibre propagation delay which is known to affect the timing restrictions imposed by the MAC protocol. Every WLAN-over-fibre network can therefore only support a certain maximum length of fibre depending on the ACK_TIMEOUT parameter of the AP. As different lengths of fibre were unavailable for the experiments, the maximum length of fibre supported by the designed WLAN over fibre link could not be determined. However, the results presented do emphasize the importance of the ACK_TIMEOUT parameter for designing WLAN-over-fibre links.

For multiple clients accessing the AP via a single RAU, the throughput performance (of especially the uplink) was seen to be influenced heavily by the type of wireless card being used.

Finally, the feasibility of using multiple RAUs fed by a single AP was demonstrated. For such a deployment, scenarios involving both non-hidden nodes and hidden nodes have been examined. An improvement in throughput performance for the case where MUs are in the receiving range of more than one RAU is seen when equal lengths of fibre are used for the RAUs. Configuring the RAUs to emulate a hidden-node case, it is seen that the throughput is severely affected when hidden nodes are introduced in the network. Measurements have been carried out for a total of two and four MUs, with equal numbers of station pairs being hidden in each case. For both cases, switching on the RTS/CTS mechanism results in improved throughput. However, the results suggest the existence of an optimal RTS threshold value which in turn will depend on the frame size being transmitted. For the four-MU case, a comparison between the basic access and RTS/CTS mechanisms confirms that the improvement in throughput with RTS/CTS increases with the increase in the number of mutually hidden stations.

References

[1] B.P. Crow, I. Widjaja, J.G. Kim, and P.T. Sakai, "IEEE 802.11 Wireless Local Area Networks," *IEEE Communications Magazine*, Vol. 35, Issue 9, pp. 116-126, September 1997.

[2] B. O'Hara and A. Petrick, "*The IEEE 802.11 Handbook – A Designer's Companion*," published by *Standards Information Network, IEEE Press, The Institute of Electrical and Electronics Engineers Inc.*, 1999.

[3] IEEE Std 802.11, 1999 Edition (R2003), *Information technology - Telecommunications and information exchange between systems - Local and metropolitan area networks - Specific requirements - Part 11: Wireless LAN Medium Access Control (MAC) and Physical Layer (PHY) specifications*, 2003.

[4] M.S. Gast, "*802.11 Wireless Networks – The Definitive Guide*," published by O'Reilly & Associates, Inc., CA, USA, 2002.

[5] IEEE Std 802.11a-1999 (R2003), *Supplement to IEEE standard IEEE 802.11a for Information technology - Telecommunications and information exchange between systems - Local and metropolitan area networks - Specific requirements - Part 11: Wireless LAN Medium Access Control (MAC) and Physical Layer (PHY) specifications, High-speed Physical Layer in the 5 GHz band*, 2003.

[6] IEEE Std 802.11b-1999 (R2003), *Supplement to IEEE standard IEEE 802.11a for Information technology - Telecommunications and information exchange between systems - Local and metropolitan area networks - Specific requirements - Part 11: Wireless LAN Medium Access Control (MAC) and Physical Layer (PHY) specifications: Higher-speed Physical Layer extension in the 2.4 GHz band*, 2003.

[7] IEEE Std 802.11g-2003, *IEEE Standard for Information technology - Telecommunications and information exchange between systems - Local and metropolitan area networks - Specific requirements - Part 11: Wireless LAN Medium Access Control (MAC) and Physical Layer (PHY) specifications, Amendment 4: Further Higher Data Rate Extension in the 2.4 GHz Band*, 2003.

[8] D. Vassis, G. Kormentzas, A. Rouskas, and I. Maglogiannis, "The IEEE 802.11g standard for high data rate WLANs," *IEEE Network*, May/June 2005.

[9] Ming-Ju Ho, J. Wang, K. Shelby, and H. Haisch, "IEEE 802.11g OFDM WLAN throughput performance," *Proceedings of the IEEE 58th Vehicular Technology Conference*, Vol. 4, pp. 2252-2256, October 2003.

[10] C. Chaudet, D. Dhoutaut, and I.G. Lassous, "Performance issues with IEEE 802.11 in adhoc networking," *IEEE Communications Magazine*, Vol. 43, Issue 7, pp. 110-116, July 2005.

[11] M.U. Ilyas, M.A.B. Ilyas, Z. Ul-Mustafa, and M. Mufti, "Effects of fragmentation in IEEE 802.11b networks," in *Proceedings of the Computer and Communication Networks (CCN 2004)*, Cambridge, USA, Proceeding 438-093, ACTA Press Publishing, August – October 2004.

[12] A. Das, M. Mjeku, A. Nkansah, and N.J. Gomes, "Effects on IEEE 802.11 MAC throughput in wireless LAN over fiber systems," *Journal of Lightwave Technology* (special issue), November 2007 (in press).

[13] N.J. Gomes, A. Das, A. Nkansah, M. Mjeku, and D. Wake, "Multimode fiber-fed indoor wireless network," Invited paper, *International Topical Meeting on Microwave Photonics (MWP) 2006*, October 2006.

[14] M.G. Larrode, A.M.J. Koonen, and P.F.M. Smulders, "Impact of radio-over-fibre links on the wireless access protocols," *Proceedings NEFERTITI Workshop*, Belgium, January 2005.

[15] B.L. Dang and I. Niemegeers, "Analysis of IEEE 802.11 in radio over fiber home networks," *Proceedings of the 30th IEEE Conference on Local Computer Networks (LCN) 2005*, pp. 744-747, November 2005.

[16] B.L. Dang, V. Prasad, and I. Niemegeers, "On the MAC protocols for radio over fiber networks," *International Conference on Communication and Electronics (ICCE) 2006*, Hanoi, October 2006.

[17] A. Di Stefano, G. Terrazzino, L. Scalia, I. Tinnirello, G. Bianchi, and C. Giaconia, "An experimental testbed and methodology for characterizing IEEE 802.11 network cards," *Proceedings of the 2006 International Symposium on a World of Wireless, Mobile and Multimedia Networks (WoWMoM) 2006*, pp. 513-518, June 2006.

[18] R. Bruno, M. Conti, and E. Gregori, "IEEE 802.11 optimal performances: RTS/CTS mechanism vs. Basic Access," *Proceedings of the 13th IEEE International Symposium on Personal and Indoor Mobile Communications (PIMRC) 2002*, Vol. 4, pp. 1747-1751, September 2002.

[19] Fun Ye, Shiann-Tsong Sheu, Tobias Chen, and Jenhui Chen, "The impact of RTS threshold on IEEE 802.11 MAC protocol," *Tamkang Journal of Science and Engineering*, Vol. 6, No. 1, pp. 57-63, 2003.

[20] S. Khurana, A. Kahol, and A.P. Jayasumana, "Effect of hidden terminals on the performance of IEEE 802.11 MAC protocol," *Proceedings of the 23rd annual conference on Local Computer Networks (LCN) 1998*, pp. 12-20, October 1998.

[21] I. Tinnirello, S. Choi, and Y. Kim, "Revisit of RTS/CTS exchange in high-speed IEEE 802.11 networks," *Proceedings of the 6th IEEE International Symposium on a World of Wireless, Mobile and Multimedia Networks (WoWMoM) 2005*, pp. 240-248, June 2005.

[22] M. Mjeku and N.J. Gomes, "Analysis of RTS/CTS exchange in WLAN over fiber networks," *IEEE Transactions on Wireless Communications*, submitted for publication, 2006.

[23] M. Mjeku, B. Kalantari-Sabet, J.E. Mitchell, and N.J. Gomes, "TCP and UDP performance over fibre-fed 802.11b networks," *12th Microcoll Conference*, Budapest, Hungary, May 2007.

CHAPTER 8
CONCLUSION AND FUTURE WORK

8.1 Introduction

This thesis has provided a detailed description of the research work conducted during a project that focused on the use of radio-over-fibre technology in order to improve in-building coverage for mobile communication networks. Most of the fibre-based DAS products for in-building coverage available in the market today use single-mode fibre for RF signal distribution[1]. Multimode fibre that is pre-installed in most buildings today offers a more cost-effective option. During the course of the research presented in this thesis, a commercial product that emerged in the market was the Zinwave DAS [1] which employed pre-installed MMF to distribute mobile and wireless signals in the frequency range 370 MHz – 2.5 GHz. However, uncooled DFB lasers operating at 1300 nm were utilised as optical sources in this product. A more inexpensive alternative in this respect could be commercially available vertical-cavity surface-emitting lasers (operating at 850 nm). Therefore, the main aim of the research presented in this thesis was to design and implement a distributed antenna system fed by VCSEL-MMF-based optical links.

Specifically, a system demonstrator was designed for the transmission of WLAN signals (frequency: 2.4 GHz) using vertical cavity surface emitting lasers at 850 nm as optical transmitters and multimode fibres as the optical link. The system demonstrator performance was characterized using signal strength and throughput measurements and the effect of the IEEE 802.11 WLAN protocol on the performance of the RoF link was also investigated.

[1] Some examples of currently available commercial DAS products have been listed in Table 1.1, Section 1.2, Chapter 1.

8.2 Summary

A summary of some of the key results that have been obtained in this research is listed below:

- A link budget has been developed for the design and operation of a bi-directional fibre-fed indoor wireless network [2]. The link budget was implemented using a Microsoft Excel spreadsheet and the calculations were automated using macros. It allows for efficient mathematical analysis of the effect of different component parameters on the combined optical and wireless link performance. In order to obtain the best possible coverage, the link budget analysis enables the optimisation of the various component parameters utilised.

- A WLAN system demonstrator using low cost components has been designed [2]. In particular, commercially available vertical cavity surface emitting lasers (at 850 nm) were used as optical transmitters and multimode fibres (OM1/OM2) as the optical link. The main attraction of using multimode fibres is that they are pre-installed in most buildings today which results in lower system costs. Inexpensive, purpose-built, omnidirectional multiband antennas were utilised in the wireless path.

- Component characterisation measurements were carried out for the 850 nm VCSELs and MMF to be used in the system demonstrator. Slope efficiency (using P-I characteristics) and relative intensity noise values (at different wireless system frequencies) were determined for the VCSELs. Frequency response measurements were also carried out for the VCSEL-PD and VCSEL-MMF-PD links. Third-order intermodulation measurements gave SFDR values as high as 97 $dB.Hz^{2/3}$ for the complete optical link. Additionally, EVM measurements were used to analyse the the transmission performance of various digitally modulated signals (emulated GSM, DPRS and UMTS) over the VCSEL-MMF-PD link.

- Two different types of remote antenna units (single-antenna RAU and two-antenna RAU) were designed for use in the demonstrator. The two-antenna RAU employs separate transmit and receive antennas while the single-antenna RAU

uses a single-antenna for both transmission and reception with the uplink and downlink paths separated by a power-splitter/combiner.

- Using two different sets of component parameters, the link budget calculations predict maximum achievable ranges of 32 m and 45 m for the transmission of IEEE 802.11b (at 11 Mbps) signals over the WLAN system demonstrator employing the two-antenna RAU and single-antenna RAU designs respectively; the corresponding values for the transmission of IEEE 802.11g signals (at 54 Mbps) are 9.0 m and 9.5 m. Based on a theoretical analysis, it was concluded that the range performances of the RoF link using the two RAU systems strongly depended on parameters such as the path loss exponent and isolation values at the two ends of the RAU, and also on the limitation (UL capping and loop gain) imposed on the range calculations.

- For both RAU designs employed in the WLAN demonstrator, the link budget calculations were also used to predict the amplifier gains required for providing complete coverage of a standard office room.

- Successful transmission of IEEE 802.11b signals at 11 Mbps and IEEE 802.11g signals at 54 Mbps (generated using a commercial access point) was achieved over the WLAN system demonstrator. The link quality was assessed by streaming video signals over the WLAN system demonstrator. High quality signal reception was achieved throughout the office room.

- The performance of the demonstrator was characterized using signal strength and throughput measurements. Signal strength measurements helped in verifying the link budget calculations. Throughputs as high as 5 Mbps for IEEE 802.11b and 20 Mbps for IEEE 802.11g were recorded at distances close to the RAU. These values are very close to the approximate maximum throughput values of 6 Mbps for IEEE 802.11b and 22 Mbps for IEEE 802.11g (at 54 Mbps) reported in literature [3]. Additionally, with particular reference to the IEEE 802.11b system, the throughput values were observed to remain relatively stable over the entire measurement range for both RAU configurations.

- Theoretical range predictions for different radio systems such as GSM 900, GSM 1800, UMTS (both FDD and TDD), as well as IEEE 802.11 b and g, have been carried out for a system using better available measured component parameters. The radio range predictions computed for the different systems are listed in the following table. The results illustrate that reasonable cell sizes may be achieved for all the systems.

TABLE 8.1 THEORETICAL RANGE PREDICTIONS USING THE LINK BUDGET FOR THE TRANSMISSION OF DIFFERENT WIRELESS SYSTEMS

System	Range (m)
GSM 900	64
GSM 1800	74
UMTS (FDD)	23
UMTS (TDD)	22
IEEE 802.11b	40
IEEE 802.11g	12

- Simultaneous dual-band transmission of different combinations of wireless signals (DPRS, GSM, UMTS and IEEE 802.11g) has been demonstrated for the first time over another RoF link (also fed by low-cost 850 nm VCSELs and multimode fibre) [4]. The results indicate that the signal qualities for each of the transmitted systems are within the maximum allowed rms EVM values.

- The performance of WLAN-over-fibre networks using different MAC mechanisms has been experimentally analysed for the first time in this research [5]. When demonstrating the different MAC mechanisms, the experimental observations have been corroborated using simulations carried out using the OPNET modeler, wherever possible. The effect of parameters such as fragmentation, fibre propagation delay and the use of RTS/CTS when hidden nodes are present have been experimentally investigated for the transmission of IEEE 802.11b (at 11 Mbps) and IEEE 802.11g (at 54 Mbps) signals via the two different RAUs.

- Specifically, when using either RAU, the fragmentation of the transmitted packet causes a decrease in throughput for both IEEE 802.11b and IEEE

802.11g signals. Simulations and experiments show that the throughput becomes stable once the fragmentation threshold reaches the transmitted MSDU size (an MSDU size of 1500 bytes was used for the simulations).

- Throughput measurements for the transmission of IEEE 802.11g signals over the two-antenna RAU system have been carried out using access points from two different manufacturers. For both the access points, it was observed that the fragmentation threshold ceases to have an effect on the throughput after attaining a value of 1500 bytes. These results indicate that the type of access point being used does not heavily influence the throughput performance. However, testing the performance of access points from other manufacturers would be helpful.

- Fibre propagation delay results obtained for the available fibre lengths (1.2 km, 1.7 km and 21.2 km) experimentally confirm the importance of the ACK_TIMEOUT parameter for WLAN-over-fibre links.

- For multiple clients accessing the access point via a single RAU, with particular reference to the uplink, it was established that the throughput performance is influenced by the type of wireless card being used.

- The feasibility of using multiple RAUs fed by a single access point has also been demonstrated. For such a deployment, scenarios involving both non-hidden nodes and hidden nodes have been examined. An improvement in throughput performance for the case where mobile units are in the receiving range of more than one RAU is seen when equal lengths of fibre are used for the RAUs. When the RAUs are configured to emulate a hidden-node case, it is seen that the throughput is severely affected when hidden nodes are introduced in the network. Measurements have been carried out for a total of two and four mobile units, with equal numbers of station pairs being hidden in each case. For both cases, switching on the RTS/CTS mechanism results in improved throughput. However, the results suggest the existence of an optimal RTS threshold value which in turn will depend on the frame size being transmitted. For the four-MU case, a comparison between the basic access and RTS/CTS mechanisms

confirms that the improvement in throughput with RTS/CTS increases with the increase in the number of mutually hidden stations.

8.3 Key Achievements

This section discusses the key achievements of the research presented in this thesis.

8.3.1 Link Budget Analysis

- A link budget has been developed which allows for component parameter optimisation and range prediction for a number of wireless systems. This aids in efficient design and performance analysis of the RoF link before practically implementing it. The automation of the calculations further improves the efficiency. A similar link budget was developed in [6] for carrying out radio range predictions for an RoF link using a passive EAT. However, the link budget analysis presented in this thesis not only allows the prediction of maximum achievable ranges for different wireless systems, but also takes into account restrictions such as crosstalk and noise emissions which are important for practical system transmissions.

- Range predictions carried out using the link budget analysis have been experimentally verified for the transmission of 'real' WLAN signals over a low-cost RoF link employing commercially available 850 nm VCSELs and OM1/OM2 MMF.

- Additionally, using this experimentally verified link budget, it has been theoretically calculated that reasonable cell sizes may be achieved for the transmission of several mobile/wireless systems (up to a transmission frequency of 2.5 GHz).

8.3.2 Experimental Demonstration of a Low-Cost Multimode Fibre-Fed Indoor WLAN Network

Most of the previous work demonstrating the transmission of WLAN signals over low-cost RoF links ([7]-[9]) mainly concentrate on the optical path transmission performance. Even though in [9], the transmission of 'real' video signals over a WLAN-over-fibre link has been demonstrated, the wireless range over which this has been achieved has not been mentioned.

- In this research, both the optical and wireless paths of the designed multimode fibre-fed WLAN system have been characterised for the transmission of IEEE 802.11b (at 11 Mbps) and IEEE 802.11g (at 54 Mbps) signals using signal strength and throughput measurements. The link quality was also assessed by streaming video signals over the WLAN-over-fibre link.

- A remote antenna unit was developed which was successfully implemented as part of the WLAN system demonstrator.

- Complete coverage of a standard office room (5 m x 6 m x 2.7 m) was demonstrated using the system demonstrator, with the recorded throughput values close to the approximate maximum throughput values reported in literature [3].

8.3.3 Simultaneous Dual-Band Transmission over an RoF Link

One of the advantages of implementing a radio-over-fibre link is that it enables the simultaneous provision of multiple wireless services over the same infrastructure. In this respect, the transmission of different combinations of emulated mobile/wireless systems in a dual-band configuration has been demonstrated for the first time in this research (over another RoF link also employing 850 nm VCSELs and multimode fibre). The transmitted systems included GSM at 1.8 GHz, DPRS at 1.88 GHz, UMTS at 2.0 GHz and IEEE 802.11g at 2.4 GHz. EVM measurements indicated acceptable signal quality after transmission over the combined optical and wireless paths.

8.3.4 Experimental Analysis of the IEEE 802.11 MAC Throughput Performance for WLAN-over-Fibre Networks

Previous research investigating IEEE 802.11 MAC protocol issues with respect to WLAN signal transmission over fibre has primarily been carried out by means of either theoretical analysis [10], [11] or by simulations [11]-[13]. The work presented in this thesis experimentally investigates for the first time, the throughput performance of WLAN-over-fibre networks using different MAC mechanisms for the transmission of IEEE 802.11b and IEEE 802.11g signals. The experimental results have been corroborated by simulations wherever possible using the OPNET Modeler. The specific achievements in this context have been listed below:

- In practical WLAN-over-fibre networks, more often than not, there will be multiple clients accessing the access point via a single remote antenna unit (e.g. hotspots). Therefore, it is important to know how the increase in the number of clients affects throughput. By examining such scenarios for the designed WLAN-over-fibre link, it was established that the type of wireless card being used in the mobile units influenced the uplink throughput performance. Additionally, for IEEE 802.11g signals, the transmission rates (and therefore the throughput values) were seen to depend on the location of the mobile units in the room; furthermore, it was determined that a low throughput value for one mobile unit caused a reduction in throughputs for the other contending mobile units.

- In WLAN-over-fibre networks consisting of several remote antenna units placed in clearly separated areas and driven by a single access point, the occurrence of groups of mobile units hidden from each other becomes more frequent. Therefore, the effect of such hidden nodes in WLAN-over-fibre networks has been investigated in this research. Specifically, the throughput performance of the designed WLAN-over-fibre link was seen to deteriorate in the presence of hidden nodes. The advantage of using the RTS/CTS mechanism in such a scenario (as has been proved by means of simulations in [11]) has been experimentally confirmed.

- Experimental results presented in this thesis confirm that fragmentation of transmitted packets causes a decrease in the throughput performance of the

designed WLAN-over-fibre link. The throughput, however, was observed to stabilise once the fragmentation threshold reached the transmitted packet size.

- The effect of the ACK_TIMEOUT parameter (of the chipset used in the access point) on the maximum length of fibre that can be supported by a WLAN-over-fibre link has been discussed by means of a theoretical analysis in [10] and by means of simulations in [12], [13]. In this research, the importance of the ACK_TIMEOUT parameter for designing WLAN-over-fibre links has been emphasized by means of fibre propagation delay measurements.

8.4 Future Work

It is evident that the transportation of multiple wireless services over the same RoF link will be a very cost-effective scheme. The simultaneous dual-band transmission of different wireless systems – GSM, UMTS, DPRS – over the designed RoF link has been demonstrated in Chapter 6. The system was, however, not optimized for such a transmission. Consideration of factors such as isolation between the uplink and downlink paths (in the RAU), avoiding oscillation in the circuit caused by loop gain, transmit power and transmitted noise are very important to link design, as has been discussed in Chapter 5. In addition, for the simultaneous transmission of multiple systems, harmonic and intermodulation distortion also needs to be taken into account. It is important that the spurious emissions from one transmitting system in the received band of another system be maintained at levels below the specified limits in the respective standards. Moreover, the range and corresponding amplifier gain calculations should be determined by the system with the most critical parameters. For example, the uplink receiver sensitivity is an important parameter in the calculation of the uplink range and therefore influences the uplink amplifier gain. The uplink receiver sensitivities of IEEE 802.11g and GSM 900 systems are -68 dBm and -88 dBm respectively (as given in Table 6.5, Chapter 6). Considering the simultaneous transmission of IEEE 802.11g and GSM 900 systems over the RoF link, the system parameters of IEEE 802.11g (with a higher value of receiver sensitivity) should be used for the range calculations. These are just a few of the important aspects that need to be considered for the transmission of multiple wireless systems over an RoF link. Further research on improvements to the current link to support multiple wireless system transmission will be useful.

The performance of the RoF link for the transmission of WLAN signals has been assessed using throughput measurements in this work. Another parameter that has been used extensively by researchers for characterising WLAN-over-fibre link performance is EVM. Optimum VCSEL bias as well as optimum input RF power from the AP that can be fed into the VCSEL without the onset of non-linearity, can be more accurately determined using EVM measurements. This, however, will require a vector signal analyser with WLAN decoding capabilities. As such equipment was unavailable during the experiments carried out in this research, EVM measurements for the WLAN-over-fibre link were not possible.

With respect to the IEEE 802.11 MAC, an attempt has been made to analyse the performance of the WLAN-over-fibre link using different MAC mechanisms such as fragmentation and RTS/CTS. However, such measurements have been carried out using a single access point. Using access points from different manufacturers could help achieve a better understanding of the influence of IEEE 802.11 MAC on WLAN-over-fibre networks.

Another interesting aspect of WLAN-over-fibre networks that can be looked at in the future is the use of multiple access points driving a single RAU or multiple RAUs. Increasing the number of users in a given area (for example, hotspots) will result in a decrease in the throughput performance of the WLAN-over-fibre link (compared to the single user case), as discussed in Section 7.6, Chapter 7. This can be solved by using multiple access points to feed a single RAU. An example of an experimental set-up for an RAU being fed by two access-points, which may be used for such measurements, is presented in Figure 8.1. Here, the combined WLAN signals from the two access points are used to modulate the laser. In such a scenario, intermodulation distortion caused by laser non-linearity can be an important concern. As the frequency separation between the two WLAN channels can be as small as 5 MHz (minimum channel spacing), it is possible that the resulting third-order intermodulation products may interfere with either of the transmitted channels. It is therefore important that the amplitudes of the third-order products be controlled so as to minimise interference. One way of doing this will be to perform two-tone measurements on the VCSEL and determine the maximum input RF power beyond which the amplitude of the third-order products exceeds the spurious emission limit specified in the WLAN standard.

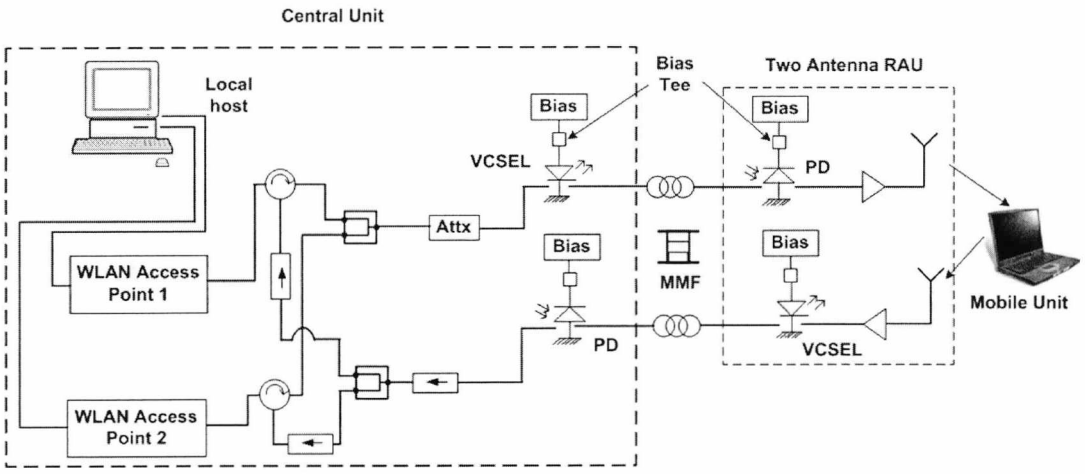

Figure 8.1. An example of the experimental configuration for multiple access points feeding the two-antenna RAU

The various issues under investigation in this thesis are of direct relevance in the planning and design of low-cost radio-over-fibre indoor wireless networks. The measurements and accompanying analyses that have been presented provide a useful addition to the limited information available in this area.

References

[1] www.zinwave.com, Zinwave 2700 Distributed Antenna System.

[2] A. Das, A. Nkansah, N.J. Gomes, I.J. Garcia, J.C. Batchelor, and D. Wake, "Design of low-cost multimode fibre-fed indoor wireless networks," *IEEE Transactions on Microwave Theory and Techniques*, Volume 54, Issue 8, pp. 3426-3432, August 2006.

[3] R. Seide, "Capacity, coverage, and deployment considerations for IEEE 802.11g," *Cisco Systems white paper*, San Jose, CA, October 2003.

[4] A. Nkansah, A. Das, C. Lethien, J-P. Vilcot, N.J. Gomes, I.J. Garcia, J.C. Batchelor, and D. Wake, "Simultaneous dual band transmission over multimode fibre-fed indoor wireless network," *IEEE Microwave and Wireless Component Letters*, Volume 16, Issue 11, pp. 627-629, November 2006.

[5] A. Das, M. Mjeku, A. Nkansah, and N.J. Gomes, "Effects on IEEE 802.11 MAC throughput in wireless LAN over fiber systems," accepted for publication in *Journal of Lightwave Technology*, (special issue), November 2007 (in press).

[6] D. Wake and K. Beacham, "Passive electroabsorption tranceivers for broadband wireless access," *Proceedings of the IEEE International Topical Meeting on Microwave Photonics (MWP '02)*, pp. 21-24, November 2002.

[7] C. Lethien, C. Loyez, and J-P. Vilcot, "Potentials of radio over multimode fiber systems for the in-buildings coverage of mobile and wireless LAN applications," *IEEE Photonics Technology Letters*, Vol. 17, No. 12, pp. 2793-2795, December 2005.

[8] P. Hartmann, X. Qian, R.V. Penty, and I.H. White, "Broadband multimode fibre (MMF) based IEEE 802.11a/b/g WLAN distribution system," *Proceedings of the IEEE International Topical Meeting on Microwave Photonics (MWP '04)*, pp. 173-176, October 2004.

[9] P. Hartmann, M. Webster, A. Wonfor, J.D. Ingham, R.V. Penty, I.H. White, D. Wake, and A.J. Seeds, "Low-cost multimode fibre-based wireless LAN distribution system using uncooled, directly modulated DFB laser diodes," *29th European Conference on Optical Communication (ECOC-ICOC '03)*, Italy, pp. Vol. 3, 804-805, September 2003.

[10] M.G. Larrode, A.M.J. Koonen, and P.F.M. Smulders, "Impact of radio-over-fibre links on the wireless access protocols," *Proceedings NEFERTITI Workshop, Belgium*, January 2005.

[11] M. Mjeku and N.J. Gomes, "Analysis of RTS/CTS exchange in WLAN over fiber networks," *IEEE Transactions for Wireless Communications*, submitted for publication, 2006.

[12] B.L. Dang and I. Niemegeers, "Analysis of IEEE 802.11 in Radio over Fiber Home Networks," *Proceedings of the 30th IEEE Conference on Local Computer Networks (LCN) 2005*, pp. 744-747, November 2005.

[13] N.J. Gomes, A. Das, A. Nkansah, M. Mjeku, and D. Wake, "Multimode fiber-fed indoor wireless network," Invited paper, *International Topical Meeting on Microwave Photonics (MWP) 2006*, October 2006.

APPENDIX A

This appendix contains the datasheets for the *ULM* 850 nm VCSEL and the *Appointech* photodiode used for measurements in this research.

A.1 Datasheet for *ULM* 850 nm VCSEL

U·L·M PHOTONICS

3mW / 6mW VCSEL
SMA Receptacle / Chip

- Vertical Cavity Surface-Emitting Laser
- 3mW / 6mW peak power
- >2,5 Gbps speed
- e.g. for storage, free space, sensing
- other wavelengths available, e.g. for WDM

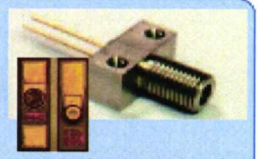

ELECTRO-OPTICAL CHARACTERISTICS Receptacle (Chip)

PARAMETER	SYMBOL	UNITS	MIN	TYP	MAX	TEST CONDITIONS
Emission wavelength	λ_E	nm	835	850	860	T=20°C
Fiber-coupled mean power (power)	mW		3(6)			Fiber 125µm, 0.37NA, T=20°C
Threshold current	I_{TH}	mA			2	T=20°C
Variation of I_{TH} over Temp.	$\Delta I_{TH}(T)$	mA		0.3		T=0 .. 70°C
Threshold voltage	U_{TH}	V	1.5	1.8	2.0	
Laser current	I_{OP}	mA		9		P_{opt}=3mW*
Laser voltage	U_{OP}	V	1.8	2.0	2.2	P_{opt}=3mW*
Wallplug efficiency	η_{WP}	%	5	10	30	P_{opt}=3mW*
Slope Efficiency	η_S	W/A	0.3	0.4	0.6	T= 20°C
Variation of η_S over Temp.	$\Delta\eta_S(T)$	W/A		0.2		T= 0 .. 70°C
Differential series resistance	R_S	Ω		25		P_{opt}=3mW*
3dB modulation bandwidth	f_{3dB}	GHz	3			P_{opt}=3mW*
Rise and fall time	t_R/t_F	ps		90	150	20%..80% ; $P_{OPTICAL}$=0.5/3.0mW*
Relative intensity noise	RIN	dB/Hz		-130	-120	P_{opt} = 3 mW* @ 1 GHz
Wavelength tuning over temperature		nm/K		0.07		
Thermal resistance	$R_{thermal}$	K/mW			2	
Spectral bandwidth	$\Delta\lambda$	nm			1	rms
far field angle chip		deg		25		6mW chip output power
far field angle TO56 package		deg		20		6mW TO56 output power

* in optical Fiber 125µm, NA 0,37

ABSOLUTE MAXIMUM RATINGS

Storage temperature	-55 ... 125°C
Operating temperature	-40 ... 85°C
Electrical power dissipation	40 mW
Continous forward current	15 mA
Reverse voltage	8V
Soldering temperature	330°C

NOTICE: Stresses greater than those listed under „Absolute Maximum Ratings" may cause permanent damage to the device. These are stress ratings only and functional operation of the device at these or any other condition beyond those indicated for extended periods of time may effect device reliability.

ATTENTION: Electrostatic Sensitive Devices
Observe Precautions for Handling

www.ulm-photonics.de v18

U·L·M PHOTONICS

LIV (optical fiber 125µm, NA 0.37)

Other fiber core diameters available upon request

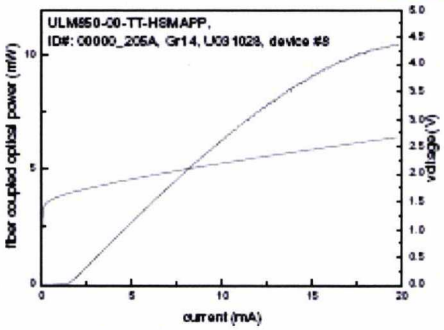

Description	3mW VCSEL SMA Receptacle	6mW VCSEL TO56	6mW VCSEL Chip
Cap	-	Ball lense	-
Common	anode	anode	-
Type			
with Monitor (PD)	ULM850-00-TT-HSMAPP	ULM850-00-TT-H56BPP	-
without Monitor	ULM850-00-TT-HSMAOP	ULM850-00-TT-H56BOP	ULM850-00-TT-H0101U

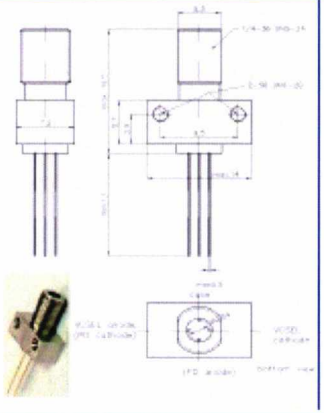

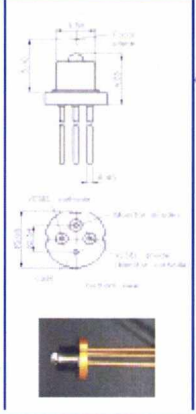

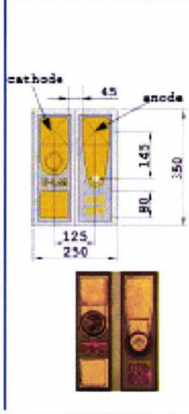

Contact U-L-M photonics GmbH / D | SESNA-Corp. / Japan | HIKARI-Inc. / Japan | Lantron Co., Ltd. / Korea
Fon (Fax) +49(0)731 ss0194-011 (-026) | +81(0)3 5978 13-71 (-74) | +81(0)3 39331-17 (-18) | +82 31 719 4331 (4339)
Email sales@ulm-photonics.de | kumazawa@sesna.net | ohta@hikari-trading.com | william88@hanalce.com

www.ulm-photonics.de

v19

A.2 Datasheet for *Appointech* Photodiode

APPOINTECH, Inc.

1.5GHz GaAs PIN Photodiode Module

GaAs PIN Photodiode Module

Features

- High Responsivity
- High speed, typical 1.5 GHz
- Low dark current, < 1nA
- Low capacitance, typical 0.7pF
- Operating temperature range -40°C to 85°C
- Hermetically sealed TO-18 package in pigtailed or receptacle housing with FC, ST, SC, LC, MU or SMA connector

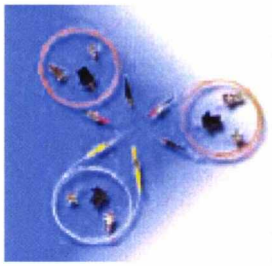

Specifications (T=25°C, -5V)

Parameter	Symbol	Test Condition	Min.	Typ.	Max.	Unit
Responsivity(62.5/125 um fiber)	R	LED source of 10 uW	0.3	0.4	-	A/W
Spectral Range	λ	-	800	-	900	nm
Dark Current	Id	V_R=5V	-	0.1	1.0	nA
Capacitance	Ct	V_R=5V,f=1MHz	-	0.6	0.7	pF
Rise/Fall Time	tr/tf	20% to 80%	-	100	130	ps
Bandwidth	B	V_R=2V,R_L=50Ω	-	1.5	-	GHz
Return Loss						
-1(Receptacle)			14	-	-	dB
-4(Receptacle or Pigtail)			40	-	-	dB
-5(Pigtail)			50	-	-	dB

Absolute Maximum Rating

	Symbol	Min.	Max.	Unit
Operating Temperature	To	-40	85	°C
Storage Temperature	T_{stg}	-40	125	°C
Forward Current	I_F	-	5	MA
Reverse Voltage	V_R	-	30	V
Reverse Current	I_R	-	500	UA
Lead Soldering Temperature (10 sec)	T_L	-	260	°C

Ordering Information

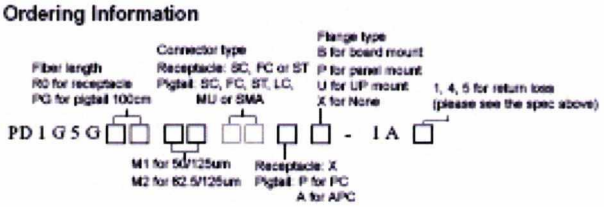

1.5GHz GaAs PIN Photodiode Module

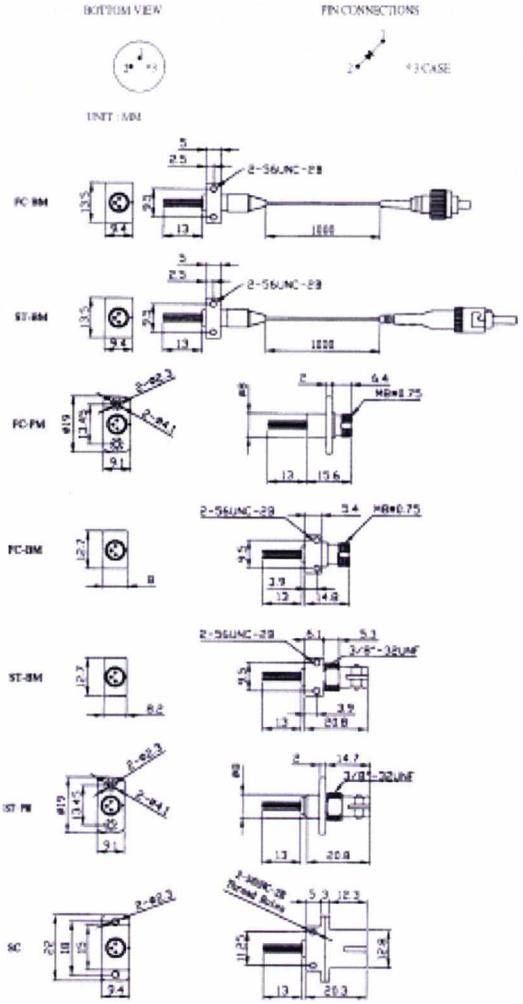

APPENDIX B

The derivations presented here are mainly aimed at verifying the results obtained in Table 6.4 (Section 6.2.1, Chapter 6). As has been discussed in Chapter 5 (Section 5.5), the link budget calculations are carried out based on certain limitations. The results presented in Table 6.4 show the amplifier gain and range values obtained for the two RAU systems using two different limitations: uplink capping and loop gain. The equations presented in this appendix can be used to explain how imposing these two different limitations can lead to changes in the relationships between amplifier gains and maximum achievable ranges for the two RAU systems. Note that for obtaining the results in Table 6.4, all the input parameters to the two-antenna RAU and single-antenna RAU link budget spreadsheets (listed in Tables 6.1a and 6.1b (Section 6.2.1, Chapter 6) respectively) have been set to be equal.

B.1 Uplink Capping Condition

According to the UL capping limitation, a maximum is set for the amplified RF power received at the uplink RAU VCSEL at the minimum distance (d_{min}). For the calculations, this maximum RF power ($P_{r,max}$) was set to be equal to the input RF power for the downlink CU VCSEL ($P_{in,RF}$). Referring to Equations 5.36 and 5.37 in Chapter 5, $P_{r,max}$ for the two-antenna and single-antenna RAU systems repectively, may be written as:

$$P_{r,\max(2)} = \frac{P_{mt} G_{au,r} G_{up(2)}}{L_{ul,\min}} \tag{B.1a}$$

$$P_{r,\max(1)} = \frac{P_{mt} G_{au} G_{up(1)}}{L_{ul,\min} \beta} \tag{B.1b}$$

where, P_{mt} is the mobile transmit power, $G_{au,r}$ is the gain of the receive antenna (for the two-antenna RAU), G_{au} is the gain of the antenna used in the single-antenna RAU, G_{up} is the uplink amplifier gain, $L_{ul,min}$ is the path loss calculated at d_{min} and β is the splitter ratio for the power-splitter/combiner used in the single-antenna RAU.

The subscripts (1) and (2) in the two equations correspond to the values for the single-antenna and the two-antenna RAU systems respectively. Note that since the same path loss exponent (n) and minimum distance (d_{min}) values have been input to both spreadsheets, $L_{ul,min}$ consequently has identical values for the single-antenna as well as two-antenna RAU systems (Equation 5.2 in Chapter 5). $P_{in,RF}$, being an input parameter to the spreadsheets, is equal for both RAU systems. This means that $P_{r,max}$ which is equal to $P_{in,RF}$ for the UL capping condition, is also equal for both RAU systems. Therefore,

$$P_{r,\max(2)} = P_{r,\max(1)} \tag{B.2}$$

Now, substituting Equations B.1a and B.1b in Equation B.2, the following relation may be derived:

$$\frac{G_{up(1)}}{G_{up(2)}} = \beta \tag{B.3}$$

For calculating the uplink range, the maximum tolerable path losses (L_{ul}) for each RAU may be written (using Equation 5.23) as:

$$L_{ul(2)} = \frac{P_{mt}}{P_{r(2)}} \tag{B.4a}$$

$$L_{ul(2)} = \frac{P_{mt}}{P_{r(1)}} \tag{B.4b}$$

where, P_r is the minimum uplink power at the receive antenna.

Substituting the values of $P_{r(2)}$ and $P_{r(1)}$ from Equations 5.21 and 5.22 into Equations B.4a and B.4b respectively:

$$L_{ul(2)} = \frac{P_{mt} G_{au,r} G_{up(2)}}{S_{ul} L_{opt,ul}} \tag{B.5a}$$

$$L_{ul(1)} = \frac{P_{mt} G_{au} G_{up(1)}}{S_{ul} L_{opt,ul} \beta} \tag{B.5b}$$

where, S_{ul} is the minimum detectable signal at the uplink receiver and $L_{opt,ul}$ is the UL optical insertion loss.

Therefore, dividing Equation B.5a by Equation B.5b and noting that $G_{au,r} = G_{au}$, the following relation is obtained:

$$\frac{L_{ul(1)}}{L_{ul(2)}} = \left(\frac{G_{up(1)}}{G_{up(2)}}\right)\left(\frac{1}{\beta}\right) \tag{B.6}$$

Now substituting Equation B.3 in Equation B.6, the following relation may be derived:

$$L_{ul(1)} = L_{ul(2)} \tag{B.7}$$

Since the maximum tolerable uplink path losses for both RAU systems are equal, the maximum achievable ranges calculated using the two link budget spreadsheets should be equal (Equation 5.2, Chapter 5). The link budget calculations are automated such that the uplink (L_{ul}) and downlink (L_{dl}) path losses and therefore, the corresponding ranges are equal for each RAU system. Therefore,

$$L_{ul(1)} = L_{dl(1)} \tag{B.8a}$$

$$L_{ul(2)} = L_{dl(2)} \tag{B.8b}$$

Using Equation B.7 in Equations B.8a and B.8b:

$$L_{dl(1)} = L_{dl(2)} \tag{B.9}$$

Substituting the expression for L_{dl} from Equation 5.11 (from Chapter 5) in Equation B.9, the following relation is obtained:

$$\frac{P_{t(1)}G_{at}}{S_{dl}} = \frac{P_{t(2)}G_{at}}{S_{dl}} \tag{B.10}$$

where, P_t is the effective isotropic radiated power, S_{dl} is the downlink receiver (i.e. the mobile unit) sensitivity specified for each standard, and G_{at} is the mobile terminal antenna gain.

Finally, substituting the values of $P_{t(2)}$ and $P_{t(1)}$ from Equations 5.9 and 5.10 in Equation B.10,

$$\frac{G_{dl(1)}}{L_{iso-au}L_p} = G_{dl(2)} \tag{B.11}$$

where, $L_{iso\text{-}au}$ and L_p are the insertion losses of the isolator and the power-splitter/combiner respectively, used in the single-antenna RAU.

The downlink amplifier gains for the two RAU systems are therefore related by the following equation:

$$\frac{G_{dl(1)}}{G_{dl(2)}} = L_{iso-au}L_p \tag{B.12}$$

B.2 Loop Gain Limitation

As stated in Section 5.5.1, Chapter 5, each RAU system forms a loop with its DL and UL branches. The loop gain limitation is imposed on the link budget calculations so that the total loop gain always remains less than the total isolation in the loop (in order to avoid oscillation). Referring to Equations 5.33 and 5.35 (Chapter 5), the worst case scenario is when the total loop gain is only one-tenth (0.1 times) the total isolation in the loop. For the two RAU systems, this may be written as:

$$\frac{G_{up(2)}G_{dl(2)}}{\gamma_a\gamma_{pl}} = 0.1 \tag{B.13a}$$

$$\frac{G_{up(1)}G_{dl(1)}}{\gamma_p\gamma_{pl}L_{iso-au}} = 0.1 \tag{B.13b}$$

where, γ_a is the isolation between the two antennas (for the two-antenna RAU), γ_p is the isolation between the two ports of the power-splitter/combiner (for the single-antenna RAU), and γ_{pl} is the isolation between the DL and UL paths in both RAU systems. Again, the subscripts (1) and (2) in the two equations correspond to the values for the single-antenna and the two-antenna RAU systems respectively.

Dividing Equation B.13b by B.13a, the following relation between the amplifier gains for the two RAU systems may be derived:

$$\frac{G_{up(1)}G_{dl(1)}}{G_{up(2)}G_{dl(2)}} = L_{iso-au} \tag{B.14}$$

The maximum tolerable uplink propagation losses for the two RAU systems are given in Equations B.5a and B.5b. Dividing these two equations, the relation between L_{ul} for the two RAU systems is obtained:

$$\frac{L_{ul(2)}}{L_{ul(1)}} = \beta\left(\frac{G_{up(2)}}{G_{up(1)}}\right) \tag{B.15}$$

Referring again to Chapter 5 and substituting Equations 5.9 and 5.10 in Equation 5.11, the maximum tolerable downlink propagation loss for the two-antenna RAU and the single-antenna RAU (respectively) may be written as:

$$L_{dl(2)} = \frac{P_{in,RF}G_{dl(2)}G_{au,t}G_{at}}{S_{dl}L_{opt,dl}} \tag{B.16a}$$

$$L_{dl(1)} = \frac{P_{in,RF}G_{dl(1)}G_{au}G_{at}}{S_{dl}L_{opt,dl}L_{iso-au}L_p} \tag{B.16b}$$

where, $G_{au,t}$ is the gain of the transmit antenna for the two-antenna RAU and $L_{opt,dl}$ is the downlink optical insertion loss.

Dividing Equations B.16a and B.16b and noting that $G_{au,t} = G_{au}$, the relation between L_{dl} for the two RAU systems may be written as:

$$\frac{L_{dl(2)}}{L_{dl(1)}} = L_{iso-au} L_p \left(\frac{G_{dl(2)}}{G_{dl(1)}} \right) \tag{B.17}$$

Multiplying Equations B.15 and B.17, the following relation may be derived:

$$\frac{L_{dl(2)} L_{ul(2)}}{L_{dl(1)} L_{ul(1)}} = \beta L_{iso-au} L_p \left(\frac{G_{dl(2)} G_{up(2)}}{G_{dl(1)} G_{up(1)}} \right) \tag{B.18}$$

As in Section B.1, the link budget calculations are automated such that the uplink (L_{ul}) and downlink (L_{dl}) path losses are equal for each RAU system. Now, substituting Equation B.14 in Equation B.18, the relation between maximum tolerable path losses ($L_{ul} = L_{dl} = L$) for the two RAU systems may be derived as:

$$\frac{L_2}{L_1} = \sqrt{\beta L_p} \tag{B.19}$$

Finally, after substituting Equation 5.2 (Chapter 5) in Equation B.19, a relation between the maximum achievable ranges (d_{max}) for the two RAU systems may be derived as:

$$\left(\frac{d_{\max(2)}}{d_{\max(1)}} \right)^n = \sqrt{\beta L_p} \tag{B.20}$$